Charles University

Faculty of Science

Department of Biochemistry

Study of structure and interaction of human lymphocyte receptors

Jan Bláha

Ph. D. Thesis

Supervisor: RNDr. Ondřej Vaněk, Ph.D.

Prague 2017

DECLARATION

I declare that I have worked on this thesis under the guidance of my supervisor and that all sources of the previous knowledge are properly cited. No part of this work was used and will not be used for obtaining any other academic degree than Ph. D. from Charles University.

Prague …… ……

Jan Bláha

DECLARATION OF AUTHORSHIP

I declare that Jan Bláha contributed significantly (30-90%) to the experiments and to all 4 scientific publications contained in this Ph.D. thesis. He performed most of the experiments; substantially contributed to their planning, and took a significant part in the primary data interpretation and their preparation for the publication.

Prague …… ……

RNDr. Ondřej Vaněk, Ph.D.

ACKNOWLEDGEMENTS

I would like to express a very special thank you to my supervisor Ondřej Vaněk, who gave me guidance and valuable advice during the work on this thesis, whilst giving me a great creative freedom to experiment with and adopt new modern techniques.

Next, I would like to express my gratitude towards all past lab members, namely to Petra Celadová, Barbora Mikulová, Anna Dvorská, Helena Pucholtová, Romana Čuperková, Edita Poláchová, Iveta Hradilová, Dorota Zawadová, Adrian Leontovyč, Lukáš Slavata, David Iléš, Lajos Gáthy, Tereza Prokopová, Jiří Nový, Romana Petermannová, Ondřej Skořepa, Samuel Pažický, and Barbora Kalousková who all participated in breathing inspiration into our beloved workplace, thereby helping me to overcome all seeming obstacles. Many thanks also go to Anna Amerová for her constant good spirit and helping hand at any time there was a need to lift something heavy.

I would like to thank Jan Dohnálek, Pavlína Řezáčová, Tereza Skálová, and Jan Stránský for introducing me to the world of protein crystallography and teaching me how to build models that fit the experimental data. To Petr Novák for constructive discussions, support of my experimental work and showing me that mass spectrometry is a useful technique.

I am forever grateful to the European infrastructure for structural biology Instruct for their continued support throughout my work on this thesis and for promoting cooperation instead of division. Namely, I would like to thank Claudia Alen Amaro, Madalena Gallagher, Callum Smith and Susan Daenke. I would like to express my gratitude to David Stuart for allowing me to carry out an internship in the laboratory of the Division of Structural Biology at the University of Oxford; and to Yuguang Zhao, Karl Harlos, Tom Walter, Weixian Lu and Margaret Jones for helping me during the many visits I made to Oxford. Also to Ray Owens, Louise Bird and Joanne Nettleship from the Oxford Protein Production Facility for pointing out the obvious solution.

My wife for her infinite patience with a man trying to understand the reality and my son Přemysl for sharing his biscuits with a man writing Ph.D. thesis. My parents and my brother for their lifelong support not only during my Ph.D. years.

This work was supported by Czech Science Foundation (15-15181S), Charles University (UNCE 204025/2012, SVV 260079/2014, GAUK 161216), Foundation "Nadání Josefa, Marie a Zdeňky Hlávkových", the Ministry of Education, Youth and Sports of the Czech Republic (LTC17065 in frame of COST Action CA15126 MOBIEU), BioStruct-X (EC FP7 project 227764 and 283570), and Instruct R&D pilot scheme APPID 56 and 286, the staff of beamline I02, I03 and I04-1 at Diamond Light Source (proposal MX10627) and BM14.1 at BESSY II for technical assistance and help with data collection.

.

ABSTRACT

Natural killer (NK) cells are an essential part of immune system, providing self-surveillance of virally infected, stress transformed or cancerous cells. NKR-P1 receptors and their ligands from *clec2* gene family represent an alternate missing-self recognition system of NK cells based on interaction of highly related C-type lectin-like receptors. Human NKR-P1 has been described more than twenty years ago but still remains the sole human orthologue of this receptor family, particularly numerous in rodents. Upon binding to its cognate ligand LLT1, NKR-P1 can relay inhibitory or co-stimulatory signals. Although being interesting targets for their potential role in tumor immune evasion and autoimmunity, nature of their interaction is still unclear.

To elucidate the architecture of their interaction, we developed a generally applicable method for recombinant expression of human NKR-P1 and LLT1 and their homologues based on transfection of HEK293S GnTI$^-$ cell line. Further, we described a stabilizing His176Cys mutation, that enables for expression of highly stable and soluble LLT1. Finally, we have crystallized LLT1 and human NKR-P1 in different glycosylation states both as individual proteins and in complex. While both structures of LLT1 and NKR-P1 follow the classical C-type lectin-like superfamily fold, contrary to LLT1, NKR-P1 forms a unique homodimer centered by its helix α1 that is similar to Dectin-1. Moreover, in the structure of their complex the α1/α2-centered dimers alternate in bivalent interaction of two distinct types. While the first type is similar to manner of interaction of related human NKp65:KACL and mouse NKR-P1B:m12 complexes, the second one is unique.

ABSTRAKT

Přirozené zabíječské (Natural killer, NK) buňky jsou důležitou složkou imunitního systému poskytující dohled nad viry infikovanými, stresem transformovanými nebo rakovinnými buňkami. Receptory NKR-P1 a jejich přirozené ligandy z genové rodiny *clec2* představují alternativní „missing-self" NK buněčný systém rozpoznávání, založený na interakci vysoce příbuzných receptorů podobných C-lektinům. Lidské NKR-P1 bylo objeveno před vice než dvaceti lety, přesto stále zůstává jediným lidským orthologem této receptorové rodiny početné především u hlodavců. Po navázání na svůj přirozený ligand LLT1 receptor NKR-P1 může předávat inhibiční nebo kostimulační signály. Pro svou potenciální roli v imunitním úniku nádorů a autoimunitě jsou zajímavými cíli výzkumu, přesto je povaha jejich interakce stále nejasná.

Abychom objasnili strukturní povahu jejich interakce, vyvinuli jsme obecně použitelnou metodu pro rekombinantní expresi lidského NKR-P1 a LLT1 a jejich homologů založenou na transfekci buněčné linie HEK293S GnTI$^-$. Popsali jsme stabilizující mutaci His176Cys umožňující přípravu vysoce stabilního rozpustného receptoru LLT1. Připravený receptor LLT1 a lidské NKR-P1 jsme vykrystalizovali v různých glykosylačních stavech jednak samostatně a také v jejich komplexu. Struktury LLT1 i NKR-P1 obsahují klasické strukturní prvky proteinů podobných lektinům C-typu. Avšak na rozdíl od LLT1 NKR-P1 tvoří unikátní homodimer centrovaný podle svého α1 helixu, který je velmi podobný receptoru Dectin-1. Ve struktuře komplexu tyto α1/α2 centrované dimery alternují v bivalentní interakci dvou různých typů. Jeden typ je velice podobný interakci příbuzného lidského NKp65:KACL i myšího NKR-P1B:m12 komplexu, druhý je unikátní.

ABBREVIATIONS

ADCC	Antibody-dependent cellular cytotoxicity
aFGF	Acidic fibroblast growth factor
AICL	Activation-induced C-type lectin
CD	Cluster of differentiation
clec2	C-type lectin receptor cluster 2
Clr	C-type lectin related protein
CRD	Carbohydrate recognition domain
CTLD	C-type lectin-like domain
CTLR	C-type lectin-like receptor
GlcNAc	N-acetylglucosamine
GST	Glutathione S-transferase
HEK293	Human embryonic kidney cell line 293
HER2	Human epidermal growth factor receptor 2
HLA	Human leukocyte antigen
IFN	Interferon
Ig	Immunoglobulin
IL	Interleukin
ITAM	Immunoreceptor tyrosine-based activation motif
ITIM	Immunoreceptor tyrosine-based inhibition motif
KACL	Keratinocyte associated C-type lectin
KIR	Killer-cell immunoglobulin-like receptor
klr	Killer cell lectin-like receptor
LIR	Leukocyte immunoglobulin-like receptor
LLT1	Lectin like transcript 1
lPEI	Linear polyethyleneimine
MAIT	Mucosal associated invariant T cell
Man	Mannose
MCMV	Mouse cytomegalovirus
MHC	Major histocompatibility complex
MIC	MHC class I polypeptide-related sequence
NCR	Natural cytotoxicity receptor

NHL	Non-Hodgkin's lymphoma
NK	Natural killer
NKp	Natural killer protein
NKR-P1	Natural killer receptor protein 1
NKT	Natural killer T cells
Ocil	Osteoclast inhibitory lectin
p27	Cyclin-dependent kinase inhibitor 1B
RA	Rheumatoid arthritis
RAG	Recombination-activating genes
SLT	Secondary lymphoid tissue
SNP	Single nucleotide polymorphism
SUMO	Small ubiquitin-like modifier
Tc	Cytotoxic T lymphocytes
TGF	Transforming growth factor
Th	Helper T lymphocyte
TNF	Tumor necrosis factor
TRX	Thioredoxin
ULBP	UL16 binding protein

TABLE OF CONTENTS

1. INTRODUCTION

1.1 NATURAL KILLER CELLS

Recently a 40-years anniversary marked the discovery of innate lymphoid cells obtained from unimmunized mice that were reported to be able to spontaneously kill allogeneic tumor cells [Greenberg and Playfair, 1974; Herberman *et al.*, 1975; Kiessling *et al.*, 1975]. Their importance for cancer immune-surveillance was understood early on [Kiessling *et al.*, 1976; Glimcher *et al.*, 1977], however the mechanisms of tumor recognition and elimination remained elusive. At first a specific reaction against some antigens of viral origin was suggested [Herberman *et al.*, 1975; Kiessling *et al.*, 1975]. However, throughout the next decade it became evident that these lymphoid cells recognize and eliminate tumor cells that express low levels of self-class I molecules of the major histocompatibility complex (MHC) [Ljunggren and Karre, 1985; Karre *et al.*, 1986]. This "missing-self" concept sufficiently explained the ability to eliminate emerging malignant cells, while sparing healthy tissues [Ljunggren and Karre, 1990]. For their naturally occurring cytotoxicity not reliant on antigen sensitization, these cells were dubbed natural killer (NK) cells.

NK cells are large granular lymphocytes arising from a common lymphoid progenitor shared by T and B cells (Figure 1, pg. 12) [Kondo *et al.*, 1997]. Lacking the T and B cell receptors they are traditionally characterized by the $CD3^-CD16^{+/-}CD56^+CD161^{+/-}$ phenotype [Trinchieri, 1989]. However, expression of CD56, the isoform of neural cell adhesion molecule found on NK cells and minority of T cells, have not been observed on murine NK cells [Walzer *et al.*, 2007]. It has been suggested that expression of activating natural cytotoxicity receptor NKp46 best defines NK cells across the species [Sivori *et al.*, 1997; Moretta *et al.*, 2002; Walzer *et al.*, 2007]. However, NKp46 was reported on a small subset of human cytotoxic T lymphocytes and some $CD3^-CD56^+$ cells have very low-density of NKp46 expression [Meresse *et al.*, 2006; Walzer *et al.*, 2007]. Therefore, a truly specific pan-NK cell marker is still missing [Caligiuri, 2008].

NK cells are short lived and estimated to constitute 5 to 15 % of circulating mononuclear cells (likely more than 2 billion circulating in an adult at any time [Blum and Pabst, 2007]) and as much as 25 % of all lymphoid cells in lymphoid organs [Whiteside *et al.*, 1998]. Although NK cells are derived from the $CD34^+$ hematopoietic progenitor cells

in bone marrow or thymus [Shibuya *et al.*, 1993; Miller *et al.*, 1994; Galy *et al.*, 1995], their development does not occur wholly in primary lymphoid organs, as originally thought, but also in secondary lymphoid tissue (SLT) [Freud *et al.*, 2014; Scoville *et al.*, 2017].

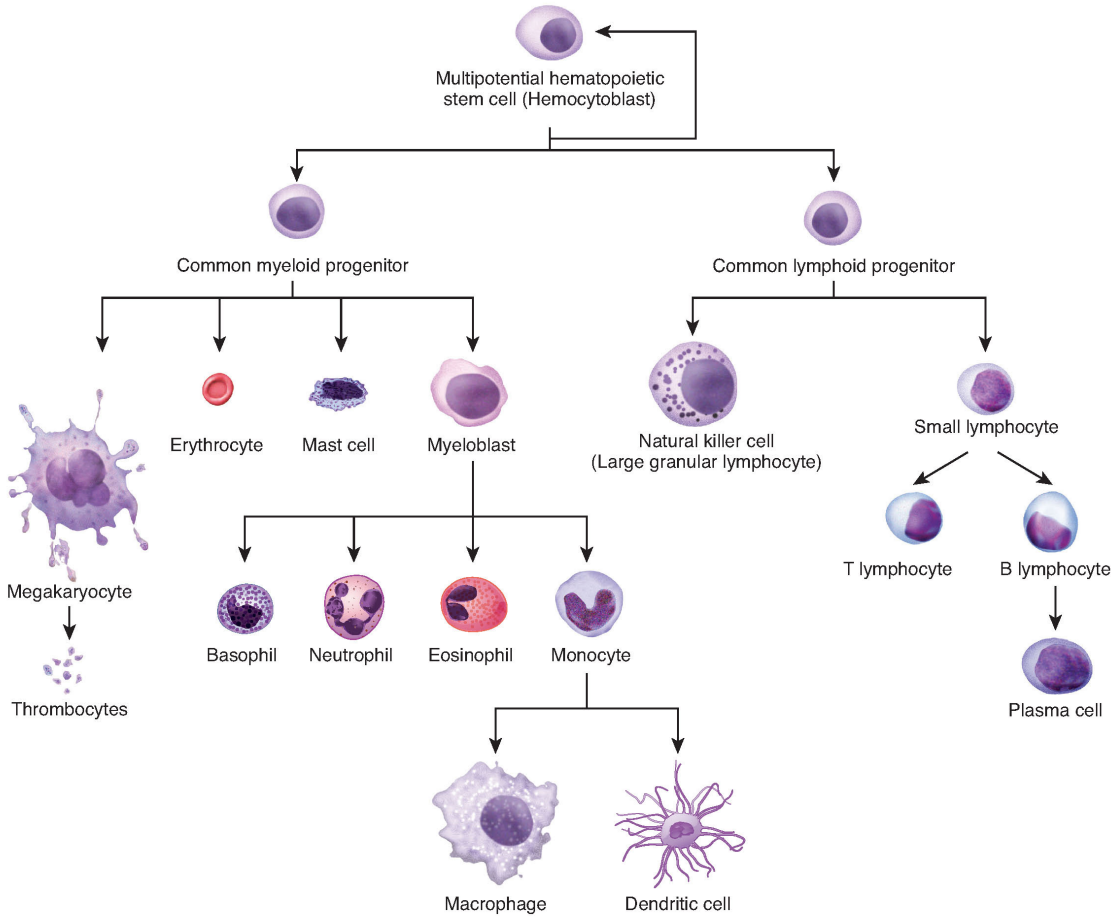

***Figure 1: Origin of natural killer cells**. Simplified differentiation tree of pluripotent hematopoietic stem cells branching into various types of myeloid and lymphoid cells. Natural killer cells originate from a common lymphoid progenitor, same as T and B lymphocytes [OpenStax, 2013].*

This is suggested mainly by selective enrichment of unique population of $CD34^{+}$ $CD45RA^{+}$ pre-NK as well as the immature $CD56^{bright}$ (with high density surface expression of CD56) NK cells in SLT relative to bone marrow and blood, where the more mature $CD56^{dim}$ NK cells are abundant [Fehniger *et al.*, 2003; Freud *et al.*, 2005]. Furthermore, SLT contains large quantities of dendritic and antigen presenting cells expressing membrane-bound IL-15 [Mattei *et al.*, 2001; Meresse *et al.*, 2006] required for NK cell maturation [Mrozek *et al.*, 1996; Kennedy *et al.*, 2000; Koka *et al.*, 2003]. As early as during the fetal development, bipotent T/NK progenitor cells can be found in the liver as well as in thymus [Sanchez *et al.*, 1994; Carlyle *et al.*, 1997; Spits *et al.*, 1998; Ikawa *et al.*, 1999; Douagi *et al.*, 2002].

In terms of stages, activation antigens and the dynamics of precursor migration into and out of the primary site of development, NK cell development bears similarities of T cell development occurring in thymus [Freud and Caligiuri, 2006; Caligiuri, 2008]. Moreover, the cytotoxic action of NK cells is akin to that of cytotoxic T cells and of a T cell subpopulation named NKT cells for bearing typical NK cell surface markers (NKR-P1) as well as T cell receptors [Hammond and Godfrey, 2002].

The innate response of NK cells is rapid and targeted against tumor, viral or intracellular bacteria infected cells. It relies on directed exocytosis of specialized lysosomes – cytotoxic granules containing proteins such as perforin, granzymes and Fas ligand [Bossi and Griffiths, 1999; de Saint Basile *et al.*, 2010; Voskoboinik *et al.*, 2015]. Moreover, NK cells express the low affinity FcγRIIIA receptor (CD16) that facilitates antibody-dependent cellular cytotoxicity (ADCC) which contributes to immune surveillance of infected cells. NK cells can also shape adaptive immune responses and prevent excessive inflammation by killing other activated immune cells [Soderquest *et al.*, 2011; Waggoner *et al.*, 2011; Lang *et al.*, 2012; Sepulveda *et al.*, 2015]. Deficiency in such cell-mediated cytotoxicity in immunodeficient patients is associated with potentially fatal hyperinflammatory syndromes usually triggered by intracellular infections [Meeths *et al.*, 2014; Voskoboinik *et al.*, 2015].

Besides immunoregulatory activity through natural cytotoxicity, NK cells are a major source of chemokines and cytokines [Caligiuri, 2008]. Upon interaction with susceptible target cell or activation by combinations of IL-2, IL-15, IL-12 and IL-18, NK cells produce IFN-γ and TNF cytokines [Fehniger *et al.*, 1999; Fauriat *et al.*, 2010]. IFN-γ protects activated T cells from NK cell cytotoxicity, promotes Th1 cell differentiation, enhances MHC class I expression and has potent anti-mycobacterial, anti-viral and growth inhibitory effects [Schroder *et al.*, 2004; Crouse *et al.*, 2014; Xu *et al.*, 2014]. TNF initiates pro-inflammatory cytokine cascades. In addition, recent findings showed that NK cells are capable of maintaining a form of immunological memory [Cooper *et al.*, 2009; Vivier *et al.*, 2011; Cerwenka and Lanier, 2016]. Thus, although historically regarded as a part of non-adaptive immunity, NK cells play rather a role of a “connective tissue” between adaptive and innate immunity whilst being complementary to the cytotoxic T lymphocytes [Vivier *et al.*, 2011].

The anti-tumor functions of NK cells are of a particular interest for cancer immunotherapy. Indeed, NK cells major role in surveillance of tumor growth and metastasis

has been demonstrated in animal models as well as in a wide range of clinical data. Notably, mice deficient in NK cell numbers [Kim *et al.*, 2000; Sathe *et al.*, 2014] or functions [Talmadge *et al.*, 1980] are more susceptible to transplanted tumors, while patients with high abundance of NK cells show reduced cancer incidence [Imai *et al.*, 2000] or less abundant metastases with improved survival rates [Delahaye *et al.*, 2011; Remark *et al.*, 2013].

However, the anticancer activity of NK cells can be hampered by tumor mediated immune suppression. Physical contacts with tumor cells as well as soluble factors – *i.e.* TGF-β, migration inhibitory factor; were described to alter expression of NK cell receptors and to suppress their functions [Greenberg and Playfair, 1974; Krockenberger *et al.*, 2008; Carlsten *et al.*, 2009; Mamessier *et al.*, 2011]. A well-known contributing mechanism is the shedding of the NKG2D ligands (MICA, MICB) from the surface of tumors, causing internalization of the activating receptor NKG2D upon interaction with them [Baragano Raneros *et al.*, 2014]. Also hypoxia – a prominent feature of the tumor microenvironment has been shown to disrupt expression of activating NK cell receptors [Balsamo *et al.*, 2013]. Indeed, NK cell cytotoxic activity is dramatically reduced at low concentrations of dioxygen [Sarkar *et al.*, 2013]. Defective NK cell activity can also have a negative impact on monoclonal antibody therapies introduced in recent years in the clinical fight against several malignancies [Weiner *et al.*, 2010], where reduced CD16 expression on tumor associated NK cells impairs ADCC toward antibody coated carcinoma cells [Carrega *et al.*, 2008]. Therefore, it is possible that many such antibody therapeutics fail to induce ADCC in cancer patients, despite their ability to efficiently trigger ADCC of healthy donor NK cells *in vitro*. Apart from cancer induced alteration of NK cell functions the tumor cell editing by NK cells is another undesirable mechanism [Dunn *et al.*, 2004]. Cancer immunoediting process consists of natural selection of escaping tumor clones that harbor mutations rendering them more resistant to the immune attack. Unfortunately, most tumors do not become clinically apparent until in the escape phase [Vesely *et al.*, 2011].

1.2 NK CELL RECOGNITION

As mentioned above, unlike B and T lymphocytes, NK cells do not require a prior antigen sensitization for specific recognition of target cells. For this purpose, NK cells are equipped with a plethora of surface inhibitory and activating receptors governing their activation through a fine balance of induced signals (Figure 2, pg. 15) [Vivier *et al.*, 2008].

Their activation is therefore dependent on the presence of specific NK receptors as well as the amount of their specific ligands on the surface of the target cells. These receptors are germline encoded and do not involve gene rearrangement mediated by the RAG recombinases, contrary to the T and B cell receptors [Lanier *et al.*, 1986]. Since their discovery, three hypotheses elucidating the NK cell recognition withstood the test of time.

The missing-self recognition describes the ability of NK cells to attack target cells that express insufficient levels of MHC class I molecules. MHC class I molecules are

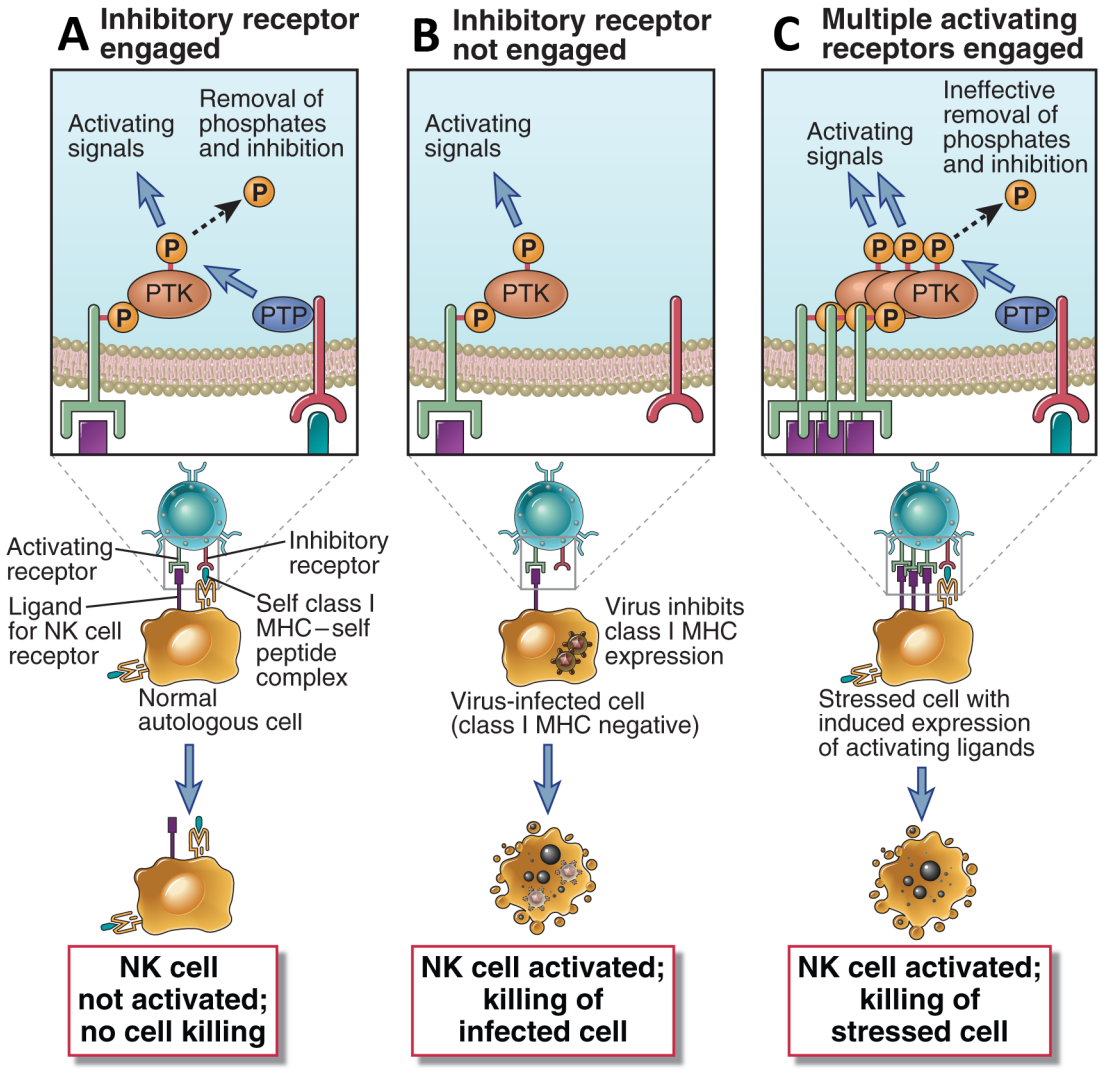

Figure 2: Simplified modes of action of NK cells. A. *Upon encountering healthy self-cell, NK cell activating signals are inhibited through action of phosphatases coupled with inhibitory receptors.* ***B.*** *Missing-self recognition. Virus infected cell has downregulated expression of MHC class I molecules, ligands of inhibitory receptors. Upon interaction with NK cell, non-suppressed activating signal triggers killing of the target cell.* ***C.*** *Induced-self recognition. Stressed cell expresses activating ligands. Although it also expresses MHC class I molecules, upon interaction with NK cell insufficient inhibitory signal does not suppress NK cell activation. PTK – protein tyrosine kinase, PTP – protein tyrosine phosphatase [Abbas et al., 2012].*

markers of health recognized by specific inhibitory NK receptors. These include mainly NK receptors from the Ly49 protein family in mice and killer-cell immunoglobulin-like receptors (KIR) [Dimasi and Biassoni, 2005] and leukocyte immunoglobulin-like receptors (LIR) [Davidson *et al.*, 2010] in humans and heterodimeric CD96/NKG2A and B [Borrego *et al.*, 1998; Vance *et al.*, 1998] in both species (Figure 3A). Indeed, downregulation of MHC class I molecules is a common strategy of virally infected and tumor cells to evade cytolysis by Tc lymphocytes, thus missing-self recognition can be understood as a defensive countermeasure of the immune system [Karre *et al.*, 1986; Ljunggren and Karre, 1990; Orr and Lanier, 2010]. Although NK cells could in theory kill any target cells that fail to engage with their inhibitory receptors (Figure 2, pg. 15), the absence of MHC class I molecules is not sufficient for complete activation of NK cell cytotoxicity. In addition, a sufficiently potent activating signal has to be obtained through NK activating receptors [Bryceson *et al.*, 2006]. This explains why under homeostasis NK cells do not engage targets with no (erythrocytes) or low (neurons) expression of MHC class I molecules [Lanier, 2005].

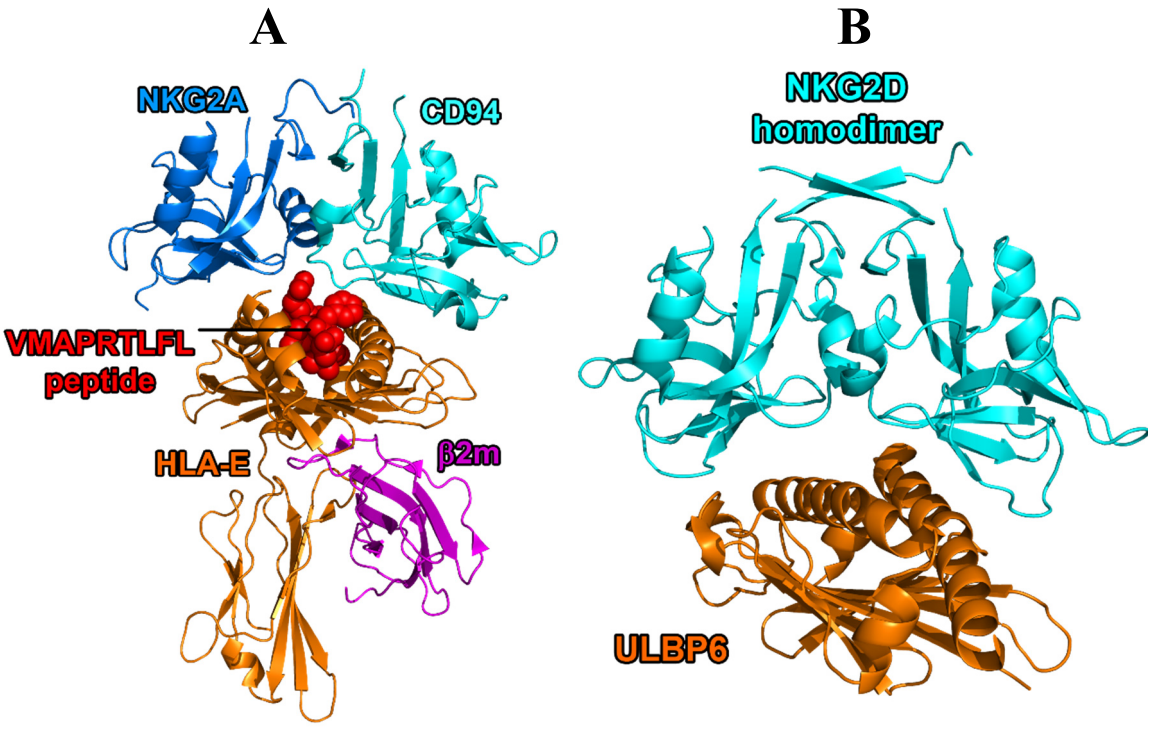

Figure 3: Inhibitory and activating receptors. A. *Side view of the inhibitory heterodimeric CD94/NKG2A bound to MHC class I molecule HLA-E. CD94/NKG2A subunits are represented as cyan and blue cartoon structures, respectively. The heavy chain of HLA-E and β2-microglobulin are shown as orange and violet cartoon, respectively, with the VMAPRTLFL peptide bound to HLA-E as red space-filling model (PDB ID: 3CD6) [Petrie et al., 2008].* ***B.*** *Side view of activating homodimeric NKG2D bound to viral infection induced ligand ULBP6. Subunits of NKG2D and ULBP6 are represented as cyan and orange cartoon structures, respectively (PDB ID: 4S0U) [Zuo et al., 2017].*

Certain internal changes in expression level or localization of self-molecules in stressed or disease-damaged tissues have been shown to activate NK cell cytotoxicity. This stress induced-self recognition relies on interaction of activating NK receptors with ligands that are under homeostasis negligibly presented on cell surface (Figure 2, pg. 15) [Bottino *et al.*, 2005; Brandt *et al.*, 2009; Raulet and Guerra, 2009]. These ligands are upregulated and presented on the cellular surface under diseased conditions to signal the immune system a self-target for killing. Recognition of B7 proteins [Matta *et al.*, 2013] or nuclear BAG-6 [Pogge von Strandmann *et al.*, 2015] by activating receptor NKp30 [Brandt *et al.*, 2009; Li *et al.*, 2011], or recognition of stress inducible MICA and MICB or recently described ULBP6 by activating receptor NKGD2 [Bauer *et al.*, 1999; Cosman *et al.*, 2001; Eagle *et al.*, 2009] are prime examples of this recognition strategy (Figure 3B, pg. 16).

Lastly and as already mentioned, NK cells express the low affinity FcγRIIIA receptor (CD16) that relates activation signal upon interaction with Fc fragment of antibody. NK cells can thus attack antibody coated targets in ADCC manner. The power of NK cells ADCC has been already utilized in antibody based cancer immunotherapies. Currently, there are several

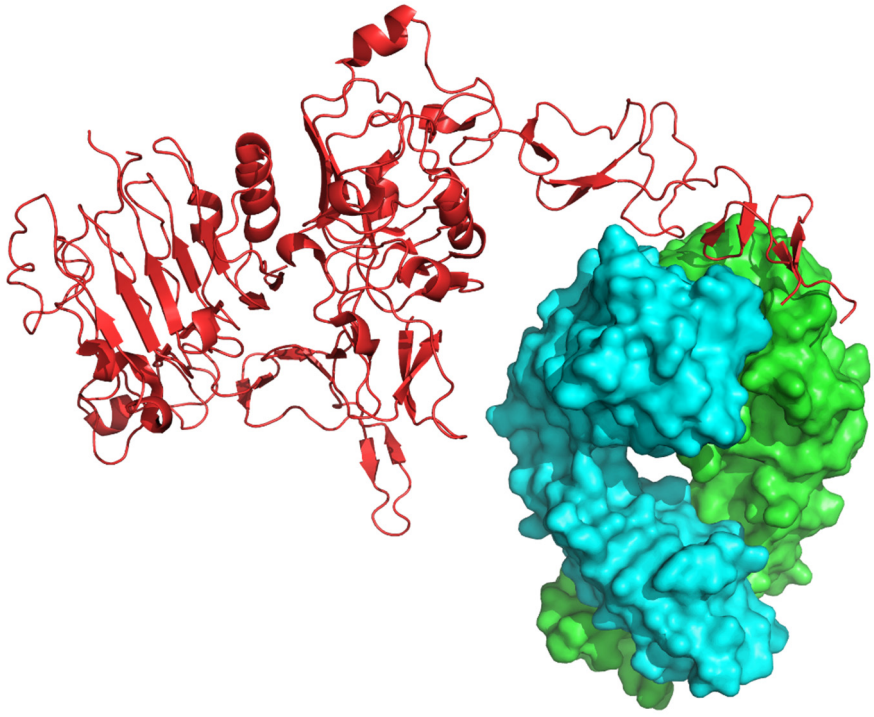

Figure 4: Utilization of antibody dependent cellular cytotoxicity in cancer immunotherapy*. Crystal structure of extracellular domain of human HER2 bound to Herceptin Fab. HER2 is shown as red cartoon structure. Subunits of Herceptin Fab are shown as cyan and green solvent accessible surface models (PDB ID: 1N8Z) [Cho et al., 2003]. HER2 antigen expression is upregulated on breast cancer cells. Herceptin binds to the tumor marker and presents its Fc portion for stimulation of antibody dependent cellular cytotoxicity.*

such clinically approved antibodies – e.g. anti-HER2 Trastuzumab (Herceptin, breast cancer; Figure 4, pg. 17) [Triulzi *et al.*, 2015] or anti-CD20 Rituximab (Rituxan, malignancies connected with B lymphocytes dysfunctions) [Meiners *et al.*, 2011; Veeramani *et al.*, 2011]. Although these therapies could be successful, the aforementioned cancer mediated immune suppression may disrupt their effects.

1.3 NK CELL TOLERANCE AND RESPONSIVENESS

NK cells can acquire autoreactivity just like T and B lymphocytes, even though NK receptors do not undergo somatic diversification. This is mainly due to lack of inhibitory receptors that bind to the MHC class I molecules of the host [Fernandez *et al.*, 2005; Kim *et al.*, 2005] or expression of activating receptors recognizing self-ligands – including MHC class I molecules [Moretta *et al.*, 1995; Lanier, 2005; Stewart *et al.*, 2005]. The array of inhibitory and activating receptors that the individual NK cell expresses during development is largely random [Parham, 2005]. In addition, the genes for the NK receptors and the MHC ligands lie on different chromosomes, thereby it is possible to inherit an allelic set of activating receptors recognizing a self-ligand, while the inhibitory receptors are unable to recognize the given MHC ligands.

To acquire tolerance to self, the immature NK cells take part in so called NK cell education. In order to gain full spectrum of effector functions, developing NK cell inhibitory receptors are engaged by self MHC class I molecules. Thereby, the inhibitory receptors have a rather positive effect on functional development pathway, opposed to delivering inhibitory signals in mature NK cell cellular recognition. During this unique process, the potentially autoreactive NK cells are selected, but rather than clonally deleted a state of hyperresponsiveness is induced. Thus, the autoreactive NK cells are defused, while NK cells tolerant to self molecules continue to mature. Indeed, in MHC class I deficient mice and humans NK cell levels are normal, but they fail to exert detectable autoimmunity or to kill MHC class I deficient autologous cell both *in vivo* and *in vitro* [Liao *et al.*, 1991; Hoglund *et al.*, 1998; Zimmer *et al.*, 1998]. These NK cells are not only unresponsive to self but are also hyporesponsive to tumor cells or to crosslinking by antibodies specific for activating receptors [Liao *et al.*, 1991; Kim *et al.*, 2005; Lanier, 2005; Anfossi *et al.*, 2006; Cooley *et al.*, 2007].

This static model of NK cell education and responsiveness is currently being challenged by a dynamic "rheostat" model (Figure 5). According to this hypothesis NK cell education doesn't function as an on/off switch, but is rather dependent on the strength of the educating signal from MHC class I molecules [Brodin *et al.*, 2009; Joncker *et al.*, 2009; Brodin *et al.*, 2010; Joncker *et al.*, 2010]. In addition, it is proposed that this molecular rheostat is continuously tuned, even in the mature NK cells by combined interpretation of signals from inhibitory, activating and cytokine receptors [Hoglund and Brodin, 2010]. Thus, the NK cell function is proposed to be seamlessly adjusted (re-educated) to the unique environment of different organs, inflammatory responses in autoimmunity or tissue damage during infections. The relevance of the dynamic model is of a particular interest for the use of NK cells as donor infusions for cancer treatment. If NK cells completely adapt to the new host MHC class I molecules setup of surrounding cells, they could not only become tolerant to the patient's cells, but may also lose the capacity to kill the malignant cells.

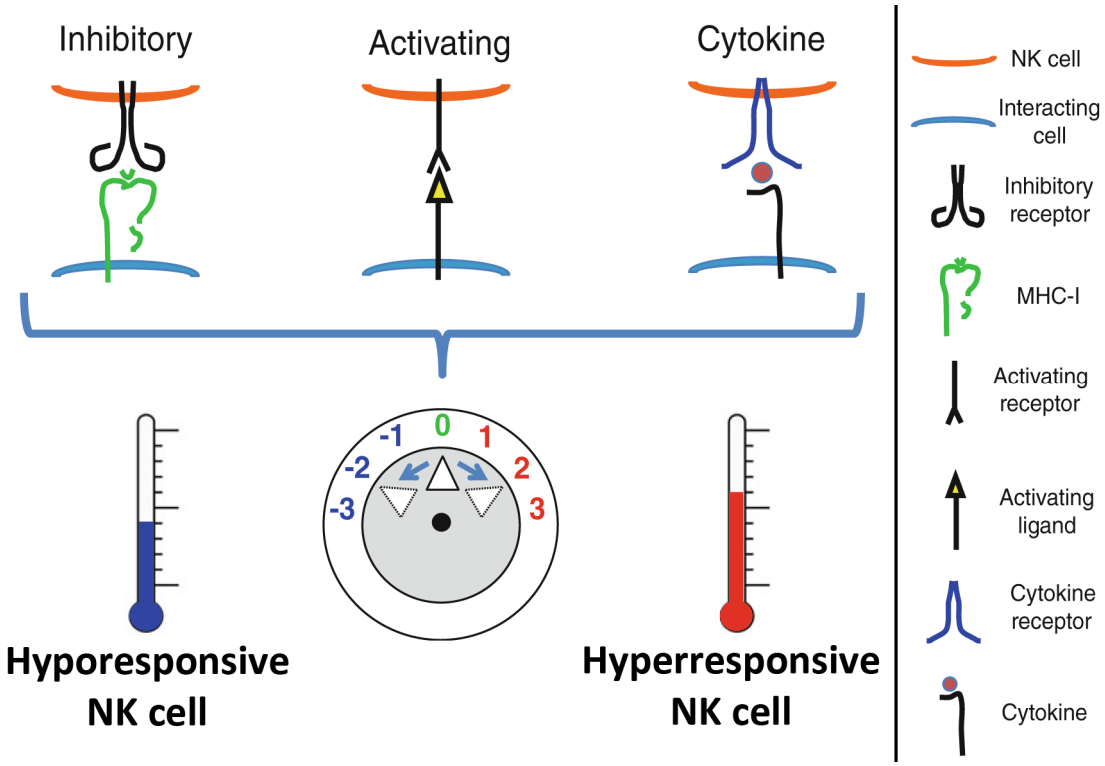

Figure 5: The dynamic "rheostat" model describing tuning of NK cells responsiveness. *Signals from inhibitory, activating and cytokine receptors are integrated to set a threshold for responsiveness. Depending on the input, NK cell responsiveness will be turned down (blue) or up (red), reflected by an increased or decreased threshold for responsiveness, respectively. A given stimulus will be less likely to trigger response in a blue NK cell compared to the red and vice versa [Kadri et al., 2016].*

Several results speaking in favor of this dynamic model have been reported; for example, it was shown that both in mice and humans NK cell responsiveness is tuned depending on the amount of inhibitory ligand input it had encountered during education and in the normal environment [Joncker *et al.*, 2009; Brodin *et al.*, 2010; Sleiman *et al.*, 2014]. However, the question of tunability of NK cell responsiveness remains ambiguous and further work in this field has to be conducted in order to obtain a definitive answer.

1.4 NK RECEPTORS

Unlike B and T cell receptors, targeting of NK cells is not defined by one type of antigen specific receptor. NK cells possess plethora of constitutively expressed surface receptors that cooperate in delivering a verdict of target cell life or death. Moreover, recent studies using multiparameter mass cytometry revealed existence of 6.000 – 30.000 phenotypically distinct peripheral NK cell types in an individual [Horowitz *et al.*, 2013; Leavy, 2013; Lanier, 2014]. According to the signalization influence on NK cell activation we can categorize NK receptors as inhibitory or activating.

Common feature of inhibitory receptors is long cytoplasmic tail containing at least one immunoreceptor tyrosine-based inhibition motif (ITIM) defined by consensus sequence Ile/Val/Leu/Ser-x-Tyr-x-x-Ile/Val/Leu. Upon interaction with its ligand the ITIMs of the inhibition receptor become phosphorylated by kinases of Src family, this allows them to engage and activate phosphotyrosine phosphatases such as SH2 domain phosphatase SHP1 and SHP2 and SH2 domain-containing inositol 5-phosphatase SHIP (Figure 6, pg. 21). These phosphatases interfere with NK cell response by dephosphorylating signal mediators downstream of activating receptors – thus preventing activation of cytotoxicity and maintaining self-tolerance [Long, 2008; Afzali *et al.*, 2013; Long *et al.*, 2013; Shifrin *et al.*, 2014]. Most common inhibitory ligands are the MHC class I molecules; however, there are NK inhibitory receptors recognizing different molecules (*e.g.* inhibitory NKR-P1 receptors in both mice and human recognize molecules of Clr family) [Vogler and Steinle, 2011]. Most notable examples of NK inhibitory receptors are representatives of the KIR family (Figure 6, pg. 21) in humans and Ly49 protein family in mice and the CD94/NKG2A and CD94/NKG2B heterodimers in both (Figure 3A, pg. 16).

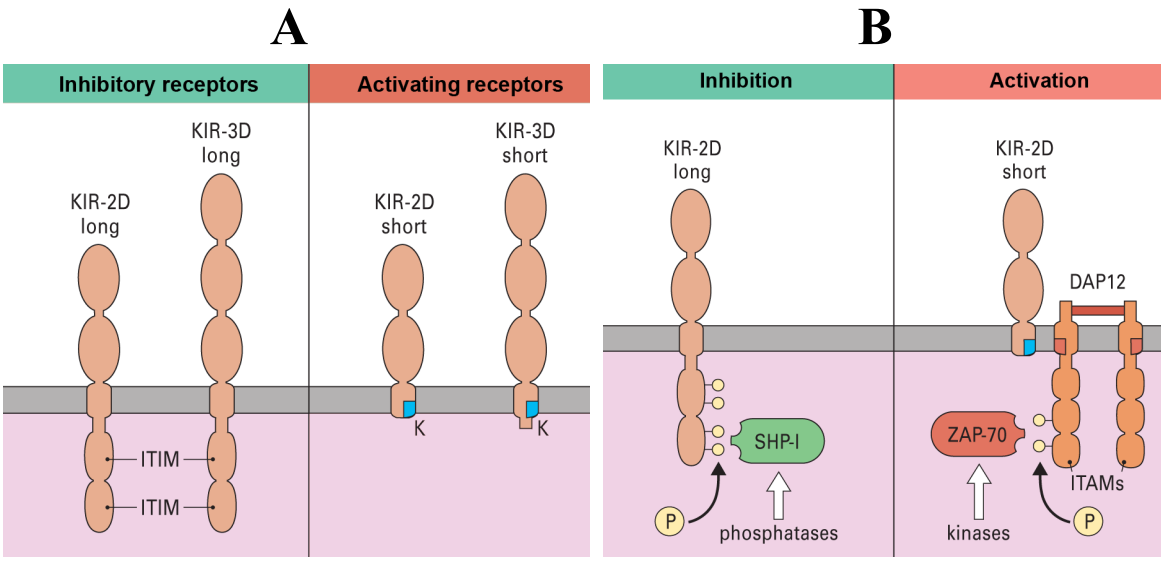

Figure 6: Physiology of inhibitory and activating NK receptors. A. *NK receptors of immunoglobulin superfamily consist of either two (2D) or three (3D) extracellular immunoglobulin domains. The inhibitory forms are longer and have intracellular ITIMs, whereas the activating forms are shorter and have charged residues in the transmembrane part.* ***B.*** *Following phosphorylation of its ITIMs, the inhibitory receptors of NK cells can bind to phosphatases, including SHP-1, SHP-2 and SHIP, which inhibits the killing. The activating receptors associate with adaptor proteins (DAP12) via complementary charged residues in their transmembrane regions. DAP12 contains immunoreceptor tyrosine activation motifs (ITAMs) that upon being phosphorylated recruit kinases of the Syk family or ZAP-70 that propagate the activation signal [Roitt et al., 2001].*

Similarly to the inhibitory receptors, activating receptors utilize phosphorylation of cytoplasmic immunoreceptor tyrosine-based activating motif (ITAM) for recruitment and activation of tyrosine kinases Syk or ZAP-70 (Figure 6B), propagating signal for Ca^{2+} influx, degranulation and production of cytokines. The ITAM consensus sequence consists of Tyr-x-x-Ile/Leu signature quartet. Typically two of these quartets are present separated by 6 to 8 amino acids. Unlike the inhibitory receptors, activating receptors have usually short cytoplasmic tails rich in charged residues close to their transmembrane region. In order to function correctly, association with adaptor proteins containing ITAMs is necessary (Figure 6) – e.g. DAP10 associating with NKG2D, DAP12 associating with KIR-2DS or FcεRIγ and CD3ζ associating with CD16 [Anderson *et al.*, 1989; Hibbs *et al.*, 1989; Lanier *et al.*, 1998; Wu *et al.*, 1999]. Activating receptors do not have a common ligand, they usually recognize a malignant transformed or stress induced molecules. Prominent representatives of activating receptors are homodimeric NKG2D (Figure 3B, pg. 16) and the natural cytotoxicity receptors (NCR) NKp30, NKp44 and NKp46. Many NK receptors can be expressed as different isoforms differing in point mutation, small deletions or insertions.

This NK receptor diversity is explained by their co-evolution with genes for MHC molecules – coding one of the most polymorphic molecules in mammalian genome. However, interesting functional consequence is described for KIRs that can be expressed with long or short cytoplasmic tail (denominated L or S isoform), thereby changing their signalization purpose from activating to inhibitory, respectively (Figure 6, pg. 21). In addition to sufficient activation signal, in the absence of inhibitory one, some coreceptors and adhesion molecules can potentiate NK cell functions.

From a structural point of view, we can distinguish two divergent classes among NK receptors – immunoglobulin-like receptors and C-type lectin-like receptors (CTLR). The immunoglobulin-like receptors are type I integral membrane proteins belonging to the immunoglobulin (Ig) superfamily. They contain two [Colonna and Samaridis, 1995] or three [D'Andrea *et al.*, 1995] Ig domains in their extracellular portion (denominated 2D and 3D, respectively) (Figure 6A, pg. 21) and usually recognize MHC class I molecules. Although the functional significance of expression of 2D or 3D is unclear, there is definite tendency of 2D receptors to recognize HLA-C alleles, whereas 3D receptors appear restricted to HLA-A and HLA-B MHC class I molecules [D'Andrea and Lanier, 1998]. The most studied representatives of this group are KIRs, LIRs and NCRs.

The CTLRs are type II integral membrane proteins containing one C-type lectin-like domain in their extracellular portion. Most prominent representatives of this group are receptors of Ly49, CD94/NKG2, NKR-P1 and Clr receptor families [Yokoyama and Plougastel, 2003; Bartel *et al.*, 2013], discussed below. Despite the obvious structural differences of these two groups they signal through the same mechanisms described above and therefore both can relate either inhibitory or activating signals as determined by the length and amino acid composition of their cytoplasmic tails.

1.5 C-TYPE LECTIN-LIKE RECEPTORS

C-type lectins are a distinct group of animal lectins, with unique requirement of calcium ions for correct function of its carbohydrate recognition domain (CRD). The CRD of C-type lectins has a compact highly conserved globular structure of a double loop (Figure 7, pg. 23), typically containing two α-helices and two anti-parallel β-sheets connected by random coils and stabilized by two or three intradomain disulfide bonds in configuration Cys^{I}-Cys^{II}, Cys^{III}-Cys^{VI} and Cys^{IV}-Cys^{V} (Figure 7, pg. 23). A distinct region

of random coil named the long loop region is involved in calcium dependent carbohydrate binding and in domain swapping dimerization [Mizuno *et al.*, 1997; Feinberg *et al.*, 2000; Hirotsu *et al.*, 2001; Mizuno *et al.*, 2001; Liu and Eisenberg, 2002]. A highly conserved "WIGL" amino acid motif within the hydrophobic core of the CRD is of particular usefulness for sequence analysis. These lectins are generally multidomain proteins with broad range of biological functions – e.g. cellular adhesion, endocytosis or pathogen neutralization [Drickamer and Taylor, 1993]. Some members of this group lost the ability to bind calcium ions, carbohydrates or both, while acquiring different substrate specificity. Although these proteins do not bind carbohydrates, due to their sequential and structural homology to C-type lectins they are designated as C-type lectin-like receptors and are thus believed to have descended from a common C-type lectin-like superfamily ancestor by a process of divergent evolution [Dodd and Drickamer, 2001].

The CTLRs of NK cells are type II integral transmembrane proteins belonging to the fifth group of C-type lectin-like superfamily. These proteins contain one C-type lectin-like domain (CTLD) at the extracellular C-terminus. Their CTLD is usually glycosylated and can form disulfide linked homodimers (with the notable exception of CD94/NKG2 heterodimers). The NK cell receptors CTLD does not contain the sequence motifs associated with carbohydrate binding. However, carbohydrate binding has been reported for some members of this group – e.g. Dectin-1 binds fungal β-glucans [Chaturvedi *et al.*, 2017; Ishimoto *et al.*, 2017] and Mast cell-associated functional antigen exhibits Ca^{2+} dependent binding to terminal mannose [Binsack and Pecht, 1997]. With the exception of Dectin-1, roles of carbohydrate recognition in the function of NK cell receptors have not been

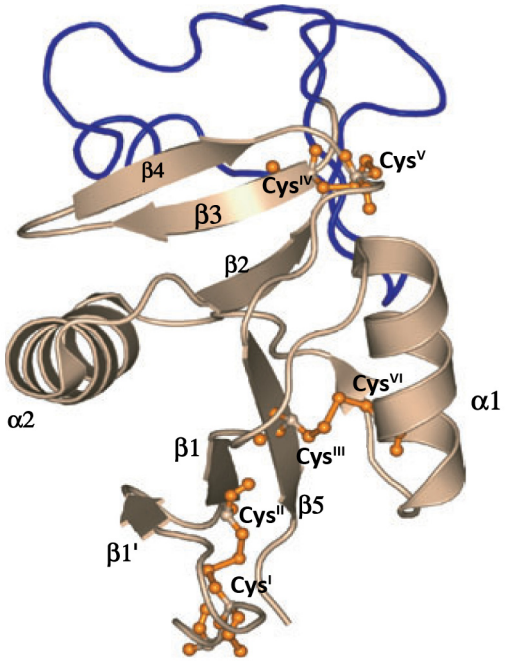

Figure 7: C-type lectin-like domain. *A cartoon representation of a typical CTLD structure (DC-SIGN receptor, PDB ID: 1K9I). The long loop region is shown in blue. Disulfide bridges are shown as orange sticks. Conserved cysteine residues are numbered from N-terminus [Zelensky and Gready, 2005].*

established and in case of NKR-P1 receptor family they have been rather controversial [Rozbesky *et al.*, 2014].

The NKG2D, CD94/NKG2 and Ly49 receptor groups belong to NK cell CTLRs recognizing MHC class I molecules [Bauer *et al.*, 1999; Yokoyama and Plougastel, 2003; Kane *et al.*, 2004]. However, this is not true of NKR-P1 receptor family that have been shown to recognize highly related Clr/Ocil CTLRs from *clec2* gene subfamily, encoded in tight genetic linkage with the NKR-P1 *klrb/f* genes. These two genetic families thus represent an alternate missing-self recognition system utilizing an unique CTLR:CTLR interaction mechanism [Yokoyama and Plougastel, 2003; Zelensky and Gready, 2005; Bartel *et al.*, 2013].

1.5.1 LY49 FAMILY

Receptors of Ly49 family are 44 kDa homodimeric disulfide-linked type II transmembrane proteins. From a structural point of view, Ly49 receptors follow the classic double loop CTLD fold with two anti-parallel β-sheets, two α-helices and with six conserved cysteine residues stabilizing the domain by three disulfide bonds [Dimasi and Biassoni, 2005]. Their extracellular portion contains single CTLD connected by a helical stalk region of ca. 70 residues to the transmembrane part. Their intracellular part contains either a long or short cytoplasmic tail – with respect to their activating or inhibitory function.

Together with KIRs, Ly49 receptors are prime examples of differential evolutionary expansion of NK CTLRs in primates and rodents since their divergence from a common ancestor. While the Ly49 receptors are most prominent in mice (encoded by at least 23 genes) and rats (at least 26 genes) only single Ly49L pseudogene have been found encoded in primates. Conversely, KIR locus has rapidly expanded in primates, while only three KIR genes can be found in rodents [Mager *et al.*, 2001].

The 23 different members of the mice Ly49 protein family (named Ly49A-W) are not all expressed in every mouse strain and their number varies among different strains as well [Yokoyama *et al.*, 1989; Brown *et al.*, 2001; Carlyle *et al.*, 2008]. They are stochastically expressed on cell surface of NK cells as well as of NKT, monocytes, macrophages, and dendritic cells. Inhibitory function dominates the Ly49 family gene complex. In fact, the missing-self hypothesis was first demonstrated on inhibitory Ly49A. Their natural ligands belong to a group of classical MHC class Ia molecules (H-2D, H-2K,

H-2L). However, recent studies demonstrate that Ly49 repertoire also includes non-classical MHC class Ib molecules [Andrews *et al.*, 2012; Sullivan *et al.*, 2016]. The big variation of Ly49 receptors and their ligands results in different mutual affinity that affects the host resistance to various pathogens, thus complicating their use as animal models in immunological studies [Carlyle *et al.*, 2008].

Many crystal structures of different Ly49 receptors have been reported [Tormo *et al.*, 1999; Dimasi *et al.*, 2002; Dam *et al.*, 2003; Dam *et al.*, 2006; Deng *et al.*, 2008; Back *et al.*, 2009], collectively showing that Ly49 receptors can adopt two distinct conformations. In backfolded conformation Ly49 dimer CTLDs are backfolded onto the helical stalk region enabling them to engage two MHC class I molecules in *trans* mode of interaction (Figure 8A and C). In extended conformation CTLDs of the dimer are extended away from the stalk, allowing Ly49 to bind one MHC class I molecule in *cis* mode of interaction (on the same cellular surface) (Figure 8B and D). In addition, Ly49 receptors appear to be able to switch between these two conformations [Back *et al.*, 2009].

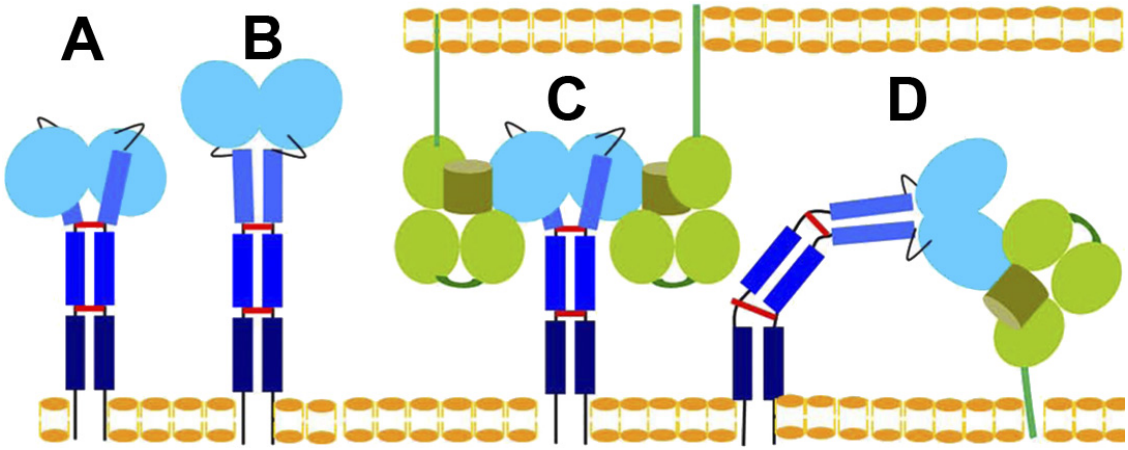

Figure 8: Conformations adopted by Ly49 receptors and interaction with MHC class I molecule. A. *The backfolded conformation of Ly49 on the NK cell membrane (bottom). The CTLDs of the Ly49 homodimer (blue ovals) are backfolded onto the α-helical stalk region (blue rectangles) with interchain disulfides drawn as red bars.* ***B.*** *The extended conformation of Ly49 in which the CTLDs extend away from the stalk.* ***C.*** *Ly49 in the backfolded conformation binding in trans to two MHC class I molecules (green) exposed on the target cell membrane (top). The interaction with MHC class I is mediated by the CTLDs.* ***D.*** *Ly49 in the extended conformation binding in cis to one MHC class I molecule on the same NK cell [Romasanta et al., 2014].*

1.5.2 CD94/NKG2 FAMILY

Receptors of CD94/NKG2 group are type II membrane proteins expressed on NK cells and subsets of T lymphocytes in humans as well as in rodents. They form disulfide

linked heterodimer of CD94 and one of at least five NKG2 receptors (named NKG2A, -B, -C, -E and -F). Structurally, both subunits consist of one extracellular CTLD linked to transmembrane helix by short stalk region. The CD94 subunit has a short cytoplasmic tail, that does not contain scaffold for association with adaptor proteins, whereby the NKG2 subunits have either long cytoplasmic tail and mediate inhibitory signalization (NKG2A and NKG2B) or possess short cytoplasmic tail with number of charged residues for association with adaptor proteins and activating signalization (NKG2C, -E and -F) (Figure 9).

CD94/NKG2 receptors prominently recognize MHC class Ib molecules. In contrast to classic MHC class Ia molecules, MHC class Ib molecules (which include HLA-E, HLA-F and HLA-G in humans and H2-M3 and Qa-1 in mice) are much less polymorphic and their tissue distribution is often restricted [Rodgers and Cook, 2005; Sullivan *et al.*, 2006]. The high degree of conservation limits MHC class Ib molecules in the diversity of peptides they can present. Utilizing five anchor sites they are ideally suited to bind peptides derived from other MHC class I molecules. Thus, interaction between MHC class Ib molecules

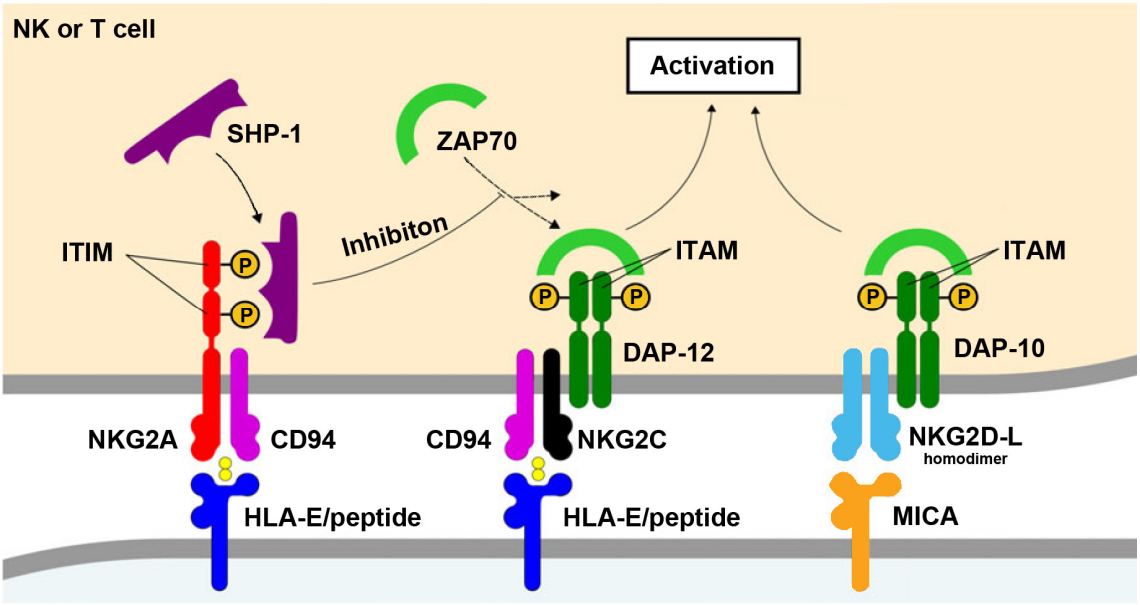

Figure 9: CD94/NKG2 and NKGD2 activating and inhibitory signalization. *The NKG2D and CD94/NKG2C activating receptors (shown on the right in light blue and in the middle in purple and black, respectively) interacts with MICA (orange) or peptide-presenting HLA-E molecule (blue), this leads to binding of adapter molecule DAP-10/DAP-12 (dark green) containing immunoreceptor tyrosine-based activation motifs (ITAM), that interacts with ZAP70 adaptor protein (light green), triggering the signal cascade resulting in NK or T cell activation. The CD94/NKG2A inhibitory receptor (shown on the left in red and purple) interacts with peptide-presenting HLA-E molecule (blue), resulting in phosphorylation of NKG2A immunoreceptor tyrosine-based inhibition motifs (ITIM), and finally recruitment of SHP-1 protein (dark purple), which causes dephosphorylation of ZAP70 protein, preventing its binding to ITAM, thus restraining the activating pathway [Iwaszko and Bogunia-Kubik, 2011].*

and CD94/NKG2 receptors represents a central innate mechanism by which NK cells indirectly monitor the expression of other MHC class I molecules within cells.

Recently structure of CD94/NKG2A and HLA-E complex with bound peptide revealed dominant role of CD94 in this protein complex – no NKG2A residues were identified as being critical to the interaction (Figure 3A, pg. 16) [Petrie *et al.*, 2008]. Surprisingly, there is ca. six-fold difference in the affinity of CD94/NKG2A vs. CD94/NKG2C for the HLA-E molecule with the same bound peptide. Upon comparison of NKG2A with NKG2C there is a sequence difference lying at the interface with CD94 that has been shown to modulate the affinity for HLA-E [Hoare *et al.*, 2008]. Therefore, it is possible that different NKG2 subunits indirectly influence affinity and specificity of CD94 through slight conformational changes.

1.5.3 NKG2D RECEPTOR

One of the most studied activating receptor within the past two decades is NKG2D [Lanier, 2015; Jelencic *et al.*, 2017]. In contrast to other members of NKG2 family, NKG2D forms a covalent homodimer that recognizes stress-induced MHC class I-like proteins. NKG2D has a very short cytoplasmic tail associating with DAP10 or DAP12 adaptor proteins for signal transduction [Wu *et al.*, 2000; Diefenbach *et al.*, 2002; Gilfillan *et al.*, 2002]. NKG2D can be expressed in two alternative splicing forms differing in thirteen residues within the cytoplasmic region. The longer isoform (NKG2D-L, the only one expressed in humans) has restricted association only to DAP10 adaptor, while the shorter isoform (NKG2D-S) can bind also to DAP12 [Rosen *et al.*, 2004; Rabinovich *et al.*, 2006]. Its extracellular portion contain one CTLD with short stalk region connecting it to the transmembrane helix. Low level expression of NKG2D has been detected for the earliest NK-committed progenitors in bone marrow [Carotta *et al.*, 2011]. It is becoming apparent that, besides inhibitory receptors, NKG2D participates in NK cell education process in setting thresholds for responsiveness of activating receptors [Kim *et al.*, 2005; Gasser and Raulet, 2006; Afzali *et al.*, 2013]. NKG2D is also expressed on several subsets of T lymphocytes.

Although NKG2D is coded by single gene with limited polymorphism, this receptor recognizes a remarkable diverse array of ligands encoded by numerous genes. In humans, NKG2D recognizes proteins encoded by the MICA and MICB locus located on

chromosome 6. At least 106 alleles of MICA encoding 82 protein variants and 42 alleles of MICB encoding 28 protein variants have been identified in human population [Robinson *et al.*, 2010]. In addition, NKG2D recognizes less polymorphic viral associated ligands of the ULBP family (Figure 3B, pg. 16). Ligands for NKG2D are not expressed in healthy tissues; however, they are upregulated upon exposure to various types of cellular stress, viral infection or malignancy [Carapito and Bahram, 2015]. NKG2D can thus facilitate cytotoxic activation of NK cells via the induced-self mechanism.

Interestingly, primary tumors frequently avoid detection and elimination by NK cells and T cells, although they express NKG2D ligands. One mechanism that permit escape of these tumors is the systemic release of NKG2D ligands from tumor cells. These can be secreted, proteolytically cleaved from the cell surface (shedded) or released as exosomes [Salih *et al.*, 2002; Wu *et al.*, 2004; Fernandez-Messina *et al.*, 2010]. Upon interaction with NKG2D, these soluble ligands cause internalization of the receptor and its downregulation. This represents an exploitation of a likely feedback mechanism regulating the response of these lymphocytes. Interestingly, this regulation is most effectively achieved by interaction with membrane-bound rather than soluble ligands. The membrane-bound NKGD2 ligands can cluster and crosslink the NKG2D receptors and thus trigger the internalization more efficiently.

1.5.4 NKR-P1 AND CLR RECEPTORS

NK cell gene complex (NKC), located on chromosome 12 and 6 in humans and rodents, respectively, encodes for NK CTLRs. Genes for these receptors are subgrouped into Killer cell lectin-like receptor (*klr*) genes – encoding for CTLRs on NK cells; and C-type lectin receptor (*clec*) genes – encoding all remaining CTLRs [Hao *et al.*, 2006]. Apart from this functional distinction, there seem to be no clear structural or sequence differences that would stand out. Unlike the previously discussed NK cell receptors, receptors of NKR-P1 family, belonging to the *klrb/f* gene subfamily, do not recognize MHC class I molecules. Surprisingly, they have been shown to bind the highly related CTLRs from *clec2* gene subfamily. Interestingly, the *clec2* genes are interspersed within the *klrb/f* locus, with the genes for respective ligands being located next to the genes of the receptors, thus underlining the genetic linkage of this unique CTLR:CTLR interaction system [Iizuka *et al.*, 2003; Yokoyama and Plougastel, 2003]. Structurally, both of these protein families represent type

II integral membrane proteins with one extracellular CTLD connected to the transmembrane part via a short flexible stalk region, usually forming disulfide-linked homodimers.

The first described NKR-P1 receptor, discovered more than 40 years ago [Glimcher *et al.*, 1977], was the mouse NKR-P1C, then designated and today still recognized as "NK1.1" marker of murine NK cells that has been since then widely used for their characterization. Antibody crosslinking of NKR-P1C triggers degranulation and IFN-γ secretion, denoting mouse NKR-P1C as an activating receptor. For signal transduction mouse NKR-P1C associates with FcεRIγ adaptor bearing ITAM [Arase *et al.*, 1997]. Since then four additional mouse NKR-P1 receptors have been described (NKR-P1A, -B/D, -F and -G) [Aust *et al.*, 2009] (Figure 10). The mouse NKR-P1E seems to be a pseudogene while the NKR-P1B expressed in BALB/c mice appears to be an allelic variant of NKR-P1D in C57BL/6 mice [Carlyle *et al.*, 2008].

Most NKR-P1 receptor genes exhibit low polymorphism, with the notable exception of highly polymorphic NKR-P1B/D and NKR-P1C. An inhibitory function is described for mouse NKR-P1B/D mediated through associating phosphatase SHP1. Similarly to mouse NKR-P1C, mouse NKR-P1A and F contain positively charged residues in the transmembrane domain suggestive of association with FcεRIγ adaptor protein – implying an activating function. However, antibody mediated crosslinking of these receptors did not enhance NK cell effector functions and thus these receptors could play rather a co-stimulatory role [Aust *et al.*, 2009]. Mouse NKR-P1 receptors recognize Clr

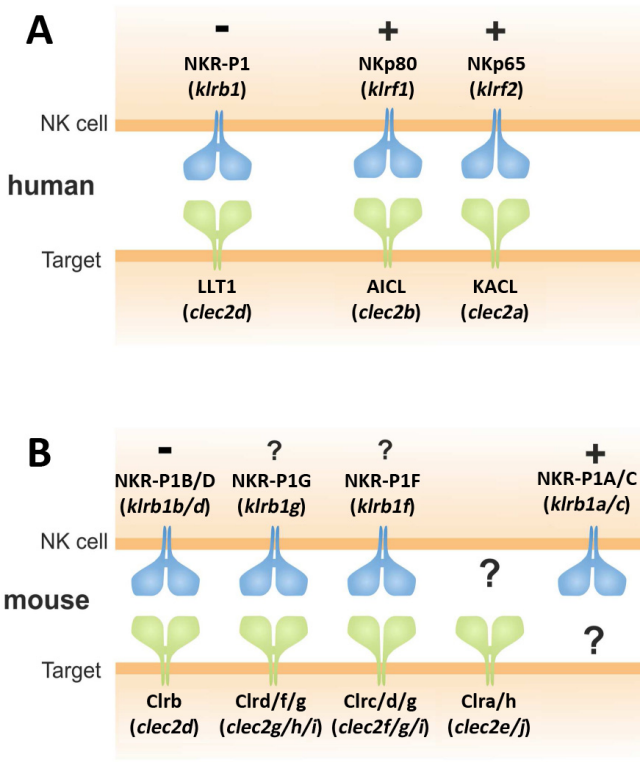

Figure 10: Overview of receptors of klrb/f subfamily and their ligands. *Human (**A**) and mouse (**B**) klrb/f receptors (blue) recognize ligands of clec2 superfamily (green) encoded in tight genetic linkage to their respective receptors. Ligands for mouse NKR-P1A/C and Clra/h remain unknown. Activating (+), inhibitory (-) or unknown (?) function is denoted above receptors. For mouse NKR-P1A, F and G functional consequences remain to be addressed [Bartel et al., 2013].*

proteins from *clec2* gene subfamily. However thus far, only ligands for mouse NKR-P1B/D, -G and -F were determined with the rest remaining orphan [Iizuka *et al.*, 2003; Chen *et al.*, 2011; Kveberg *et al.*, 2011]. Mouse *clec2* gene subfamily encodes at least 7 functional Clr proteins and an early activation marker CD69. Apart from CD69, the best characterized member is mouse Clrb, a ligand of mouse NKR-P1B/D. Mouse Clrb is expressed by almost all hematopoietic cells and exhibits tissue-broad expression, similar to the MHC class I molecules [Kartsogiannis *et al.*, 2008]. Accordingly, mouse Clrb has been observed to be downregulated on many tumor cell lines, thus facilitating missing-self axis of NK cell-mediated lysis [Carlyle *et al.*, 2004]. Expression and function for other representatives is scarcely characterized.

Although similar sets of NKR-P1 and Clr orthologues have been described in rat, in human only one representative of *klrb* gene subfamily has been described so far – human NKR-P1 recognizing lectin like transcript 1 (LLT1) as its cognate ligand (discussed below). However, recently two representatives of the *klrf* gene subfamily in humans – encoding NKp65 and NKp80; have been proposed as an activating counterparts of the orphan human NKR-P1 (Figure 10, pg. 29) [Vogler and Steinle, 2011; Bartel *et al.*, 2013]. NKp80 is characterized as a disulfide-linked homodimer expressed on the surface of NK cells and subsets of T lymphocytes. Although signalization pathway of NKp80 remains unknown, Ca^{2+} influx and cell mediated cytotoxicity has been reported upon engagement of its *clec2b* encoded ligand AICL [Welte *et al.*, 2006]. Similarly, NKp65 recognizes a *clec2a* encoded ligand KACL, triggering NK cell cytotoxicity. KACL is broadly expressed on keratinocytes and forms a non-disulfide-linked homodimer while also lacking the canonical Cys^{IV}-Cys^{V} disulfide bridge within the CTLD. Cellular expression of NKp65 *in vivo* remains unclear. NKp65 was characterized as non-disulfide-linked homodimer [Spreu *et al.*, 2010]. Crystal structure of NKp65 and KACL complex remains the only structure of *klrb:clec2* interacting complex published till now. Surprisingly, it shows two monomeric NKp65 subunits in symmetric interaction with non-covalent KACL homodimer [Li *et al.*, 2013], thus the question of NKp65 stoichiometry remains unclear.

1.6 HUMAN RECEPTORS NKR-P1 AND LLT1

While there were described several inhibitory and activating rodent NKR-P1 receptors, the human NKR-P1 (CD161, gene *klrb1*) identified in 1994 is the only human

orthologue described so far. NKR-P1 was at first identified as a marker of human NK cells where it acts as an inhibitory receptor [Lanier *et al.*, 1994; Aldemir *et al.*, 2005; Rosen *et al.*, 2005], that is upregulated by IL-12 [Poggi *et al.*, 1998]. However, NKR-P1 is also expressed by NKT type I (Vα24JαQ T cells) [Exley *et al.*, 1998], MAIT cells [Ussher *et al.*, 2014] and other subsets of T lymphocytes [Fergusson *et al.*, 2014] where it surprisingly functions as a co-stimulatory receptor, increasing secretion of IFN-γ [Aldemir *et al.*, 2005; Germain *et al.*, 2011]. NKR-P1 is already present on immature $CD16^-$ $CD56^-$ NK cells [Bennett *et al.*, 1996] and also on precursors of Th17 and MAIT cells in the umbilical cord blood [Cosmi *et al.*, 2008; Walker *et al.*, 2012]. Of particular interest is the presence of NKR-P1 on IL-17 producing regulatory T cells [Afzali *et al.*, 2013], on subsets of Tc17 cells [Billerbeck *et al.*, 2010], and on all Th17 cells – for which NKR-P1 is considered their marker [Cosmi *et al.*, 2008]. These IL-17 producing T lymphocytes are implicated in development of several autoimmune diseases – e.g. Crohn's disease [Smith and Colbert, 2014], multiple sclerosis [Brucklacher-Waldert *et al.*, 2009; Jamshidian *et al.*, 2013], rheumatoid arthritis (RA) [Estrada-Capetillo *et al.*, 2013] or psoriasis [Michalak-Stoma *et al.*, 2013]; with NKR-P1 considered to aim or promote transendothelial migration of these lymphocytes into immunologically privileged niches upon interaction with its endogenous ligand – LLT1 [Poggi *et al.*, 1997; Poggi *et al.*, 1997; Cosmi *et al.*, 2008; Annibali *et al.*, 2011; Chalan *et al.*, 2015]. Interestingly, LLT1 expression levels have been reported to be strikingly high in immune-privileged sites such as the brain, placenta and testes [Llibre *et al.*, 2016].

LLT1 (gene *clec2d*) has been described to be primarily expressed on activated monocytes (antigen presenting cells) and B-cells [Mathew *et al.*, 2004; Rosen *et al.*, 2008] where it presumably contributes to defense against NK cell self-reaction [Rosen *et al.*, 2008; Vogler and Steinle, 2011]. However its expression can be induced on NK cells and T cells by IL-2 [Boles *et al.*, 1999]. Furthermore, it was shown that LLT1 is upregulated on glioblastoma cells [Roth *et al.*, 2007] and on B-cell non-Hodgkin's lymphoma (NHL) [Germain *et al.*, 2015] and prostate cancer cells [Mathew *et al.*, 2016]. There LLT1 contributes to immune evasion by dampening the NK cell cytotoxicity. Interestingly, Th17 cells ($CD161^+$) have been reported to be increased and present in the glioma tumor [Zambrano-Zaragoza *et al.*, 2014]. There have been also a report of increased LLT1 expression in RA tissue and increased systemic presence of soluble form of LLT1 in RA patients [Chalan *et al.*, 2015]. LLT1 is currently considered as a marker for B-cell NHL [Germain *et al.*, 2015].

Being genetically coupled C-type lectin-like receptor:ligand pair, both the human NKR-P1 and LLT1 share the same general morphology [Bartel *et al.*, 2013]. They are type II transmembrane glycoproteins with an N-terminal cytoplasmic signalization tail, transmembrane helix, flexible stalk region and C-terminal CTLD [Lanier *et al.*, 1994; Yokoyama and Plougastel, 2003; Germain *et al.*, 2010]. The CTLD has classical double loop structure build up by two antiparallel β-sheets and two α-helices and stabilized by two (LLT1 lacs Cys^V) or three (NKR-P1) conserved intramolecular disulfide bridges and a conserved stretch of four hydrophobic amino acids that forms the core of the domain known as the "WIGL" motif [Yokoyama and Plougastel, 2003; Zelensky and Gready, 2005]. Both NKR-P1 and LLT1 were characterized on cell surface as disulfide-linked homodimers [Lanier *et al.*, 1994; Mathew *et al.*, 2004] presumably coupled by cysteine residues in their stalk regions. The cytoplasmic tail of NKR-P1 contains a non-canonical ITIM signalization sequence – AIYAEL; that relays inhibitory signal through recruitment of phosphatases, dampening activating signals [Lanier, 2005]. However, instead of an Ile/Val/Leu/Ser residue typical in the -2 position relative to the tyrosine residue of ITIM, NKR-P1 contains an alanine residue in this position [Ravetch and Lanier, 2000]. This substitution in the ITIM has been previously shown to decrease the inhibitory potential [Burshtyn and Long, 1997] and could explain the NKR-P1 NK cell inhibitory [Rosen *et al.*, 2005; Rosen *et al.*, 2008] and T/NKT cell co-stimulatory ambidexterity [Exley *et al.*, 1998; Aldemir *et al.*, 2005; Pozo *et al.*, 2006; Germain *et al.*, 2011; Fergusson *et al.*, 2014].

A single nucleotide polymorphism (SNP) within the intron 1 of *klrb1* gene was implicated as a risk allele for multiple sclerosis [D'Netto *et al.*, 2009]; however, Sondergaard *et al.* showed that this SNP has a marginal role in multiple sclerosis susceptibility and that rather the overall increase of the *klrb1* gene expression is involved in the pathogenesis of the disease [Sondergaard *et al.*, 2011]. Six alternatively spliced isoforms of the *clec2d* gene have been identified, with isoform 1 (coding for LLT1) being the only one confirmed to interact with NKR-P1. However, isoform 5 represents an soluble form of LLT1 that was reported to express poorly, but was recently found elevated in sera of RA patients [Germain *et al.*, 2010; Chalan *et al.*, 2015]. SPR analysis of NKR-P1:LLT1 complex reported a fast kinetics and low affinity ($K_D \sim 50\ \mu M$) interaction [Kamishikiryo *et al.*, 2011; Kita *et al.*, 2015].

2. AIMS OF THE THESIS

- To develop suitable transfection protocol for efficient transient transfection of suspension adapted HEK293S GnTI$^-$ cells.

- To develop suitable protocol for rapid selection of stably transfected polyclonal HEK293S GnTI$^-$ cell pools.

- To develop expression and purification protocol providing sufficient amount of stable and soluble human LLT1 for structural and functional studies.

- To develop expression and purification protocol providing sufficient amount of stable and soluble human NKR-P1 for structural and functional studies.

- To study the structure of LLT1, NKR-P1 and their complex by protein crystallography and other biophysical techniques.

3. METHODS

The selected publications in this Ph.D. thesis include a detailed description of all used methods describing all technical details necessary for their reproducibility. Part 3 presents only list of used research methods.

List of research methods:

- Sequence and phylogeny analysis
- Gene cloning and DNA manipulation
- In-Fusion cloning
- High-throughput expression construct optimization
- Flow cytometry
- Mammalian suspension cell culture
- Protein expression and purification
- Disulfide bond mapping using mass spectrometry
- Analytical ultracentrifugation
- Protein crystallization and X-ray crystallography
- Protein structure modeling and structure refinement
- Dynamic light scattering
- Multi-angle light scattering
- Small angle X-ray scattering

4. RESULTS AND DISCUSSION

The main focus of this thesis was to contribute to the ongoing research of NK receptors, particularly from human NKR-P1 family, by developing a suitable expression approach for soluble forms of these receptors, thus providing enough material for their biophysical characterization and structural studies. Although NKR-P1 receptors belong to the most prominent NK cell markers, we have not started to gain insight into their structure and ligand-interaction only until very recently [Kolenko *et al.*, 2011; Rozbesky *et al.*, 2016; Aguilar *et al.*, 2017]. Recombinant expression of NKR-P1 receptors proved to be a big obstacle to overcome in their research. Previous efforts of my colleagues to prepare soluble forms of these receptors in classical expression system based on *E. coli* led to precipitation of the recombinant NKR-P1 into inclusion bodies. Their renaturation was difficult and in most cases unsuccessful – the exceptions being mouse NKR-P1A and NKR-P1C [Kolenko *et al.*, 2011; Rozbesky *et al.*, 2014].

To overcome this primary problem in investigation of NKR-P1 receptors and their ligands we have been working on implementation and optimization of mammalian expression system based on transient transfection of HEK293 cells. The transient transfection of HEK293 cell line and its derivatives is well established in structural biology community. Although it is not as widely used as recombinant expression in *E. coli* or insect cell lines – mostly due to expensive maintenance demands; it is steadily becoming the expression method of choice for difficult targets and membrane proteins, when cheaper approaches fail. On comparison with prokaryotic expression systems recombinant proteins produced in HEK293 cells do not aggregate into inclusion bodies and, due to mammalian post-translational modification, possess glycosylation of complex human type. However, the absolute yields of recombinant protein tend to be lower, thus increasing the price per mg of final product.

Although the N-linked glycosylation of complex human type can make such recombinant proteins more suitable for *in vivo* studies or medical applications, the lack of uniformity of bound glycans and their flexibility makes them worse targets for protein crystallization. This obstacle is amendable by disrupting the N-linked glycosylation pathway with inhibitors of its key enzymes – e.g. kifunensine; or by utilizing a knock-out cell line (Figure 11, pg. 36). The gene for N-acetylglucosaminyl transferase I is not expressed in HEK293S GnTI$^-$ cell line, thereby recombinant glycoproteins produced in this cell line

contain homogeneous and simple $GlcNAc_2Man_5$ N-linked glycans (Figure 11). Although there could still be differences in occupation of the N-linked glycosylation sites, the glycoproteins exhibit much higher degree of homogeneity. Moreover, due to lack of bound fucose on the first GlcNAc unit, the N-linked glycans are easily cleavable after the first GlcNAc unit by endoglycosidases like Endo H or Endo F1 (Figure 11). Although this enzymatic cleavage does not provide complete removal of the N-linked glycans, in further text this process will be referred as deglycosylation, as it is commonly referred in the same way within recombinant protein expression and structural biology fields.

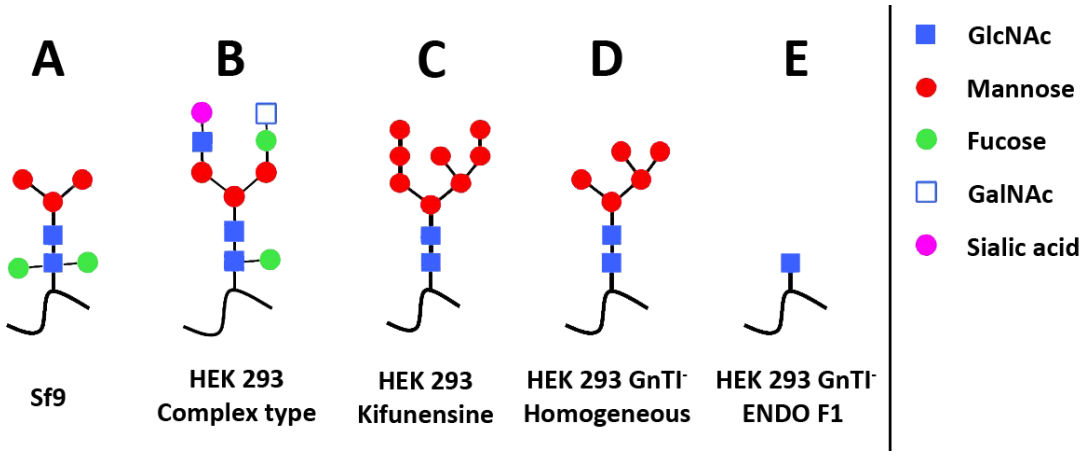

Figure 11: Types of N-linked glycosylation with regards to the recombinant expression host. *Diagrams are showing examples of N-linked glycans obtained from different recombinant expression hosts:* ***A.*** *Insect cell line.* ***B.*** *Human cell line.* ***C.*** *Human cell line with added mannosidase I inhibitor kifunensine [Shi and Jarvis, 2007].* ***D.*** *Human cell line lacking N-acetylglucosaminyltransferase I activity [Reeves et al., 2002].* ***E.*** *Remnant of N-linked glycan obtained from HEK293S GnTI- cell line after cleavage by endoglycosidase Endo F1. The bound fucose in case of insect cell line is optional, also the mammalian complex type has a high degree of variability mostly with regards to the terminal saccharide units.*

In the publication Bláha *et al.*, 2015 [Blaha *et al.*, 2015], we describe adaptation of HEK293S GnTI- cell line for suspension growth in mixture of serum free media (EX-CELL293, Freestyle293 F17) in shaken square bottles with permeable caps. However, our routinely used protocol for chemical transfection based on endocytosis of positively charged polyplexes of linear polyethyleneimine (lPEI) and plasmid DNA, previously optimized for HEK293T cell line, have proved to be quite inefficient for transfection of HEK293S GnTI- cells. The obvious difference between these two cell lines is the lack of complex glycans in HEK293S GnTI- cell line, resulting also in loss of negatively charged sulfated glycans at the cell surface. We have theorized that the decrease in attraction

of positively charged lPEI:DNA polyplexes could be overcome by increasing the cell density and the DNA and lPEI concentrations during the process of transfection. Similar protocol has been reported for HEK293E suspension grown cells with increased transfection efficiency [Backliwal *et al.*, 2008]. Indeed, transfection at cell density 20×10^6 cells/ml in EX-CELL293 with final concentration of plasmid DNA 20 μg/ml (ten times higher than optimized for HEK293T cell line while still keeping the ratio of 1 μg of plasmid DNA to 1×10^6 cells) resulted in 5-fold increase of transfection efficiency as measured by percentage of GFP positive viable cells. While the volumetric yield of recombinant protein was still significantly lower than from HEK293T cell line, the easily cleavable homogenous glycosylation proved more critical for further crystallization experiments. Following further optimization, we have been able to improve the productivity of HEK293S GnTI$^-$ cells by co-transfection with anti-apoptotic factors p27 and aFGF, currently routinely used in the group of Dr. O. Vaněk, prolonging the viable production phase of transiently transfected culture and thus increasing the yields by more than 50% (unpublished results).

In addition, in Bláha *et al*., 2015 [Blaha *et al.*, 2015] we described successful utilization of the high-density transfection protocol for transient production of soluble CTLD of LLT1 in HEK293S GnTI$^-$ cells. The ectodomain was chosen because we were mainly interested in characterization of the poorly understood interaction interface of human NKR-P1:LLT1 complex and because this interaction is mediated by the CTLDs of these two receptors. Taking into account previous experiences with recombinant expression of highly stable CD69 in *E. coli* [Vanek *et al.*, 2008], we have designed similar expression construct for soluble LLT1 (Gln72-Va191, omitting the flexible stalk region). Additionally, the construct contained N-terminal secretion signal and C-terminal His_8-tag, thus flanking the secreted protein with ITG- and GTKHHHHHHHHG at N- and C-termini, respectively.

The CTLD of LLT1 contains five out of six conserved cysteine residues. Thereby, only two out of three putative disulfide bridges are conceivable to stabilize the wild-type (WT) CTLD domain of LLT1. Our initial attempts to prepare the WT ectodomain resulted in heterogenous product that was prone to aggregation. Moreover, mass spectrometry analysis pointed out heterogeneous configuration of intramolecular disulfides with the Cys163 participating in covalent bond with both Cys184 and Cys75, while only small percentage of Cys163 was left unbound. Based on the conserved disulfide pattern of CTLD we would expect WT LLT1 to have disulfide configuration of Cys75-Cys86 and Cys103-Cys184 with Cys163 left unpaired due to His176 at the position of the sixth

canonical cysteine residue (Figure 12). In order to amend the disruptive influence of the odd cysteine residue we have attempted to prepare Cys163Ser mutant form of the LLT1 ectodomain. Unfortunately, this led to almost no recoverable product. Changing our approach to the problem, we have tried to produce His176Cys mutant form of the LLT1 ectodomain with the aim to reconstruct the third disulfide bond and thereby occupy the odd cysteine. This strategy proved to be successful, as we have been able to obtain monodisperse and stable product in sufficient yields for further structural characterization. Although this stabilizing mutation of LLT1 was not new at the time of our publication [Kamishikiryo *et al.*, 2011], using mass spectrometry approach we were the first to experimentally prove the reconstruction of the Cys163-Cys176 as well as the conserved CTLD disulfide pattern in the His176Cys mutant form of LLT1. Furthermore, using sedimentation equilibrium analysis in analytical ultracentrifuge we have shown that the LLT1 mutant forms in solution primarily non-covalent dimer, similarly to the related CTLD of CD69 [Vanek *et al.*, 2008]. The His176Cys LLT1 has been reported to interact with human NKR-P1 with comparable affinity as WT LLT1 [Kamishikiryo *et al.*, 2011].

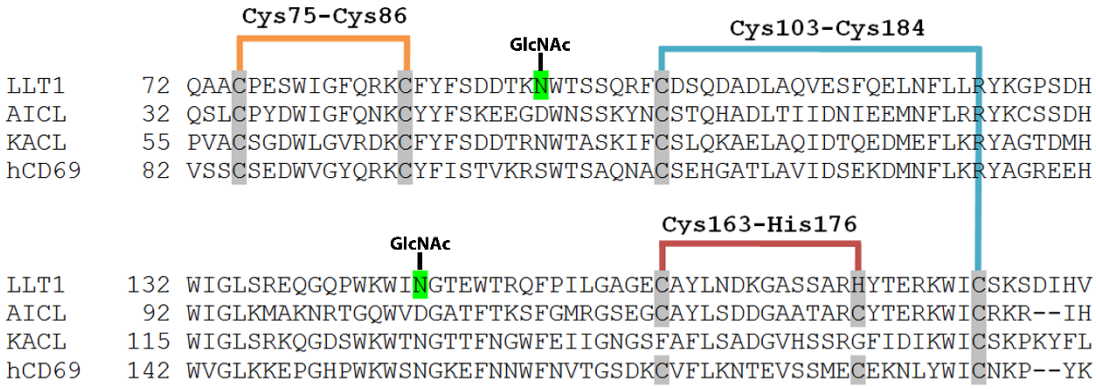

Figure 12: Conserved disulfide pattern in human clec2 CTLDs. *Multiple sequence alignment of CTLD sequences of receptors from human clec2 gene subfamily. Conserved cysteine residues are highlighted in grey, including the His176 residue in sequence of LLT1, canonical CTLD disulfide bonds are shown by connecting color lines. N-linked glycosylation sites occupied in LLT1 as confirmed by mass spectrometry are highlighted in green.*

The role of Cys163 on stability of LLT1 ectodomain or its influence on interaction with human NKR-P1 is still unclear. The detrimental impact of Cys163Ser mutation on the amount of produced recombinant protein points out that at least in the expressed WT construct formation of random disulfide bonds has a meta-stabilizing influence. However, the biological function of such LLT1 disulfide isoforms is questionable. It can be argued,

that in case of full length LLT1 its membrane anchoring can reduce the spatial degrees of freedom, compared to the soluble form, so that for example the C-terminal Cys184 cannot form a bond with Cys163. The close proximity of Cys163 to His176 is evocative of enzyme active center or at least of possible coordination of metal ion. However, no such activity or ligands have been reported, and although this is probably mostly due to the instability of the WT form of LLT1 ectodomain, it seems to be unlikely. One plausible explanation could be that LLT1 is in an evolutionary transitional state of a removal of the second canonical Cys^{IV}-Cys^{V} disulfide within the CTLD, that is notably missing in homologous KACL and orthologous mouse Clrb and Clrg NK receptors from *clec2* gene subfamily. The Cys^{IV}-Cys^{V} disulfide is in the canonical CTLD located at the base of the long loop region and its role is presumably to stabilize the long loop region (Figure 7, pg. 23) [Zelensky and Gready, 2003]. Thus, we cannot rule out that a more flexible long loop region of LLT1 has some functional impact on the interaction with human NKR-P1. However, there are many examples of canonical CTLD sequences lacking either Cys^{IV} or Cys^{V} both in mammals and *C. elegans*, suggesting that their presence is not functionally essential.

Although the optimized protocol for transient expression in HEK293S GnTI$^-$ cells was successful in case of LLT1 and other related NK receptors (unpublished data), it was inefficient in the case of human NKR-P1. Initial expression construct for human NKR-P1 (Gly90-Ser225, N-terminal secretion signal, C-terminal His_8-tag) was based on the highly stable CD69 as well as the aforementioned soluble LLT1. Interestingly, group of prof. Maenaka from Hokkaido University reported successful expression of the same human NKR-P1 expression construct in HEK293T cells. Although said publication have not stated the yield of the protein, the reported use for immobilization on SPR chip does not necessarily suggest high yields [Kamishikiryo *et al.*, 2011]. Indeed, our efforts to transiently express this construct in HEK293T as well as HEK293S GnTI$^-$ cell lines resulted in meager 100 μg of pure protein per liter of costly production media. Such low yields were neither sufficient nor economical for structural studies, therefore we have attempted further optimization of the expression construct of soluble human NKR-P1.

In the publication Bláha *et al*., 2017 [Blaha *et al.*, 2017] we describe several construct optimization strategies. The extracellular part of human NKR-P1 consists of 25 amino acids long putative flexible stalk region and 135 amino acids long C-terminal CTLD. We have theorized that by adding the correct length of the stalk region to the initial expression

construct (containing only the C-terminal CTLD) we could find a more stable and higher yielding expression construct.

Firstly, we have attempted to improve the solubility of human NKR-P1 expressed in *E. coli*. We have tested three constructs: with full (Ile66-Ser225), half (Gln80-Ser225), or without (Gly90-Ser225) the stalk region; in combination with a different N-terminal fusion protein tags (SUMO, TRX, MsyB, and GST), or with periplasm targeting signal sequence (PelB). Expression tests were performed in *E. coli* B834(DE3) and *E. coli* Rosetta2(DE3) pLysS strains using two different production conditions – an overnight production at 20°C after induction with 1 mM IPTG and a production in auto-induction medium at 25°C for 20 h. Unfortunately, any of the tested conditions did not lead to soluble product. It cannot be ruled out that some of the insoluble products would be renaturable with better result than in any of our previous attempts. Moreover, bacterial strains with an oxidizing cytoplasm designed for expression of disulfide rich proteins (i.e. SHuffle, Rosetta-gami) could be more efficient, although several such previous attempts to express similar constructs of mouse NKR-P1 receptors provided negative results, too.

Secondly, we have prepared stalk region deletion library of expression constructs in pOPING expression plasmid. The pOPING expression plasmid allows for secreted expression with C-terminal His_6-tag both in insect cell baculoviral and mammalian expression systems simultaneously. From expression tests performed in Sf9 cells we could identify region of best expression constructs with N-termini of NKR-P1 ranging from Cys74 to Gln79, albeit expression level was low for all of them. We have further attempted unsuccessful scale-up production of Ser75-Ser225 expression construct. Interestingly, within the region of best expressing constructs in Sf9 cells, the JPred4 secondary structure analysis predicts an α-helix, which may explain the observed stabilizing effect. Such secondary structure in the stalk region could provide a scaffold for formation of the presumed intermolecular disulfide bridge of human NKR-P1. Analysis of the expression tests in HEK293T cells showed positive albeit again low level of expression for most of the tested constructs. Interestingly, a very low signal corresponding to the NKR-P1 covalent dimer could be detected within the range Ser69-Glu72 as well as sudden electrophoretic mobility shift suggesting presence of N-linked glycan at Asn83.

Thirdly, we have attempted to improve the yield of the initial expression construct of human NKR-P1 in HEK293S GnTI$^-$ cells by stable instead of transient transfection. Utilizing the high-density transfection protocol, we have transfected HEK293S GnTI$^-$ cells with

expression vector pOPINGTTneo containing the Gly90-Ser225 expression construct of human NKR-P1. This expression plasmid provides secreted production, C-terminal His_6-tag and selection marker for neomycin resistance. A pool of resistant HEK293S GnTI$^-$ cells was selected on Geneticin G418 antibiotic yielding on average 2.5 mg of pure protein per liter of production media. This represented more than 20-fold improvement in expression level and enabled us to continue with further characterization and crystallization attempts. Although this shortest construct performed poorly in the aforementioned transient expression tests and may be suboptimal with respect to possible expression yield, based on our previous work on structural elucidation of related CTLR, constructs lacking the N-terminal stalk region and containing only the well-defined CTLD are the most suitable targets for further structural experiments. However, it would be worth to further utilize this expression strategy for expression of the constructs that provided detectable amounts of covalent dimer of human NKR-P1.

This success in expression of human NKR-P1 CTLD has prompted us to apply the production in stably transfected HEK293 polyclonal cell pools to other previously impossible-to-prepare NK cell receptors with some promising first results. Certainly, this expression method has its own pitfalls – e.g. unsuccessful or partial integration of gene of interest expression cassette or time dependent silencing of expression; however, we have already introduced some improvements to make this method more robust and reliable – e.g. enzyme driven integration of expression cassette into chromosomal DNA or utilizing viral ubiquitous chromatin opening element (UCOE, [Muller-Kuller *et al.*, 2015]) anti-silencing DNA sequence (unpublished data).

Following the expression of soluble human NKR-P1 we have confirmed that its intramolecular disulfide bonds match the canonical CTLD configuration by mass spectrometry. Although human NKR-P1 was identified as a covalent dimer on cell surface [Lanier *et al.*, 1994], we have shown by calibrated size exclusion chromatography as well as liquid chromatography coupled with multi-angle laser light scattering detector that the prepared soluble protein is monomeric with low degree of polydispersity. This was further corroborated by sedimentation equilibrium and sedimentation velocity analysis in analytical ultracentrifuge for maximum concentration of 12.5 mg/ml. This result could be expected due to the absence of putative dimerization cysteine residue located in the stalk region of said product and is in accord with reported monomeric state of soluble mouse NKR-P1A and NKR-P1C. Furthermore, even with the dimerization cysteine included in the expression

construct a covalent dimeric form of the product could be detected only in minority, with majority being monomeric. On the other hand, highly homologous receptors from *clec2* gene family, including LLT1, prepared without the dimerization cysteines form non-covalent dimers quite easily. It is thereby possible that the low propensity for formation of NKR-P1 dimers is due to different or weaker mode of dimerization compared to *clec2* proteins while its stalk region could be critical for its stabilization.

The successful expression of both LLT1 and NKR-P1 enabled us to attempt their crystallization by vapor diffusion method both as individuals and in their mixture. Firstly, LLT1 provided protein monocrystals suitable for diffraction experiment obtained from three different crystallization conditions, one for LLT1 with $GlcNAc_2Man_5$ N-glycosylation and two for endoglycosidase Endo F1 treated LLT1. These crystallization conditions differed mainly in pH of used reservoir solutions – 4.2 for the glycosylated form and 7.0 and 3.5 for the deglycosylated form. Diffraction data were collected from single crystals at synchrotron radiation source BESSY II in Helmholtz-Zentrum Berlin and at Diamond Light Source. The phase problem was solved by molecular replacement using the extracellular domain of CD69 (PDB ID: 3HUP) [Kolenko *et al.*, 2009] and the structures of glycosylated and two deglycosylated forms of LLT1were refined to 2.7, 1.8 and 1.95 Å, respectively. These first structures of LLT1 were described in Skálová *et al.*, 2015 [Skalova *et al.*, 2015].

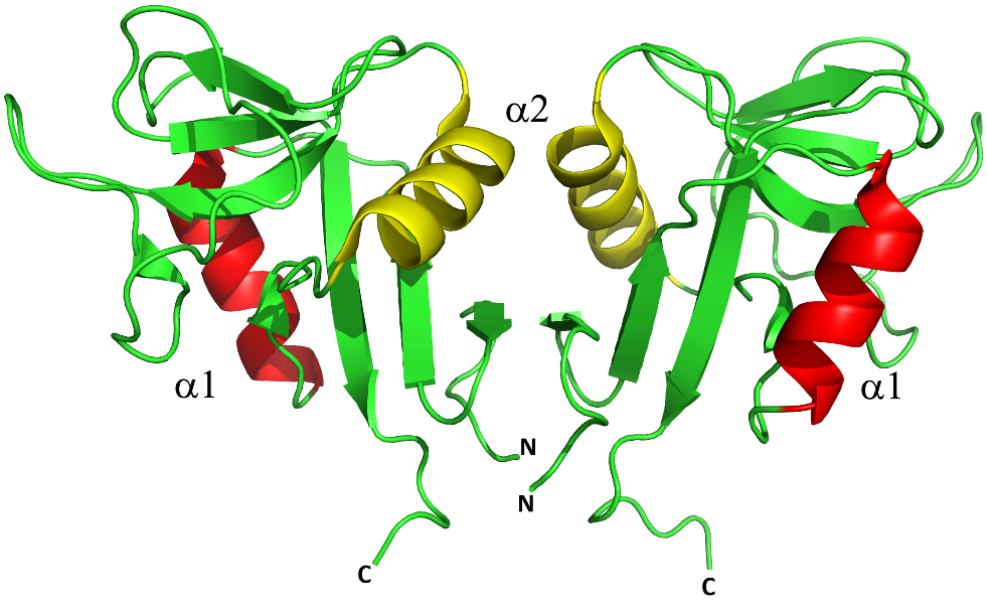

Figure 13: Structure of LLT1. *Homodimer of deglycosylated form of LLT1 (PDB ID: 4QKI, [Skalova et al., 2015]) is shown as green cartoon structure. The helices α1 (red) and α2 (yellow) of CTLD and the N- and C- termini are labeled.*

The overall fold of LLT1 follows that of a typical CTLD – with two α-helices, two antiparallel β-sheets and three disulfide bonds. The artificial disulfide bond induced by the His176Cys mutation is located in the same position as the canonical Cys^{IV}-Cys^{V} disulfide bond naturally occurring in CD69 (Figure 13, pg. 42). With the exception of structure obtained from crystal grown in pH ~ 3.5, the manner of dimerization of both glycosylated and deglycosylated LLT1 forms corresponds to the classical dimerization mode of human CD69 or mouse Clrg. Subunits of the dimer are centered by its helix α2 while the N- and C-termini of both chains are localized on the same side, thus allowing for protein anchoring in the cell membrane which supports biological relevancy of given structure. Furthermore, on comparison of different LLT1 dimer structures we have showed that the dimer interface is based on common hydrophobic core while it retains some degree of flexibility. This ability to adapt the dimer shape could be an advantage enabling binding of the protein partner as discussed before [Sullivan *et al.*, 2007; Skalova *et al.*, 2012]. The dimeric state of LLT1 is in good agreement with reported sedimentation equilibrium and sedimentation velocity analysis in analytical ultracentrifuge and dynamic light scattering results for LLT1 in solution [Blaha *et al.*, 2015; Skalova *et al.*, 2015]. In LLT1 structure obtained from crystal grown in pH ~ 3.5 electron densities for residues 147-160 of the outer loop of the long loop region were poorly resolved and these residues were not built into the final model. The approximate position of the loop differs significantly from the other structures and we could observe only monomeric state in this structure. However, this is probably due to the low pH which corresponds to the changed preferred intermolecular contacts and the formation of oligomers.

Secondly, crystallization of human NKR-P1 alone and in mixture with LLT1 also provided suitable monocrystals – in deglycosylated state for both samples and also with homogeneous $GlcNAc_2Man_5$ N-glycosylation for NKR-P1 alone. Diffraction data were collected from single crystals at Diamond Light Source synchrotron radiation source. The phase problem was solved by molecular replacement using the extracellular domain of KLRG1 bound to E-cadherin (PDB ID: 3FF7) [Li *et al.*, 2009] for glycosylated NKR-P1; extracellular domain of mouse NKR-P1A (PDB ID: 3T3A) [Kolenko *et al.*, 2011] for deglycosylated NKR-P1; and extracellular domain of mouse Dectin-1 (PDB ID: 2BPD) [Brown *et al.*, 2007] for complex of deglycosylated NKR-P1 and LLT1. These structures were refined to 1.8, 1.9 and 1.9 Å, respectively. Obtained results described in Bláha *et al*., 2017 (submitted for publication) represent the first crystal structure of dimeric NKR-P1 and

of complex of dimeric NKR-P1 with dimeric *clec2* ligand.

In both deglycosylated and glycosylated structures human NKR-P1 follows classical CTLD fold of double loop with two α-helices, two antiparallel β-sheets and three canonical intramolecular disulfide bridges stabilizing the domain. NKR-P1 monomers are in both structures arranged into very similar homodimers (pairwise RMSD on Cα atoms up to 0.5 Å only). Interestingly, these homodimers are of an unexpected type, not resembling the classical dimerization of CD69 or other *clec2* ligands (including LLT1, Figure 13, pg. 42) that all utilize helix α2 in the dimerization interface. The observed homodimer of human NKR-P1 is instead formed by helix α1 while still having N- and C- termini of both chains localized on the same side and thus allowing for protein anchoring in cell membrane – as expected for biological dimer (Figure 14A). This is very similar to overall position and orientation of subunits in homodimer of C-type lectin-like pattern recognition receptor Dectin-1 (PDB ID: 2BPD) [Brown *et al.*, 2007].

In comparison with the classical α2-centred dimer of LLT1 the α1-centred dimer of NKR-P1 is realized through smaller contact surface area with fewer contact residues. However, in both structures the first localized GlcNAc units at Asn116 and Asn157 form intermolecular contacts with the opposite subunit and thus contribute to stabilization of the homodimer (Figure 14B). Interestingly, in deglycosylated structure GlcNAc units

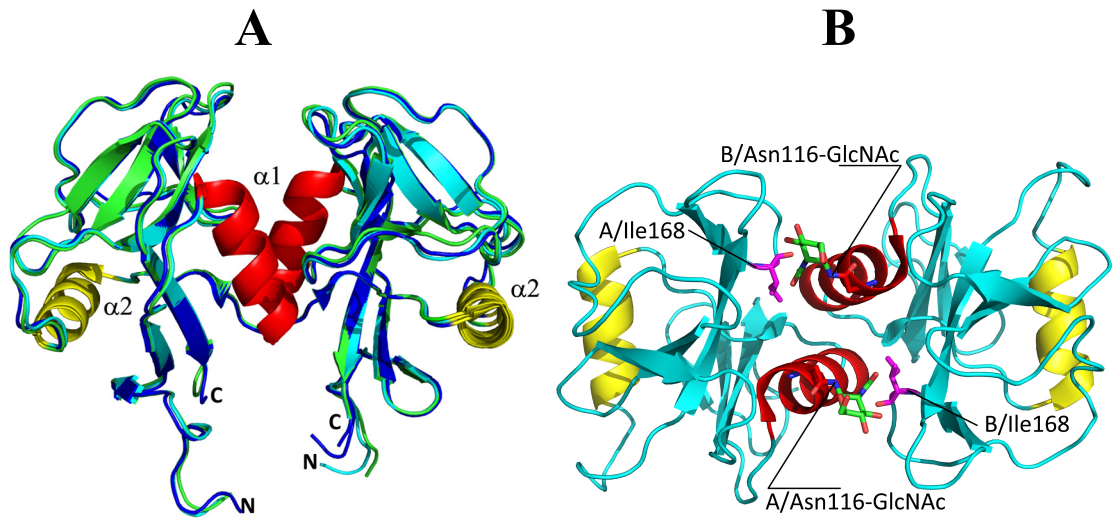

***Figure 14: Structure of human NKR-P1**. **A.** Comparison of NKR-P1 dimer formation of glycosylated (cyan ribbon), deglycosylated free (green ribbon) and complex-bound (blue ribbon) form of NKR-P1 (PDB ID: unreleased). **B.** Top view of the glycosylated homodimer of NKR-P1 (cyan ribbon). The N-linked GlcNAc units bound to Asn116 at both chains localized at the dimerization interface are shown in green. The polymorphic Ile168 residue is show in magenta at both chains. The helices α1 (red) and α2 (yellow) of CTLD and the N- and C- termini are labeled.*

on Asn116 and Asn157 of the opposite protein chains of the dimer occupy the same space and are found in alternative conformations together with Asn116. On the other hand, in the glycosylated structure the GlcNAc at Asn116 is well defined with full occupancy in both chains, while no electron density is present for glycosylation at Asn157. We can speculate that the glycosylation at both Asn116 and Asn157 on opposing subunits could preclude such dimerization and that in the deglycosylated structure we observe sampling of different glycoforms of NKR-P1; whereas in the glycosylated structure with more spacious $GlcNAc_2Man_5$ glycan only one glycoform crystallized. Indeed, the N-linked glycosylation could have both a stabilizing and regulatory role for formation of the proposed dimer.

Recently, a single nucleotide polymorphism c.503T>C of human NKR-P1 that results in point mutation of Ile168 residue to Thr168 within its CTLD [Rother *et al.*, 2015] has been described. The authors reported 37% frequency of the Thr168 allele and showed that the Thr168 isoform of NKR-P1 has lower ability to bind LLT1 and subsequently smaller inhibitory effect on NK cells [Rother *et al.*, 2015]. Although the authors speculate that Ile168 is participating in the interaction with LLT1, it is obvious from the structure that Ile168 is localized rather in the lateral region than at the distal region that is expected to participate in the interaction with LLT1. Although we cannot rule out a long-distance effect of this amino acid exchange, it seems more probable that the Thr168 mutation destabilizes the hydrophobic core in which Ile168 participates at the dimerization interface of the observed α1-centred dimer (Figure 14B, pg. 44). Thus, this SNP can actually have indirect influence on the NKR-P1:LLT1 interaction by forming less stable NKR-P1 homodimers.

Although we were not able to capture any non-covalent dimer of human NKR-P1 in solution by SEC-MALS or analytical ultracentrifugation techniques, the weaker dimerization interface of this novel proposed homodimer would be in accord with the observed small propensity to form dimers. As mentioned above, it would be interesting to attempt to recombinantly express and characterize human NKR-P1 construct containing the stalk region with the intermolecular cysteine residue to further investigate this question.

The crystal structure of the NKR-P1:LLT1 complex is formed by deglycosylated NKR-P1 and LLT1 ectodomains. The asymmetric unit of the crystal contains a complex of dimeric NKR-P1 with dimeric LLT1 and an extra dimer of NKR-P1 not participating in the interaction (Figure 15A, pg. 47). The dimerization mode of NKR-P1 is of the same α1-centred type as discussed above, while the LLT1 dimer follows the classical α2-centred dimerization as described previously in Skálová *et al.*, 2015 [Skalova *et al.*, 2015]. The LLT1

homodimer engages its partner bivalently, i.e. one dimer interacts with two dimers of NKR-P1 related by crystallographic symmetry: each monomer of LLT1 binds to a different subunit of a distinct NKR-P1 homodimer. There is no apparent induced fit of the binding partners. The localized N-linked glycosylation chains do not directly contribute to this interaction.

Two distinct interaction modes between NKR-P1 and LLT1 can be observed in the structure. While the first interaction mode corresponds closely to the interface found in the structure of homologous human NKp65:KACL complex (Figure 15B, pg. 47) [Li *et al.*, 2013], it also agrees with the more recent structure of mouse NKR-P1B bound to the MCMV-encoded immunoevasin m12 [Aguilar *et al.*, 2017] – in that the footprint of m12 on NKR-P1B overlaps the footprint of LLT1 on NKR-P1. Most importantly, the primary interaction mode is confirmed by a previous mutational analysis of the NKR-P1:LLT1 binding interaction using SPR [Kamishikiryo *et al.*, 2011]. To the best of our knowledge no protein-protein interaction similar to the second interaction mode is known and we cannot rule out that this is only the result of crystal packing. The residues employed in both interaction modes remain virtually the same in case of human NKR-P1, but they are quite different, albeit sharing a small number of residues, for LLT1. However, both interaction modes place the membrane-proximal parts of the receptor and of the ligand on the opposite sides of the complex and suggest a plausible model of interaction realized between two cells.

Moreover, the bivalent engagement of alternating α1/α2-centred homodimeric state of NKR-P1/LLT1 has a chain-forming effect. Interestingly, an avidity effect of multimerization upon mutual interaction was suggested by several authors as a means of compensation for the low affinity of the NKR-P1:LLT1 complex [Skalova *et al.*, 2012; Li *et al.*, 2013; Kita *et al.*, 2015]. Although such functional multimerization of NK CTLRs have not been much explored, formation of similar nanoclusters is well described for the immunoglobulin family of KIRs interacting with MHC class I glycoproteins [Davis *et al.*, 1999] as well as in the co-stimulatory immunocomplexes B7-1:CTLA-4 and B7-2:CTLA-4 where a periodic zipper-like network of interaction dimers was reported [Schwartz *et al.*, 2001; Stamper *et al.*, 2001].

Although both LLT1 and NKR-P1 were shown to form covalent homodimers on the cell surface as full-length proteins [Lanier *et al.*, 1994; Germain *et al.*, 2010], the dimeric state of their CTLDs was, to the best of our knowledge, not yet evaluated in native cells. It would be therefore interesting to assess the actual stoichiometry of NKR-P1 CTLD on

cellular surface since similarly to B7-1/CD28 there could be an equilibrium of the monomeric/dimeric states (stabilized by cystic bond in the flexible stalk region) influencing the formation and dissociation of the above proposed interaction multimer and thus regulating the strength and signalization of the NKR-P1:LLT1 system. Whether this hypothesis of multimerization upon interaction of NKR-P1:LLT1 or other low affinity NK CTLRs has biological relevance remains to be tested.

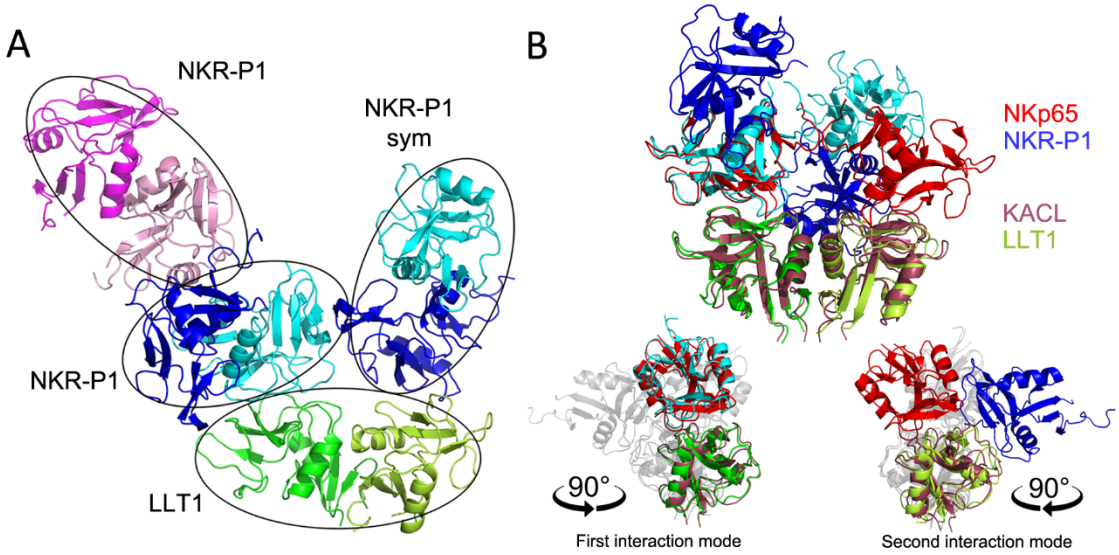

Figure 15: Structure of human NKR-P1:LLT1 complex. A. *Overall organization of the complex crystal structure (PDB ID: unreleased). The LLT1 dimer (green/lemon) has contact with the NKR-P1 dimer formed by the blue monomer and the cyan monomer. The second blue-cyan NKR-P1 dimer is related to the first one by crystal symmetry. The cyan NKR-P1 monomer forms the first observed type of contact with LLT1, while the blue NKR-P1 monomer forms the second type. Additionally, the asymmetric unit of the crystal contains another NKR-P1 dimer (pink/magenta), not engaging in any contacts with LLT1.* ***B.*** *Overall comparison of the structure of dimeric KACL in the complex with two NKp65 monomers (dark purple and red, respectively; PDB ID: 4IOP, [Li et al., 2013]) and the structure of the LLT1 dimer (green/lemon) with two NKR-P1 dimers in the primary (cyan, left side) and secondary (blue, right side) binding modes. In the lower part the comparisons with only the primary or secondary (both in side-view using 90° y-axis rotation) interaction modes of NKR-P1:LLT1 are highlighted; the second molecules in NKR-P1 dimers were omitted for clarity.*

5. SUMMARY

- A new method for recombinant expression of stable LLT1 ectodomain based on efficient transfection of HEK293 GnTI$^-$ cells and for human NKR-P1 ectodomain based on stably transfected polyclonal HEK293S GnTI$^-$ cell pool selection has been developed. These methods have general applicability for homologous NK receptors.

- The crystal structures of glycosylated and deglycosylated states of human LLT1 have been determined by molecular replacement with highest resolution of 1.8 Å.

- In the crystal structures of LLT1 the overall fold was similar to the other C-type lectin-like domains, forming a classical α2-centered homodimer similar to CD69.

- The crystal structures of glycosylated and deglycosylated states of human NKR-P1 have been determined by molecular replacement with highest resolution of 1.7 Å.

- In the crystal structure of NKR-P1 the overall fold was similar to the other C-type lectin-like domains, but differed significantly in the formation of unique α1-centered homodimer similar to Dectin-1.

- The crystal structure of complex of deglycosylated human NKR-P1 and LLT1 has been determined by molecular replacement with highest resolution of 1.7 Å.

- In the crystal structure of NKR-P1 and LLT1 complex α1/α2-centered dimers alternate in bivalent interaction of two distinct types. The first type is similar to human NKp65:KACL and mouse NKR-P1B:m12 complexes interactions, while the second type is unique.

- A hypothesis of formation of interaction multimer of alternating NKR-P1 and LLT1 molecules upon cellular contact and their mutual engagement has been proposed.

REFERENCES

Abbas, A. K., Lichtman, A. H. and Pillai, S. (2012). Cellular and molecular immunology. Philadelphia, Elsevier/Saunders.

Afzali, B., Mitchell, P. J., Edozie, F. C., Povoleri, G. A., Dowson, S. E., Demandt, L., Walter, G., Canavan, J. B., Scotta, C., Menon, B., Chana, P. S., Khamri, W., Kordasti, S. Y., Heck, S., Grimbacher, B., Tree, T., Cope, A. P., Taams, L. S., Lechler, R. I., John, S. and Lombardi, G. (2013). "CD161 expression characterizes a subpopulation of human regulatory T cells that produces IL-17 in a STAT3-dependent manner." Eur J Immunol **43**(8): 2043-2054.

Aguilar, O. A., Berry, R., Rahim, M. M., Reichel, J. J., Popovic, B., Tanaka, M., Fu, Z., Balaji, G. R., Lau, T. N., Tu, M. M., Kirkham, C. L., Mahmoud, A. B., Mesci, A., Krmpotic, A., Allan, D. S., Makrigiannis, A. P., Jonjic, S., Rossjohn, J. and Carlyle, J. R. (2017). "A Viral Immunoevasin Controls Innate Immunity by Targeting the Prototypical Natural Killer Cell Receptor Family." Cell **169**(1): 58-71 e14.

Aldemir, H., Prod'homme, V., Dumaurier, M. J., Retiere, C., Poupon, G., Cazareth, J., Bihl, F. and Braud, V. M. (2005). "Cutting edge: lectin-like transcript 1 is a ligand for the CD161 receptor." J Immunol **175**(12): 7791-7795.

Anderson, P., Caligiuri, M., Ritz, J. and Schlossman, S. F. (1989). "CD3-negative natural killer cells express zeta TCR as part of a novel molecular complex." Nature **341**(6238): 159-162.

Andrews, D. M., Sullivan, L. C., Baschuk, N., Chan, C. J., Berry, R., Cotterell, C. L., Lin, J., Halse, H., Watt, S. V., Poursine-Laurent, J., Wang, C. R., Scalzo, A. A., Yokoyama, W. M., Rossjohn, J., Brooks, A. G. and Smyth, M. J. (2012). "Recognition of the nonclassical MHC class I molecule H2-M3 by the receptor Ly49A regulates the licensing and activation of NK cells." Nat Immunol **13**(12): 1171-1177.

Anfossi, N., Andre, P., Guia, S., Falk, C. S., Roetynck, S., Stewart, C. A., Breso, V., Frassati, C., Reviron, D., Middleton, D., Romagne, F., Ugolini, S. and Vivier, E. (2006). "Human NK cell education by inhibitory receptors for MHC class I." Immunity **25**(2): 331-342.

Annibali, V., Ristori, G., Angelini, D. F., Serafini, B., Mechelli, R., Cannoni, S., Romano, S., Paolillo, A., Abderrahim, H., Diamantini, A., Borsellino, G., Aloisi, F., Battistini, L. and Salvetti, M. (2011). "CD161(high)CD8+T cells bear pathogenetic potential in multiple sclerosis." Brain **134**(Pt 2): 542-554.

Arase, N., Arase, H., Park, S. Y., Ohno, H., Ra, C. and Saito, T. (1997). "Association with FcRgamma is essential for activation signal through NKR-P1 (CD161) in natural killer (NK) cells and NK1.1+ T cells." J Exp Med **186**(12): 1957-1963.

Aust, J. G., Gays, F., Mickiewicz, K. M., Buchanan, E. and Brooks, C. G. (2009). "The expression and function of the NKRP1 receptor family in C57BL/6 mice." J Immunol **183**(1): 106-116.

Back, J., Malchiodi, E. L., Cho, S., Scarpellino, L., Schneider, P., Kerzic, M. C., Mariuzza, R. A. and Held, W. (2009). "Distinct conformations of Ly49 natural killer cell receptors mediate MHC class I recognition in trans and cis." Immunity **31**(4): 598-608.

Backliwal, G., Hildinger, M., Hasija, V. and Wurm, F. M. (2008). "High-density transfection with HEK-293 cells allows doubling of transient titers and removes need for a priori DNA complex formation with PEI." Biotechnol Bioeng **99**(3): 721-727.

Balsamo, M., Manzini, C., Pietra, G., Raggi, F., Blengio, F., Mingari, M. C., Varesio, L., Moretta, L., Bosco, M. C. and Vitale, M. (2013). "Hypoxia downregulates the expression of activating receptors involved in NK-cell-mediated target cell killing without affecting ADCC." Eur J Immunol **43**(10): 2756-2764.

Baragano Raneros, A., Suarez-Alvarez, B. and Lopez-Larrea, C. (2014). "Secretory pathways generating immunosuppressive NKG2D ligands: New targets for therapeutic intervention." Oncoimmunology **3**: e28497.

Bartel, Y., Bauer, B. and Steinle, A. (2013). "Modulation of NK cell function by genetically coupled C-type lectin-like receptor/ligand pairs encoded in the human natural killer gene complex." Front Immunol **4**: 362.

Bauer, S., Groh, V., Wu, J., Steinle, A., Phillips, J. H., Lanier, L. L. and Spies, T. (1999). "Activation of NK cells and T cells by NKG2D, a receptor for stress-inducible MICA." Science **285**(5428): 727-729.

Bennett, I. M., Zatsepina, O., Zamai, L., Azzoni, L., Mikheeva, T. and Perussia, B. (1996). "Definition of a natural killer NKR-P1A+/CD56-/CD16- functionally immature human NK cell subset that differentiates in vitro in the presence of interleukin 12." J Exp Med **184**(5): 1845-1856.

Billerbeck, E., Kang, Y. H., Walker, L., Lockstone, H., Grafmueller, S., Fleming, V., Flint, J., Willberg, C. B., Bengsch, B., Seigel, B., Ramamurthy, N., Zitzmann, N., Barnes, E. J., Thevanayagam, J., Bhagwanani, A., Leslie, A., Oo, Y. H., Kollnberger, S., Bowness, P., Drognitz, O., Adams, D. H., Blum, H. E., Thimme, R. and Klenerman, P. (2010). "Analysis of CD161 expression on human CD8+ T cells defines a distinct functional subset with tissue-homing properties." Proc Natl Acad Sci U S A **107**(7): 3006-3011.

Binsack, R. and Pecht, I. (1997). "The mast cell function-associated antigen exhibits saccharide binding capacity." Eur J Immunol **27**(10): 2557-2561.

Blaha, J., Kalouskova, B., Skorepa, O., Pazicky, S., Novak, P. and Vanek, O. (2017). "High-level expression and purification of soluble form of human natural killer cell receptor NKR-P1 in HEK293S GnTI- cells." Protein Expr Purif **140**: 36-43.

Blaha, J., Pachl, P., Novak, P. and Vanek, O. (2015). "Expression and purification of soluble and stable ectodomain of natural killer cell receptor LLT1 through high-density transfection of suspension adapted HEK293S GnTI(-) cells." Protein Expr Purif **109**: 7-13.

Blum, K. S. and Pabst, R. (2007). "Lymphocyte numbers and subsets in the human blood. Do they mirror the situation in all organs?" Immunol Lett **108**(1): 45-51.

Boles, K. S., Barten, R., Kumaresan, P. R., Trowsdale, J. and Mathew, P. A. (1999). "Cloning of a new lectin-like receptor expressed on human NK cells." Immunogenetics **50**(1-2): 1-7.

Borrego, F., Ulbrecht, M., Weiss, E. H., Coligan, J. E. and Brooks, A. G. (1998). "Recognition of human histocompatibility leukocyte antigen (HLA)-E complexed with HLA class I signal sequence-derived peptides by CD94/NKG2 confers protection from natural killer cell-mediated lysis." J Exp Med **187**(5): 813-818.

Bossi, G. and Griffiths, G. M. (1999). "Degranulation plays an essential part in regulating cell surface expression of Fas ligand in T cells and natural killer cells." Nat Med **5**(1): 90-96.

Bottino, C., Castriconi, R., Moretta, L. and Moretta, A. (2005). "Cellular ligands of activating NK receptors." Trends Immunol **26**(4): 221-226.

Brandt, C. S., Baratin, M., Yi, E. C., Kennedy, J., Gao, Z., Fox, B., Haldeman, B., Ostrander, C. D., Kaifu, T., Chabannon, C., Moretta, A., West, R., Xu, W., Vivier, E. and Levin,

S. D. (2009). "The B7 family member B7-H6 is a tumor cell ligand for the activating natural killer cell receptor NKp30 in humans." J Exp Med **206**(7): 1495-1503.

Brodin, P., Karre, K. and Hoglund, P. (2009). "NK cell education: not an on-off switch but a tunable rheostat." Trends Immunol **30**(4): 143-149.

Brodin, P., Lakshmikanth, T., Mehr, R., Johansson, M. H., Duru, A. D., Achour, A., Salmon-Divon, M., Karre, K., Hoglund, P. and Johansson, S. (2010). "Natural killer cell tolerance persists despite significant reduction of self MHC class I on normal target cells in mice." PLoS One **5**(10).

Brown, J., O'Callaghan, C. A., Marshall, A. S., Gilbert, R. J., Siebold, C., Gordon, S., Brown, G. D. and Jones, E. Y. (2007). "Structure of the fungal beta-glucan-binding immune receptor dectin-1: implications for function." Protein Sci **16**(6): 1042-1052.

Brown, M. G., Scalzo, A. A., Stone, L. R., Clark, P. Y., Du, Y., Palanca, B. and Yokoyama, W. M. (2001). "Natural killer gene complex (Nkc) allelic variability in inbred mice: evidence for Nkc haplotypes." Immunogenetics **53**(7): 584-591.

Brucklacher-Waldert, V., Stuerner, K., Kolster, M., Wolthausen, J. and Tolosa, E. (2009). "Phenotypical and functional characterization of T helper 17 cells in multiple sclerosis." Brain **132**(Pt 12): 3329-3341.

Bryceson, Y. T., March, M. E., Ljunggren, H. G. and Long, E. O. (2006). "Synergy among receptors on resting NK cells for the activation of natural cytotoxicity and cytokine secretion." Blood **107**(1): 159-166.

Burshtyn, D. N. and Long, E. O. (1997). "Regulation through inhibitory receptors: Lessons from natural killer cells." Trends Cell Biol **7**(12): 473-479.

Caligiuri, M. A. (2008). "Human natural killer cells." Blood **112**(3): 461-469.

Carapito, R. and Bahram, S. (2015). "Genetics, genomics, and evolutionary biology of NKG2D ligands." Immunol Rev **267**(1): 88-116.

Carlsten, M., Norell, H., Bryceson, Y. T., Poschke, I., Schedvins, K., Ljunggren, H. G., Kiessling, R. and Malmberg, K. J. (2009). "Primary human tumor cells expressing CD155 impair tumor targeting by down-regulating DNAM-1 on NK cells." J Immunol **183**(8): 4921-4930.

Carlyle, J. R., Jamieson, A. M., Gasser, S., Clingan, C. S., Arase, H. and Raulet, D. H. (2004). "Missing self-recognition of Ocil/Clr-b by inhibitory NKR-P1 natural killer cell receptors." Proc Natl Acad Sci U S A **101**(10): 3527-3532.

Carlyle, J. R., Mesci, A., Fine, J. H., Chen, P., Belanger, S., Tai, L. H. and Makrigiannis, A. P. (2008). "Evolution of the Ly49 and Nkrp1 recognition systems." Semin Immunol **20**(6): 321-330.

Carlyle, J. R., Michie, A. M., Furlonger, C., Nakano, T., Lenardo, M. J., Paige, C. J. and Zuniga-Pflucker, J. C. (1997). "Identification of a novel developmental stage marking lineage commitment of progenitor thymocytes." J Exp Med **186**(2): 173-182.

Carotta, S., Pang, S. H., Nutt, S. L. and Belz, G. T. (2011). "Identification of the earliest NK-cell precursor in the mouse BM." Blood **117**(20): 5449-5452.

Carrega, P., Morandi, B., Costa, R., Frumento, G., Forte, G., Altavilla, G., Ratto, G. B., Mingari, M. C., Moretta, L. and Ferlazzo, G. (2008). "Natural killer cells infiltrating human nonsmall-cell lung cancer are enriched in CD56 bright CD16(-) cells and display an impaired capability to kill tumor cells." Cancer **112**(4): 863-875.

Cerwenka, A. and Lanier, L. L. (2016). "Natural killer cell memory in infection, inflammation and cancer." Nat Rev Immunol **16**(2): 112-123.

Chalan, P., Bijzet, J., Huitema, M. G., Kroesen, B. J., Brouwer, E. and Boots, A. M. (2015). "Expression of Lectin-Like Transcript 1, the Ligand for CD161, in Rheumatoid Arthritis." PLoS One **10**(7): e0132436.

Chaturvedi, N., Yadav, B. S., Pandey, P. N. and Tripathi, V. (2017). "The effect of beta-glucan and its potential analog on the structure of Dectin-1 receptor." J Mol Graph Model **74**: 315-325.

Chen, P., Belanger, S., Aguilar, O. A., Zhang, Q., St-Laurent, A., Rahim, M. M., Makrigiannis, A. P. and Carlyle, J. R. (2011). "Analysis of the mouse 129-strain Nkrp1-Clr gene cluster reveals conservation of genomic organization and functional receptor-ligand interactions despite significant allelic polymorphism." Immunogenetics **63**(10): 627-640.

Cho, H. S., Mason, K., Ramyar, K. X., Stanley, A. M., Gabelli, S. B., Denney, D. W., Jr. and Leahy, D. J. (2003). "Structure of the extracellular region of HER2 alone and in complex with the Herceptin Fab." Nature **421**(6924): 756-760.

Colonna, M. and Samaridis, J. (1995). "Cloning of immunoglobulin-superfamily members associated with HLA-C and HLA-B recognition by human natural killer cells." Science **268**(5209): 405-408.

Cooley, S., Xiao, F., Pitt, M., Gleason, M., McCullar, V., Bergemann, T. L., McQueen, K. L., Guethlein, L. A., Parham, P. and Miller, J. S. (2007). "A subpopulation of human peripheral blood NK cells that lacks inhibitory receptors for self-MHC is developmentally immature." Blood **110**(2): 578-586.

Cooper, M. A., Colonna, M. and Yokoyama, W. M. (2009). "Hidden talents of natural killers: NK cells in innate and adaptive immunity." EMBO Rep **10**(10): 1103-1110.

Cosman, D., Mullberg, J., Sutherland, C. L., Chin, W., Armitage, R., Fanslow, W., Kubin, M. and Chalupny, N. J. (2001). "ULBPs, novel MHC class I-related molecules, bind to CMV glycoprotein UL16 and stimulate NK cytotoxicity through the NKG2D receptor." Immunity **14**(2): 123-133.

Cosmi, L., De Palma, R., Santarlasci, V., Maggi, L., Capone, M., Frosali, F., Rodolico, G., Querci, V., Abbate, G., Angeli, R., Berrino, L., Fambrini, M., Caproni, M., Tonelli, F., Lazzeri, E., Parronchi, P., Liotta, F., Maggi, E., Romagnani, S. and Annunziato, F. (2008). "Human interleukin 17-producing cells originate from a CD161+CD4+ T cell precursor." J Exp Med **205**(8): 1903-1916.

Crouse, J., Bedenikovic, G., Wiesel, M., Ibberson, M., Xenarios, I., Von Laer, D., Kalinke, U., Vivier, E., Jonjic, S. and Oxenius, A. (2014). "Type I interferons protect T cells against NK cell attack mediated by the activating receptor NCR1." Immunity **40**(6): 961-973.

D'Andrea, A., Chang, C., Franz-Bacon, K., McClanahan, T., Phillips, J. H. and Lanier, L. L. (1995). "Molecular cloning of NKB1. A natural killer cell receptor for HLA-B allotypes." J Immunol **155**(5): 2306-2310.

D'Andrea, A. and Lanier, L. L. (1998). "Killer cell inhibitory receptor expression by T cells." Curr Top Microbiol Immunol **230**: 25-39.

D'Netto, M. J., Ward, H., Morrison, K. M., Ramagopalan, S. V., Dyment, D. A., DeLuca, G. C., Handunnetthi, L., Sadovnick, A. D. and Ebers, G. C. (2009). "Risk alleles for multiple sclerosis in multiplex families." Neurology **72**(23): 1984-1988.

Dam, J., Baber, J., Grishaev, A., Malchiodi, E. L., Schuck, P., Bax, A. and Mariuzza, R. A. (2006). "Variable dimerization of the Ly49A natural killer cell receptor results in differential engagement of its MHC class I ligand." J Mol Biol **362**(1): 102-113.

Dam, J., Guan, R., Natarajan, K., Dimasi, N., Chlewicki, L. K., Kranz, D. M., Schuck, P., Margulies, D. H. and Mariuzza, R. A. (2003). "Variable MHC class I engagement by

Ly49 natural killer cell receptors demonstrated by the crystal structure of Ly49C bound to H-2K(b)." Nat Immunol **4**(12): 1213-1222.

Davidson, C. L., Li, N. L. and Burshtyn, D. N. (2010). "LILRB1 polymorphism and surface phenotypes of natural killer cells." Hum Immunol **71**(10): 942-949.

Davis, D. M., Chiu, I., Fassett, M., Cohen, G. B., Mandelboim, O. and Strominger, J. L. (1999). "The human natural killer cell immune synapse." Proc Natl Acad Sci U S A **96**(26): 15062-15067.

de Saint Basile, G., Menasche, G. and Fischer, A. (2010). "Molecular mechanisms of biogenesis and exocytosis of cytotoxic granules." Nat Rev Immunol **10**(8): 568-579.

Delahaye, N. F., Rusakiewicz, S., Martins, I., Menard, C., Roux, S., Lyonnet, L., Paul, P., Sarabi, M., Chaput, N., Semeraro, M., Minard-Colin, V., Poirier-Colame, V., Chaba, K., Flament, C., Baud, V., Authier, H., Kerdine-Romer, S., Pallardy, M., Cremer, I., Peaudecerf, L., Rocha, B., Valteau-Couanet, D., Gutierrez, J. C., Nunes, J. A., Commo, F., Bonvalot, S., Ibrahim, N., Terrier, P., Opolon, P., Bottino, C., Moretta, A., Tavernier, J., Rihet, P., Coindre, J. M., Blay, J. Y., Isambert, N., Emile, J. F., Vivier, E., Lecesne, A., Kroemer, G. and Zitvogel, L. (2011). "Alternatively spliced NKp30 isoforms affect the prognosis of gastrointestinal stromal tumors." Nat Med **17**(6): 700-707.

Deng, L., Cho, S., Malchiodi, E. L., Kerzic, M. C., Dam, J. and Mariuzza, R. A. (2008). "Molecular architecture of the major histocompatibility complex class I-binding site of Ly49 natural killer cell receptors." J Biol Chem **283**(24): 16840-16849.

Diefenbach, A., Tomasello, E., Lucas, M., Jamieson, A. M., Hsia, J. K., Vivier, E. and Raulet, D. H. (2002). "Selective associations with signaling proteins determine stimulatory versus costimulatory activity of NKG2D." Nat Immunol **3**(12): 1142-1149.

Dimasi, N. and Biassoni, R. (2005). "Structural and functional aspects of the Ly49 natural killer cell receptors." Immunol Cell Biol **83**(1): 1-8.

Dimasi, N., Sawicki, M. W., Reineck, L. A., Li, Y., Natarajan, K., Margulies, D. H. and Mariuzza, R. A. (2002). "Crystal structure of the Ly49I natural killer cell receptor reveals variability in dimerization mode within the Ly49 family." J Mol Biol **320**(3): 573-585.

Dodd, R. B. and Drickamer, K. (2001). "Lectin-like proteins in model organisms: implications for evolution of carbohydrate-binding activity." Glycobiology **11**(5): 71R-79R.

Douagi, I., Colucci, F., Di Santo, J. P. and Cumano, A. (2002). "Identification of the earliest prethymic bipotent T/NK progenitor in murine fetal liver." Blood **99**(2): 463-471.

Drickamer, K. and Taylor, M. E. (1993). "Biology of animal lectins." Annu Rev Cell Biol **9**: 237-264.

Dunn, G. P., Old, L. J. and Schreiber, R. D. (2004). "The three Es of cancer immunoediting." Annu Rev Immunol **22**: 329-360.

Eagle, R. A., Traherne, J. A., Hair, J. R., Jafferji, I. and Trowsdale, J. (2009). "ULBP6/RAET1L is an additional human NKG2D ligand." Eur J Immunol **39**(11): 3207-3216.

Estrada-Capetillo, L., Hernandez-Castro, B., Monsivais-Urenda, A., Alvarez-Quiroga, C., Layseca-Espinosa, E., Abud-Mendoza, C., Baranda, L., Urzainqui, A., Sanchez-Madrid, F. and Gonzalez-Amaro, R. (2013). "Induction of Th17 lymphocytes and Treg cells by monocyte-derived dendritic cells in patients with rheumatoid arthritis and systemic lupus erythematosus." Clin Dev Immunol **2013**: 584303.

Exley, M., Porcelli, S., Furman, M., Garcia, J. and Balk, S. (1998). "CD161 (NKR-P1A) costimulation of CD1d-dependent activation of human T cells expressing invariant V alpha 24 J alpha Q T cell receptor alpha chains." J Exp Med **188**(5): 867-876.

Fauriat, C., Long, E. O., Ljunggren, H. G. and Bryceson, Y. T. (2010). "Regulation of human NK-cell cytokine and chemokine production by target cell recognition." Blood **115**(11): 2167-2176.

Fehniger, T. A., Cooper, M. A., Nuovo, G. J., Cella, M., Facchetti, F., Colonna, M. and Caligiuri, M. A. (2003). "CD56bright natural killer cells are present in human lymph nodes and are activated by T cell-derived IL-2: a potential new link between adaptive and innate immunity." Blood **101**(8): 3052-3057.

Fehniger, T. A., Shah, M. H., Turner, M. J., VanDeusen, J. B., Whitman, S. P., Cooper, M. A., Suzuki, K., Wechser, M., Goodsaid, F. and Caligiuri, M. A. (1999). "Differential cytokine and chemokine gene expression by human NK cells following activation with IL-18 or IL-15 in combination with IL-12: implications for the innate immune response." J Immunol **162**(8): 4511-4520.

Feinberg, H., Park-Snyder, S., Kolatkar, A. R., Heise, C. T., Taylor, M. E. and Weis, W. I. (2000). "Structure of a C-type carbohydrate recognition domain from the macrophage mannose receptor." J Biol Chem **275**(28): 21539-21548.

Fergusson, J. R., Smith, K. E., Fleming, V. M., Rajoriya, N., Newell, E. W., Simmons, R., Marchi, E., Bjorkander, S., Kang, Y. H., Swadling, L., Kurioka, A., Sahgal, N., Lockstone, H., Baban, D., Freeman, G. J., Sverremark-Ekstrom, E., Davis, M. M., Davenport, M. P., Venturi, V., Ussher, J. E., Willberg, C. B. and Klenerman, P. (2014). "CD161 defines a transcriptional and functional phenotype across distinct human T cell lineages." Cell Rep **9**(3): 1075-1088.

Fernandez-Messina, L., Ashiru, O., Boutet, P., Aguera-Gonzalez, S., Skepper, J. N., Reyburn, H. T. and Vales-Gomez, M. (2010). "Differential mechanisms of shedding of the glycosylphosphatidylinositol (GPI)-anchored NKG2D ligands." J Biol Chem **285**(12): 8543-8551.

Fernandez, N. C., Treiner, E., Vance, R. E., Jamieson, A. M., Lemieux, S. and Raulet, D. H. (2005). "A subset of natural killer cells achieves self-tolerance without expressing inhibitory receptors specific for self-MHC molecules." Blood **105**(11): 4416-4423.

Freud, A. G., Becknell, B., Roychowdhury, S., Mao, H. C., Ferketich, A. K., Nuovo, G. J., Hughes, T. L., Marburger, T. B., Sung, J., Baiocchi, R. A., Guimond, M. and Caligiuri, M. A. (2005). "A human CD34(+) subset resides in lymph nodes and differentiates into CD56bright natural killer cells." Immunity **22**(3): 295-304.

Freud, A. G. and Caligiuri, M. A. (2006). "Human natural killer cell development." Immunol Rev **214**: 56-72.

Freud, A. G., Yu, J. and Caligiuri, M. A. (2014). "Human natural killer cell development in secondary lymphoid tissues." Semin Immunol **26**(2): 132-137.

Galy, A., Travis, M., Cen, D. and Chen, B. (1995). "Human T, B, natural killer, and dendritic cells arise from a common bone marrow progenitor cell subset." Immunity **3**(4): 459-473.

Gasser, S. and Raulet, D. H. (2006). "Activation and self-tolerance of natural killer cells." Immunol Rev **214**: 130-142.

Germain, C., Bihl, F., Zahn, S., Poupon, G., Dumaurier, M. J., Rampanarivo, H. H., Padkjaer, S. B., Spee, P. and Braud, V. M. (2010). "Characterization of alternatively spliced transcript variants of CLEC2D gene." J Biol Chem **285**(46): 36207-36215.

Germain, C., Guillaudeux, T., Galsgaard, E. D., Hervouet, C., Tekaya, N., Gallouet, A. S., Fassy, J., Bihl, F., Poupon, G., Lazzari, A., Spee, P., Anjuere, F., Pangault, C., Tarte,

K., Tas, P., Xerri, L. and Braud, V. M. (2015). "Lectin-like transcript 1 is a marker of germinal center-derived B-cell non-Hodgkin's lymphomas dampening natural killer cell functions." Oncoimmunology **4**(8): e1026503.

Germain, C., Meier, A., Jensen, T., Knapnougel, P., Poupon, G., Lazzari, A., Neisig, A., Hakansson, K., Dong, T., Wagtmann, N., Galsgaard, E. D., Spee, P. and Braud, V. M. (2011). "Induction of lectin-like transcript 1 (LLT1) protein cell surface expression by pathogens and interferon-gamma contributes to modulate immune responses." J Biol Chem **286**(44): 37964-37975.

Gilfillan, S., Ho, E. L., Cella, M., Yokoyama, W. M. and Colonna, M. (2002). "NKG2D recruits two distinct adapters to trigger NK cell activation and costimulation." Nat Immunol **3**(12): 1150-1155.

Glimcher, L., Shen, F. W. and Cantor, H. (1977). "Identification of a cell-surface antigen selectively expressed on the natural killer cell." J Exp Med **145**(1): 1-9.

Greenberg, A. H. and Playfair, J. H. (1974). "Spontaneously arising cytotoxicity to the P-815-Y mastocytoma in NZB mice." Clin Exp Immunol **16**(1): 99-109.

Hammond, K. J. and Godfrey, D. I. (2002). "NKT cells: potential targets for autoimmune disease therapy?" Tissue Antigens **59**(5): 353-363.

Hao, L., Klein, J. and Nei, M. (2006). "Heterogeneous but conserved natural killer receptor gene complexes in four major orders of mammals." Proc Natl Acad Sci U S A **103**(9): 3192-3197.

Herberman, R. B., Nunn, M. E., Holden, H. T. and Lavrin, D. H. (1975). "Natural cytotoxic reactivity of mouse lymphoid cells against syngeneic and allogeneic tumors. II. Characterization of effector cells." Int J Cancer **16**(2): 230-239.

Hibbs, M. L., Selvaraj, P., Carpen, O., Springer, T. A., Kuster, H., Jouvin, M. H. and Kinet, J. P. (1989). "Mechanisms for regulating expression of membrane isoforms of Fc gamma RIII (CD16)." Science **246**(4937): 1608-1611.

Hirotsu, S., Mizuno, H., Fukuda, K., Qi, M. C., Matsui, T., Hamako, J., Morita, T. and Titani, K. (2001). "Crystal structure of bitiscetin, a von Willebrand factor-dependent platelet aggregation inducer." Biochemistry **40**(45): 13592-13597.

Hoare, H. L., Sullivan, L. C., Clements, C. S., Ely, L. K., Beddoe, T., Henderson, K. N., Lin, J., Reid, H. H., Brooks, A. G. and Rossjohn, J. (2008). "Subtle changes in peptide conformation profoundly affect recognition of the non-classical MHC class I molecule HLA-E by the CD94-NKG2 natural killer cell receptors." J Mol Biol **377**(5): 1297-1303.

Hoglund, P. and Brodin, P. (2010). "Current perspectives of natural killer cell education by MHC class I molecules." Nat Rev Immunol **10**(10): 724-734.

Hoglund, P., Glas, R., Menard, C., Kase, A., Johansson, M. H., Franksson, L., Lemmonier, F. and Karre, K. (1998). "Beta2-microglobulin-deficient NK cells show increased sensitivity to MHC class I-mediated inhibition, but self tolerance does not depend upon target cell expression of H-2Kb and Db heavy chains." Eur J Immunol **28**(1): 370-378.

Horowitz, A., Strauss-Albee, D. M., Leipold, M., Kubo, J., Nemat-Gorgani, N., Dogan, O. C., Dekker, C. L., Mackey, S., Maecker, H., Swan, G. E., Davis, M. M., Norman, P. J., Guethlein, L. A., Desai, M., Parham, P. and Blish, C. A. (2013). "Genetic and environmental determinants of human NK cell diversity revealed by mass cytometry." Sci Transl Med **5**(208): 208ra145.

Iizuka, K., Naidenko, O. V., Plougastel, B. F., Fremont, D. H. and Yokoyama, W. M. (2003). "Genetically linked C-type lectin-related ligands for the NKRP1 family of natural killer cell receptors." Nat Immunol **4**(8): 801-807.

Ikawa, T., Kawamoto, H., Fujimoto, S. and Katsura, Y. (1999). "Commitment of common T/Natural killer (NK) progenitors to unipotent T and NK progenitors in the murine fetal thymus revealed by a single progenitor assay." J Exp Med **190**(11): 1617-1626.

Imai, K., Matsuyama, S., Miyake, S., Suga, K. and Nakachi, K. (2000). "Natural cytotoxic activity of peripheral-blood lymphocytes and cancer incidence: an 11-year follow-up study of a general population." Lancet **356**(9244): 1795-1799.

Ishimoto, Y., Ishibashi, K. I., Yamanaka, D., Adachi, Y., Kanzaki, K., Okita, K., Iwakura, Y. and Ohno, N. (2017). "Modulation of an innate immune response by soluble yeast beta-glucan prepared by a heat degradation method." Int J Biol Macromol **104**(Pt A): 367-376.

Iwaszko, M. and Bogunia-Kubik, K. (2011). "Clinical significance of the HLA-E and CD94/NKG2 interaction." Arch Immunol Ther Exp (Warsz) **59**(5): 353-367.

Jamshidian, A., Shaygannejad, V., Pourazar, A., Zarkesh-Esfahani, S. H. and Gharagozloo, M. (2013). "Biased Treg/Th17 balance away from regulatory toward inflammatory phenotype in relapsed multiple sclerosis and its correlation with severity of symptoms." J Neuroimmunol **262**(1-2): 106-112.

Jelencic, V., Lenartic, M., Wensveen, F. M. and Polic, B. (2017). "NKG2D: A versatile player in the immune system." Immunol Lett.

Joncker, N. T., Fernandez, N. C., Treiner, E., Vivier, E. and Raulet, D. H. (2009). "NK cell responsiveness is tuned commensurate with the number of inhibitory receptors for self-MHC class I: the rheostat model." J Immunol **182**(8): 4572-4580.

Joncker, N. T., Shifrin, N., Delebecque, F. and Raulet, D. H. (2010). "Mature natural killer cells reset their responsiveness when exposed to an altered MHC environment." J Exp Med **207**(10): 2065-2072.

Kadri, N., Wagner, A. K., Ganesan, S., Karre, K., Wickstrom, S., Johansson, M. H. and Hoglund, P. (2016). "Dynamic Regulation of NK Cell Responsiveness." Curr Top Microbiol Immunol **395**: 95-114.

Kamishikiryo, J., Fukuhara, H., Okabe, Y., Kuroki, K. and Maenaka, K. (2011). "Molecular basis for LLT1 protein recognition by human CD161 protein (NKRP1A/KLRB1)." J Biol Chem **286**(27): 23823-23830.

Kane, K. P., Lavender, K. J. and Ma, B. J. (2004). "Ly-49 receptors and their functions." Crit Rev Immunol **24**(5): 321-348.

Karre, K., Ljunggren, H. G., Piontek, G. and Kiessling, R. (1986). "Selective rejection of H-2-deficient lymphoma variants suggests alternative immune defence strategy." Nature **319**(6055): 675-678.

Kartsogiannis, V., Sims, N. A., Quinn, J. M., Ly, C., Cipetic, M., Poulton, I. J., Walker, E. C., Saleh, H., McGregor, N. E., Wallace, M. E., Smyth, M. J., Martin, T. J., Zhou, H., Ng, K. W. and Gillespie, M. T. (2008). "Osteoclast inhibitory lectin, an immune cell product that is required for normal bone physiology in vivo." J Biol Chem **283**(45): 30850-30860.

Kennedy, M. K., Glaccum, M., Brown, S. N., Butz, E. A., Viney, J. L., Embers, M., Matsuki, N., Charrier, K., Sedger, L., Willis, C. R., Brasel, K., Morrissey, P. J., Stocking, K., Schuh, J. C., Joyce, S. and Peschon, J. J. (2000). "Reversible defects in natural killer and memory CD8 T cell lineages in interleukin 15-deficient mice." J Exp Med **191**(5): 771-780.

Kiessling, R., Klein, E. and Wigzell, H. (1975). ""Natural" killer cells in the mouse. I. Cytotoxic cells with specificity for mouse Moloney leukemia cells. Specificity and distribution according to genotype." Eur J Immunol **5**(2): 112-117.

Kiessling, R., Petranyi, G., Klein, G. and Wigzell, H. (1976). "Non-T-cell resistance against a mouse Moloney lymphoma." Int J Cancer **17**(2): 275-281.

Kim, S., Iizuka, K., Aguila, H. L., Weissman, I. L. and Yokoyama, W. M. (2000). "In vivo natural killer cell activities revealed by natural killer cell-deficient mice." Proc Natl Acad Sci U S A **97**(6): 2731-2736.

Kim, S., Poursine-Laurent, J., Truscott, S. M., Lybarger, L., Song, Y. J., Yang, L., French, A. R., Sunwoo, J. B., Lemieux, S., Hansen, T. H. and Yokoyama, W. M. (2005). "Licensing of natural killer cells by host major histocompatibility complex class I molecules." Nature **436**(7051): 709-713.

Kita, S., Matsubara, H., Kasai, Y., Tamaoki, T., Okabe, Y., Fukuhara, H., Kamishikiryo, J., Krayukhina, E., Uchiyama, S., Ose, T., Kuroki, K. and Maenaka, K. (2015). "Crystal structure of extracellular domain of human lectin-like transcript 1 (LLT1), the ligand for natural killer receptor-P1A." Eur J Immunol **45**(6): 1605-1613.

Koka, R., Burkett, P. R., Chien, M., Chai, S., Chan, F., Lodolce, J. P., Boone, D. L. and Ma, A. (2003). "Interleukin (IL)-15R[alpha]-deficient natural killer cells survive in normal but not IL-15R[alpha]-deficient mice." J Exp Med **197**(8): 977-984.

Kolenko, P., Rozbesky, D., Vanek, O., Kopecky, V., Jr., Hofbauerova, K., Novak, P., Pompach, P., Hasek, J., Skalova, T., Bezouska, K. and Dohnalek, J. (2011). "Molecular architecture of mouse activating NKR-P1 receptors." J Struct Biol **175**(3): 434-441.

Kolenko, P., Skalova, T., Vanek, O., Stepankova, A., Duskova, J., Hasek, J., Bezouska, K. and Dohnalek, J. (2009). "The high-resolution structure of the extracellular domain of human CD69 using a novel polymer." Acta Crystallogr Sect F Struct Biol Cryst Commun **65**(Pt 12): 1258-1260.

Kondo, M., Weissman, I. L. and Akashi, K. (1997). "Identification of clonogenic common lymphoid progenitors in mouse bone marrow." Cell **91**(5): 661-672.

Krockenberger, M., Dombrowski, Y., Weidler, C., Ossadnik, M., Honig, A., Hausler, S., Voigt, H., Becker, J. C., Leng, L., Steinle, A., Weller, M., Bucala, R., Dietl, J. and Wischhusen, J. (2008). "Macrophage migration inhibitory factor contributes to the immune escape of ovarian cancer by down-regulating NKG2D." J Immunol **180**(11): 7338-7348.

Kveberg, L., Dai, K. Z., Inngjerdingen, M., Brooks, C. G., Fossum, S. and Vaage, J. T. (2011). "Phylogenetic and functional conservation of the NKR-P1F and NKR-P1G receptors in rat and mouse." Immunogenetics **63**(7): 429-436.

Lang, P. A., Lang, K. S., Xu, H. C., Grusdat, M., Parish, I. A., Recher, M., Elford, A. R., Dhanji, S., Shaabani, N., Tran, C. W., Dissanayake, D., Rahbar, R., Ghazarian, M., Brustle, A., Fine, J., Chen, P., Weaver, C. T., Klose, C., Diefenbach, A., Haussinger, D., Carlyle, J. R., Kaech, S. M., Mak, T. W. and Ohashi, P. S. (2012). "Natural killer cell activation enhances immune pathology and promotes chronic infection by limiting CD8+ T-cell immunity." Proc Natl Acad Sci U S A **109**(4): 1210-1215.

Lanier, L. L. (2005). "NK cell recognition." Annu Rev Immunol **23**: 225-274.

Lanier, L. L. (2014). "Of snowflakes and natural killer cell subsets." Nat Biotechnol **32**(2): 140-142.

Lanier, L. L. (2015). "NKG2D Receptor and Its Ligands in Host Defense." Cancer Immunol Res **3**(6): 575-582.

Lanier, L. L., Chang, C. and Phillips, J. H. (1994). "Human NKR-P1A. A disulfide-linked homodimer of the C-type lectin superfamily expressed by a subset of NK and T lymphocytes." J Immunol **153**(6): 2417-2428.

Lanier, L. L., Corliss, B. C., Wu, J., Leong, C. and Phillips, J. H. (1998). "Immunoreceptor DAP12 bearing a tyrosine-based activation motif is involved in activating NK cells." Nature **391**(6668): 703-707.

Lanier, L. L., Phillips, J. H., Hackett, J., Jr., Tutt, M. and Kumar, V. (1986). "Natural killer cells: definition of a cell type rather than a function." J Immunol **137**(9): 2735-2739.

Leavy, O. (2013). "Natural killer cells: a virtual pick and mix." Nat Rev Immunol **13**(12): 844-845.

Li, Y., Hofmann, M., Wang, Q., Teng, L., Chlewicki, L. K., Pircher, H. and Mariuzza, R. A. (2009). "Structure of natural killer cell receptor KLRG1 bound to E-cadherin reveals basis for MHC-independent missing self recognition." Immunity **31**(1): 35-46.

Li, Y., Wang, Q., Chen, S., Brown, P. H. and Mariuzza, R. A. (2013). "Structure of NKp65 bound to its keratinocyte ligand reveals basis for genetically linked recognition in natural killer gene complex." Proc Natl Acad Sci U S A **110**(28): 11505-11510.

Li, Y., Wang, Q. and Mariuzza, R. A. (2011). "Structure of the human activating natural cytotoxicity receptor NKp30 bound to its tumor cell ligand B7-H6." J Exp Med **208**(4): 703-714.

Liao, N. S., Bix, M., Zijlstra, M., Jaenisch, R. and Raulet, D. (1991). "MHC class I deficiency: susceptibility to natural killer (NK) cells and impaired NK activity." Science **253**(5016): 199-202.

Liu, Y. and Eisenberg, D. (2002). "3D domain swapping: as domains continue to swap." Protein Sci **11**(6): 1285-1299.

Ljunggren, H. G. and Karre, K. (1985). "Host resistance directed selectively against H-2-deficient lymphoma variants. Analysis of the mechanism." J Exp Med **162**(6): 1745-1759.

Ljunggren, H. G. and Karre, K. (1990). "In search of the 'missing self': MHC molecules and NK cell recognition." Immunol Today **11**(7): 237-244.

Llibre, A., Garner, L., Partridge, A., Freeman, G. J., Klenerman, P. and Willberg, C. B. (2016). "Expression of lectin-like transcript-1 in human tissues." F1000Res **5**: 2929.

Long, E. O. (2008). "Negative signaling by inhibitory receptors: the NK cell paradigm." Immunol Rev **224**: 70-84.

Long, E. O., Kim, H. S., Liu, D., Peterson, M. E. and Rajagopalan, S. (2013). "Controlling natural killer cell responses: integration of signals for activation and inhibition." Annu Rev Immunol **31**: 227-258.

Mager, D. L., McQueen, K. L., Wee, V. and Freeman, J. D. (2001). "Evolution of natural killer cell receptors: coexistence of functional Ly49 and KIR genes in baboons." Curr Biol **11**(8): 626-630.

Mamessier, E., Sylvain, A., Thibult, M. L., Houvenaeghel, G., Jacquemier, J., Castellano, R., Goncalves, A., Andre, P., Romagne, F., Thibault, G., Viens, P., Birnbaum, D., Bertucci, F., Moretta, A. and Olive, D. (2011). "Human breast cancer cells enhance self tolerance by promoting evasion from NK cell antitumor immunity." J Clin Invest **121**(9): 3609-3622.

Mathew, P. A., Chuang, S. S., Vaidya, S. V., Kumaresan, P. R., Boles, K. S. and Pham, H. T. (2004). "The LLT1 receptor induces IFN-gamma production by human natural killer cells." Mol Immunol **40**(16): 1157-1163.

Mathew, S. O., Chaudhary, P., Powers, S. B., Vishwanatha, J. K. and Mathew, P. A. (2016). "Overexpression of LLT1 (OCIL, CLEC2D) on prostate cancer cells inhibits NK cell-mediated killing through LLT1-NKRP1A (CD161) interaction." Oncotarget **7**(42): 68650-68661.

Matta, J., Baratin, M., Chiche, L., Forel, J. M., Cognet, C., Thomas, G., Farnarier, C., Piperoglou, C., Papazian, L., Chaussabel, D., Ugolini, S., Vely, F. and Vivier, E. (2013). "Induction of B7-H6, a ligand for the natural killer cell-activating receptor NKp30, in inflammatory conditions." Blood **122**(3): 394-404.

Mattei, F., Schiavoni, G., Belardelli, F. and Tough, D. F. (2001). "IL-15 is expressed by dendritic cells in response to type I IFN, double-stranded RNA, or lipopolysaccharide and promotes dendritic cell activation." J Immunol **167**(3): 1179-1187.

Meeths, M., Chiang, S. C., Lofstedt, A., Muller, M. L., Tesi, B., Henter, J. I. and Bryceson, Y. T. (2014). "Pathophysiology and spectrum of diseases caused by defects in lymphocyte cytotoxicity." Exp Cell Res **325**(1): 10-17.

Meiners, P. M., Vissink, A., Kallenberg, C. G., Kroese, F. G. and Bootsma, H. (2011). "Treatment of primary Sjogren's syndrome with anti-CD20 therapy (rituximab). A feasible approach or just a starting point?" Expert Opin Biol Ther **11**(10): 1381-1394.

Meresse, B., Curran, S. A., Ciszewski, C., Orbelyan, G., Setty, M., Bhagat, G., Lee, L., Tretiakova, M., Semrad, C., Kistner, E., Winchester, R. J., Braud, V., Lanier, L. L., Geraghty, D. E., Green, P. H., Guandalini, S. and Jabri, B. (2006). "Reprogramming of CTLs into natural killer-like cells in celiac disease." J Exp Med **203**(5): 1343-1355.

Michalak-Stoma, A., Bartosinska, J., Kowal, M., Juszkiewicz-Borowiec, M., Gerkowicz, A. and Chodorowska, G. (2013). "Serum levels of selected Th17 and Th22 cytokines in psoriatic patients." Dis Markers **35**(6): 625-631.

Miller, J. S., Alley, K. A. and McGlave, P. (1994). "Differentiation of natural killer (NK) cells from human primitive marrow progenitors in a stroma-based long-term culture system: identification of a CD34+7+ NK progenitor." Blood **83**(9): 2594-2601.

Mizuno, H., Fujimoto, Z., Atoda, H. and Morita, T. (2001). "Crystal structure of an anticoagulant protein in complex with the Gla domain of factor X." Proc Natl Acad Sci U S A **98**(13): 7230-7234.

Mizuno, H., Fujimoto, Z., Koizumi, M., Kano, H., Atoda, H. and Morita, T. (1997). "Structure of coagulation factors IX/X-binding protein, a heterodimer of C-type lectin domains." Nat Struct Biol **4**(6): 438-441.

Moretta, A., Sivori, S., Vitale, M., Pende, D., Morelli, L., Augugliaro, R., Bottino, C. and Moretta, L. (1995). "Existence of both inhibitory (p58) and activatory (p50) receptors for HLA-C molecules in human natural killer cells." J Exp Med **182**(3): 875-884.

Moretta, L., Bottino, C., Pende, D., Mingari, M. C., Biassoni, R. and Moretta, A. (2002). "Human natural killer cells: their origin, receptors and function." Eur J Immunol **32**(5): 1205-1211.

Mrozek, E., Anderson, P. and Caligiuri, M. A. (1996). "Role of interleukin-15 in the development of human CD56+ natural killer cells from CD34+ hematopoietic progenitor cells." Blood **87**(7): 2632-2640.

Muller-Kuller, U., Ackermann, M., Kolodziej, S., Brendel, C., Fritsch, J., Lachmann, N., Kunkel, H., Lausen, J., Schambach, A., Moritz, T. and Grez, M. (2015). "A minimal ubiquitous chromatin opening element (UCOE) effectively prevents silencing of juxtaposed heterologous promoters by epigenetic remodeling in multipotent and pluripotent stem cells." Nucleic Acids Res **43**(3): 1577-1592.

OpenStax (2013). "Cellular Differentiation " OpenStax CNX Retrieved Jul 20 2017 from http://cnx.org/contents/966c32cc-3d6f-4f4e-af4f-ea0c975e825c@4

Orr, M. T. and Lanier, L. L. (2010). "Natural killer cell education and tolerance." Cell **142**(6): 847-856.

Parham, P. (2005). "MHC class I molecules and KIRs in human history, health and survival." Nat Rev Immunol **5**(3): 201-214.

Petrie, E. J., Clements, C. S., Lin, J., Sullivan, L. C., Johnson, D., Huyton, T., Heroux, A., Hoare, H. L., Beddoe, T., Reid, H. H., Wilce, M. C., Brooks, A. G. and Rossjohn, J. (2008). "CD94-NKG2A recognition of human leukocyte antigen (HLA)-E bound to an HLA class I leader sequence." J Exp Med **205**(3): 725-735.

Pogge von Strandmann, E., Shatnyeva, O. and Hansen, H. P. (2015). "NKp30 and its ligands: emerging players in tumor immune evasion from natural killer cells." Ann Transl Med **3**(20): 314.

Poggi, A., Costa, P., Tomasello, E. and Moretta, L. (1998). "IL-12-induced up-regulation of NKRP1A expression in human NK cells and consequent NKRP1A-mediated down-regulation of NK cell activation." Eur J Immunol **28**(5): 1611-1616.

Poggi, A., Costa, P., Zocchi, M. R. and Moretta, L. (1997). "NKRP1A molecule is involved in transendothelial migration of CD4+ human T lymphocytes." Immunol Lett **57**(1-3): 121-123.

Poggi, A., Costa, P., Zocchi, M. R. and Moretta, L. (1997). "Phenotypic and functional analysis of CD4+ NKRP1A+ human T lymphocytes. Direct evidence that the NKRP1A molecule is involved in transendothelial migration." Eur J Immunol **27**(9): 2345-2350.

Pozo, D., Vales-Gomez, M., Mavaddat, N., Williamson, S. C., Chisholm, S. E. and Reyburn, H. (2006). "CD161 (human NKR-P1A) signaling in NK cells involves the activation of acid sphingomyelinase." J Immunol **176**(4): 2397-2406.

Rabinovich, B., Li, J., Wolfson, M., Lawrence, W., Beers, C., Chalupny, J., Hurren, R., Greenfield, B., Miller, R. and Cosman, D. (2006). "NKG2D splice variants: a reexamination of adaptor molecule associations." Immunogenetics **58**(2-3): 81-88.

Raulet, D. H. and Guerra, N. (2009). "Oncogenic stress sensed by the immune system: role of natural killer cell receptors." Nat Rev Immunol **9**(8): 568-580.

Ravetch, J. V. and Lanier, L. L. (2000). "Immune inhibitory receptors." Science **290**(5489): 84-89.

Reeves, P. J., Callewaert, N., Contreras, R. and Khorana, H. G. (2002). "Structure and function in rhodopsin: high-level expression of rhodopsin with restricted and homogeneous N-glycosylation by a tetracycline-inducible N-acetylglucosaminyltransferase I-negative HEK293S stable mammalian cell line." Proc Natl Acad Sci U S A **99**(21): 13419-13424.

Remark, R., Alifano, M., Cremer, I., Lupo, A., Dieu-Nosjean, M. C., Riquet, M., Crozet, L., Ouakrim, H., Goc, J., Cazes, A., Flejou, J. F., Gibault, L., Verkarre, V., Regnard, J. F., Pages, O. N., Oudard, S., Mlecnik, B., Sautes-Fridman, C., Fridman, W. H. and Damotte, D. (2013). "Characteristics and clinical impacts of the immune environments in colorectal and renal cell carcinoma lung metastases: influence of tumor origin." Clin Cancer Res **19**(15): 4079-4091.

Robinson, J., Mistry, K., McWilliam, H., Lopez, R. and Marsh, S. G. (2010). "IPD--the Immuno Polymorphism Database." Nucleic Acids Res **38**(Database issue): D863-869.

Rodgers, J. R. and Cook, R. G. (2005). "MHC class Ib molecules bridge innate and acquired immunity." Nat Rev Immunol **5**(6): 459-471.

Roitt, I. M., Brostoff, J. and Male, D. K. (2001). Immunology. Edinburgh ; New York, Mosby.

Romasanta, P. N., Curto, L. M., Urtasun, N., Sarratea, M. B., Chiappini, S., Miranda, M. V., Delfino, J. M., Mariuzza, R. A., Fernandez, M. M. and Malchiodi, E. L. (2014). "A

positive cooperativity binding model between Ly49 natural killer cell receptors and the viral immunoevasin m157: kinetic and thermodynamic studies." J Biol Chem **289**(8): 5083-5096.

Rosen, D. B., Araki, M., Hamerman, J. A., Chen, T., Yamamura, T. and Lanier, L. L. (2004). "A Structural basis for the association of DAP12 with mouse, but not human, NKG2D." J Immunol **173**(4): 2470-2478.

Rosen, D. B., Bettadapura, J., Alsharifi, M., Mathew, P. A., Warren, H. S. and Lanier, L. L. (2005). "Cutting edge: lectin-like transcript-1 is a ligand for the inhibitory human NKR-P1A receptor." J Immunol **175**(12): 7796-7799.

Rosen, D. B., Cao, W., Avery, D. T., Tangye, S. G., Liu, Y. J., Houchins, J. P. and Lanier, L. L. (2008). "Functional consequences of interactions between human NKR-P1A and its ligand LLT1 expressed on activated dendritic cells and B cells." J Immunol **180**(10): 6508-6517.

Roth, P., Mittelbronn, M., Wick, W., Meyermann, R., Tatagiba, M. and Weller, M. (2007). "Malignant glioma cells counteract antitumor immune responses through expression of lectin-like transcript-1." Cancer Res **67**(8): 3540-3544.

Rother, S., Hundrieser, J., Pokoyski, C., Kollrich, S., Borns, K., Blasczyk, R., Poehnert, D., Klempnauer, J. and Schwinzer, R. (2015). "The c.503T>C Polymorphism in the Human KLRB1 Gene Alters Ligand Binding and Inhibitory Potential of CD161 Molecules." PLoS One **10**(8): e0135682.

Rozbesky, D., Adamek, D., Pospisilova, E., Novak, P. and Chmelik, J. (2016). "Solution structure of the lymphocyte receptor Nkrp1a reveals a distinct conformation of the long loop region as compared to in the crystal structure." Proteins **84**(9): 1304-1311.

Rozbesky, D., Krejzova, J., Krenek, K., Prchal, J., Hrabal, R., Kozisek, M., Weignerova, L., Fiore, M., Dumy, P., Kren, V. and Renaudet, O. (2014). "Re-evaluation of binding properties of recombinant lymphocyte receptors NKR-P1A and CD69 to chemically synthesized glycans and peptides." Int J Mol Sci **15**(1): 1271-1283.

Salih, H. R., Rammensee, H. G. and Steinle, A. (2002). "Cutting edge: down-regulation of MICA on human tumors by proteolytic shedding." J Immunol **169**(8): 4098-4102.

Sanchez, M. J., Muench, M. O., Roncarolo, M. G., Lanier, L. L. and Phillips, J. H. (1994). "Identification of a common T/natural killer cell progenitor in human fetal thymus." J Exp Med **180**(2): 569-576.

Sarkar, S., Germeraad, W. T., Rouschop, K. M., Steeghs, E. M., van Gelder, M., Bos, G. M. and Wieten, L. (2013). "Hypoxia induced impairment of NK cell cytotoxicity against multiple myeloma can be overcome by IL-2 activation of the NK cells." PLoS One **8**(5): e64835.

Sathe, P., Delconte, R. B., Souza-Fonseca-Guimaraes, F., Seillet, C., Chopin, M., Vandenberg, C. J., Rankin, L. C., Mielke, L. A., Vikstrom, I., Kolesnik, T. B., Nicholson, S. E., Vivier, E., Smyth, M. J., Nutt, S. L., Glaser, S. P., Strasser, A., Belz, G. T., Carotta, S. and Huntington, N. D. (2014). "Innate immunodeficiency following genetic ablation of Mcl1 in natural killer cells." Nat Commun **5**: 4539.

Schroder, K., Hertzog, P. J., Ravasi, T. and Hume, D. A. (2004). "Interferon-gamma: an overview of signals, mechanisms and functions." J Leukoc Biol **75**(2): 163-189.

Schwartz, J. C., Zhang, X., Fedorov, A. A., Nathenson, S. G. and Almo, S. C. (2001). "Structural basis for co-stimulation by the human CTLA-4/B7-2 complex." Nature **410**(6828): 604-608.

Scoville, S. D., Freud, A. G. and Caligiuri, M. A. (2017). "Modeling Human Natural Killer Cell Development in the Era of Innate Lymphoid Cells." Front Immunol **8**: 360.

Sepulveda, F. E., Maschalidi, S., Vosshenrich, C. A., Garrigue, A., Kurowska, M., Menasche, G., Fischer, A., Di Santo, J. P. and de Saint Basile, G. (2015). "A novel immunoregulatory role for NK-cell cytotoxicity in protection from HLH-like immunopathology in mice." Blood **125**(9): 1427-1434.

Shi, X. and Jarvis, D. L. (2007). "Protein N-glycosylation in the baculovirus-insect cell system." Curr Drug Targets **8**(10): 1116-1125.

Shibuya, A., Kojima, H., Shibuya, K., Nagayoshi, K., Nagasawa, T. and Nakauchi, H. (1993). "Enrichment of interleukin-2-responsive natural killer progenitors in human bone marrow." Blood **81**(7): 1819-1826.

Shifrin, N., Raulet, D. H. and Ardolino, M. (2014). "NK cell self tolerance, responsiveness and missing self recognition." Semin Immunol **26**(2): 138-144.

Sivori, S., Vitale, M., Morelli, L., Sanseverino, L., Augugliaro, R., Bottino, C., Moretta, L. and Moretta, A. (1997). "p46, a novel natural killer cell-specific surface molecule that mediates cell activation." J Exp Med **186**(7): 1129-1136.

Skalova, T., Blaha, J., Harlos, K., Duskova, J., Koval, T., Stransky, J., Hasek, J., Vanek, O. and Dohnalek, J. (2015). "Four crystal structures of human LLT1, a ligand of human NKR-P1, in varied glycosylation and oligomerization states." Acta Crystallogr D Biol Crystallogr **71**(Pt 3): 578-591.

Skalova, T., Kotynkova, K., Duskova, J., Hasek, J., Koval, T., Kolenko, P., Novak, P., Man, P., Hanc, P., Vanek, O., Bezouska, K. and Dohnalek, J. (2012). "Mouse Clr-g, a ligand for NK cell activation receptor NKR-P1F: crystal structure and biophysical properties." J Immunol **189**(10): 4881-4889.

Sleiman, M., Brons, N. H., Kaoma, T., Dogu, F., Villa-Forte, A., Lenoble, P., Hentges, F., Kotsch, K., Gadola, S. D., Vilches, C. and Zimmer, J. (2014). "NK cell killer Ig-like receptor repertoire acquisition and maturation are strongly modulated by HLA class I molecules." J Immunol **192**(6): 2602-2610.

Smith, J. A. and Colbert, R. A. (2014). "Review: The interleukin-23/interleukin-17 axis in spondyloarthritis pathogenesis: Th17 and beyond." Arthritis Rheumatol **66**(2): 231-241.

Soderquest, K., Walzer, T., Zafirova, B., Klavinskis, L. S., Polic, B., Vivier, E., Lord, G. M. and Martin-Fontecha, A. (2011). "Cutting edge: CD8+ T cell priming in the absence of NK cells leads to enhanced memory responses." J Immunol **186**(6): 3304-3308.

Sondergaard, H. B., Sellebjerg, F., Hillert, J., Olsson, T., Kockum, I., Linden, M., Mero, I. L., Myhr, K. M., Celius, E. G., Harbo, H. F., Christensen, J. R., Bornsen, L., Sorensen, P. S. and Oturai, A. B. (2011). "Alterations in KLRB1 gene expression and a Scandinavian multiple sclerosis association study of the KLRB1 SNP rs4763655." Eur J Hum Genet **19**(10): 1100-1103.

Spits, H., Blom, B., Jaleco, A. C., Weijer, K., Verschuren, M. C., van Dongen, J. J., Heemskerk, M. H. and Res, P. C. (1998). "Early stages in the development of human T, natural killer and thymic dendritic cells." Immunol Rev **165**: 75-86.

Spreu, J., Kuttruff, S., Stejfova, V., Dennehy, K. M., Schittek, B. and Steinle, A. (2010). "Interaction of C-type lectin-like receptors NKp65 and KACL facilitates dedicated immune recognition of human keratinocytes." Proc Natl Acad Sci U S A **107**(11): 5100-5105.

Stamper, C. C., Zhang, Y., Tobin, J. F., Erbe, D. V., Ikemizu, S., Davis, S. J., Stahl, M. L., Seehra, J., Somers, W. S. and Mosyak, L. (2001). "Crystal structure of the B7-1/CTLA-4 complex that inhibits human immune responses." Nature **410**(6828): 608-611.

Stewart, C. A., Laugier-Anfossi, F., Vely, F., Saulquin, X., Riedmuller, J., Tisserant, A., Gauthier, L., Romagne, F., Ferracci, G., Arosa, F. A., Moretta, A., Sun, P. D., Ugolini, S. and Vivier, E. (2005). "Recognition of peptide-MHC class I complexes by activating killer immunoglobulin-like receptors." Proc Natl Acad Sci U S A **102**(37): 13224-13229.

Sullivan, L. C., Berry, R., Sosnin, N., Widjaja, J. M., Deuss, F. A., Balaji, G. R., LaGruta, N. L., Mirams, M., Trapani, J. A., Rossjohn, J., Brooks, A. G. and Andrews, D. M. (2016). "Recognition of the Major Histocompatibility Complex (MHC) Class Ib Molecule H2-Q10 by the Natural Killer Cell Receptor Ly49C." J Biol Chem **291**(36): 18740-18752.

Sullivan, L. C., Clements, C. S., Beddoe, T., Johnson, D., Hoare, H. L., Lin, J., Huyton, T., Hopkins, E. J., Reid, H. H., Wilce, M. C., Kabat, J., Borrego, F., Coligan, J. E., Rossjohn, J. and Brooks, A. G. (2007). "The heterodimeric assembly of the CD94-NKG2 receptor family and implications for human leukocyte antigen-E recognition." Immunity **27**(6): 900-911.

Sullivan, L. C., Hoare, H. L., McCluskey, J., Rossjohn, J. and Brooks, A. G. (2006). "A structural perspective on MHC class Ib molecules in adaptive immunity." Trends Immunol **27**(9): 413-420.

Talmadge, J. E., Meyers, K. M., Prieur, D. J. and Starkey, J. R. (1980). "Role of NK cells in tumour growth and metastasis in beige mice." Nature **284**(5757): 622-624.

Tormo, J., Natarajan, K., Margulies, D. H. and Mariuzza, R. A. (1999). "Crystal structure of a lectin-like natural killer cell receptor bound to its MHC class I ligand." Nature **402**(6762): 623-631.

Trinchieri, G. (1989). "Biology of natural killer cells." Adv Immunol **47**: 187-376.

Triulzi, T., De Cecco, L., Sandri, M., Prat, A., Giussani, M., Paolini, B., Carcangiu, M. L., Canevari, S., Bottini, A., Balsari, A., Menard, S., Generali, D., Campiglio, M., Di Cosimo, S. and Tagliabue, E. (2015). "Whole-transcriptome analysis links trastuzumab sensitivity of breast tumors to both HER2 dependence and immune cell infiltration." Oncotarget **6**(29): 28173-28182.

Ussher, J. E., Bilton, M., Attwod, E., Shadwell, J., Richardson, R., de Lara, C., Mettke, E., Kurioka, A., Hansen, T. H., Klenerman, P. and Willberg, C. B. (2014). "CD161++ CD8+ T cells, including the MAIT cell subset, are specifically activated by IL-12+IL-18 in a TCR-independent manner." Eur J Immunol **44**(1): 195-203.

Vance, R. E., Kraft, J. R., Altman, J. D., Jensen, P. E. and Raulet, D. H. (1998). "Mouse CD94/NKG2A is a natural killer cell receptor for the nonclassical major histocompatibility complex (MHC) class I molecule Qa-1(b)." J Exp Med **188**(10): 1841-1848.

Vanek, O., Nalezkova, M., Kavan, D., Borovickova, I., Pompach, P., Novak, P., Kumar, V., Vannucci, L., Hudecek, J., Hofbauerova, K., Kopecky, V., Jr., Brynda, J., Kolenko, P., Dohnalek, J., Kaderavek, P., Chmelik, J., Gorcik, L., Zidek, L., Sklenar, V. and Bezouska, K. (2008). "Soluble recombinant CD69 receptors optimized to have an exceptional physical and chemical stability display prolonged circulation and remain intact in the blood of mice." FEBS J **275**(22): 5589-5606.

Veeramani, S., Wang, S. Y., Dahle, C., Blackwell, S., Jacobus, L., Knutson, T., Button, A., Link, B. K. and Weiner, G. J. (2011). "Rituximab infusion induces NK activation in lymphoma patients with the high-affinity CD16 polymorphism." Blood **118**(12): 3347-3349.

Vesely, M. D., Kershaw, M. H., Schreiber, R. D. and Smyth, M. J. (2011). "Natural innate and adaptive immunity to cancer." Annu Rev Immunol **29**: 235-271.

Vivier, E., Raulet, D. H., Moretta, A., Caligiuri, M. A., Zitvogel, L., Lanier, L. L., Yokoyama, W. M. and Ugolini, S. (2011). "Innate or adaptive immunity? The example of natural killer cells." Science **331**(6013): 44-49.

Vivier, E., Tomasello, E., Baratin, M., Walzer, T. and Ugolini, S. (2008). "Functions of natural killer cells." Nat Immunol **9**(5): 503-510.

Vogler, I. and Steinle, A. (2011). "Vis-a-vis in the NKC: genetically linked natural killer cell receptor/ligand pairs in the natural killer gene complex (NKC)." J Innate Immun **3**(3): 227-235.

Voskoboinik, I., Whisstock, J. C. and Trapani, J. A. (2015). "Perforin and granzymes: function, dysfunction and human pathology." Nat Rev Immunol **15**(6): 388-400.

Waggoner, S. N., Cornberg, M., Selin, L. K. and Welsh, R. M. (2011). "Natural killer cells act as rheostats modulating antiviral T cells." Nature **481**(7381): 394-398.

Walker, L. J., Kang, Y. H., Smith, M. O., Tharmalingham, H., Ramamurthy, N., Fleming, V. M., Sahgal, N., Leslie, A., Oo, Y., Geremia, A., Scriba, T. J., Hanekom, W. A., Lauer, G. M., Lantz, O., Adams, D. H., Powrie, F., Barnes, E. and Klenerman, P. (2012). "Human MAIT and CD8alphaalpha cells develop from a pool of type-17 precommitted CD8+ T cells." Blood **119**(2): 422-433.

Walzer, T., Blery, M., Chaix, J., Fuseri, N., Chasson, L., Robbins, S. H., Jaeger, S., Andre, P., Gauthier, L., Daniel, L., Chemin, K., Morel, Y., Dalod, M., Imbert, J., Pierres, M., Moretta, A., Romagne, F. and Vivier, E. (2007). "Identification, activation, and selective in vivo ablation of mouse NK cells via NKp46." Proc Natl Acad Sci U S A **104**(9): 3384-3389.

Walzer, T., Jaeger, S., Chaix, J. and Vivier, E. (2007). "Natural killer cells: from CD3(-)NKp46(+) to post-genomics meta-analyses." Curr Opin Immunol **19**(3): 365-372.

Weiner, L. M., Surana, R. and Wang, S. (2010). "Monoclonal antibodies: versatile platforms for cancer immunotherapy." Nat Rev Immunol **10**(5): 317-327.

Welte, S., Kuttruff, S., Waldhauer, I. and Steinle, A. (2006). "Mutual activation of natural killer cells and monocytes mediated by NKp80-AICL interaction." Nat Immunol **7**(12): 1334-1342.

Whiteside, T. L., Vujanovic, N. L. and Herberman, R. B. (1998). "Natural killer cells and tumor therapy." Curr Top Microbiol Immunol **230**: 221-244.

Wu, J., Cherwinski, H., Spies, T., Phillips, J. H. and Lanier, L. L. (2000). "DAP10 and DAP12 form distinct, but functionally cooperative, receptor complexes in natural killer cells." J Exp Med **192**(7): 1059-1068.

Wu, J., Song, Y., Bakker, A. B., Bauer, S., Spies, T., Lanier, L. L. and Phillips, J. H. (1999). "An activating immunoreceptor complex formed by NKG2D and DAP10." Science **285**(5428): 730-732.

Wu, J. D., Higgins, L. M., Steinle, A., Cosman, D., Haugk, K. and Plymate, S. R. (2004). "Prevalent expression of the immunostimulatory MHC class I chain-related molecule is counteracted by shedding in prostate cancer." J Clin Invest **114**(4): 560-568.

Xu, H. C., Grusdat, M., Pandyra, A. A., Polz, R., Huang, J., Sharma, P., Deenen, R., Kohrer, K., Rahbar, R., Diefenbach, A., Gibbert, K., Lohning, M., Hocker, L., Waibler, Z., Haussinger, D., Mak, T. W., Ohashi, P. S., Lang, K. S. and Lang, P. A. (2014). "Type I interferon protects antiviral CD8+ T cells from NK cell cytotoxicity." Immunity **40**(6): 949-960.

Yokoyama, W. M., Jacobs, L. B., Kanagawa, O., Shevach, E. M. and Cohen, D. I. (1989). "A murine T lymphocyte antigen belongs to a supergene family of type II integral membrane proteins." J Immunol **143**(4): 1379-1386.

Yokoyama, W. M. and Plougastel, B. F. (2003). "Immune functions encoded by the natural killer gene complex." Nat Rev Immunol **3**(4): 304-316.

Zambrano-Zaragoza, J. F., Romo-Martinez, E. J., Duran-Avelar Mde, J., Garcia-Magallanes, N. and Vibanco-Perez, N. (2014). "Th17 cells in autoimmune and infectious diseases." Int J Inflam **2014**: 651503.

Zelensky, A. N. and Gready, J. E. (2003). "Comparative analysis of structural properties of the C-type-lectin-like domain (CTLD)." Proteins **52**(3): 466-477.

Zelensky, A. N. and Gready, J. E. (2005). "The C-type lectin-like domain superfamily." FEBS J **272**(24): 6179-6217.

Zimmer, J., Donato, L., Hanau, D., Cazenave, J. P., Tongio, M. M., Moretta, A. and de la Salle, H. (1998). "Activity and phenotype of natural killer cells in peptide transporter (TAP)-deficient patients (type I bare lymphocyte syndrome)." J Exp Med **187**(1): 117-122.

Zuo, J., Willcox, C. R., Mohammed, F., Davey, M., Hunter, S., Khan, K., Antoun, A., Katakia, P., Croudace, J., Inman, C., Parry, H., Briggs, D., Malladi, R., Willcox, B. E. and Moss, P. (2017). "A disease-linked ULBP6 polymorphism inhibits NKG2D-mediated target cell killing by enhancing the stability of NKG2D ligand binding." Sci Signal **10**(481).

PUBLICATION I

Bláha, J., Pachl, P., Novák, P., Vaněk, O.

Expression and purification of soluble and stable ectodomain of natural killer receptor LLT1 through high-density transfection of suspension adapted HEK293S GnTI$^-$ cells

Protein Expr. Purif. 109, 7-13 (2015)

My contribution to the publication: *performing research (cloning, protein expression and purification, transfection optimization, protein characterization and crystallization), data collection, data analysis and interpretation, manuscript writing*

Protein Expression and Purification 109 (2015) 7–13

Contents lists available at ScienceDirect

Protein Expression and Purification

journal homepage: www.elsevier.com/locate/yprep

Expression and purification of soluble and stable ectodomain of natural killer cell receptor LLT1 through high-density transfection of suspension adapted HEK293S GnTI$^-$ cells

Jan Bláha [a], Petr Pachl [b], Petr Novák [a,c], Ondřej Vaněk [a,*]

[a] Department of Biochemistry, Faculty of Science, Charles University in Prague, Hlavova 8, Prague 12840, Czech Republic
[b] Institute of Organic Chemistry and Biochemistry, Academy of Sciences of the Czech Republic, Flemingovo nám. 2, Prague 16610, Czech Republic
[c] Institute of Microbiology, Academy of Sciences of the Czech Republic, Vídeňská 1083, Prague 14220, Czech Republic

ARTICLE INFO

Article history:
Received 12 December 2014
and in revised form 15 January 2015
Available online 24 January 2015

Keywords:
LLT1
HEK293S GnTI$^-$
C-type lectin-like
NK cell
Glycosylation
Transfection

ABSTRACT

Lectin-like transcript 1 (LLT1, gene *clec2d*) was identified to be a ligand for the single human NKR-P1 receptor present on NK and NK-T lymphocytes. Naturally, LLT1 is expressed on the surface of NK cells, stimulating IFN-γ production, and is up-regulated upon activation of other immune cells, e.g. TLR-stimulated dendritic cells and B cells or T cell receptor-activated T cells. While in normal tissues LLT1:NKR-P1 interaction (representing an alternative "missing-self" recognition system) play an immunomodulatory role in regulation of crosstalk between NK and antigen presenting cells, LLT1 is upregulated in glioblastoma cells, one of the most lethal tumors, where it acts as a mediator of immune escape of glioma cells.

Here we report transient expression and characterization of soluble His176Cys mutant of LLT1 ectodomain in an eukaryotic expression system of human suspension-adapted HEK293S GnTI$^-$ cell line with uniform N-glycans. The His176Cys mutation is critical for C-type lectin-like domain stability, leading to the reconstruction of third canonical disulfide bridge in LLT1, as shown by mass spectrometry. Purified soluble LLT1 is homogeneous, deglycosylatable and forms a non-covalent homodimer whose dimerization is not dependent on presence of its N-glycans.

As a part of production of soluble LLT1, we have adapted HEK293S GnTI$^-$ cell line to growth in suspension in media facilitating transient transfection and optimized novel high cell density transfection protocol, greatly enhancing protein yields. This transfection protocol is generally applicable for protein production within this cell line, especially for protein crystallography.

Introduction

Natural killer (NK[1]) cells are large granular lymphocytes that are able to destroy tumor, virally infected or stressed cells based on equilibrium between stimulatory and inhibitory signals mediated by their surface recognition receptors [1]. While the role of some NK cell receptors in antitumor immunity is described in relatively great detail, on the other hand, the possible utilization of soluble receptor domains in antitumor therapy is only beginning to be explored. The main NK cell activating receptors studied in this respect include C-type lectin-like NKG2D receptor and immunoglobulin-like receptor NKp30 [1]. For example, the soluble NKp30–Fc_IgG fusion protein was shown to inhibit the growth of prostate cancer cell line *in vivo*, including complete tumor removal in 50% of mice [2]. In another study, a synergy was observed when bifunctional anti-CD20 scFv fusions with natural ligands for NKp30 and NKG2D receptors were combined [3] and it could be expected that further increase in antitumor potency might be reached by simultaneous targeting of other activation or co-stimulatory receptors, e.g. NKp80, NKp65 or LLT1. Therefore technologies leading to production of soluble domains of these receptors as well as of their ligands in good yield and stability are needed.

Lectin-like transcript 1 (LLT1, gene *clec2d*) is a type II transmembrane receptor belonging to the C-type lectin like (CTL) superfamily of natural killer cell receptors. Six alternatively spliced transcripts of *clec2d* gene were identified, with the isoform 1

* Corresponding author at: Department of Biochemistry, Faculty of Science, Charles University in Prague, Hlavova 2030, Prague 12840, Czech Republic. Tel.: +420 22195 1272; fax: +420 22195 1283.
E-mail address: ondrej.vanek@natur.cuni.cz (O. Vaněk).

[1] *Abbreviations used:* CTL, C-type lectin-like; dpt, days post-transfection; GFP, green fluorescent protein; GnTI$^-$, N-acetylglucosaminyltransferase I negative; HEK, human embryonic kidney; NK, natural killer; LLT1, lectin-like transcript 1; lPEI, linear polyethylenimine; PBS, phosphate buffered saline; pNPP, *p*-nitrophenyl phosphate; SEAP, secreted alkaline phosphatase; SEC, size exclusion chromatography; WT, wild-type.

http://dx.doi.org/10.1016/j.pep.2015.01.006
1046-5928/

(designated as LLT1) being the only one presented on the cell surface, thus being the only isoform able to participate in the cell to cell signal transmission [4]. LLT1 is expressed mainly on activated lymphocytes (NK cells, T cells, B cells) and antigen presenting cells, i.e. macrophages and dendritic cells [5].

Almost a decade ago, LLT1 was identified as a physiological ligand of NKR-P1 (CD161, gene *klrb1*) – the only described representative of human NKR-P1 subfamily [6,7]. NK cell cytotoxicity and IFNγ production is inhibited upon engagement of NKR-P1 on NK cell with LLT1 on target cell [6,7]. It has been shown that this mechanism contributing to NK self-tolerance is being exploited by the human glioblastoma cells that are escaping the appropriate immunological response by up-regulating the surface expression of LLT1 [8]. However, in response to microbial and viral stimuli LLT1 expression is up-regulated on surface of epithelial cells [9], and also IFNγ increases LLT1 expression on B cells and antigen presenting cells [5]. Upon ligation with CD161 these cells can co-stimulate T cell proliferation, cytokine secretion and proinflammatory responses. Therefore LLT1:NKR-P1 signalization represents a system that regulates both innate and adaptive immune responses and may provide a link between pathogen pattern recognition and lymphocyte activation [9].

The polypeptide chain of LLT1 can be divided into the N-terminal cytoplasmic part, transmembrane and stalk regions and C-terminal CTL ectodomain with two predicted N-glycosylation sites. While homologous CTL receptors usually contain two or three canonical disulfide bonds corresponding to four or six cysteines within their CTL domain, respectively [10], the CTL domain of LLT1 contains five conserved cysteine residues. Thus, two putative canonical disulfide bridges (Cys75–Cys86 and Cys103–Cys184) may be formed leaving Cys163 unpaired. Previously [11] reported that the mutation of His176 residue to Cys176 improves on stability of recombinant LLT1 ectodomain expressed in *Escherichia coli* and refolded from inclusion bodies *in vitro*, hence proposing that this mutation might reconstruct the third disulfide bridge.

Here we report a transient gene expression of LLT1 ectodomain H176C mutant in suspension adapted HEK293S N-acetylglucosaminyltransferase I negative (GnTI$^-$) cell line, originally developed for expression of rhodopsin mutants [12], that provides recombinant proteins with homogeneous $GlcNAc_2Man_5$ N-linked oligosaccharides, making them excellent for structural and biophysical studies. Unfortunately this quality is often repaid by lower yields of protein [13]. Current production protocols reported so far are based either on rather slow generation of stably transfected cell lines [12] or transient transfection using adherent cell culture which might get laborious and material consuming when scaling-up with the yields reportedly being lower when compared to other HEK293 cell line derivatives, e.g. HEK293T or HEK293E [14]. In order to improve the transfection efficiency and productivity of HEK293S GnTI$^-$ cell line we have adapted these cells to growth in suspension and optimized for them a high-density transfection protocol previously reported for HEK293E cells [15–17], thus greatly enhancing the protein yields when compared to standard low-density transfection. This transfection protocol is generally applicable for protein production within this cell line, especially for protein crystallography.

Materials and methods

Vectors and cloning

The pTTo3c_SSH and pTTo_GFPq vectors containing SEAP and GFP, respectively, were kindly provided by Dr. Yves Durocher [18] as well as pTT28 plasmid, a derivative of pTT5 [18] containing N-terminal secretion leader and C-terminal His_8-tag sequence (leaving ITG- and -GTKHHHHHHHHG at expressed protein N- and C-termini), whose multiple cloning site was further modified to include AgeI and KpnI restriction sites. Total RNA was isolated from human spleen with TRIzol and used as template for single stranded cDNA synthesis using Superscript III reverse transcriptase (both Invitrogen, USA). DNA fragment coding for LLT1 was amplified using 5′ TGCAAGCTGCATGCCCAGAAAG 3′ and 5′ CCTCGA GCTAGACATGTATATCTGATTTGGA 3′ primers and the PCR product was subcloned into the SmaI site of pBluescript SK + cloning vector (Stratagene, USA). The extracellular portion of LLT1 (Q72-V191) was amplified from the cloning vector using 5′ AAAAAAACC GGTCAAGCTGCATGCCCAGAAAGC 3′ and 5′ AAAAAAGGTACCGAC ATGTATATCTGATTTGGAACAAATC 3′ primers and subcloned into the pTT28 expression plasmid using AgeI and KpnI sites. Mutant constructs of LLT1 were prepared by overlap extension PCR [19,20], using the prepared expression plasmid as template and aforementioned primers as forward and reverse primers. The specific forward primers used for preparation of C163S and H176C mutants have been 5′ GAGCAGGAGAGTCTGCCTATTTGAA 3′ and 5′ GTAGTGCCAGGTGCTACACAGAGAG 3′, respectively.

Cell culture

The HEK293T cells were kindly provided by Dr. Radu A. Aricescu [14]. The HEK293S GnTI$^-$ cell line was purchased from ATCC (CRL-3022) [12]. These adherent cultures were firstly adapted to growth in EX-CELL293 serum-free medium (Sigma, USA) supplemented with 4 mM L-glutamine on Petri dishes by consecutive subcultivations until the cells resumed normal growth rate (doubling time approx. 24 h) and later were adapted to growth in suspension in mixture of equal volumes of EX-CELL293 supplemented as above and Freestyle F17 (Invitrogen, USA) supplemented with 4 mM L-glutamine and 0.1% Pluronic F-68 (Sigma, USA) in shaken square-shaped glass bottles with permeable filter caps (DURAN, Germany) using 30-40% filling volume at 135 rpm (Orbit1000 shaker; Labnet, USA) in humidified 37 °C, 5% CO_2 incubator. The cell density was kept between 0.2 and 6.0 × 10^6 cells/ml.

Low-scale transfection

Day before transfection cells were centrifuged and resuspended in fresh supplemented F17 medium (1.0 × 10^6 cells/ml). Next day, cell density was adjusted to 2.0 × 10^6 cells/ml and 1 ml was distributed per well in 12-well plate. Transfection mix was prepared by diluting DNA (1 μg/10^6 cells) to 0.1 ml PBS (1/10 transfection culture volume), 1 mg/ml solution of 25 kDa linear polyethylenimine (lPEI; Polysciences, USA) was added to desired ratio, the mixture was immediately vigorously shaken and following 5 min incubation added to the cell suspension. After 4 h incubation the suspension was diluted with 1 ml of EX-CELL293 to 1.0 × 10^6/ml final density. For high-density transfection the cells were prepared on the day of transfection. Cells were centrifuged and resuspended in fresh supplemented EX-CELL293 medium (25 × 10^6 cells/ml) and 0.4 ml was distributed per well in 12-well plate. The suspension was then diluted with approximately 0.1 ml of transfection mix (prepared as above) to 20 × 10^6 cells/ml. After 4 h incubation 0.1 ml of this suspension was diluted with 1.9 ml of EX-CELL293 in new 12-well plate to final density of 1.0 × 10^6/ml.

SEAP and GFP analysis

Determination of SEAP activity (ΔA_{410}/min) was performed as previously described [18]. Briefly, HEK293 cells were transfected with 19:1 (w/w) mixture of pTTo3c_SSH and pTTo_GFPq plasmids. Three dpt culture supernatants were diluted with water as required (typically 1/1000), 180 μl were transferred to 96-well

plate, 20 μl of SEAP assay solution (20 mM *p*-nitrophenyl phosphate (pNPP), 1 mM $MgCl_2$ and 1 M diethanolamine, pH 9.8) were added and absorbance was read at 410 nm at 1 min intervals to determine pNPP hydrolysis rates (Safire reader; Tecan, Austria). Each sample was assayed for SEAP activity three times independently to avoid pipetting errors. Transfection efficiency was assayed by BD LSR II flow cytometer (BD Biosciences, USA). GFP-positive viable cells were quantified by using appropriate gating to exclude dead cells (stained with propidium iodide), debris and aggregates in forward vs. side scatter plot. Data are shown as mean of one experiment performed in triplicate with error bars representing standard deviation.

Protein production and purification

For LLT1 production, 400 μg of the respective expression plasmid was diluted in PBS, filter-sterilized and 25 kDa lPEI was added in 1:3 weight ratio to final volume of 4 ml, the mixture was shaken and incubated for 5 min. Meanwhile, 400×10^6 HEK293S GnTI$^-$ cells were centrifuged and resuspended in EX-CELL293 (if not specified otherwise) at 25×10^6 cells/ml and immediately transfected. Following 4 h incubation culture was diluted to 400 ml with EX-CELL293. Two dpt, culture was fed with 0.5% Tryptone N1 (Organotechnie, France) [21]. 5-7 dpt culture medium was harvested by centrifugation (4000×*g*, 30 min), filtered (0.22 μm Steritop filter; Millipore, USA), and stored at −20 °C or immediately processed. Medium was diluted twofold with PBS (50 mM Na_2HPO_4, 300 mM NaCl, 10 mM NaN_3) and pH was adjusted to 7.0. The protein was recovered by batch IMAC chromatography on TALON beads (Clontech, USA; elution by 250 mM imidazole within the PBS buffer) with subsequent SEC on Superdex 200 10/300 GL column (GE Healthcare, USA) in 10 mM HEPES, 150 mM NaCl, 10 mM NaN_3, pH 7.5 buffer and concentrated on AmiconUltra concentrator (10,000 MWCO; Millipore, USA).

Sedimentation analysis

Molecular weight of the produced protein was analyzed in an analytical ultracentrifuge ProteomeLab XL-I equipped with An-50 Ti rotor (BeckmanCoulter, USA) using sedimentation equilibrium experiment. Native and deglycosylated LLT1(H176C) diluted with SEC buffer to 0.07 and 0.09 mg/ml, respectively, were measured at 4 °C using absorbance optics at 280 nm in 0.11 ml total volume at 12–15–18–21–24–27–30,000 rpm after reaching the equilibrium for 18 h at each given speed. Buffer density and protein partial specific volume were estimated in Sednterp 1.09 (www.jphilo.mailway.com). The data were analyzed using Sedphat 10.58d software [22] using single non-interacting discrete species model.

Mass spectrometry

Disulfide bonds in LLT1 were determined according to the previously published protocol [23]. Briefly, the protein was separated by SDS–PAGE, deglycosylated by ENDO Hf (New England Biolabs, USA) and digested by trypsin (Sigma, USA) under non-reducing conditions in the presence of 200 μM cystamine. The peptide mixtures were desalted on peptide MacroTrap and separated on reverse phase MAGIC C18 columns (both Michrom BioResources, USA) connected directly to an APEX-Q 9.4 T FT-ICR mass spectrometer (Bruker Daltonics, USA) using an electrospray ion source. Data were acquired using ApexControl 3.0.0 and processed with DataAnalysis 4.0. The disulfide bonds and saccharide moieties were identified using Links software [24].

Protein crystallization

LLT1 solution concentrated to 13.8 mg/ml was crystallized using vapor diffusion method in sitting drop (50 μl reservoir volume). Drops were set up by crystallization robot Crystal Gryphon (Art Robbins Instruments, USA) by mixing 200 nl of both reservoir (JCSG + Suite; Qiagen, USA) and protein solutions at 15 °C. The successful crystallization condition reservoir contained 40% (v/v) PEG 300 and 0.1 M citrate phosphate buffer (pH 4.2). Rod shaped crystals of approximately $150 \times 50 \times 50$ μm in size grew within 14 days.

Results and discussion

Reconstruction of third disulfide bridge is crucial for stability of LLT1 ectodomain

The C-type lectin-like ectodomain of LLT1 contains five cysteine residues and the multiple alignment analysis shows that only two out of three putative disulfide bonds are thus conceivable, with Cys163 residue left unpaired (Fig. 1A). Earlier it has been proposed that mutation of His176 to Cys176 leads to reconstruction of the third disulfide bridge [11]. Initially, we have produced the wild-type (WT) LLT1 ectodomain (Q72-V191) in HEK293T cells; however the purified protein was heterogeneous and was prone to aggregation (Fig. 1B). Based on these results and assumptions we have prepared C163S and H176C mutant forms of soluble LLT1 ectodomain. While the mutation of odd Cys163 residue to Ser163 led to very low yield of recoverable product, the mutation of His176 to Cys176 led to monodisperse and stable product (Fig. 1B). These findings correlate very well with previously reported data of unstable WT and C163S mutant LLT1 ectodomain renaturated from *E. coli* expressed inclusion bodies [11] and suggest structurally stabilizing role of the third disulfide bridge in LLT1(H176C) ectodomain.

Furthermore, using mass spectrometry approach [23] we were able to identify the cystine peptides in the H176C mutant and WT soluble LLT1. While in case of WT we have observed quite heterogeneous configuration of disulfide bridges with majority of Cys163 participating in covalent bond with Cys184 and only very small percentage left unpaired (supplementary data, Table S1), we were able to confirm the reconstruction of Cys163–Cys176 putative disulfide bridge in H176C mutant protein (Fig. 1C and supplementary data, Table S2). Moreover, we were able to confirm the presence of saccharide moiety at both predicted N-glycosylation sites (Fig. 1A and supplementary data, Table S2). The incomplete occupancy of these two possible sites accounts for two different glycoforms as observed on SDS–PAGE (see below).

High-density transfection of HEK293S GnTI$^-$ cells substantially improves transfection efficiency and expression yields

In order to produce glycosylated ectodomain of LLT1 with homogeneous N-glycans for structural and biophysical studies we have investigated the optimal transfection conditions for suspension adapted HEK293S GnTI$^-$ cell line [12], based on previously published transfection protocols for suspension adapted HEK293E cells [15,18]. The adherent HEK293S GnTI$^-$ and HEK293T cultures were adapted to growth in suspension in equal mixture of serum-free EX-CELL293 and Freestyle F17 media in shaken square bottles, as described in methods (2.2). For evaluation of transfection efficiency and production of secreted recombinant protein we have used previously adopted reporter genes – green fluorescent protein (GFP) and secreted alkaline phosphatase (SEAP), respectively [18]. Initially we have found that protocol optimized

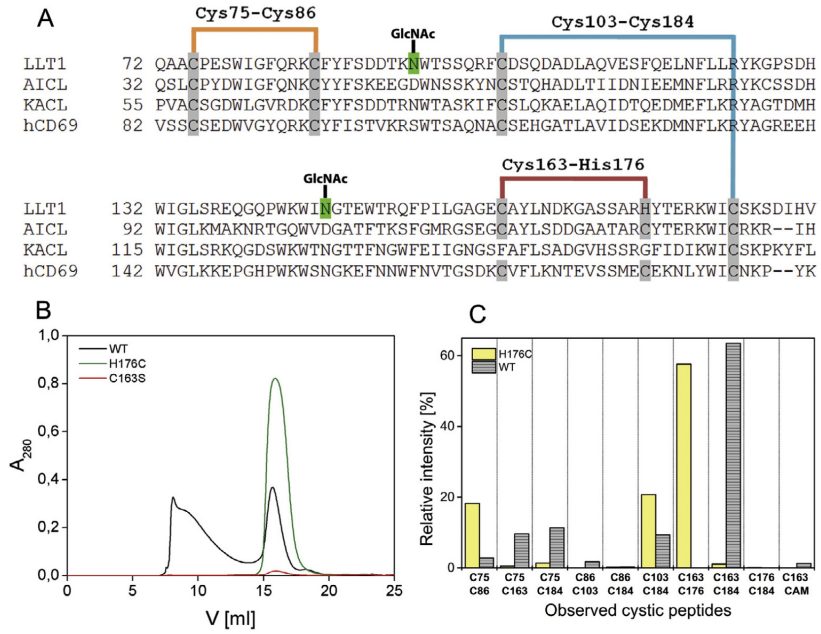

Fig. 1. The reconstruction of disulfide bridge improves folding and yield of soluble LLT1. (A) Multiple sequence alignment of C-type lectin-like domain sequences of receptors from human *clec2* gene family showing conserved cysteines in gray and their disulfidic pairing; reconstructed disulfide bridge in LLT1(H176C) mutant is high-lighted in red and N-glycosylation sites in green. (B) Size exclusion chromatography of soluble LLT1 wild-type (black) and mutant H176C (green) and C163S (red) proteins produced in HEK293T cell line. (C) Mass spectrometry analysis of disulfide bond pattern in wild-type and LLT1(H176C) mutant; proteins produced in HEK293S GnTI$^-$ cell line were purified by IMAC and SEC chromatography and samples corresponding to peak at 16 ml position on SEC run shown in B were deglycosylated, digested and the resultant cystic peptides were analyzed by FT-ICR MS as described in methods, the relative intensity of observed cystic peptides (error below 3 ppm) is shown. (For interpretation of the references to color in this figure legend, the reader is referred to the web version of this article.)

for suspension adapted HEK293T cells used routinely in our laboratory – transfection at density of 2.0×10^6 cells/ml in Freestyle F17 (medium exchanged one day prior to transfection), transfection complexes formed *a priori* with 2 μg/ml of DNA (final concentration) at optimal 1:3 DNA:PEI weight to weight ratio – was quite inefficient for transfection of HEK293S GnTI$^-$ cells (Fig. 2, yellow vs. cyan columns).

The obvious difference between the HEK293T and HEK293S GnTI$^-$ cells is the lack of complex glycans resulting also in loss of a sulfated negatively charged glycans displayed at the cell surface that might attract positively charged DNA:PEI polyplexes. We have thus theorized that by increasing the concentration of DNA and PEI during the transfection process we could improve the transfection efficiency. This prompted us to test the previously reported protocol for transient transfection of suspension adapted HEK293E cells in EX-CELL293 medium at high cell density [15]. Interestingly, transfection of HEK293S GnTI$^-$ cells at high cell density (20×10^6 cells/ml in EX-CELL293 with final DNA concentration of 20 μg/ml) proved to be much more efficient with up to 5-fold increase in transfection efficiency measured as percentage of GFP positive

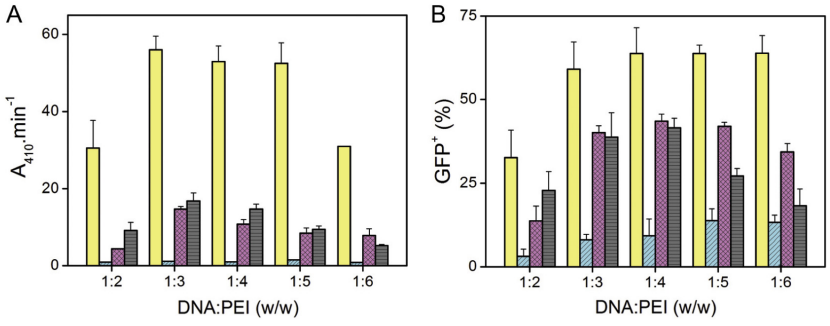

Fig. 2. High-density transfection of HEK293SGnTI$^-$ cells under optimized DNA:PEI ratio increases transfection efficiency and cell productivity. (A) Secreted protein production (measured as SEAP activity) and (B) transfection efficiency (GFP$^+$ viable cells) of suspension adapted HEK293T cells (yellow) and HEK293S GnTI$^-$ cells (cyan) transfected at density of 2.0×10^6 cells/ml and HEK293S GnTI$^-$ cells transfected at density of 20×10^6 cells/ml with transfection complex formed *a priori* (gray) or *in situ* (magenta) was monitored 3 dpt; error bars – standard deviations (one experiment performed in triplicate). (For interpretation of the references to color in this figure legend, the reader is referred to the web version of this article.)

viable cells (Fig. 2B). While the yield of model secreted protein was still quite lower when compared to our routine protocol with HEK293T cells (such trend is not unusual for HEK293S GnTI⁻ cell line and was observed in previous studies [13]), it was still substantially increased when compared to the original low density transfection protocol (Fig. 2A). Furthermore, we compared both the *a priori* and *in situ* approach for formation of DNA:PEI transfection complexes in small scale (Fig. 2) and found the effect of both these approaches comparable with the *a priori* approach giving slightly better results. This is in very good agreement with previously reported higher yields with *a priori* complex formation [15,25].

High-density transfection of HEK293S GnTI⁻ cells has comparable yield for a priori and in situ DNA:PEI complex formation

To confirm our results on non-model secreted protein we have used our optimized high-density transfection protocol for production of mutant LLT1(H176C) ectodomain in HEK293S GnTI⁻ cells at 400 ml scale. We have further investigated the effect of *a priori* and *in situ* approach for transfection complexes formation at this scale as well as the effect of Freestyle F17 as the medium for incubation of cells at high density during the transfection. Unlike to the transfection at low cell density (data not shown) we were able to recover substantial amount of recombinant protein using the high-density transfection, routinely yielding approx. 3 mg per liter of HEK293S GnTI⁻ production culture. And in agreement with the previous data we recovered higher yields with the *a priori* transfection complexes approach (Fig. 3A). However, we found that the high-density transfection in Freestyle F17 media with *a priori* complex formation is performing quite worse than in the EX-CELL293 – about 2-fold decrease in yield was observed (Fig. 3A). Based on these results we can recommend transfecting the suspension adapted HEK293S GnTI⁻ cells in EX-CELL293 using the *a priori* approach, although we recognize that the *in situ* approach would be more suitable at even larger production scale, e.g. in bioreactor where it would allow for sequential addition of DNA and lPEI solutions through sterile filter equipped inlet ports (DNA:lPEI polyplexes cannot be sterile filtered).

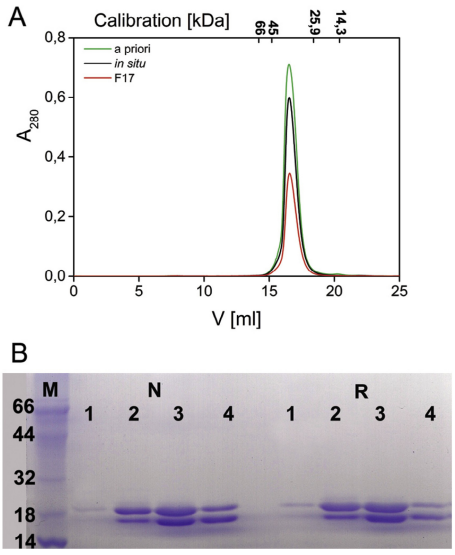

Fig. 3. EX-CELL293 medium is suitable for high-density transfection of HEK293S GnTI⁻ cell line. (A) Size exclusion chromatography profiles of LLT1(H176C) protein purified from cell culture supernatants of HEK293S GnTI⁻ cells transfected at 20×10^6 cells/ml in Freestyle F17 medium (red) or in EX-CELL293 medium with *a priori* (green) or *in situ* (black) transfection complexes formation; position of elution peaks of protein molecular weight standards is shown on the top axis. (B) Representative SDS–PAGE analysis of elution peak fractions from size exclusion chromatography analyzed under non-reducing (N) and reducing (R) conditions; M – molecular weight standards in kDa. (For interpretation of the references to color in this figure legend, the reader is referred to the web version of this article.)

LLT1 forms non-covalent dimer in solution independently of its N-glycans

While on SDS–PAGE, under both reducing and non-reducing conditions, the soluble LLT1(H176C) mutant migrates as two distinct monomeric glycoforms (Fig. 3B), SEC on Superdex 200 10/300 GL column used as final purification step suggested that LLT1(H176C) soluble ectodomain elutes as a non-covalent dimer (Fig. 3A). This finding was further corroborated using sedimentation equilibrium analysis in analytical ultracentrifuge (Fig. 4A). Fitting the data with the single ideal species model yielded a weight average molecular weight of 35,500 ± 500 Da which is in good agreement with a theoretical 36,191 Da weight of LLT1(H176C) dimer (including $GlcNAc_2Man_5$ oligosaccharides at both N-glycosylation sites), especially given the partial occupancy of the N-glycosylation sites. This observation is in contrast to previously published data for *E. coli* expressed and refolded LLT1(H176C) ectodomain obtained via SEC suggesting monomeric soluble protein [11].

We were therefore interested whether the presence of glycosylation might be the reason for dimer association. Towards this end we performed deglycosylation of various forms of LLT1 soluble ectodomain with endoglycosidase F1 [26]. As could be seen from SDS–PAGE analysis performed under non-reducing conditions, wild-type LLT1 ectodomain (fraction taken from the peak at 16 ml position on SEC run shown in Fig. 1B) forms besides monomer also a disulfidic dimer of approx. 40 kDa (Fig. 4C, lane WT), most probably an artifact caused by mixed disulfide pairing due to the presence of odd cysteine residue. For LLT1(H176C) mutant only monomer is observed, with N-glycans heterogeneity dramatically reduced when expressed in HEK293S GnTI⁻ cells, allowing also for complete protein deglycosylation (Fig. 4C, lanes GnTI⁻ and $GnTI_D$, respectively). However, sedimentation equilibrium analysis of deglycosylated protein (Fig. 4B) yielded weight average molecular weight of 32,400 ± 500 Da, again pointing for non-covalent dimer (theor. 32,135 Da for deglycosylated protein dimer). It should be noted that molecular weights derived from sedimentation equilibrium analysis are far more precise than that from SEC since it is direct thermodynamical method not dependent on calibration or interaction with column matrice. Also, the closest homologs of LLT1 from *clec2* gene family, i.e. CD69 and KACL, were found to form non-covalent dimers in solution and dimerization of KACL is presumed to increase affinity towards its monomeric ligand [27,28]. Furthermore, the prepared soluble LLT1(H176C) mutant with homogeneous $GlcNAc_2Man_5$ N-glycans (although still being inhomogeneous with respect to incomplete N-glycosylation site occupancy) was readily crystallized using the vapor diffusion method in sitting drop, forming hexagonal 3D rods (Fig. 4D) up to 150 μm in size. These primary crystals already provided protein diffraction up to resolution of 3.2 Å and were later optimized leading to solution of LLT1 crystal structure [29].

Conclusions

To conclude, we have optimized high-density transfection protocol for suspension adapted HEK293S GnTI⁻ cell line and used it

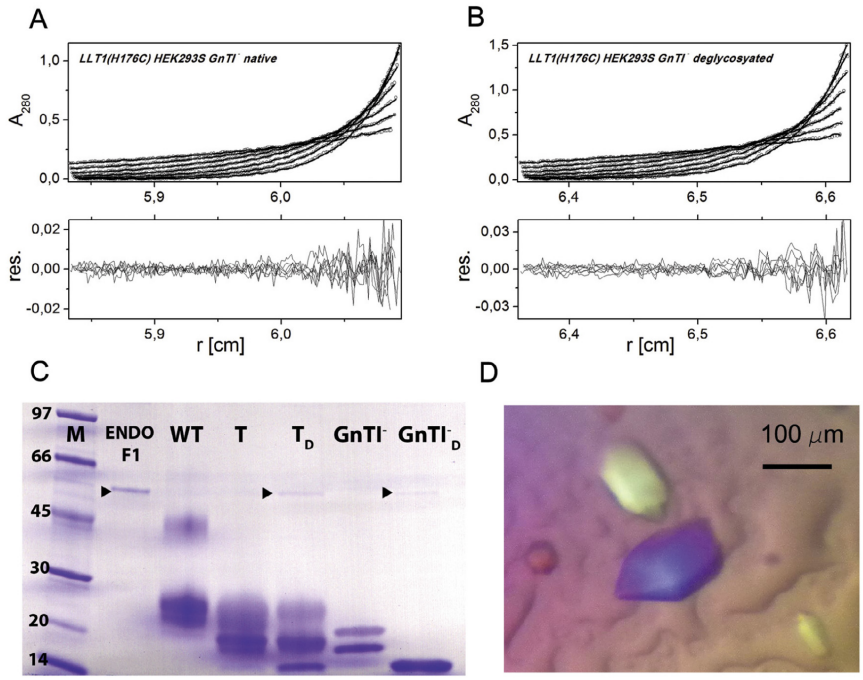

Fig. 4. LLT1(H176C) protein forms non-covalent dimer in solution, is easily deglycosylated and crystallizes. (A) and (B) Sedimentation equilibrium analysis in analytical ultracentrifuge has shown that both native and deglycosylated LLT1(H176C) produced in HEK293S GnTI⁻ cells behaves as non-covalent homodimer in solution; upper panels – absorbance data with fitted curves (single non-interacting discrete species model), lower panels – residual plot showing the goodness of fit. (C) SDS–PAGE analysis of LLT1(H176C) deglycosylation under non-reducing conditions; M – molecular weight standards in kDa, ENDO F1 – endoglycosidase F1 used for deglycosylation (arrow), WT – wild-type LLT1 produced in HEK293T cells, T and T_D – native and deglycosylated LLT1(H176C) produced in HEK293T cells, GnTI⁻ and $GnTI^-_D$ – native and deglycosylated LLT1(H176C) produced in HEK293S GnTI⁻ cells. (D) Crystals of native LLT1(H176C) protein produced in HEK293S GnTI⁻ cell line.

for production of LLT1(H176C) mutant ectodomain that forms stable, deglycosylatable and crystallizable non-covalent homodimer in solution which formation is not dependent upon presence of N-glycans. To our knowledge, this is the first attempt at structural characterization of human LLT1 immunoreceptor. The strategy of construct design described herein for LLT1 – i.e. the restoration of disulfidic bond pairing pattern – might be considered also for other C-type lectin-like receptors of NK cells, either for protein production aimed at structural characterization or for production of stable soluble receptor domains that could be utilized in clinical therapy. Apart from LLT1, the high-density transfection protocol described here was within our laboratory successfully used for production of different soluble receptor domains as well as other recombinant proteins and is generally applicable for protein production within HEK293S GnTI⁻ cell line, especially for protein crystallography.

Acknowledgments

We thank Dr. Yves Durocher for the pTT28, pTTo3c_SSH and pTTo_GFPq plasmids and Dr. Radu A. Aricescu for HEK293T cell line. This work was supported by Charles University in Prague (GAUK 403211/2010, UNCE 204025/2012, SVV 260079/2014), High Education Development Fund (FRVS 669/2013), Institutional Research Concept of the Institute of Microbiology (RVO61388971) and grants from Ministry of Education, Youth and Sports of the Czech Republic and European Regional Development Funds (CZ.1.07/2.3.00/30.0003 and CZ.1.05/1.1.00/02.0109). Access to instrumental and other facilities was supported by EU (Operational Program Prague – Competitiveness project CZ.2.16/3.1.00/24023). The research leading to these results has received funding from the European Community's Seventh Framework Programme (FP7/2007-2013) under BioStruct-X (grant agreement N°283570) and from Instruct, part of the European Strategy Forum on Research Infrastructures (ESFRI) supported by national member subscriptions.

Appendix A. Supplementary data

Supplementary data associated with this article can be found, in the online version, at http://dx.doi.org/10.1016/j.pep.2015.01.006.

References

[1] E. Vivier, E. Tomasello, M. Baratin, T. Walzer, S. Ugolini, Functions of natural killer cells, Nat. Immunol. 9 (2008) 503–510.
[2] T.I. Arnon, G. Markel, A. Bar-Ilan, J. Hanna, E. Fima, F. Benchetrit, R. Galili, A. Cerwenka, D. Benharroch, N. Sion-Vardy, A. Porgador, O. Mandelboim, Harnessing soluble NK cell killer receptors for the generation of novel cancer immune therapy, PLoS One 3 (2008) e2150.
[3] C. Kellner, T. Maurer, D. Hallack, R. Repp, J.G. van de Winkel, P.W. Parren, T. Valerius, A. Humpe, M. Gramatzki, M. Peipp, Mimicking an induced self phenotype by coating lymphomas with the NKp30 ligand B7–H6 promotes NK cell cytotoxicity, J. Immunol. 189 (2012) 5037–5046.
[4] C. Germain, F. Bihl, S. Zahn, G. Poupon, M.J. Dumaurier, H.H. Rampanarivo, S.B. Padkjaer, P. Spee, V.M. Braud, Characterization of alternatively spliced transcript variants of CLEC2D gene, J. Biol. Chem. 285 (2010) 36207–36215.

[5] C. Germain, A. Meier, T. Jensen, P. Knapnougel, G. Poupon, A. Lazzari, A. Neisig, K. Hakansson, T. Dong, N. Wagtmann, E.D. Galsgaard, P. Spee, V.M. Braud, Induction of lectin-like transcript 1 (LLT1) protein cell surface expression by pathogens and interferon-gamma contributes to modulate immune responses, J. Biol. Chem. 286 (2011) 37964–37975.
[6] H. Aldemir, V. Prod'homme, M.J. Dumaurier, C. Retiere, G. Poupon, J. Cazareth, F. Bihl, V.M. Braud, Cutting edge: lectin-like transcript 1 is a ligand for the CD161 receptor, J. Immunol. 175 (2005) 7791–7795.
[7] D.B. Rosen, J. Bettadapura, M. Alsharifi, P.A. Mathew, H.S. Warren, L.L. Lanier, Cutting edge: lectin-like transcript-1 is a ligand for the inhibitory human NKR-P1A receptor, J. Immunol. 175 (2005) 7796–7799.
[8] P. Roth, M. Mittelbronn, W. Wick, R. Meyermann, M. Tatagiba, M. Weller, Malignant glioma cells counteract antitumor immune responses through expression of lectin-like transcript-1, Cancer Res. 67 (2007) 3540–3544.
[9] S. Satkunanathan, N. Kumar, M. Bajorek, M.A. Purbhoo, F.J. Culley, Respiratory syncytial virus infection, TLR3 ligands, and proinflammatory cytokines induce CD161 ligand LLT1 expression on the respiratory epithelium, J. Virol. 88 (2014) 2366–2373.
[10] A.N. Zelensky, J.E. Gready, The C-type lectin-like domain superfamily, FEBS J. 272 (2005) 6179–6217.
[11] J. Kamishikiryo, H. Fukuhara, Y. Okabe, K. Kuroki, K. Maenaka, Molecular basis for LLT1 protein recognition by human CD161 protein (NKRP1A/KLRB1), J. Biol. Chem. 286 (2011) 23823–23830.
[12] P.J. Reeves, N. Callewaert, R. Contreras, H.G. Khorana, Structure and function in rhodopsin: high-level expression of rhodopsin with restricted and homogeneous N-glycosylation by a tetracycline-inducible N-acetylglucosaminyltransferase I-negative HEK293S stable mammalian cell line, Proc. Natl. Acad. Sci. U.S.A. 99 (2002) 13419–13424.
[13] Y. Zhao, B. Bishop, J.E. Clay, W. Lu, M. Jones, S. Daenke, C. Siebold, D.I. Stuart, E.Y. Jones, A.R. Aricescu, Automation of large scale transient protein expression in mammalian cells, J. Struct. Biol. 175 (2011) 209–215.
[14] A.R. Aricescu, W. Lu, E.Y. Jones, A time- and cost-efficient system for high-level protein production in mammalian cells, Acta Crystallogr. D Biol. Crystallogr. 62 (2006) 1243–1250.
[15] G. Backliwal, M. Hildinger, V. Hasija, F.M. Wurm, High-density transfection with HEK-293 cells allows doubling of transient titers and removes need for a priori DNA complex formation with PEI, Biotechnol. Bioeng. 99 (2008) 721–727.
[16] D.L. Hacker, D. Kiseljak, Y. Rajendra, S. Thurnheer, L. Baldi, F.M. Wurm, Polyethyleneimine-based transient gene expression processes for suspension-adapted HEK-293E and CHO-DG44 cells, Protein Expr. Purif. 92 (2013) 67–76.
[17] C. Raymond, R. Tom, S. Perret, P. Moussouami, D. L'Abbe, G. St-Laurent, Y. Durocher, A simplified polyethylenimine-mediated transfection process for large-scale and high-throughput applications, Methods 55 (2011) 44–51.
[18] Y. Durocher, S. Perret, A. Kamen, High-level and high-throughput recombinant protein production by transient transfection of suspension-growing human 293-EBNA1 cells, Nucleic Acids Res. 30 (2002) E9.
[19] R. Higuchi, B. Krummel, R.K. Saiki, A general method of in vitro preparation and specific mutagenesis of DNA fragments: study of protein and DNA interactions, Nucleic Acids Res. 16 (1988) 7351–7367.
[20] S.N. Ho, H.D. Hunt, R.M. Horton, J.K. Pullen, L.R. Pease, Site-directed mutagenesis by overlap extension using the polymerase chain reaction, Gene 77 (1989) 51–59.
[21] P.L. Pham, S. Perret, B. Cass, E. Carpentier, G. St-Laurent, L. Bisson, A. Kamen, Y. Durocher, Transient gene expression in HEK293 cells: peptone addition posttransfection improves recombinant protein synthesis, Biotechnol. Bioeng. 90 (2005) 332–344.
[22] P. Schuck, On the analysis of protein self-association by sedimentation velocity analytical ultracentrifugation, Anal. Biochem. 320 (2003) 104–124.
[23] P. Pompach, P. Man, D. Kavan, K. Hofbauerova, V. Kumar, K. Bezouska, V. Havlicek, P. Novak, Modified electrophoretic and digestion conditions allow a simplified mass spectrometric evaluation of disulfide bonds, J. Mass Spectrometry 44 (2009) 1571–1578.
[24] M.M. Young, N. Tang, J.C. Hempel, C.M. Oshiro, E.W. Taylor, I.D. Kuntz, B.W. Gibson, G. Dollinger, High throughput protein fold identification by using experimental constraints derived from intramolecular cross-links and mass spectrometry, Proc. Natl. Acad. Sci. U.S.A. 97 (2000) 5802–5806.
[25] E.J. Schlaeger, K. Christensen, Transient gene expression in mammalian cells grown in serum-free suspension culture, Cytotechnology 30 (1999) 71–83.
[26] F. Grueninger-Leitch, A. D'Arcy, B. D'Arcy, C. Chene, Deglycosylation of proteins for crystallization using recombinant fusion protein glycosidases, Protein Sci. 5 (1996) 2617–2622.
[27] O. Vanek, M. Nalezkova, D. Kavan, I. Borovickova, P. Pompach, P. Novak, V. Kumar, L. Vannucci, J. Hudecek, K. Hofbauerova, V. Kopecky Jr., J. Brynda, P. Kolenko, J. Dohnalek, P. Kaderavek, J. Chmelik, L. Gorcik, L. Zidek, V. Sklenar, K. Bezouska, Soluble recombinant CD69 receptors optimized to have an exceptional physical and chemical stability display prolonged circulation and remain intact in the blood of mice, FEBS J. 275 (2008) 5589–5606.
[28] Y. Li, Q. Wang, S. Chen, P.H. Brown, R.A. Mariuzza, Structure of NKp65 bound to its keratinocyte ligand reveals basis for genetically linked recognition in natural killer gene complex, Proc. Natl. Acad. Sci. U.S.A. 110 (2013) 11505–11510.
[29] T. Skalova, J. Blaha, K. Harlos, J. Duskova, T. Koval, J. Stransky, J. Hasek, O. Vanek, J. Dohnalek, Four crystal structures of human LLT1, a ligand for human NKR-P1, in varied glycosylation and oligomerization state, *Acta Crystallogr. D Biol. Crystallogr.* (in press).

Supplementary data

First column shows identified peptides / cystic dipeptides (numbered relative to the expressed construct ITG-Q72-V191-GTKHHHHHHHG) based on which a disulfide bridge or a free cysteine labeled with carboxyamidomethyl (CAM) was assigned in the second column (presence of N-bound HexNAc is also indicated). Theoretical and experimental masses of measured peptides, mass error and intensity are shown in the third, fourth, fifth and sixth columns, respectively.

Table S1. Table of cystic peptides identified for LLT1(WT)

Identified peptide(s)	Cys-Cys crosslink	Theoretical mass	Experimental mass	Error (ppm)	Intensity
113-118/86-101	C163-C184	2500.2366	2500.2349	0.7	3.23E+08
114-118/86-101	C163-C184	2372.1416	2372.1387	1.3	2.65E+08
86-101/1-16	C75-C163	3499.6775	3499.6729	1.4	9.30E+07
114-118/1-16	C75-C184	2397.1482	2397.1467	0.6	7.40E+07
114-118/34-56	C103-C184	3321.5559	3321.5513	1.4	6.70E+07
113-118/86-107	C163-C184	3029.4976	3029.4937	1.3	6.70E+07
113-118/1-16	C75-C184	2525.2432	2525.2402	1.2	4.56E+07
113-118/34-56	C103-C184	3449.6509	3449.6465	1.3	3.23E+07
114-118/86-107	C163-C184	2901.4026	2901.4006	0.7	2.37E+07
18-26/1-16	C75-C86	2886.2864	2886.2832	1.1	1.41E+07
86-101	C163-CAM	1795.8688	1795.8671	1	1.38E+07
17-26/1-16	C75-C86	3014.3813	3014.3823	0.3	1.24E+07
86-101/1-17	C75-C163	3627.7725	3627.7678	1.3	6.31E+06
1-16/86-107	C75-C163	4028.9385	4028.9316	1.7	3.92E+06
113-118/18-26	C86-C184	1886.8456	1886.8511	2.9	3.07E+06
1-16/34-56	C75-C86	4449.0918	4449.0854	1.4	2.57E+06
113-118/1-17	C75-C184	2653.3381	2653.3354	1	1.58E+06
1-26	C75-C86	2996.3711	2996.3677	1.1	1.55E+06
108-118/86-101	C163-C184	3186.5503	3186.5488	0.5	8.09E+05
113-118/34-69	C103-C184	4946.4028	4946.3975	1.1	7.18E+05
77-85c	N147-HexNAc	1365.6438	1365.6423	1.1	6.88E+08
70-85	N147-HexNAc	2219.052	2219.05	0.9	2.14E+08
1-16/18-33	C75-C86 N95-HexNAc	3948.7595	3948.7554	1	5.72E+05

Table S2. Table of cystic peptides identified for LLT1(H176C)

Identified peptide(s)	Cys-Cys crosslink	Theoretical mass	Experimental mass	Error (ppm)	Intensity
108-112/86-101	C163-C176	2407.106	2407.102	1.8	1.74E+08
18-26/1-16	C75-C86	2886.286	2886.283	1.1	3.26E+07
114-118/34-56	C103-C184	3321.556	3321.552	1.2	3.18E+07
113-118/34-56	C103-C184	3449.651	3449.647	1.1	3.17E+07
17-26/1-16	C75-C86	3014.381	3014.381	0.3	2.05E+07
114-118/1-16	C103-C184	2397.148	2397.146	0.9	4.21E+06
1-26	C75-C86	2996.371	2996.367	1.4	1.44E+06
114-126/18-33	C103-C184	3455.579	3455.585	1.7	7.58E+05
108-113/86-101	C163-C176	2535.201	2535.198	1.1	3.90E+05
77-85	N147-HexNAc	1365.644	1365.642	1.6	1.43E+08
70-85	N147-HexNAc	2219.052	2219.05	1	1.14E+07
1-16/18-33	C75-C86 N95-HexNAc	3948.76	3948.755	1.1	1.36E+06
17-33	N95-HexNAc	2373.046	2373.05	1.7	4.56E+06
108-112/114-126	C176-C184	2142.011	2142.013	0.9	2.06E+06
86-101/1-16	C75-C163	3499.678	3499.672	1.5	1.62E+06
113-118/86-101	C163-C184	2500.237	2500.236	0.2	1.34E+06
114-118/1-16	C75-C184	2397.148	2397.146	0.9	4.21E+06
108-112/113-118	C176-C184	1432.672	1432.67	1.3	4.31E+05

PUBLICATION II

Skálová, T., Bláha, J., Harlos, K., Dušková, J., Koval', T., Stránský, J., Hašek, J., Vaněk, O., Dohnálek, J.

Four crystal structures of human LLT1, a ligand of human NKR-P1, in varied glycosylation and oligomerization states

Acta Crystallogr. Sect. D Biol. Crystallogr. 71, 578-591 (2015)

My contribution to the publication: *performing research (protein characterization and crystallization), data collection, data analysis and interpretation, manuscript writing*

research papers

BIOLOGICAL CRYSTALLOGRAPHY

ISSN 1399-0047

Four crystal structures of human LLT1, a ligand of human NKR-P1, in varied glycosylation and oligomerization states

Tereza Skálová,[a]* Jan Bláha,[b] Karl Harlos,[c] Jarmila Dušková,[a] Tomáš Koval',[d] Jan Stránský,[a] Jindřich Hašek,[a] Ondřej Vaněk[b] and Jan Dohnálek[a,d]*

[a]Institute of Biotechnology, Academy of Sciences of the Czech Republic, v.v.i., Vídeňská 1083, 142 20 Praha 4, Czech Republic, [b]Department of Biochemistry, Faculty of Science, Charles University Prague, Hlavova 8, 128 40 Praha, Czech Republic, [c]Division of Structural Biology, The Wellcome Trust Centre for Human Genetics, University of Oxford, Roosevelt Drive, Oxford OX3 7BN, England, and [d]Institute of Macromolecular Chemistry, Academy of Sciences of the Czech Republic, v.v.i., Heyrovského nám. 2, 162 06 Praha 6, Czech Republic. *Correspondence e-mail: t.skalova@gmail.com, dohnalek007@gmail.com

Received 18 September 2014
Accepted 22 December 2014

Keywords: LLT1; C-type lectin-like ligand.

PDB references: human LLT1, dimeric form, 4qkh; 4qki; hexameric form, 4qkj; monomeric form, 4qkg

Supporting information: this article has supporting information at journals.iucr.org/d

Human LLT1 is a C-type lectin-like ligand of NKR-P1 (CD161, gene *KLRB1*), a C-type lectin-like receptor of natural killer cells. Using X-ray diffraction, the first experimental structures of human LLT1 were determined. Four structures of LLT1 under various conditions were determined: monomeric, dimeric deglycosylated after the first *N*-acetylglucosamine unit in two forms and hexameric with homogeneous $GlcNAc_2Man_5$ glycosylation. The dimeric form follows the classical dimerization mode of human CD69. The monomeric form keeps the same fold with the exception of the position of an outer part of the long loop region. The hexamer of glycosylated LLT1 consists of three classical dimers. The hexameric packing may indicate a possible mode of interaction of C-type lectin-like proteins in the glycosylated form.

1. Introduction

Natural killer (NK) cells are innate immune lymphocytes that possess the ability to recognize and induce the death of a broad range of target cells without prior antigen sensitization, including tumour, virally infected or stressed cells. Apart from direct cell-mediated cytotoxicity, NK cells also participate in the initiation and development of the adaptive immune response through the production and secretion of cytokines (Caligiuri, 2008; Vivier *et al.*, 2011). Their function is regulated by a fine balance of signals induced by the interaction of a vast array of surface-activating and surface-inhibitory receptors with ligands on the surface of target cells (Lanier, 2008; Vivier *et al.*, 2008; Bartel *et al.*, 2013). The activation of NK cells and the killing of the target cell is triggered when the expression of cellular health markers (MHC class I-like glycoproteins) that engage the inhibitory NK receptors is too low ('missing-self' recognition mode) or when the ligands for activating NK receptors are upregulated, usually in virally infected, stressed or malignant cells ('induced-self' mode).

The NK cell receptors are divided into two main structural classes: the immunoglobulin and C-type lectin-like (CTL) superfamilies. The CTL family of NK cells encoded within the natural gene complex (human chromosome 12) comprises proteins related to C-type lectins that have lost the ability to bind carbohydrates but have instead gained the ability to

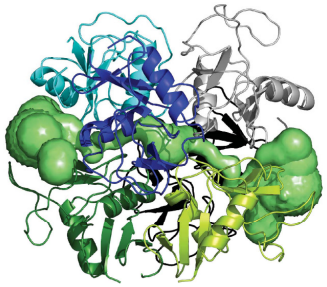

OPEN ACCESS

recognize protein ligands (Yokoyama & Plougastel, 2003; Zelensky & Gready, 2005; Grobárová *et al.*, 2013). While certain CTL receptors are known to bind proteins with the MHC class I-like fold (*e.g.* NKG2D, CD94/NKG2A and murine Ly49 receptors; Bartel *et al.*, 2013), the NKR-P1 receptor subfamily does not share this specificity. Although the ligands for some rodent NKR-P1 receptors are still unknown, it has been shown that many of them recognize genetically and structurally highly related Clr/Ocil CTL receptors from the *CLEC2* gene subfamily (Aust *et al.*, 2009; Kveberg *et al.*, 2009). It is now accepted that this unique system of CTL receptor–CTL ligand interaction represents an alternative form of 'missing-self' recognition (Bartel *et al.*, 2013).

Lectin-like transcript 1 (LLT1, gene *CLEC2D*) was identified as a physiological ligand of NKR-P1, the sole described representative of the human NKR-P1 subfamily (CD161, gene *KLRB1*; Aldemir *et al.*, 2005; Rosen *et al.*, 2005). LLT1 is expressed primarily on activated lymphocytes (NK cells, T cells and B cells) and antigen-presenting cells (macrophages and dendritic cells; Germain *et al.*, 2011). Six alternatively spliced transcripts of the *CLEC2D* gene have been identified, with isoform 1 (coding for LLT1) being the only one able to interact with NKR-P1 (Germain *et al.*, 2010). The engagement of NKR-P1 on the NK cell with LLT1 on the target cell inhibits NK cell cytotoxicity and IFNγ production (Aldemir *et al.*, 2005; Rosen *et al.*, 2005, 2008) and contributes to NK self-tolerance in a similar way to the orthologous rodent NKR-P1B–Clr-b receptor–ligand pair (Voigt *et al.*, 2007; Fine *et al.*, 2010; Williams *et al.*, 2012). It has been shown that human glioblastoma exploits this mechanism by the upregulation of the surface expression of LLT1 to escape the immunological response (Roth *et al.*, 2007). On the other hand, LLT1 is upregulated in response to both microbial and viral stimuli, and stimulation of NKR-P1-expressing T cells promotes their activation, proliferation and cytokine secretion (Huarte *et al.*, 2008; Germain *et al.*, 2011; Satkunanathan *et al.*, 2014). Thus, LLT1–NKR-P1 signalization may provide a link between pathogen pattern recognition and lymphocyte activation and represents a system that regulates both the innate and the adaptive immune responses.

Recently, we have described the first three-dimensional structure of mouse Clr-g, a representative of the murine CLEC2 family (Skálová *et al.*, 2012). Similarly to mouse Clr-g, human LLT1 is a type II transmembrane glycoprotein which consists of an N-terminal cytoplasmic chain, transmembrane and stalk regions and a C-terminal CTL domain with two predicted N-linked glycosylation sites. In this study, we present several structures of LLT1 under various conditions: monomeric (LLT1_mono), dimeric deglycosylated after the first *N*-acetylglucosamine unit (LLT1_D1 and LLT1_D2) and dimeric (packed into hexamers) with homogeneous $GlcNAc_2Man_5$ glycosylation (LLT1_glyco). All structures originate from protein expressed in HEK293S GnTI$^-$ cells (Reeves *et al.*, 2002). The dimeric form follows the classical dimerization mode of human CD69 (Natarajan *et al.*, 2000; Llera *et al.*, 2001; Vaněk *et al.*, 2008; Kolenko *et al.*, 2009).

2. Materials and methods

2.1. Protein expression and purification

The lectin-like domain of LLT1 was produced in HEK293S GnTI$^-$ cells as described by Bláha *et al.* (2015). Briefly, the expression construct corresponding to the CTL extracellular domain of LLT1 (Gln72–Val191) with a His176 to Cys176 mutation was cloned into the pTT28 plasmid, a derivative of the pTT5 plasmid (Durocher *et al.*, 2002) with an altered cloning site (Bláha *et al.*, 2015). A suspension culture of HEK293S GnTI$^-$ cells (Reeves *et al.*, 2002) was transiently transfected with a 1:3 mixture of the expression plasmid and 25 kDa linear polyethyleneimine. The resulting protein contained an N-terminal secretion leader and a C-terminal His_8 tag. 5–7 d post-transfection, the secreted recombinant protein was purified from the harvested production medium by two-step chromatography using batch IMAC on Talon resin (Clontech) followed by size-exclusion chromatography on a Superdex 200 10/300 GL column (GE Healthcare) in 10 m*M* HEPES pH 7.5 with 150 m*M* NaCl and 10 m*M* NaN_3. The final product was concentrated to 20 mg ml^{-1} using an Amicon Ultra concentrator (10 kDa molecular-weight cutoff; Merck Millipore).

For deglycosylation, GST-fused Endo F1 (Grueninger-Leitch *et al.*, 1996) was added to the concentrated protein solution in a 1:200 weight ratio and incubated overnight at room temperature. The slight precipitate that developed after deglycosylation was dissolved by the addition of L-arginine–HCl to a concentration of 0.4 *M* before setting up the crystallization drops.

The C-type lectin-like ectodomain of LLT1 contains two of the three canonical disulfide bridges (Cys75–Cys86 and Cys103–Cys184) found in homologous CTL receptors. Multiple alignment analysis showed that the formation of the third canonical disulfide bridge is impaired by the absence of the sixth evolutionarily conserved Cys residue, which is substituted by His176 in the wild-type LLT1 sequence. Based on previous results (Kamishikiryo *et al.*, 2011), we decided to clone and express the extracellular part (Gln72–Val191) of LLT1 with the His176 to Cys176 mutation. This mutation dramatically improved the stability, homogeneity and yield of the product (Bláha *et al.*, 2015). Expression in HEK293S GnTI$^-$ cells and subsequent purification provided highly pure protein with artificially homogeneous ($GlcNAc_2Man_5$) N-linked glycosylation with a typical yield of 3 mg of purified protein per litre of production culture. The disulfide-bond pattern as well as the occupancy of both N-glycosylation sites was verified by mass spectrometry (Bláha *et al.*, 2015).

2.2. Crystallization and data collection

2.2.1. LLT1_mono. The protein (diluted to 14 mg ml^{-1} in 0.4 *M* arginine, 4 m*M* HEPES, 120 m*M* NaCl, 4 m*M* NaN_3 pH 7.5) was crystallized using the sitting-drop vapour-diffusion method. Drops (100 nl reservoir solution and 100 nl protein solution) were set up using a Cartesian Honeybee 961 robot (Genomic Solutions) at 294 K. The reservoir consisted of 2 *M* ammonium sulfate, 0.1 *M* sodium citrate pH 3.5. A crystal with

the shape of a hexagonal plate (dimensions of 100 × 100 × 10 µm) was cryoprotected by soaking in the reservoir solution with the addition of 25% glycerol. The diffraction data were measured on a split segment of the multi-crystal on beamline I02 of Diamond Light Source (DLS) using an ADSC Q315 CCD detector at 100 K.

2.2.2. LLT1_D1 and LLT1_D2. The protein was crystallized as above. The reservoir consisted of 30%(*w*/*v*) polyethylene glycol (PEG) 6000, 0.1 *M* HEPES pH 7.0. A cuboid-shaped crystal of dimensions ∼60 × 60 × 120 µm was cryoprotected as above. The data were measured on beamline I04-1 at DLS using a PILATUS 2M detector at 100 K. Both data sets were collected using crystals from the same crystallization condition. Interestingly, both crystals belonged to the same space group, $P2_12_12_1$, but the crystals differed in solvent content (36% for LLT1_D1 and 25% for LLT1_D2) and in unit-cell parameters (a difference of 4 Å in *b* and 8 Å in *c*).

2.2.3. LLT1_glyco. Protein diluted to 14 mg ml^{-1} in 10 m*M* HEPES, 150 m*M* NaCl, 10 m*M* NaN_3 pH 7.5 was crystallized using the hanging-drop vapour-diffusion method (with drops consisting of 1 µl reservoir solution and 1 µl protein solution) with reservoir consisting of 40%(*v*/*v*) PEG 300, 0.1 *M* citrate–phosphate buffer pH 4.2 at a temperature of 288 K. A rod-shaped crystal of dimensions ∼200 × 50 × 50 µm was vitrified without cryoprotection. Diffraction data were measured on BM 14.1 of the BESSY II synchrotron-radiation source (Mueller *et al.*, 2012) at the Hemholtz-Zentrum Berlin using a MAR Mosaic 225 CCD detector at 100 K.

2.3. Structure determination

The data sets for LLT1_mono and LLT1_glyco were processed using the *HKL*-2000 package (*DENZO* and *SCALEPACK*; Otwinowski & Minor, 1997). Intensities were converted to amplitudes and imported into the CCP4 format with *TRUNCATE* (French & Wilson, 1978). The data for LLT1_D1 and LLT1_D2 were processed in *MOSFLM* (Leslie & Powell, 2007) using the *iMosflm* interface (Battye *et al.*, 2011) and were scaled in *AIMLESS* (Evans & Murshudov, 2013). The data parameters are shown in Table 1.

The data for LLT1_glyco showed strong anisotropy; therefore, the data processed in *DENZO* and *SCALEPACK* were then rescaled using the *Diffraction Anisotropy Server* (http://services.mbi.ucla.edu/anisoscale/; Strong *et al.*, 2006). The processed data comprised 4186 reflections. An isotropic *B* factor of −23.39 Å^2 was applied to restore the magnitude of the high-resolution reflections diminished by anisotropic scaling.

The phase problem for the LLT1_D1, LLT1_D2 and LLT1_glyco structures was solved by molecular replacement in *BALBES* (Long *et al.*, 2008; Keegan *et al.*, 2013) using the structure of human CD69 as a search model (Kolenko *et al.*, 2009; PDB entry 3hup). The structure of LLT1_mono was solved in *MOLREP* (Vagin & Teplyakov, 2010) using one chain of LLT1_glyco as a search model.

All of the structures were refined in *REFMAC*5 (Murshudov *et al.*, 2011) with manual changes performed in *Coot* (Emsley *et al.*, 2010). Structure parameters are shown in Table 1. After several cycles of rigid-body refinement, the structures were refined using restrained refinement including H atoms (not deposited in the Protein Data Bank). Non-crystallographic symmetry between two monomers of the dimer was applied in the cases of LLT1_D1, LLT1_D2 and LLT1_glyco in the first steps of the refinement. The refinement was performed with the omission of 5% of the reflections (test set with $R_{\rm free}$ flag). In the case of LLT1_glyco with a lower resolution and a lower number of reflections, 6% of the reflections (223 reflections) were used for the test set. The last cycle of refinement of all four structures was performed with all reflections including the test set.

The choice of the correct space group for LLT1_glyco was ambiguous and structure refinement was tested in 16 space groups alternative to $P2_1$ using *Zanuda* (Lebedev & Isupov, 2014) and then also manually in $P2_1$, $C222$, $C222_1$, $P6_3$ and $P6_322$. Finally, $P6_322$ was chosen as the correct space group because lower symmetry space groups did not show apparent differences among the molecules in the asymmetric unit and refinement was less stable.

2.4. Structure quality: geometry and electron density

2.4.1. LLT1_mono. According to the *MolProbity* Ramachandran plot (Chen *et al.*, 2010), 95% of the residues of the structure lie in the favoured regions. There is one outlier, Gln83. This is a residue in a loop with an alternative conformation of the main chain. The residue is in good agreement with the $2mF_o - DF_c$ and $mF_o - DF_c$ electron-density Fourier maps.

One sulfate anion is localized in the structure, bound to Lys181 N$^{\zeta}$, Ser129 N and Ser129 O$^{\gamma}$. The peptide bond Lys126-Gly127 in the vicinity of the sulfate anion has *cis*–*trans* alternative conformations.

2.4.2. LLT1_D1. This structure with high resolution has residues generally well localized in $2mF_o - DF_c$ and $mF_o - DF_c$ maps; however, the Fourier maps have lower quality in the region of the long loop (residues 137–160), mainly in chain *A*. According to the *MolProbity* Ramachandran plot, 98% of the residues lie in the favoured regions and there is only one outlier, residue *A*Gln139, which is in a turn of a loop.

There are unmodelled peaks in the $2mF_o - DF_c$ Fourier maps. The electron density for the side chain of Lys186 in both chains is elongated, which may indicate covalent modification of this lysine. Moreover, arginine as added to the LLT1 sample after deglycosylation to improve protein folding is probably localized on the protein surface, bound by hydrogen bonds to residues *B*Asp104 and *B*Asp109, but the electron density is not sufficiently clear to build the whole arginine residue.

Surprisingly, the conformation of the Gln83-Arg84 peptide bond differs significantly between chain *A* (Gln83 torsion angles $\varphi = 47°$, $\psi = 51°$) and chain *B* ($\varphi = 54°$, $\psi = -122°$). Electron density is well defined in both cases. In chain *B* the value lies in the allowed region of the Ramachandran plot and *B*Gln83 O forms a water-mediated hydrogen bond to *A*Cys75 N. In chain *A*, the torsion-angle values lie in the

Table 1
Data-collection statistics and structure-refinement parameters.

Values in parentheses are for the highest resolution shell.

	LLT1_mono	LLT1_D1	LLT1_D2	LLT1_glyco
PDB code	4qkg	4qkh	4qki	4qkj
pH of crystallization condition	3.5	7.0	7.0	4.2
Glycosylation	GlcNAc	GlcNAc	GlcNAc	$GlcNAc_2Man_5$
Oligomer	Monomer	Dimer	Dimer	Hexamer
Data-collection statistics				
Resolution range (Å)	50.0–1.95 (1.98–1.95)	47.3–1.8 (1.84–1.80)	43.7–1.8 (1.84–1.80)	39.0–2.7 (2.76–2.70)
Space group	$P3_221$	$P2_12_12_1$	$P2_12_12_1$	$P6_322$
Unit-cell parameters (Å)	$a = b = 47.3$, $c = 106.1$	$a = 50.9$, $b = 57.8$, $c = 82.3$	$a = 51.3$, $b = 54.1$, $c = 74.2$	$a = b = 70.1$, $c = 101.7$
Radiation source	I02, DLS	I04-1, DLS	I04-1, DLS	BM 14.1, BESSY II
Detector	ADSC Q315 CCD	PILATUS 2M	PILATUS 2M	MAR Mosaic 225 CCD
Data-processing software	*HKL*-2000 [*DENZO*, *SCALEPACK*]	*MOSFLM*, *AIMLESS*	*MOSFLM*, *AIMLESS*	*HKL*-2000 [*DENZO*, *SCALEPACK*], anisotropy server
Wavelength (Å)	0.9796	0.9200	0.9200	0.9184
No. of images	220	900	1800	80 [images 1–50, 330–360]
Crystal-to-detector distance (mm)	256.1	325.2	251.9	288.1
Exposure time per image (s)	1	0.2	0.2	2
Oscillation width (°)	0.5	0.2	0.2	0.5
No. of observations	66670 (3340)	175131 (5869)	113353 (6521)	478731 (1201)
No. of unique reflections	10555 (506)	21104 (1087)	18996 (1050)	4431 (273)
Data completeness (%)	99.7 (100)	91.8 (81.0)	96.7 (91.6)	99.5 (99.3)
Average multiplicity	6.3 (6.6)	8.3 (5.4)	6.0 (6.2)	4.3 (4.4)
Mosaicity (°)	0.3–0.7	1.8	1.3	0.8–1.4
$\langle I/\sigma(I)\rangle$	21.2 (2.9)	11.3 (3.0)	11.8 (3.7)	16.2 (2.0)
Solvent content (%)	44	36	25	46
Matthews coefficient ($Å^3$ Da^{-1})	2.18	1.93	1.64	2.30
B factor from Wilson plot ($Å^2$)	34.0	20.7	17.7	66.1
R_{merge}†	0.074 (0.599)	0.093 (0.462)	0.082 (0.404)	0.096 (0.757)
$R_{p.i.m.}$‡	0.032 (0.251)	0.045 (0.309)	0.053 (0.257)	0.031 (0.171)
Structure parameters				
R_{work}§ (%)	19.4	17.5	17.8	22.1
R_{free}§ (%)	24.7	25.0	24.4	29.8
R_{all}§ (%)	20.1	18.0	18.3	23.1
Average *B* factor ($Å^2$)	39.8	27.6	20.9	40.1
R.m.s.d. from ideal bond lengths (Å)	0.016	0.016	0.016	0.017
R.m.s.d. from ideal bond angles (°)	1.9	1.7	1.8	2.0
No. of monomers per asymmetric unit	1	2	2	1
Amino-acid residues located	*A*72–*A*146, *A*161–*A*193	*A*70–*A*192, *B*72–*B*192	*A*73–*A*194, *B*73–*B*192	*A*74–*A*188
Asn residues with located GlcNAc	*A*95	*A*95, *A*147, *B*95, *B*147	*A*95, *A*147, *B*95, *B*147	*A*95
No. of water molecules	42	215	167	15
Other localized moieties	$1 \times SO_4^{2-}$	—	—	—
Ramachandran statistics: residues in favoured region (%)	95	98	98	87

† $R_{merge} = \sum_{hkl}\sum_i |I_i(hkl) - \langle I(hkl)\rangle|/\sum_{hkl}\sum_i I_i(hkl)$ (Diederichs & Karplus, 1997), where $I_i(hkl)$ and $\langle I(hkl)\rangle$ are the observed individual and mean intensities of a reflection with indices *hkl*, respectively, $\sum_i$ is the sum over the individual measurements of a reflection with indices *hkl* and $\sum_{hkl}$ is the sum over all reflections. ‡ $R_{p.i.m.} = \sum_{hkl}\{1/[N(hkl)-1]\}^{1/2}\sum_i |I_i(hkl) - \langle I(hkl)\rangle|/\sum_{hkl}\sum_i I_i(hkl)$ (Weiss, 2001), where $N(hkl)$ is the redundancy of the reflection with indices *hkl*. § $R_{work} = \sum_{hkl}||F_{obs}| - |F_{calc}||/\sum_{hkl}|F_{obs}|$, where F_{obs} and F_{calc} are the observed and calculated structure-factor amplitudes for the reflection with indices *hkl* for the working set of reflections. R_{free} is the same as R_{work} but is calculated for 5–6% of the data omitted from refinement. R_{all} sums over all reflections.

favoured region of the Ramachandran plot but the connection formed between chains *A* and *B* is weaker: it is mediated by hydrogen bonds formed by two water molecules connecting *A*Arg84 N and *B*Cys75 N.

2.4.3. LLT1_D2. Of the four presented structures, this structure has the best quality electron density because of its high resolution (1.8 Å) and low solvent content (25%). The long loop region of both chains is in contact with symmetry-related molecules in the crystal and is better localized in electron density than in the other presented structures. According to the *MolProbity* Ramachandran plot, 98% of residues lie in the favoured regions and there are no outliers.

Unlike in LLT1_D1, there are no signs of Lys186 modification. Solvent arginine bound to *B*Asp104 and *B*Asp109 could be present, but is less apparent than in LLT1_D1. The Gln83-Arg84 peptide bond is modelled in the same orientation in both chains, even though there are some signs of the alternative conformation in chain *A*.

2.4.4. LLT1_glyco. The structure of glycosylated LLT1 has lower resolution (2.7 Å) and the data have an anisotropic character. According to the *MolProbity* Ramachandran plot, 87% of residues lie in the favoured regions and there are two outliers, *A*Ser105 and *A*Ile146, both of which are in turns of different loops.

Tyr88 has elongated electron density which may indicate covalent modification of this tyrosine. Some positive signal in the $mF_o - DF_c$ map behind the hydroxyl group of Tyr88 is also present in chain *B* of LLT1_D1.

research papers

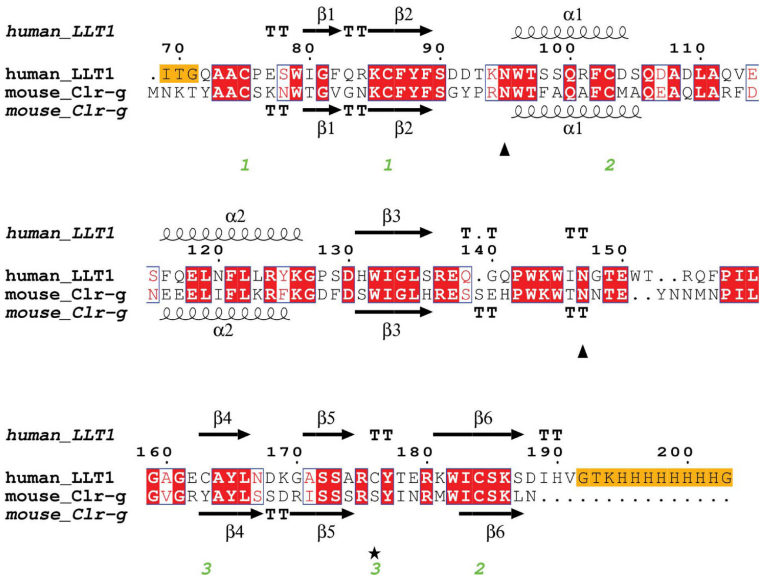

Figure 1
The LLT1 expression construct used for crystallization and its sequence alignment (*Clustal Omega*; Thompson *et al.*, 1994; Sievers *et al.*, 2011) with mouse Clr-g. The H176C mutation is denoted by an asterisk, glycosylated Asn residues are denoted by triangles and the three pairs of disulfide bonds in LLT1 are numbered. Uncleaved residues of the N-terminal signal sequence and the C-terminal tag are in orange boxes. Secondary structure was assigned by *DSSP* (Kabsch & Sander, 1983).

2.5. Electrostatic potential

The electrostatic potential of LLT1_D2 was computed by solving the Poisson–Boltzmann equation in *APBS* (Baker *et al.*, 2001). H atoms were added in *PROPKA* (Li *et al.*, 2005), including optimization of hydrogen bonds for the protein at pH 7.5. Partial charges were assigned in *PDB2PQR* (Dolinsky *et al.*, 2007) based on the AMBER potential. The Poisson–Boltzmann equation was solved using values of the dielectric constants of ε(solvent) = 78.54 and ε(protein) = 2 and assuming a 0.225 *M* concentration of ions in solution with charges $+e$ and $-e$ and radius 2 Å.

2.6. Sedimentation analysis

The oligomeric state of the produced protein was analyzed in a ProteomeLab XL-I analytical ultracentrifuge equipped with an An-50 Ti rotor (Beckman Coulter, USA) using a sedimentation-velocity experiment. Samples of glycosylated LLT1 diluted with the buffer used in size-exclusion chromatography to the desired concentration were spun at 50 000 rev min^{-1} at 20°C and 100 scans with 0.003 cm spatial resolution were recorded using absorbance optics at 280 nm. Buffer density and protein partial specific volume were estimated in *SEDNTERP* (http://sednterp.unh.edu/). The data were analyzed using *SEDPHAT* (Schuck, 2003) using the continuous size-distribution model and the monomer–dimer self-association model.

2.7. Dynamic light scattering

Measurement of dynamic light scattering was performed with a Zetasizer Nano (Malvern Instruments) and a 45 µl quartz cuvette with ~40 µl LLT1 solution (sample corresponding to LLT1_glyco) diluted to 1 mg ml^{-1} in a buffer solution consisting of 10 m*M* HEPES, 150 m*M* NaCl, 10 m*M* NaN_3 pH 7.5.

2.8. Figure preparation

Fig. 1 was prepared using *ESPript* (http://espript.ibcp.fr; Gouet *et al.*, 2003). Figs. 2–6 and Supplementary Fig. S1 were prepared in *PyMOL* (Schrödinger; http://www.pymol.org).

3. Results and discussion

The extracellular part of LLT1 was expressed in the HEK293S GnTI$^-$ cell line and was purified. Three crystal forms were grown at pH 3.5, 4.2 and 7.0 and led to four structures of LLT1: monomeric, dimeric (with altered crystal packing) and dimeric packed as hexamers. The hexameric structure of LLT1 has $GlcNAc_2Man_5$ N-glycosylation; in the other three LLT1 structures the protein is deglycosylated beyond the first GlcNAc.

3.1. Overview of the crystal structures of LLT1

The crystallized extracellular part of human LLT1 corresponds to the sequence deposited in the UniProt database under code Q9UHP7, isoform 1, starting with Gln72 and with a His176 to Cys176 mutation (for the formation of a Cys163–Cys176 disulfide bond for greater stabilization of the protein fold) and with the addition of ITG (the remnant of a secretion leader) at the beginning of the chain and of a GTKHHHHHHHHG tag at the end of the chain (Fig. 1). The calculated molecular weight of this construct is 15.7 kDa (18.1 kDa taking N-glycosylation into account).

The extracellular part of human LLT1 has the C-type lectin-like fold (Fig. 2*a*) with two α-helices, two antiparallel β-sheets and three disulfide bonds (Cys70–Cys86, Cys103–Cys184 and Cys163–Cys176). The third (artificial) disulfide bond induced by the mutation of His176 to Cys176 is located in the same position as the third disulfide bond occurring naturally in CD69. The overall manner of dimerization of both its glycosylated and deglycosylated dimeric forms (produced in a human cell line in a close-to-native form) corresponds to the classical dimerization mode of human CD69 or of mouse Clr-g (one of the mouse orthologues of LLT1) both produced in bacteria and refolded from inclusion bodies. The N- and C-termini of both chains in this type of dimer are localized on

one side (Fig. 2*b*) and their position allows protein anchoring in the cell membrane, which supports the biological relevancy of this dimer.

The protein used to obtain the LLT1_glyco structure contained homogeneous $GlcNAc_2Man_5$ glycosylation, while the protein used to obtain the LLT1_mono, LLT1_D1 and LLT1_D2 structures was deglycosylated beyond the first GlcNAc. However, only the first GlcNAc unit could be modelled in LLT1_glyco. The subsequent oligosaccharide moieties cannot be modelled but are visible at low electron-density levels.

In LLT1_mono, residues 147–160 (the outer loop of the long loop region) are poorly visible and were not built in the deposited structure. However, the approximate position of the loop is apparent in the electron density and differs significantly from its position in LLT1 in its dimeric form (Figs. 2*c* and 3*a*). The structure of LLT1_mono with the approximate position of the loop is available from the authors upon request.

3.2. Comparison of monomeric and dimeric LLT1

Superposition of chain *A* of LLT1_D2 on LLT1_mono by secondary-structure matching in *Coot* gives an r.m.s. deviation of C^{α}atoms of 0.6 Å. The core of the monomer and the dimer has the same structure, but there are some structural differences in the outer parts of the CTL domain.

As mentioned above, there is an important difference in the placement of the outer loop (residues 147–160) of the long loop region (residues 137–160). While in LLT1_D2 this loop lies in the direction of β-sheet 171–174 and α-helix 116–126 of the same chain, as is common in the structures of similar proteins (*e.g.* the CD69 dimer), in LLT1_mono the loop is

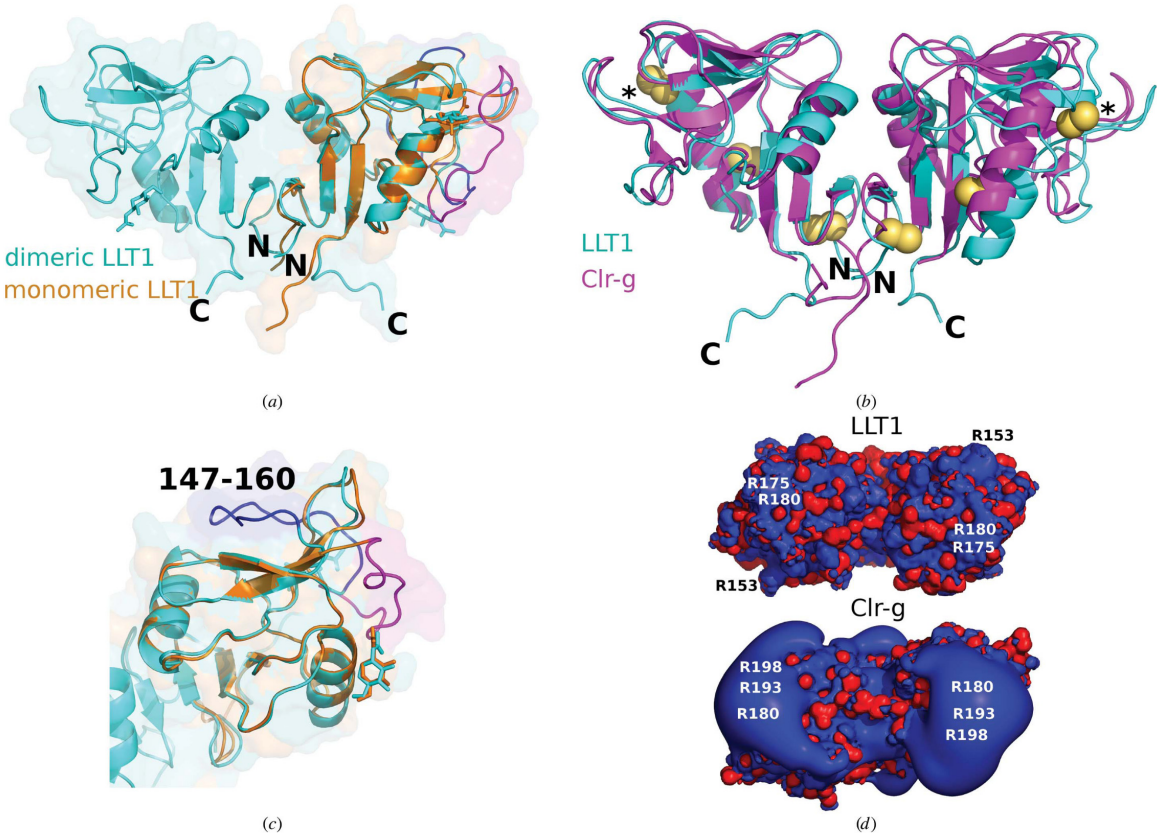

Figure 2
(*a*) Structures of the dimeric (LLT1_D2, cyan) and monomeric (LLT1_mono, orange) forms of LLT1. The loop is in its standard dimeric position in LLT1_D2 (blue) and is in the swapped position in LLT1_mono (magenta). The N- and C-termini of LLT1_D2 are denoted. (*b*) Comparison of the structure of LLT1_D2 (cyan) with its mouse orthologue Clr-g (PDB entry 3rs1, magenta). The superposition was performed in *Coot* by SSM of chains *A* (on the left). The N- and C-termini of LLT1_D2 are denoted. Disulfide bonds are shown as yellow spheres, with the artificial disulfide bonds induced by the H176C mutation denoted by asterisks. (*c*) A detailed view of the loop position discussed in (*a*). (*d*) Electrostatic equipotential surfaces of LLT1_D2 (top) and mouse Clr-g (bottom). They are displayed at the 3 kT/e (blue) and $-3kT$/e (red) levels as computed in *APBS* (Baker *et al.*, 2001). The view is from the 'top' of the dimer, *i.e.* from the termini-distal side.

turned to the opposite side with regard to the inner loop 135–145: it is situated near to α-helix 96–104 of the same chain and makes contact with α-helix 120–125 of a neighbouring monomer in the crystal (Figs. 2*c* and 3*a*).

There are also other structural differences between the monomer and dimer structures: the C-terminal part of the main chain, residues 190–194, is placed differently (Fig. 2*a*) and residues around Gln139 are mutually shifted; the distance between the C^{α} atoms in the monomeric and dimeric forms is 1.9 Å.

3.3. Dimer interface in dimeric LLT1

LLT1_glyco, LLT1_D1 and LLT1_D2 share essentially the same structure at the level of the dimer; however, they differ slightly in the mutual orientation of the monomers within a dimer. This difference is especially apparent when the dimers are overlapped by only one chain: the rotation necessary to superimpose chain *A* onto chain *B* of the selected protein is exactly 180° for the LLT1_glyco dimer crystallized in space group $P6_322$, in which the chains are related by a crystallographic rotation axis. In contrast, it is 173.7° for LLT1_D1 and 177.7° for LLT1_D2, both of which crystallized in space group $P2_12_12_1$ with one dimer in the asymmetric unit. Owing to these differences in mutual orientation, there are differences in the area of the dimer interface (obtained using the *PISA* server; Krissinel & Henrick, 2007): the size of the contact area is 530 Å^2 for LLT1_glyco (8% of the monomer surface area), 740 Å^2 for LLT1_D2 (10% of the monomer surface area) and 810 Å^2 for LLT1_D1 (11% of the monomer surface area).

The dimeric interface in all three LLT1 dimers is based on a hydrophobic core formed by phenyl rings, analogous to that observed in similar CTL dimers: Phe121, Tyr125, Phe89, Phe87 and Phe82 (Fig. 4). Additionally, there is an interaction formed by π-stacking of arginine residue Arg124 of both chains, and a pair of His190 residues forms a partial stacking interaction in the termini region (the part of the CTL domain oriented towards the cell membrane).

There are six common hydrogen bonds that connect the monomers in all three dimers: *A*Gly81 N–*B*Gly81 O, *A*Arg124 N^{ε}–*B*Tyr125 O, *A*Arg124 $N^{\eta1}$–*B*Lys126 O and the three analogous hydrogen bonds with exchanged chains. Additionally, there are some hydrogen bonds specific to individual cases: one additional hydrogen bond in the dimeric interface of LLT1_glyco, two hydrogen bonds in LLT1_D2 and six in LLT1_D1.

This variability of the mutual chain orientation has been discussed previously for similar CTL protein dimers (CD94/NKG2A, Clr-g and CD69; Sullivan *et al.*, 2007; Skálová *et al.*, 2012). Considering the flexibility of the dimer interface, it seems that the flexible hydrophobic interactions are the most important contact for the existence of the dimer, its stability and its ability to bind a protein partner. These CTL dimers differ in their main purpose, which is surface partner binding,

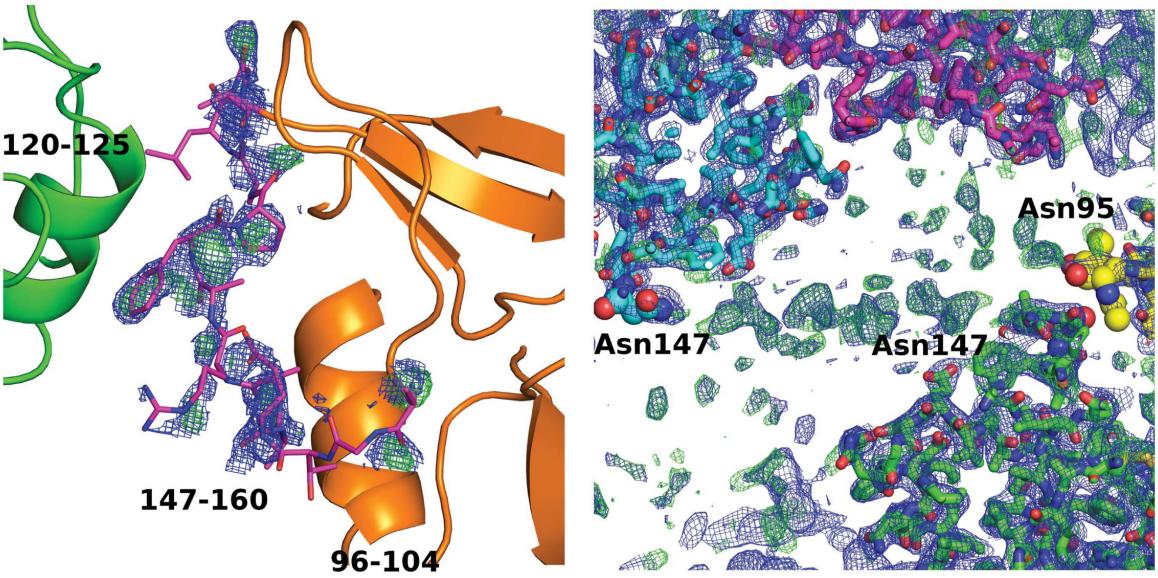

Figure 3
(*a*) Electron-density OMIT maps for the flexible loop (residues 147–160) placed in an unusual position in the monomeric structure of LLT1 (LLT1_mono). $2mF_o - DF_c$ (blue, 0.8σ) and $mF_o - DF_c$ (green, 2.5 σ) Fourier maps are drawn up to a distance of 1.6 Å from the atoms of residues 147–160. The residues are better localized in the middle of the loop, where they are stabilized by the nearby α-helix of a neighbouring molecule in the crystal (green). The loop is not modelled in the deposited structure because weak signal in this region causes unstable refinement. (*b*) Two neighbouring hexamers in the crystal of LLT1_glyco are connected by weak electron density belonging to the glycan chains. The glycosylated residues and GlcNAc units are shown as spheres. $2mF_o - DF_c$ (blue, 0.7σ) and $mF_o - DF_c$ (green, 1.8σ) Fourier maps are shown.

from for example the small aspartic proteases (such as HIV-1 protease), which in contrast require a strictly defined binding site at the dimer interface providing an environment for a specific peptide-bond cleavage. Increased flexibility within the dimer interface would be destructive for the function of proteases, unlike in this case of CTL protein–CTL ligand complexation, where the flexibility and ability to adapt the dimer shape to enable protein partner binding could be an advantage.

3.4. Crystal packing of monomeric LLT1

The crystal packing of LLT1_mono was investigated to confirm that the form of the protein in this structure is really monomeric and that no possible partner participating in oligomer formation can be found among the symmetry-related copies. The crystal packing is shown in Fig. 5(*a*). The classical dimerization interface is left open to the solvent, without any crystal contacts. The largest intermolecular interface in the crystal (according to the *PISA* server; Krissinel & Henrick, 2007) has a surface area of 724 Å^2 (11% of the monomer surface area) and includes ten hydrogen bonds. The following interface is much weaker (372 Å^2). The largest intermolecular contact is formed by the C- and N-termini of the chain with the region above the β-sheet of the neighbouring molecule where the outer loop of the long loop region is usually localized. In this structure, the outer loop (147–160) of the long loop region is turned over towards the other side along the inner loop and the terminal region of a neighbouring molecule takes its place (Figs. 2*c* and 5*a*). This contact with the C- and N-termini cannot be a biologically relevant contact, because in the cell the N-terminal chain continues to the membrane. This leads to the conclusion that in this structure the LLT1 monomer does not form any biologically relevant contacts.

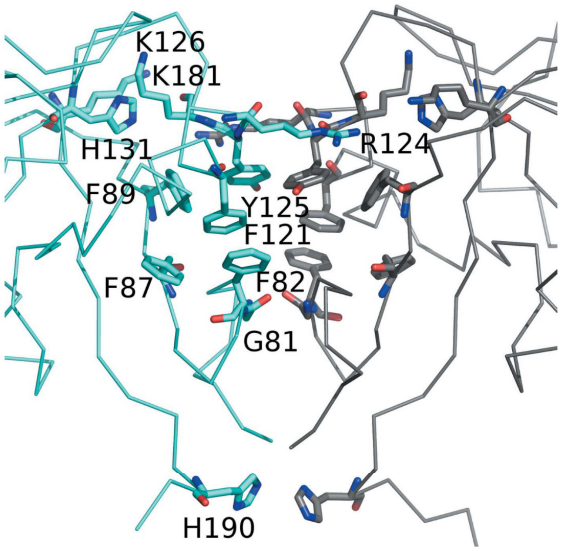

Figure 4
A detailed view of the LLT1 dimer interface (structure LLT1_D2).

3.5. Crystal packing of dimeric LLT1

The strongest dimer–dimer contact in the LLT1_D1 and LLT1_D2 crystals is the contact of the turns of three loops (around residues 139, 160 and 177) with a 'binding pocket' at the dimer interface (in the part distant from the N- and C-termini; Fig. 5*b*). The contact has an area of 620 Å^2 and includes 15 hydrogen bonds. An *N*-acetylglucosamine unit bound to Asn95 is also in this region and is close to the 'binding pocket'. This type of crystal packing would be much more complicated or impossible in the case where the protein was not deglycosylated after the first GlcNAc unit.

In our structural study of the Clr-g receptor (Skálová *et al.*, 2012), the strongest contact in the crystal was also connected with a bond to this 'binding pocket' at the dimer interface. In that case, it was the truncated N-terminus of the Clr-g chain making a tight interaction with the neighbouring dimer interface (the 'binding pocket'), a clearly strong but biologically irrelevant interaction.

3.6. Role of pH in the formation of dimers

The monomeric form of LLT1 was crystallized at pH 3.5 and the changed protonation state at low pH corresponds with the changed preferred intermolecular contacts and the formation of oligomers.

As an example, residue His190, localized near the C-terminus in the dimerization interface, is charged at low pH and destabilizes this part of the interface. It is apparent from the structures that His190 is neutral in LLT1_D1 and LLT1_D2 (pH 7.0) and is close to His190 (3.1 and 3.3 Å) from the opposite chain, participating in a partial stacking interaction. In LLT1_glyco (pH 4.2) His190 is not localized in electron density. In LLT1_mono His190 is very likely to be protonated as it forms a hydrogen bond to the N-terminal Gln72 O of the same chain.

Residues His131 and Lys181 are found in LLT1_D1 and LLT1_D2 close (with regard to interaction of charges, ~5 Å) to the site in which the guanidinium group of Arg124 reaches over from the opposite chain to 'lock' the dimer interface, which is otherwise formed mainly by the hydrophobic core. Arg124 stacks on the side chain of Tyr125 and forms additional hydrogen bonds. In the low-pH structure LLT1_mono, His131 is charged and this site attracts an SO_4^{2-} ion. Under these conditions the positive charge of Lys181 and His131 repels Arg124 from its standard position and thus contributes to dimer destabilization.

As LLT1 is expected to function as a dimer, very low pH values would disable its dimerization and its function as such. A tumour environment often shows decreased pH, but not such drastically lowered values, and a decrease of pH in some cases also leads to higher activity of cytotoxic cells. Given that we observe standard dimers at pH 4.2 in the LLT1_glyco structure and only the extreme pH of 3.5 in LLT1_mono leads to dimer disruption, this direct observation of behaviour at extremely low pH is not relevant to normal biological limits.

3.7. Hexamers of LLT1 with $GlcNAc_2Man_5$ glycosylation

The LLT1_glyco structure is packed into hexamers (Figs. 5*c* and 6). The hexamer is formed by three dimers, which are similar to those of LLT1_D1 and LLT1_D2. The hexamer has one threefold and three perpendicular twofold axes of symmetry (point symmetry 32, where the asymmetric unit is one monomer). The hexamer of ∼70 Å diameter contains a central cavity of about 10 Å in diameter. The cavity is formed by the surface depressions of the three participating dimers found on the termini-distal surface. Six Pro128 residues are exposed into the cavity and six Asp168 and Lys169 residues with their side chains near to the proline residues together form the border of the cavity. The cavity is connected to the exterior of the hexamer by a channel along the threefold axis of the hexamer (Fig. 6*b*; the channel shape was computed in *CAVER*; Chovancova *et al.*, 2012).

The tightest monomer–monomer contact in the hexamer is the standard dimerization contact (530 $Å^2$). The second largest contact has practically the same area (528 $Å^2$) but lacks hydrogen bonds. The third largest contact, with a surface area of 377 $Å^2$, involves six hydrogen bonds (*A*Cys176 N–*B*Glu138 $O^{\varepsilon1}$, *A*Tyr177 N–*B*Glu138 $O^{\varepsilon1}$, *A*Arg101 $N^{\eta2}$–*B*Asn147 O and three analogous hydrogen bonds with exchanged chains). The second and the third strongest contacts are formed to molecules of the neighbouring dimer so that the dimer–dimer contact in the hexamer is relatively strong and these additional interactions explain the weakened interactions of monomers in the LLT1_glyco dimerization interface, as described in §3.3.

The N- and C-termini of the extracellular part of LLT1 are localized on the surface of the hexamer, but in different directions for different dimers (Fig. 6*c*). This indicates that LLT1 present on the surface of one cell cannot form such hexamers. However, the dimer packing into the hexamers may

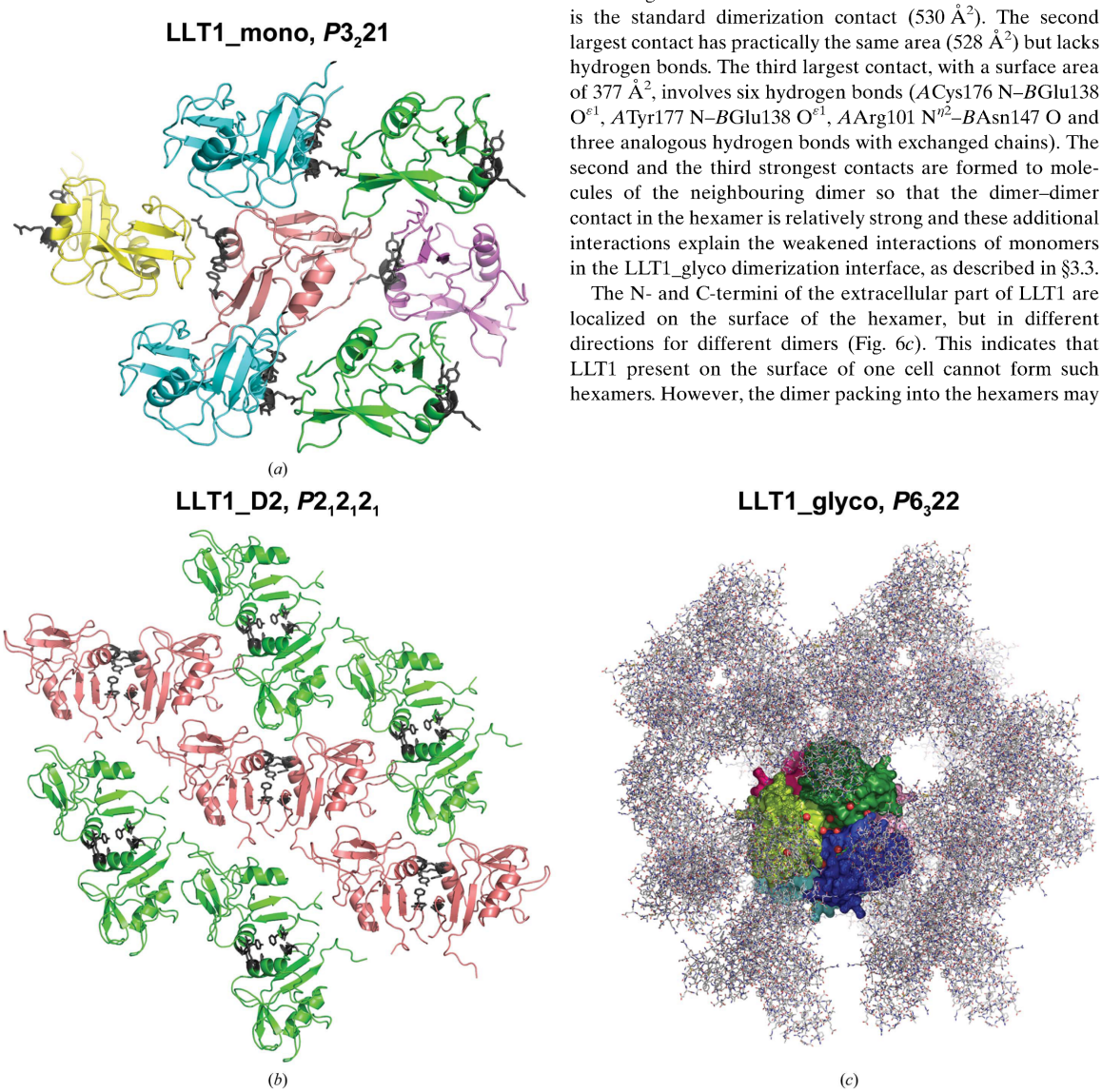

Figure 5
Crystal packing of the presented LLT1 structures. (*a*) LLT1_mono. Colours are according to the orientation of the protein molecule in the crystal. Residues that would form the dimer interface in the case of a dimer (Gly81, Phe82, Phe121, Arg124 and Tyr125) are shown as black sticks. (*b*) LLT1_D2 with the same colour coding. The dimer interface is shown as black sticks. LLT1_D1 has similar packing as LLT1_D2. (*c*) LLT1_glyco. One hexamer, containing three dimers of LLT1, is represented by a molecular surface colour-coded by individual protein chains and viewed along the crystallographic threefold axis. Surrounding symmetry-related chains are represented as sticks.

indicate a possible method of NK receptor–ligand interaction between two cells (see §3.11).

3.8. Role of glycosylation in LLT1_glyco

In the hexamer, the glycosylated Asn residues Asn95 and Asn147 are localized on its surface. Three Asn95 residues related by the threefold axis are at a mutual distance of 18 Å and are placed relatively close to the central channel. Three Asn147 residues located ∼18 Å from the Asn95 residues in the direction away from the central channel are distant from each other. The other three Asn95 and three Asn147 residues are in the same formation on the opposite side of the hexamer.

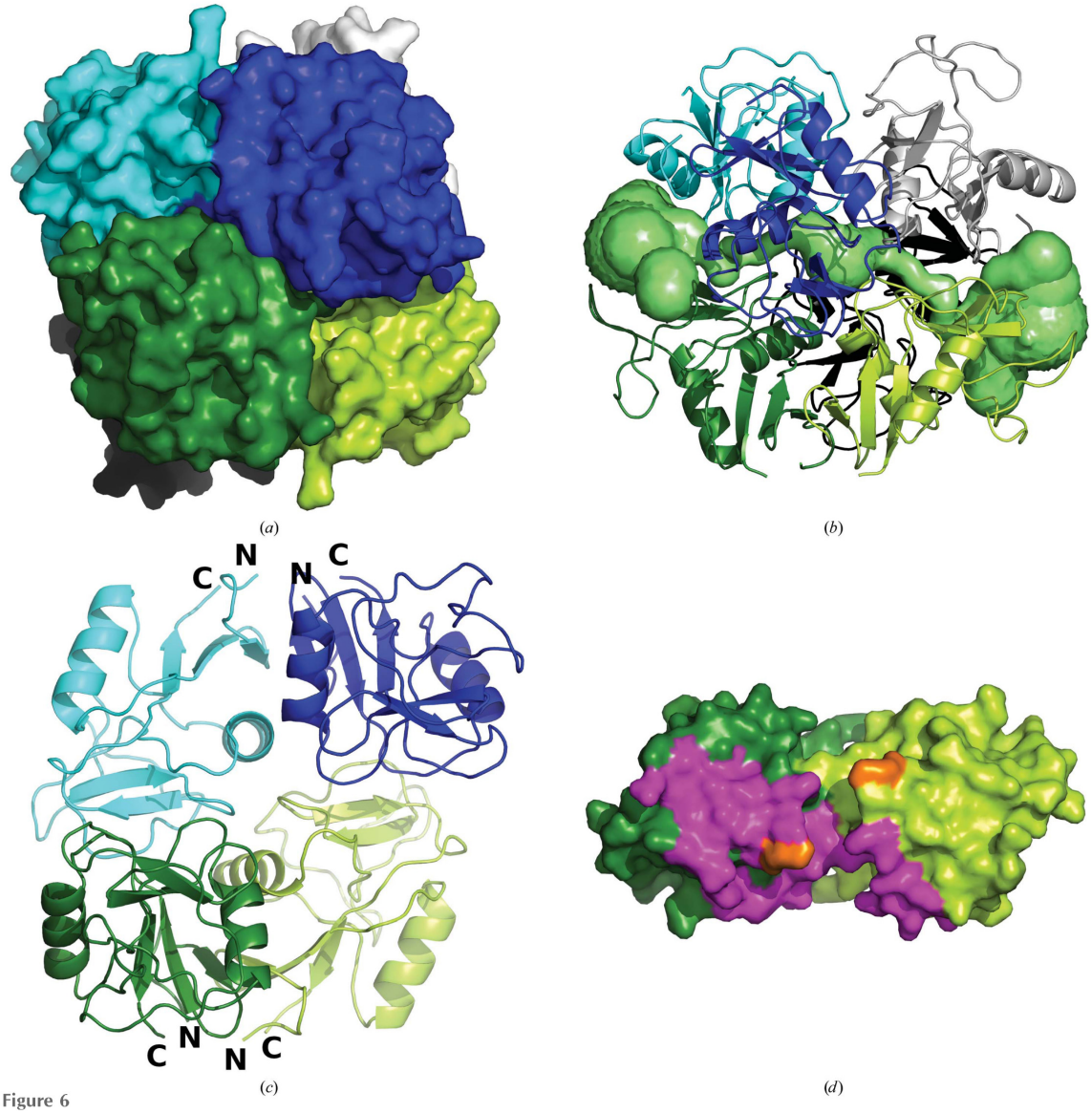

Figure 6
The fully glycosylated form of LLT1 forms hexamers in crystals which are an assembly of three classical dimers. The dimers are distinguished by colour (dark and light green, dark and light blue and black and white). (*a*) A general view of the hexamer. (*b*) Visualization of the tunnel and the central cavity of the hexamer (computed in *CAVER*). A view perpendicular to the threefold axis, which is the direction of the tunnel. (*c*) Dimer–dimer contacts in the hexamer. One dimer of the hexamer is omitted to show the mutual orientation of two dimers. The N- and C-termini of the chains are denoted. (*d*) Contact residues of a dimer with its neighbour in the hexamer. Residues forming the LLT1 dimer–dimer contact up to a distance of 5 Å are shown in magenta. Residue Lys169 (important for interaction in the NKR-P1–LLT1 complex) is coloured orange. The contact residues are localized on the termini-distal side. Interacting residues were identified using *NCONTACT* from the *CCP*4 package (Winn *et al.*, 2011).

However, Asn147 is very close to Asn95 from a symmetry-related hexamer in the unit cell: the distance between Asn147 O and Asn95 $O^{\delta1}$ from a symmetry-related molecule is 7.7 Å (Fig. 3*b*). In spite of the fact that it is not possible to model any unit of glycosylation well at Asn147 because the electron density is not sufficiently unambiguous, there is apparent continuous electron density between Asn147 and Asn147 from the neighbouring hexamer (the distance between the Asn147 $N^{\delta2}$ atoms is 33 Å; Fig. 3*b*) with peaks of up to 1.3σ in $2mF_o - DF_c$ and 3.6σ in $mF_o - DF_c$ maps, indicating that the oligosaccharide chains interconnect molecules and indeed the individual hexamers in the crystal. Thus, we conclude that we do not observe any role of glycans in the formation of the hexamer; however, it is evident that the glycans contribute to the packing of the hexamers into the crystal lattice.

3.9. Influence of the His176Cys mutation on the LLT1 structure

The mutated residue 176 is localized on the surface of LLT1 near the long loop region. It is distant from the N- and C-terminal parts and also does not lie in the dimerization interface. The additional S—S bond involving Cys176 stabilizes the protein fold. It is probable that the His176 form of LLT1 would have a longer flexible part of the loop than the flexible part 147–160 observed in the structure of the Cys176 variant. The residue lies in a crystal contact region in the dimeric and hexameric structures, and therefore the wild-type form of LLT1 with His176 would have different crystal packing.

3.10. Comparison of LLT1, CD69 and Clr-g structures

LLT1 shares relatively high three-dimensional structure similarity with other dimeric CTL proteins. All comparisons were performed with the LLT1_D2 coordinates. According to SSM structure superposition with *PDBeFold* (http://www.ebi.ac.uk/msd-srv/ssm/), LLT1 is structurally most similar to human CD69 (PDB entry 1e8i; Llera *et al.*, 2001; 36% sequence identity). Structure similarity to mouse Clr-g (PDB entry 3rs1; Skálová *et al.*, 2012; 44% sequence identity) has similar values when comparing monomers and is a little lower when comparing dimers. The parameters of the structure superpositions are as follows: LLT1 monomer/CD69 monomer, *Q*-score[1] 0.82 and r.m.s. deviation 1.10 Å, aligned on 115 residues; LLT1 dimer/CD6 dimer, *Q*-score 0.67 and r.m.s. deviation 1.67 Å, aligned on 223 residues; LLT1 monomer/Clr-g monomer, *Q*-score 0.82 and r.m.s. deviation 0.96 Å, aligned on 116 residues; LLT1 dimer/Clr-g dimer, *Q*-score 0.55 and r.m.s. deviation 2.10 Å, aligned on 219 residues.

The comparison of the structure of LLT1_D2 with that of mouse Clr-g is shown in Fig. 2(*b*). The superposition was performed in *Coot* by SSM of chains *A*. There is an apparent difference in the mutual orientation of the monomers in the dimer of LLT1 in comparison with mouse Clr-g. There are shifts in the distant part of the long loop region of up to 5 Å. Differences are also present in the N- and C-terminal parts owing to the distinct lengths of the LLT1 and Clr-g constructs. Differences between LLT1 and CD69 are found in the same regions and are of the same character as the differences between LLT1 and Clr-g (not shown).

Electrostatic equipotential surfaces of LLT1 and mouse Clr-g (Skálová *et al.*, 2012) are shown in Fig. 2(*d*). There are some positive patches in the part distant from the N- and C-termini in LLT1. A similar and much stronger effect is observed for mouse Clr-g. The large patch in Clr-g is formed mainly owing to the contributions of Arg180, Arg193 and Arg198, which correspond to Glu162, Arg175 and Arg180 in LLT1. The change from Arg180 to Glu162 may explain the weaker positive patches in the case of LLT1.

3.11. Hypotheses about NKR-P1–LLT1 complexation

The hexamer is formed by the packing of three 'standard' CTL dimers. To the best of our knowledge, no such molecular arrangement has been observed for CTL proteins. Each dimer in the hexamer interacts with two other dimers. The dimer–dimer interaction in the hexamer is analyzed in Figs. 6(*c*) and 6(*d*). Could this dimer–dimer interaction indicate the manner of NK CTL receptor–CTL ligand complex formation or other biologically relevant actions?

This interaction of LLT1–LLT1 dimers in the hexamer is not a 'face-to-face' interaction, as is classically expected for NK CTL receptor–CTL ligand interaction (Kamishikiryo *et al.*, 2011); rather, one monomer of the dimer binds to one dimer and the second monomer binds to another dimer of the hexamer. In this aspect it is similar to the model of the NKR-P1F–Clr-g complex (based on electrostatic complementarity) in our previous study (Skálová *et al.*, 2012).

The only experimentally determined structure of a CTL NK receptor–CTL ligand complex is the X-ray structure of the monomeric receptor NKp65–dimeric KACL ligand complex (PDB entry 4iop; Li *et al.*, 2013), where the binding mode is of the monomer–dimer type. The sequence identity of the CTL domain of LLT1 to the CTL domain of KACL is 49%, while that of LLT1 to NKp65 is 30%.

We have built several models of the NKR-P1–LLT1 complex. The modelling of NKR-P1 was performed in *SWISS-MODEL* (Biasini *et al.*, 2014) based on the crystal structure of mouse NKR-P1A (PDB entry 3m9z; Kolenko, Rozbeský, Vaněk, Kopecký *et al.*, 2011; 46% sequence identity). The crystal structure of mouse NKR-P1A (Kolenko, Rozbeský, Vaněk, Bezouška *et al.*, 2011; Kolenko, Rozbeský, Vaněk, Kopecký *et al.*, 2011) has extended flexible loops which form crystal contacts and most probably occupy a different position in solution (Sovová *et al.*, 2011). However, the identified receptor–ligand interaction pairs do not lie in the loops; therefore, it is possible to use the crystal structure as a modelling basis for our purposes.

The first model is based on the NKp65–KACL structure. Both the model of NKR-P1 and the structure of LLT1 were

[1] *Q*-score is the default sorting criterion of structure similarity in *PDBeFold* and is defined as $Q = N_{algn} \times N_{algn}/\{[1 + (\text{r.m.s.d.}/R_0)^2] \times N_{res1} \times N_{res2}\}$, where $R_0 = 3$ Å, N_{res1} and N_{res2} are the numbers of residues in the overlapping structures and N_{algn} is the number of overlapped residues.

superimposed on the structure of the NKp65–KACL complex to simulate a model of the NKR-P1–LLT1 complex (Supplementary Fig. S1*a*). In this rather crude model it is possible to query the interaction between Lys169 of LLT1 and Glu205 of NKR-P1, which were identified by Kamishikiryo and coworkers as the key interacting residues based on SPR experiments (Kamishikiryo *et al.*, 2011). It should be noted that these SPR experiments were performed on nonglycosylated LLT1 produced in *E. coli*. In this first model, these two residues are 10 Å away from each other.

In the second model we exchanged the positions of the receptor and the ligand, *i.e.* NKR-P1 was superimposed on KACL and the individual chains of LLT1 on the positions of the monomers of NKp65 (Supplementary Fig. S1*b*). In this model, residues Lys169 of LLT1 and Glu205 of NKR-P1 are in direct contact.

The third model is based on the LLT1–LLT1 dimer–dimer mutual position in the hexameric structure. The NKR-P1 model was superimposed on the closest LLT1 chain in the hexamer with respect to a fixed LLT1 dimer (Supplementary Figs. S1*c* and S1*d*). In this model, the distance between LLT1 Lys169 and NKR-P1 Glu205 is 20 Å.

Based on the assumption of close positioning of Lys169 and Glu205, we conclude that the LLT1 arrangement in the hexameric packing is not a probable model for NK CTL receptor–CTL ligand interaction. Interestingly, the only model enabling direct contact of Lys169 and Glu205 residues is that which requires disruption of the LLT1 dimer into monomers. It remains to be shown experimentally in the future whether this is truly the case.

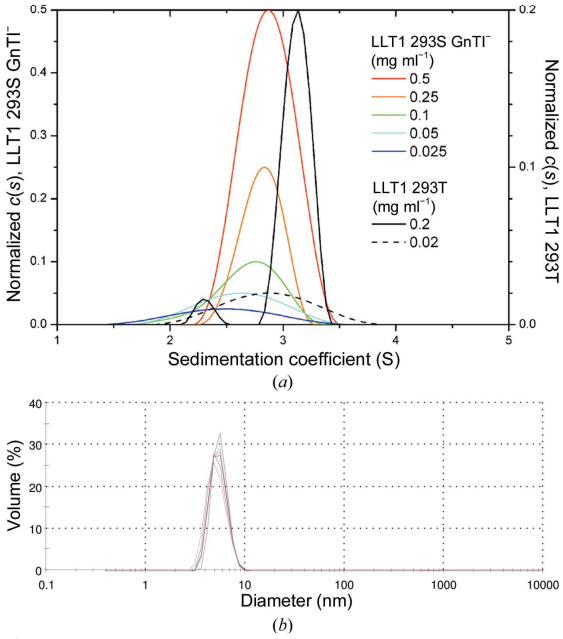

Figure 7
(*a*) Sedimentation analysis of LLT1 oligomerization. Glycosylated LLT1 with homogeneous $GlcNAc_2Man_5$ N-glycosylation produced in the HEK293S GnTI$^-$ cell line was characterized by a sedimentation-velocity experiment in an analytical ultracentrifuge at five different concentrations (coloured lines). The continuous size distribution of the sedimenting species is shown, which was normalized with respect to the difference in loading concentration. A broad size distribution that is shifted towards lower values with lower protein concentration points to monomer–dimer equilibrium; for comparison, data for LLT1 produced in the HEK293T cell line with wild-type complex N-glycosylation are shown (black and dashed lines), with separated signals for dimeric and monomeric protein at higher protein concentration. (*b*) Size distribution of LLT1 measured by dynamic light scattering and scaled by volume. Seven measurements (distributions differentiated by colour) were performed with similar results, three of them at 291 K, two at 298 K and two at 303 K.

3.12. Oligomeric state of LLT1 in solution

Sedimentation-equilibrium analysis has previously shown that LLT1 forms noncovalent dimers in solution that do not depend on its N-glycosylation (Bláha *et al.*, 2015). However, to assess for the presence of either monomers or higher oligomers (*e.g.* hexamers), we performed sedimentation-velocity measurements. Firstly, LLT1 produced in the HEK293T cell line with wild-type complex N-glycosylation was analyzed. At 0.2 mg ml^{-1} concentration, LLT1 behaves as two distinct species with $s_{20,w}$ values of 2.43 and 3.14 ± 0.1 S corresponding to a monomer and a dimer, respectively (Fig. 7*a*, black line). Upon tenfold dilution the two peaks merged into one with an average $s_{20,w}$ value of 2.87 S, pointing to a monomer–dimer equilibrium at low concentration (Fig. 7*a*, dashed line). No higher oligomers were detected. LLT1 with homogeneous $GlcNAc_2Man_5$ N-glycosylation produced in the HEK293S GnTI$^-$ cell line behaved similarly, yielding broad size distributions that shifted towards lower sedimentation-coefficient values at lower protein concentrations (Fig. 7*a*, coloured lines), thus reflecting monomer–dimer equilibrium behaviour of the protein. The fact that monomeric and dimeric forms are not separated in these distributions might suggest that LLT1 produced with shorter *N*-glycans dimerizes more weakly and/or that equilibrium exchange is faster than for LLT1 with wild-type complex *N*-glycans, with an estimated K_d lying in the low micromolar range (∼20 µ*M*).

Dynamic light scattering was performed for LLT1 with homogeneous $GlcNAc_2Man_5$ N-glycosylation produced in the HEK293S GnTI$^-$ cell line at 1 mg ml^{-1} concentration (Fig. 7*b*). The experiment was repeated at temperatures of 291, 298 and 303 K. Particles with a diameter of 55 ± 10 Å were observed in all cases. This value corresponds to a Stokes diameter of 56 Å for the LLT1 dimer, as computed based on the three-dimensional structure of LLT1 in *HYDROPRO* (Ortega *et al.*, 2011), while the Stokes diameter computed for the LLT1 hexamer is 70 Å and that for the monomer is 20 Å.

4. Conclusions

This study has introduced the first X-ray structures of LLT1. A new conformation of the outer loop in the long loop region of a CTL receptor/ligand was observed; its newly observed position near α-helix 96–104 is probably the result of conformational sampling with satisfied packing positions of the

neighbours and is without any special biological significance. Furthermore, the four structures with their mutual differences extend our understanding of the influence of glycosylation on the structure and the role of flexibility of the dimer interface in complex formation.

Glycosylation control has been shown by this study to play a very important role in structural investigations of small mammalian proteins. The fully homogeneously glycosylated extracellular domain of human LLT1 clearly gained from the uniformity of the glycosylation pattern. The longer, yet homogeneous, oligosaccharides seem to participate in crystal formation of the LLT1_glyco form. Their uniform length and type are important. It is also clear that these longer oligosaccharides would disable the crystal contacts observed for deglycosylated LLT1 in the dimeric structures LLT1_D1 and LLT1_D2. The deglycosylated protein variant enables the formation of contacts in which GlcNAc plays an important role, but longer antennae would disable such tight packing into a crystal. Both forms (uniformly glycosylated and deglycosylated) proved to be important for the structural results, thereby showing the extreme importance of controlled post-translational modifications for detailed molecular studies.

The hydrogen-bonding pattern at the LLT1 dimer interface is not the governing interaction in dimerization and can be significantly weakened, as is the case for the LLT1_glyco form. Here, the interactions with the neighbouring dimers in the hexamer are strong enough to slightly deform the dimer so that several interface hydrogen bonds near the termini region disappear (the hydrophobic core remains unchanged). The variability of the CTL receptor or ligand dimer interface reported previously, and confirmed by this study, is thus clearly related to the CTL dimer–dimer interaction for the first time. The capacity of these small proteins to form very flexible but still well defined dimers is very likely to form a part of their overall strategy for mediating plastic cell–cell interactions in the immune system.

Acknowledgements

This study was supported by BIOCEV CZ.1.05/1.1.00/02.0109 from the ERDF, the Ministry of Education, Youth and Sports of the Czech Republic (grants EE2.3.30.0029 and LG14009), the Czech Science Foundation (project P302/11/0855 and 15-15181S), Charles University (GAUK 403211/2010, UNCE 204025/2012 and SVV 260079/2014), the High Education Development Fund (FRVS 669/2013), P-CUBE (EC FP7 project 227764), BioStruct-X (EC FP7 project 283570) and Instruct, part of the European Strategy Forum on Research Infrastructures (ESFRI) supported by national member subscriptions. We thank the staff of beamlines I02 and I04-1 at Diamond Light Source and BM14.1 at BESSY II for technical support.

References

Aldemir, H., Prod'homme, V., Dumaurier, M.-J., Retiere, C., Poupon, G., Cazareth, J., Bihl, F. & Braud, V. M. (2005). *J. Immunol.* **175**, 7791–7795.
Aust, J. G., Gays, F., Mickiewicz, K. M., Buchanan, E. & Brooks, C. G. (2009). *J. Immunol.* **183**, 106–116.
Baker, N. A., Sept, D., Joseph, S., Holst, M. J. & McCammon, J. A. (2001). *Proc. Natl Acad. Sci. USA*, **98**, 10037–10041.
Bartel, Y., Bauer, B. & Steinle, A. (2013). *Front. Immunol.* **4**, 362.
Battye, T. G. G., Kontogiannis, L., Johnson, O., Powell, H. R. & Leslie, A. G. W. (2011). *Acta Cryst.* D**67**, 271–281.
Biasini, M., Bienert, S., Waterhouse, A., Arnold, K., Studer, G., Schmidt, T., Kiefer, F., Cassarino, T. G., Bertoni, M., Bordoli, L. & Schwede, T. (2014). *Nucleic Acids Res.* **42**, W252–W258.
Bláha, J., Pachl, P., Novák, P. & Vaněk, O. (2015). *Protein Expres. Purif.* **109**, 7–13.
Caligiuri, M. A. (2008). *Blood*, **112**, 461–469.
Chen, V. B., Arendall, W. B., Headd, J. J., Keedy, D. A., Immormino, R. M., Kapral, G. J., Murray, L. W., Richardson, J. S. & Richardson, D. C. (2010). *Acta Cryst.* D**66**, 12–21.
Chovancova, E., Pavelka, A., Benes, P., Strnad, O., Brezovsky, J., Kozlikova, B., Gora, A., Sustr, V., Klvana, M., Medek, P., Biedermannova, L., Sochor, J. & Damborsky, J. (2012). *PLoS Comput. Biol.* **8**, e1002708.
Diederichs, K. & Karplus, P. A. (1997). *Nature Struct. Mol. Biol.* **4**, 269–275.
Dolinsky, T. J., Czodrowski, P., Li, H., Nielsen, J. E., Jensen, J. H., Klebe, G. & Baker, N. A. (2007). *Nucleic Acids Res.* **35**, W522–W525.
Durocher, Y., Perret, S. & Kamen, A. (2002). *Nucleic Acids Res.* **30**, E9.
Emsley, P., Lohkamp, B., Scott, W. G. & Cowtan, K. (2010). *Acta Cryst.* D**66**, 486–501.
Evans, P. R. & Murshudov, G. N. (2013). *Acta Cryst.* D**69**, 1204–1214.
Fine, J. H., Chen, P., Mesci, A., Allan, D. S., Gasser, S., Raulet, D. H. & Carlyle, J. R. (2010). *Cancer Res.* **70**, 7102–7113.
French, S. & Wilson, K. (1978). *Acta Cryst.* A**34**, 517–525.
Germain, C., Bihl, F., Zahn, S., Poupon, G., Dumaurier, M. J., Rampanarivo, H. H., Padkjaer, S. B., Spee, P. & Braud, V. M. (2010). *J. Biol. Chem.* **285**, 36207–36215.
Germain, C., Meier, A., Jensen, T., Knapnougel, P., Poupon, G., Lazzari, A., Neisig, A., Håkansson, K., Dong, T., Wagtmann, N., Galsgaard, E. D., Spee, P. & Braud, V. M. (2011). *J. Biol. Chem.* **286**, 37964–37975.
Gouet, P., Robert, X. & Courcelle, E. (2003). *Nucleic Acids Res.* **31**, 3320–3323.
Grobárová, V., Benson, V., Rozbeský, D., Novák, P. & Černý, J. (2013). *Immunol. Lett.* **156**, 110–117.
Grueninger-Leitch, F., D'Arcy, A., D'Arcy, B. & Chène, C. (1996). *Protein Sci.* **5**, 2617–2622.
Huarte, E., Cubillos-Ruiz, J. R., Nesbeth, Y. C., Scarlett, U. K., Martinez, D. G., Engle, X. A., Rigby, W. F., Pioli, P. A., Guyre, P. M. & Conejo-Garcia, J. R. (2008). *Blood*, **112**, 1259–1268.
Kabsch, W. & Sander, C. (1983). *Biopolymers*, **22**, 2577–2637.
Kamishikiryo, J., Fukuhara, H., Okabe, Y., Kuroki, K. & Maenaka, K. (2011). *J. Biol. Chem.* **286**, 23823–23830.
Keegan, R. M., Long, F., Fazio, V. J., Winn, M. D., Murshudov, G. N. & Vagin, A. A. (2011). *Acta Cryst.* D**67**, 313–323.
Kolenko, P., Rozbeský, D., Vaněk, O., Bezouška, K., Hašek, J. & Dohnálek, J. (2011). *Acta Cryst.* F**67**, 1519–1523.
Kolenko, P., Rozbeský, D., Vaněk, O., Kopecký, V. Jr, Hofbauerová, K., Novák, P., Pompach, P., Hašek, J., Skálová, T., Bezouška, K. & Dohnálek, J. (2011). *J. Struct. Biol.* **175**, 434–441.
Kolenko, P., Skálová, T., Vaněk, O., Štěpánková, A., Dušková, J., Hašek, J., Bezouška, K. & Dohnálek, J. (2009). *Acta Cryst.* F**65**, 1258–1260.
Krissinel, E. & Henrick, K. (2007). *J. Mol. Biol.* **372**, 774–797.
Kveberg, L., Dai, K.-Z., Westgaard, I. H., Daws, M. R., Fossum, S., Naper, C. & Vaage, J. T. (2009). *Eur. J. Immunol.* **39**, 541–551.
Lanier, L. L. (2008). *Nature Immunol.* **9**, 495–502.
Lebedev, A. A. & Isupov, M. N. (2014). *Acta Cryst.* D**70**, 2430–2443.

Leslie, A. G. W. & Powell, H. R. (2007). *Evolving Methods for Macromolecular Crystallography*, edited by R. J. Read & J. L. Sussman, pp. 41–51. Dordrecht: Springer.
Li, H., Robertson, A. D. & Jensen, J. H. (2005). *Proteins*, **61**, 704–721.
Li, Y., Wang, Q., Chen, S., Brown, P. H. & Mariuzza, R. A. (2013). *Proc. Natl Acad. Sci. USA*, **110**, 11505–11510.
Llera, A. S., Viedma, F., Sánchez-Madrid, F. & Tormo, J. (2001). *J. Biol. Chem.* **276**, 7312–7319.
Long, F., Vagin, A. A., Young, P. & Murshudov, G. N. (2008). *Acta Cryst.* D**64**, 125–132.
Mueller, U., Darowski, N., Fuchs, M. R., Förster, R., Hellmig, M., Paithankar, K. S., Pühringer, S., Steffien, M., Zocher, G. & Weiss, M. S. (2012). *J. Synchrotron Rad.* **19**, 442–449.
Murshudov, G. N., Skubák, P., Lebedev, A. A., Pannu, N. S., Steiner, R. A., Nicholls, R. A., Winn, M. D., Long, F. & Vagin, A. A. (2011). *Acta Cryst.* D**67**, 355–367.
Natarajan, K., Sawicki, M. W., Margulies, D. H. & Mariuzza, R. A. (2000). *Biochemistry*, **39**, 14779–14786.
Ortega, A., Amorós, D. & García de la Torre, J. (2011). *Biophys. J.* **101**, 892–898.
Otwinowski, Z. & Minor, W. (1997). *Methods Enzymol.* **276**, 307–326.
Reeves, P. J., Callewaert, N., Contreras, R. & Khorana, H. G. (2002). *Proc. Natl Acad. Sci. USA*, **99**, 13419–13424.
Rosen, D. B., Bettadapura, J., Alsharifi, M., Mathew, P. A., Warren, H. S. & Lanier, L. L. (2005). *J. Immunol.* **175**, 7796–7799.
Rosen, D. B., Cao, W., Avery, D. T., Tangye, S. G., Liu, Y.-J., Houchins, J. P. & Lanier, L. L. (2008). *J. Immunol.* **180**, 6508–6517.
Roth, P., Mittelbronn, M., Wick, W., Meyermann, R., Tatagiba, M. & Weller, M. (2007). *Cancer Res.* **67**, 3540–3544.
Satkunanathan, S., Kumar, N., Bajorek, M., Purbhoo, M. A., Culley, F. J. & Lyles, D. (2014). *J. Virol.* **88**, 2366–2373.
Schuck, P. (2003). *Anal. Biochem.* **320**, 104–124.
Sievers, F., Wilm, A., Dineen, D., Gibson, T. J., Karplus, K., Li, W., Lopez, R., McWilliam, H., Remmert, M., Söding, J., Thompson, J. D. & Higgins, D. G. (2011). *Mol. Syst. Biol.* **7**, 539.
Skálová, T., Kotýnková, K., Dušková, J., Hašek, J., Koval, T., Kolenko, P., Novák, P., Man, P., Hanč, P., Vaněk, O., Bezouška, K. & Dohnálek, J. (2012). *J. Immunol.* **189**, 4881–4889.
Sovová, Ž., Kopecký, V. Jr, Pazderka, T., Hofbauerová, K., Rozbeský, D., Vaněk, O., Bezouška, K. & Ettrich, R. (2011). *J. Mol. Model.* **17**, 1353–1370.
Strong, M., Sawaya, M. R., Wang, S., Phillips, M., Cascio, D. & Eisenberg, D. (2006). *Proc. Natl Acad. Sci. USA*, **103**, 8060–8065.
Sullivan, L. C., Clements, C. S., Beddoe, T., Johnson, D., Hoare, H. L., Lin, J., Huyton, T., Hopkins, E. J., Reid, H. H., Wilce, M. C. J., Kabat, J., Borrego, F., Coligan, J. E., Rossjohn, J. & Brooks, A. G. (2007). *Immunity*, **27**, 900–911.
Thompson, J. D., Higgins, D. G. & Gibson, T. J. (1994). *Nucleic Acids Res.* **22**, 4673–4680.
Vagin, A. & Teplyakov, A. (2010). *Acta Cryst.* D**66**, 22–25.
Vaněk, O. *et al.* (2008). *FEBS J.* **275**, 5589–5606.
Vivier, E., Raulet, D. H., Moretta, A., Caligiuri, M. A., Zitvogel, L., Lanier, L. L., Yokoyama, W. M. & Ugolini, S. (2011). *Science*, **331**, 44–49.
Vivier, E., Tomasello, E., Baratin, M., Walzer, T. & Ugolini, S. (2008). *Nature Immunol.* **9**, 503–510.
Voigt, S., Mesci, A., Ettinger, J., Fine, J. H., Chen, P., Chou, W. & Carlyle, J. R. (2007). *Immunity*, **26**, 617–627.
Weiss, M. S. (2001). *J. Appl. Cryst.* **34**, 130–135.
Williams, K. J., Wilson, E., Davidson, C. L., Aguilar, O. A., Fu, L., Carlyle, J. R. & Burshtyn, D. N. (2012). *J. Immunol.* **188**, 4980–4991.
Winn, M. D. *et al.* (2011). *Acta Cryst.* D**67**, 235–242.
Yokoyama, W. M. & Plougastel, B. F. M. (2003). *Nature Rev. Immunol.* **3**, 304–316.
Zelensky, A. N. & Gready, J. E. (2005). *FEBS J.* **272**, 6179–6217.

Acta Cryst. (2015). D**71**, doi:10.1107/S1399004714027928 Supporting information

BIOLOGICAL
CRYSTALLOGRAPHY

Volume 71 (2015)

Supporting information for article:

Four crystal structures of human LLT1, a ligand for human NKR-P1, in varied glycosylation and oligomerization states

Tereza Skálová, Jan Bláha, Karl Harlos, Jarmila Dušková, Tomáš Kovaľ, Jan Stránský, Jindřich Hašek, Ondřej Vaněk and Jan Dohnálek

Acta Cryst. (2015). D**71**, doi:10.1107/S1399004714027928 Supporting information, sup-1

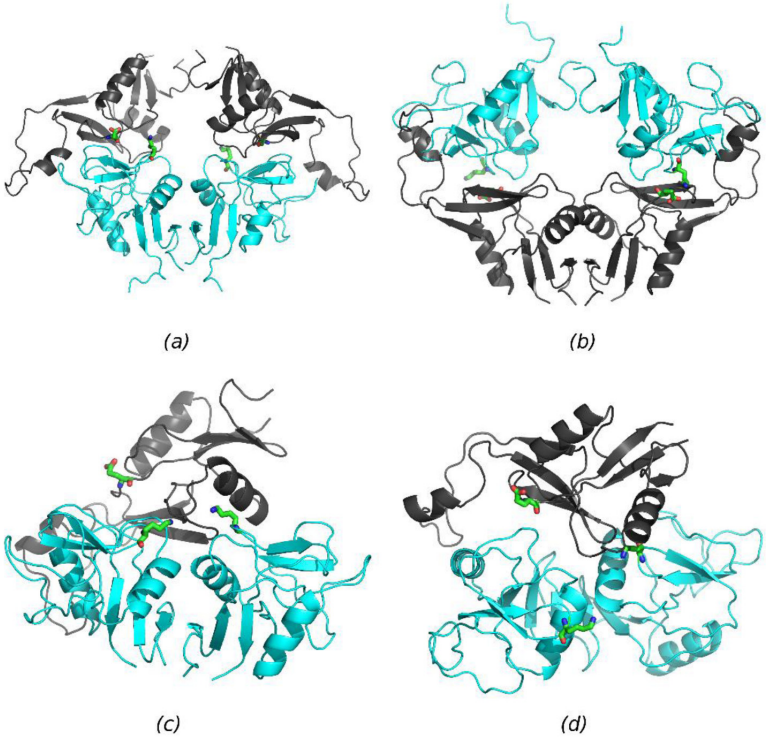

Figure S1 Discussed models of NKR-P1:LLT1 interaction. LLT1 cyan, model of NKR-P1 black. Residues LLT1 Lys169 and NKR-P1 Glu205 important for the interaction (Kamishikiryo *et al.*, 2011) are shown as green sticks. (*a*) Model based on the NKp65:KACL structure (PDB code 4iop, Li *et al.*, 2013), NKR-P1 is placed in position of NKp65 and LLT1 in position of KACL. (*b*) Model based on the same structure, but NKR-P1 takes the position of KACL and LLT1 of NKp65. (*c, d*) Model based on hexameric packing of LLT1_glyco. LLT1 dimer is in its position from the observed hexamer and NKR-P1 in the position of the closest LLT1 monomer in the hexamer. (*d*) A view from the "top" – from the termini distal side.

PUBLICATION III

Bláha, J., Kalousková, B., Skořepa, O., Pažický, S., Novák, P., Vaněk, O.

High-level expression and purification of soluble form of human natural killer cell receptor NKR-P1 in HEK293S GnTI$^-$ cells

Protein Expr. Purif. 140, 36-43 (2017)

My contribution to the publication: *performing research (cloning, protein expression, construct optimization, preparation of stable cell pool, protein characterization and crystallization), data collection, data analysis and interpretation, manuscript writing*

Protein Expression and Purification 140 (2017) 36–43

Contents lists available at ScienceDirect

Protein Expression and Purification

journal homepage: www.elsevier.com/locate/yprep

High-level expression and purification of soluble form of human natural killer cell receptor NKR-P1 in HEK293S GnTI⁻ cells

Jan Bláha [a], Barbora Kalousková [a], Ondřej Skořepa [a], Samuel Pažický [a], Petr Novák [a, b], Ondřej Vaněk [a, *]

[a] Department of Biochemistry, Faculty of Science, Charles University, Hlavova 2030/8, 12840 Prague, Czech Republic
[b] Institute of Microbiology, The Czech Academy of Sciences, BIOCEV, Průmyslová 595, 25250 Vestec, Czech Republic

ARTICLE INFO

Article history:
Received 29 May 2017
Received in revised form
21 July 2017
Accepted 25 July 2017
Available online 27 July 2017

Keywords:
NKR-P1
CD161
klrb1
NK cells
HEK293
LLT1

ABSTRACT

Human natural killer receptor protein 1 (NKR-P1, CD161, gene *klrb1*) is a C-type lectin-like receptor of natural killer (NK) cells responsible for recognition of its cognate protein ligand lectin-like transcript 1 (LLT1). NKR-P1 is the single human orthologue of the prototypical rodent NKR-P1 receptors. Naturally, human NKR-P1 is expressed on the surface of NK cells, where it serves as inhibitory receptor; and on T and NKT cells functioning as co-stimulatory receptor promoting secretion of IFNγ. Most notably, it is expressed on Th17 and Tc17 lymphocytes where presumably promotes targeting into LLT1 expressing immunologically privileged niches. We tested effect of different protein tags (SUMO, TRX, GST, MsyB) on expression of soluble NKR-P1 in *E. coli*. Then we optimized the expression construct of soluble NKR-P1 by preparing a library of expression constructs in pOPING vector containing the extracellular lectin-like domain with different length of the putative *N*-terminal stalk region and tested its expression in Sf9 and HEK293 cells. Finally, a high-level expression of soluble NKR-P1 was achieved by stable expression in suspension-adapted HEK293S GnTI⁻ cells utilizing pOPINGTTneo expression vector. Purified soluble NKR-P1 is homogeneous, deglycosylatable, crystallizable and monomeric in solution, as shown by size-exclusion chromatography, multi-angle light scattering and analytical ultracentrifugation.

1. Introduction

Natural killer (NK) cells are large granular lymphocytes described to be on the functional borderline of innate and adaptive immunity [1,2]. They are mainly recognized for their singular ability to provide defence against viral infection and tumour development without prior antigen sensitization [3], but they also contribute to the regulation of the adaptive system via secretion of cytokines [1] and are even able to form antigen specific immunologic memory [4–6]. NK cell activity is controlled by a fine balance of signals from its variety of inhibitory and activating receptors [3] that engage a broad range of health and disease markers in the accepted "missing-self" and "induced-self" modes of recognition, respectively [7–11].

NK cell receptors are divided into the immunoglobulin-like [12] and the C-type lectin-like (CTL) structural classes [13,14]. C-type lectins bind calcium and carbohydrates; however, CTL receptors recognize protein ligands instead, despite the fact that they are homologous to C-type lectins [15,16]. The NKR-P1 receptor family, encoded in the Natural Killer Cell (NKC) gene complex (human chromosome 12), encompasses the prototypical NK cell receptors belonging to the CTL class [15]. Unlike many CTL NK receptors that are recognizing MHC class I glycoproteins [14,17,18], NKR-P1 receptors interact with a genetically and structurally highly related ligands from *clec2* gene subfamily [13].

Human NKR-P1 (CD161, gene *klrb1*) was identified in 1994 as a human orthologue of rodent NKR-P1 receptors [19] and up to now remains the only described human NKR-P1 receptor. However, human NK receptors from the *klrf* subfamily – i.e. NKp65 [20] and NKp80 [21] share distinct similarity to NKR-P1 and were proposed to represent activating counterparts of human NKR-P1 [13,22].

Apart from NK cells, human NKR-P1 was found to be expressed on NKT cells [23] and subpopulations of T lymphocytes [24]. Most

Abbreviations: CTL, C-type lectin-like; GnTI⁻, *N*-acetylglucosaminyltransferase I negative; HEK, human embryonic kidney; LLT1, lectin-like transcript 1; lPEI, linear polyethylenimine; MALS, multi-angle light scattering; NK, natural killer; SEC, size-exclusion chromatography.

* Corresponding author.
E-mail address: ondrej.vanek@natur.cuni.cz (O. Vaněk).

http://dx.doi.org/10.1016/j.pep.2017.07.016
1046-5928/

notably, human NKR-P1 is present on regulatory T cells [25] and is currently recognized to be a marker for all Th17 cells [26]. It was found also on some Tc17 cells [27] which are being more and more implicated in autoimmune diseases like multiple sclerosis [28], rheumatoid arthritis [29] and Crohn's disease [30]. It was proposed that NKR-P1 could play a role in targeting of these lymphocytes and promote transendothelial extravasation into immunologically privileged niches [26,31–34].

Under homeostasis NKR-P1 functions as inhibitory receptor of NK cells [19,35,36] and co-stimulatory receptor of NKT and T cells [35,37] promoting secretion of IFNγ. However, it was also described that the inhibitory function of human NKR-P1 is in an undesirable way exploited by glioblastomas [38] and B-cell Non-Hodgkin's lymphomas [39] which overexpress the NKR-P1 physiological ligand – lectin-like transcript 1 (LLT1, gene *clec2d*) [35,36,40,41] and thus escape immune response.

From a protein point of view, human NKR-P1 shares common CTL receptor features. It was identified as a homodimeric type II. transmembrane glycoprotein lacking O-linked glycosylation [19]. Its short intracellular portion contains an immunoreceptor tyrosine-based inhibitory motif that is noncanonical for the presence of alanine residue in the −2 position relative to the tyrosine residue [42]. A transmembrane helix is followed by 25 residues long stalk region that presumably functions as a flexible linker providing a scaffold for cystine homodimerization and a *C*-terminal CTL domain that itself contains 6 conserved cysteine residues stabilizing this domain by formation of three intramolecular disulphide bridges [14].

Although there have been recently promising results for refolding of murine NKR-P1 receptors from inclusion bodies produced in *E. coli* [43,44], so far only an unsuccessful renaturation of the human orthologue have been reported [45]. Mammalian cell lines were used previously to express full-length human NKR-P1 receptor or its extracellular part in low-scale for immunological studies [35,36,40,41] or surface plasmon resonance measurements [45], respectively. Here we present an optimization of the human NKR-P1 ectodomain expression in different expression systems and finally an utilization of HEK293S GnTI$^-$ cells [46] for generation of stably transfected cell line that provides a high yield of soluble human NKR-P1 ectodomain usable for structural studies.

2. Material and methods

2.1. Vectors and NKR-P1 library cloning

A cDNA clone (GenBank accession no. BC114516) containing the entire coding sequence of *klrb1* gene was obtained from Source BioScience (GenomeCUBE IRCMp5012E0732D). A library of NKR-P1 stalk region deletion expression vectors was constructed by In-Fusion cloning at the Oxford Protein Production Facility (OPPF; Oxford, UK) as described before [47,48]. Primers used for amplification of the selected NKR-P1 constructs from the cDNA clone contained In-Fusion overlaps at the 5′ of the specific forward and the reverse primers as described in supplementary data, Table S1. For transient expression in HEK293 cells, NKR-P1 ectodomain (G90-S225) was amplified from the cDNA clone using 5′–AAAAAAACCGGTGGTCTCTTAAACTGCCCAATATATTG–3′ and 5′–AAAAAAGGTACCAGAGTCAGGATACACTTTATTTCTCAC–3′ and using *Age*I and *Kpn*I sites subcloned into pTT28 expression plasmid (kindly provided by Dr. Yves Durocher; a derivative of pTT5 [49] containing *N*-terminal secretion leader and *C*-terminal His_8-tag sequence, thus leaving ITG- and -GTKHHHHHHHHG at expressed protein *N*-and *C*-termini).

2.2. Small-scale NKR-P1 expression tests

Expression of the library of stalk region deletion constructs was performed at OPPF following standard OPPF protocols for high-throughput expression testing in *E. coli* [50] and Sf9 cells [51] as described before.

Briefly, for prokaryotic expression 150 μl of overnight cultures grown from selected colony of *E. coli* Rosetta2(DE3) pLysS or B834(DE3) strains (both Novagen) transformed with the given expression plasmid were used for inoculation of 3 ml of Power Broth (Molecular Dimensions) and Overnight Express Instant TB Medium (TBONEX; Novagen) with an appropriate antibiotic in 24-well deep well blocks. The blocks were shaken at 37 °C until an average OD_{595} reached ca 0.5. The Power Broth cultures were cooled to 20 °C and expression was induced by addition of IPTG to 1 mM final concentration and left to produce overnight. The TBONEX cultures were cooled to 25 °C and left to produce for 20 h.

Bacterial cultures were centrifuged and frozen until analysis. Defrosted cell pellets were resuspended in lysis buffer (50 mM NaH_2PO_4, 300 mM NaCl, 10 mM imidazole, 1% v/v Tween 20, pH 8.0) supplemented with lysozyme and DNAse I, incubated for 30 min and the lysates were cleared by centrifugation in deep-well block (6000 × g, 30 min, 4 °C). Expression levels were analysed by Coomassie stained reducing SDS-PAGE from soluble fraction of cell lysates [50].

For insect cell expression, to generate a P0 virus stock Sf9 cells were co-transfected with linearized bacmid DNA (Bac10:KO_{1629} [52]) and pOPIN vector from the stalk region deletion library as a transfer vector. For small-scale expression tests 3 ml of 1 × 10^6 Sf9 cells/ml in 24-well deep blocks were infected with 3 and 30 μl of P1 virus stock and left to produce at 27 °C for 72 h. For scale up, 800 ml of Sf9 production culture in shaken Thompson flask was infected with 800 μl of P2 virus stock. Media were harvested and purified after 7 days.

For mammalian expression tests, 4 μg of the given expression plasmid and 10 μl of Lipofectamine 2000 (Invitrogen, USA) were each diluted into 25 μl of Freestyle F17 media (Invitrogen, USA), incubated for 5 min, mixed and incubated for 10 min again before addition to 2 × 10^6 HEKT293T cells grown in 1 ml of Freestyle F17 medium on a shaken 24-well culture plate (Corning, USA) at 37 °C, 5% CO_2. After 4 h cell cultures were diluted with 1 ml of EX-CELL293 serum-free medium (Sigma, USA) and left to produce for 72 h.

Expression tests from insect and mammalian cell cultures were analysed by enriching the secreted products by IMAC on Ni-NTA magnetic beads (Qiagen and Biotool, USA) from 1 ml of the production media and either analysed by SDS-PAGE or by Western blot and immunodetection with primary mouse PentaHis anti-His-tag monoclonal antibody (Qiagen, USA) and secondary HRP or AP conjugated anti-mouse IgG antibody (R&D Systems, USA; Sigma, USA).

2.3. Transient NKR-P1 expression in HEK293T cells

HEK293 cell lines were grown in suspension as described in Ref. [41] in mixture of equal volumes of EX-CELL293 and Freestyle F17 media in shaken square-shaped glass bottles within humidified 37 °C, 5% CO2 incubator. For transient expression of soluble NKR-P1 ectodomain, 400 μg of the pTT28 expression plasmid were diluted in PBS, filter-sterilized and 25 kDa linear polyethylenimine (Polysciences, USA) was added in 1:3 (w/w) ratio to 4 ml final volume, the mixture was shaken and incubated for 5 min. Meanwhile, 400 × 10^6 HEK293T cells were centrifuged and resuspended in 200 ml of Freestyle F17 and immediately transfected. Following 4 h incubation, the culture was diluted with 200 ml of EX-CELL293. 5–7 days post-transfection culture medium was harvested by

centrifugation (4000 × g, 30 min), filtered (0.22 μm Steritop filter; Millipore, USA), and stored at −20 °C or immediately processed.

2.4. Stable NKR-P1 expression in HEK293S GnTI⁻ cells

For generation of stably transfected HEK293S GnTI⁻ cell pool, 30 × 10^6 cells were transfected in high cell density [41] with 30 μg of pOPINGTTneo expression plasmid. For selection, Geneticin G418 was added two days post-transfection at 100 μg/ml. The culture was split and the medium was exchanged with fresh addition of the selection antibiotic every three days. Three weeks post-transfection healthy and growing pool of polyclonal stably transfected cell culture was established. The stable culture was maintained in 1:1 mixture of EX-CELL293 and Freestyle F17 with 100 μg/ml of the Geneticin G418. For protein production 400 × 10^6 cells were split into 400 ml of 1:1 mixture of EX-CELL293 and Expi293 (Invitrogen, USA) with 100 μg/ml of the selection antibiotic. Culture medium was harvested after 10–14 days by centrifugation (4000 × g, 30 min), filtered (0.22 μm Steritop filter; Millipore, USA), and stored at −20 °C or immediately processed.

2.5. Protein purification and crystallization

Medium was diluted twofold with 50 mM Na_2HPO_4, 300 mM NaCl, 10 mM NaN_3, pH 7.5 PBS buffer and pH was adjusted to 7.5 if necessary. The His-tagged protein was recovered by IMAC chromatography on HiTrap TALON crude column (GE Healthcare, USA) with subsequent SEC on Superdex 200 10/300 GL column (GE Healthcare, USA) in 10 mM HEPES, 150 mM NaCl, 10 mM NaN_3, pH 7.5 buffer and concentrated to 20 mg/ml on Amicon Ultra concentrator (10000 MWCO; Millipore, USA). The protein was crystallized using sitting drop vapour diffusion method. Drops (100 nl of protein solution and 100 nl of reservoir) were set up using a Cartesian Honeybee 961 robot (Genomic Solutions) at 294 K. The reservoir consisted of 30% w/v PEG 6000, 100 mM Bis-Tris propane pH 9.0 (PegRx screen, condition 39, Hampton Research).

2.6. Mass spectrometry

Disulphide bonds in soluble human NKR-P1 were determined according to the previously published protocol [53]. Briefly, the protein was separated by SDS-PAGE, *N*-linked glycans were cleaved off after the first GlcNAc unit by endoglycosidase Endo Hf (New England Biolabs, USA) and digested by trypsin (Sigma, USA) or Asp-N endoproteinase (Sigma, USA) under nonreducing conditions in the presence of 200 μM cystamine. The peptide mixtures were desalted on peptide MacroTrap and separated on reversed phase MAGIC C18 columns (both Michrom BioResources, USA) connected directly to an APEX-Q 9.4 T FT-ICR mass spectrometer (Bruker Daltonics, USA) using an electrospray ion source. Data were acquired using ApexControl 3.0.0 and processed with DataAnalysis 4.0. The disulphide bonds and saccharide moieties were identified using Links software [54].

2.7. Analytical ultracentrifugation

The oligomeric state of the produced protein was analysed in ProteomeLab XL-I analytical ultracentrifuge equipped with An-50 Ti rotor (Beckman Coulter, USA). For sedimentation velocity experiment, samples of NKR-P1 diluted to the desired concentration with the SEC buffer used for its purification were spun at 48000 rpm at 20 °C and 150 scans with 0.003 cm spatial resolution were recorded in 5 min interval using absorbance optics at 280–300 nm. The data were analysed using Sedfit [55] using a c(s) continuous size distribution model. For sedimentation equilibrium experiment, NKR-P1 at 0.11 mg/ml was spun at 12-15-18-21-24000 rpm at 4 °C and 1 scan with 0.001 cm spatial resolution at 280 nm was recorded after first 34 h and then consecutively after 18 h per each velocity. The data were analysed using Sedphat [56] using multi-speed sedimentation equilibrium and single ideal species model. Buffer density and protein partial specific volume were estimated in SEDNTERP (http://sednterp.unh.edu/), figures were prepared in GUSSI [57].

2.8. SEC-MALS

Molecular weight and polydispersity of NKR-P1 and LLT1(H176C) [41] were analysed by size exclusion chromatography using an HPLC system (Shimadzu, Japan) equipped with refractive index (RI), UV and multi-angle light scattering (MALS) DAWN8 EOS detectors (Wyatt Technology, USA). A microSuperose12 column (GE Healthcare, USA) was used with 10 mM HEPES, 150 mM NaCl, 10 mM NaN_3, pH 7.5 eluent at 0.1 ml/min. Weight-average molecular weights (Mw) were calculated from the light-scattering detector based on the known injected mass while assuming 100%

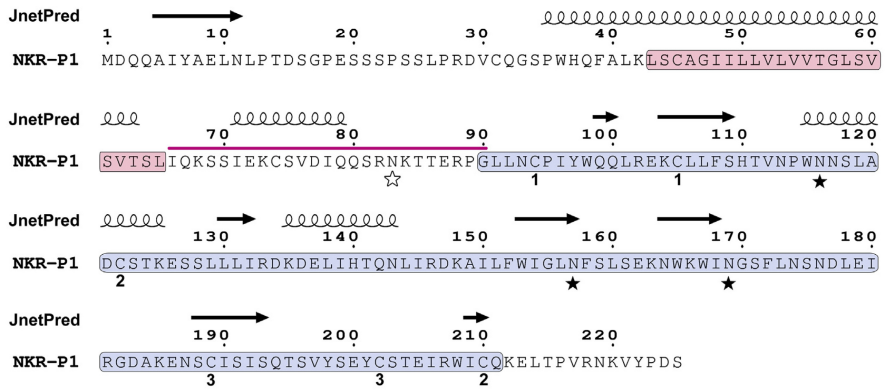

Fig. 1. The primary sequence of human NKR-P1 (CD161, *klrb1*). The transmembrane helix and C-type lectin-like domain predicted by Globplot 2 [59] are highlighted by red and blue rectangles, respectively. The stalk region optimized in this study is marked by magenta line above the sequence. JPred 4 [60] secondary structure prediction is depicted at the top. Identified cystic pairs and *N*-linked glycosylation sites are labelled by numbers and full stars, respectively. The empty star indicates the presumptive *N*-linked glycosylation site present within the stalk region. (For interpretation of the references to colour in this figure legend, the reader is referred to the web version of this article.)

Table 1
List of used expression plasmids with description of peptides flanking the expression construct.

Vector	*N*-terminal	*C*-terminal
pOPINS3C	His_6-SUMO-3C	–
pOPINTRX	His_6-TRX-3C	–
pOPINMSYB	His_6-MsyB-3C	–
pOPINJB	His_6-GST-3C	BAP
pOPINP	SS[PelB]	Lys-His_6
pOPING	SS[RPTPmu]	Lys-His_6
pOPINGTTneo	SS[RPTPmu]	Lys-His_6

His_6 – hexahistidine tag; SUMO – small ubiquitin-like modifier; 3C – cleavage site for 3C protease; TRX – *E. coli* thioredoxin; MsyB – *E. coli* MsyB; GST – glutathione S-transferase; SS[PelB] – PelB signal sequence; SS[RPTPmu] – receptor-like protein tyrosine phosphatase μ signal sequence; BAP – biotin acceptor peptide.

mass recovery. Number-average molecular weights (Mn) were determined by refractive index measurements and were calculated assuming a dn/dc value of 0.185 ml/g. Polydispersity is defined as (Mw/Mn).

3. Results and discussion

3.1. Transient expression of NKR-P1 in HEK293 cell lines

To our best knowledge, successful expression of soluble human NKR-P1 ectodomain has been previously reported only in transiently transfected HEK293 cells [45]. Although the authors haven't stated the production yield, the reported use for immobilization on SPR sensor chip doesn't necessarily suggest high yields. To evaluate this approach, we have performed transient expression of NKR-P1 ectodomain in suspension cultures of HEK293T and HEK293S GnTI$^-$ cells using the same expression construct G90-S225 as reported before [45]. This expression construct corresponds to the CTL domain of NKR-P1 (Fig. 1) and does not contain residues from the stalk region of the receptor. Similar constructs were previously successfully used within our hands for bacterial expression and refolding of mouse NKR-P1A, NKR-P1C, and Clrg ectodomains [43,44,58], as well as of human LLT1 ectodomain that was expressed in the same HEK293 cell lines [41]. However, in case of human NKR-P1 we have obtained on average yields of only about 0.1 mg of pure recombinant protein per litre of production culture from either HEK293 cell line. In contrast, we have recently reported ca 30-times higher yields in the same expression system for LLT1 [41]. Such low yields of NKR-P1 are neither sufficient nor economical for structural studies; therefore, we have attempted further optimization of its expression with regards to the expression system used and to the length of the putative *N*-terminal stalk region in its expression construct.

3.2. Screening of NKR-P1 expression in E. coli

In order to test the solubility effect of a protein tag fusion we

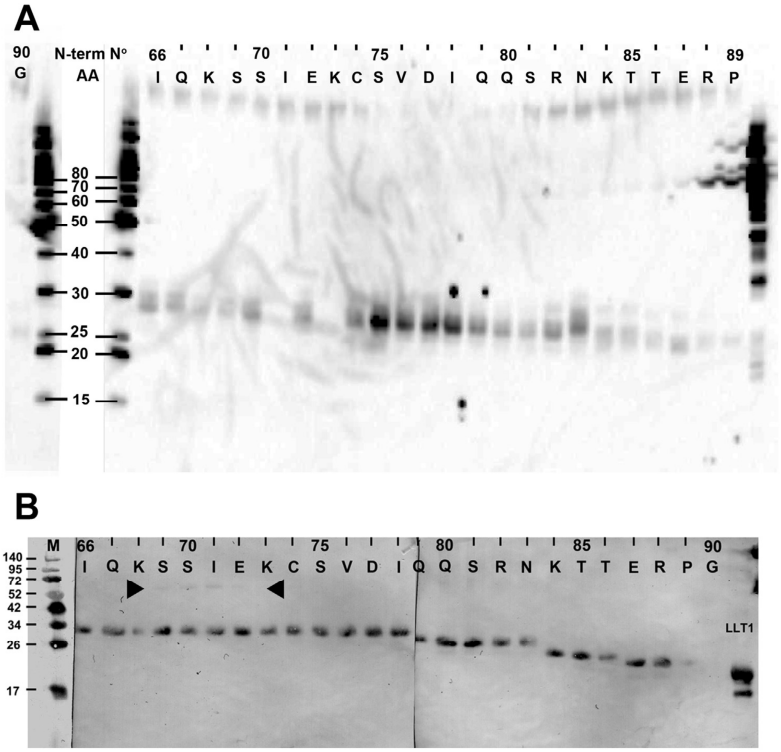

Fig. 2. Screening of the stalk region deletion library of NKR-P1 expression constructs. Western blots of His-tagged products enriched on Ni-NTA magnetic beads from small-scale expression tests of the NKR-P1 stalk region deletion library in pOPING (*C*-terminally His_6-tagged) in (A) Sf9 insect and (B) human HEK293T cell lines. The *N*-terminal residue of the stalk region included in the given construct is annotated at the top. Molecular weight standards are in kDa. Position of putative covalent dimer of NKR-P1 is marked by an arrow. Sample of NKR-P1 ligand, protein LLT1, was added for comparison.

have subcloned three expression constructs of human NKR-P1 differing in the length of the flexible *N*-terminal stalk region while containing the whole CTL domain (I66/Q80/G90-S225) (Fig. 1) into the pOPINS3C, pOPINTRX, pOPINMSYB, pOPINJB, and pOPINP expression vectors from OPPF's suite of pOPIN vectors [48] (see Table 1 for information about the expression cassettes). Expression tests were performed in *E. coli* B834(DE3) and *E. coli* Rosetta2(DE3) pLysS strains using two different production conditions – an overnight production at 20 °C after induction with 1 mM IPTG and a production in TBONEX auto-induction medium at 25 °C for 20 h. Products of 1 ml cultures were enriched using Ni-NTA magnetic beads from soluble fraction of cell lysate and analysed using Coomassie stained reducing SDS-PAGE [50] (Fig. S1). Unfortunately, we cannot report any improvement on expression of soluble human NKR-P1 in *E. coli* for any of the tested fusion constructs or conditions. It is possible that using strains with an oxidizing cytoplasm designed for expression of disulphide-containing proteins like SHuffle or Rosetta-gami would be more efficient; however, based on our previous experiences with these strains for similar constructs of mouse NKR-P1 receptors this seems unlikely, too (not shown).

3.3. Screening of stalk region deletion library in Sf9 and HEK293T cells

For simultaneous expression test in both insect cell baculoviral and mammalian expression systems, we have utilized OPPF's pOPING expression vector allowing for secreted expression with *C*-terminal His_6-tag flanking the protein of interest (Table 1). A series of 25 human NKR-P1 constructs with consecutively shortened *N*-terminal stalk region (I66–G90) (Fig. 1) ending at the CTL domain *C*-terminal S225 were subcloned into the pOPING vector. Expression tests were performed in 3 ml of Sf9 culture infected with P1 generation of baculoviruses and in 2 ml of transiently transfected suspension HEK293T cultures. Expression media were analysed for the presence of desired products 72 h post-transfection by anti-histidine tag immunodetection.

Although positive, only low expression signals were obtained from the insect cell expressions (Fig. 2A). However, a distinct region of best expressing constructs could be distinguished with the *N*-termini of NKR-P1 ranging from C74 to Q79. This could suggest stabilization of these constructs by secondary structure formation. Interestingly, a JPred 4 secondary structure prediction analysis suggests α-helix within this region (Fig. 1). Such structural stabilization could provide a scaffold for the formation of an intermolecular disulphide bridge via the C74 residue.

Analysis of the expression test in mammalian culture showed positive albeit similarly low level of expression for most of the tested constructs (Fig. 2B). Interestingly, a very low signal corresponding to the NKR-P1 covalent dimer could be detected within the range of S69-E72 *N*-terminal NKR-P1 constructs. Also, a sudden shift in the electrophoretic mobility between the N83 and K84 *N*-terminal constructs and presence of NKT consensus sequence suggest presence of *N*-linked glycan at the N83 (Fig. 1).

We have further attempted to scale-up the production of the S75-S225 construct in 800 ml of Sf9 culture infected with P2 generation of the virus. However, the low level of expression was confirmed with yield of only ca 0.4 mg of heavily contaminated protein per litre of production culture (contamination may have been caused by presence of misfolded protein aggregates). Therefore, we cannot report a suitable format of recombinant expression of soluble human NKR-P1 based on baculoviral transduction of Sf9 cells. We cannot exclude the possibility that the sequence following the signal peptide might have a negative impact on secretion in insect cells, rather than the construct itself.

3.4. High-level expression of soluble human NKR-P1 in stable HEK293S GnTI⁻ cell line

In parallel, we have attempted to express the original G90-S225 construct of human NKR-P1 ectodomain in stably transfected pool of HEK293S GnTI⁻ cells and thus test whether higher production yields might be reached by using stable instead of transient transfection. Although this construct performed poorly in the aforementioned transient expression test and may be suboptimal with respect to possible expression yield, based on our previous work on structural elucidation of CTL receptors [40,43,58,61] constructs lacking the *N*-terminal stalk region and containing only the well-defined CTL domain are the most suitable targets for further structural experiments. The expression construct was subcloned into OPPF's vector pOPINGTTneo containing neomycin selection marker. A pool of resistant HEK293S GnTI⁻ cells was selected on Geneticin G418. Following positive expression test (data not shown), the resistant pool was scaled to 300 ml of 1×10^6/ml cell suspension and left to produce for 10 days. The secreted product was purified by IMAC on HiTrap Talon column followed by SEC on Superdex 200 10/300 GL yielding on average 2.5 mg of pure protein per litre of production culture.

The HEK293S GnTI⁻ cell line provides uniform mammalian *N*-linked glycosylation of $GlcNAc_2Man_5$ type that is readily cleavable with endoglycosidase Endo F1 leaving only a single GlcNAc unit (Fig. 3A, lane D). Both under reducing and non-reducing conditions the soluble human NKR-P1 ectodomain migrates on SDS-PAGE as three distinct glycoforms corresponding to the theoretical weight of monomer with one (18.4 kDa), two (19.6 kDa) or three (20.9 kDa)

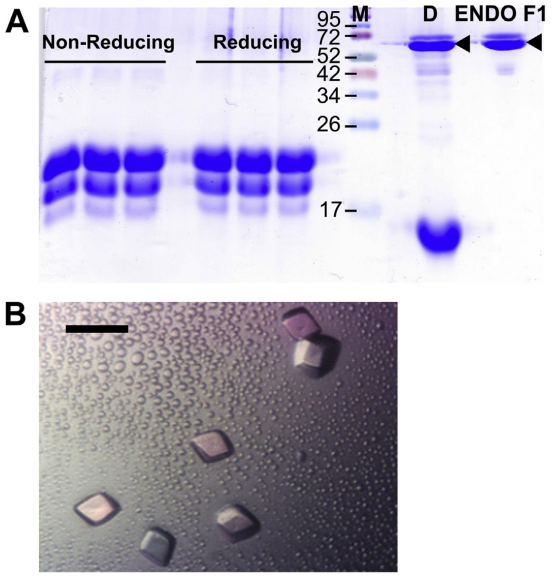

Fig. 3. Soluble NKR-P1 ectodomain forms distinct glycoforms, is easily deglycosylatable and crystallizable. (A) SDS-PAGE analysis of the final product of soluble NKR-P1 (G90-S225) with simple $GlcNAc_2Man_5$ *N*-linked glycosylation from HEK293S GnTI⁻ cells. Both under reducing and non-reducing conditions three distinct glycoforms of NKR-P1 are detectable, that migrate as a single band after cleavage of *N*-glycans with endoglycosidase Endo F1 (leaving single GlcNAc unit; lane D). M – molecular weight standard in kDa. ENDO F1 – endoglycosidase F1 (arrow). (B) Crystals of NKR-P1 produced in HEK293S GnTI⁻ cells grown by sitting drop vapour diffusion method. The black scale bar represents 100 μm.

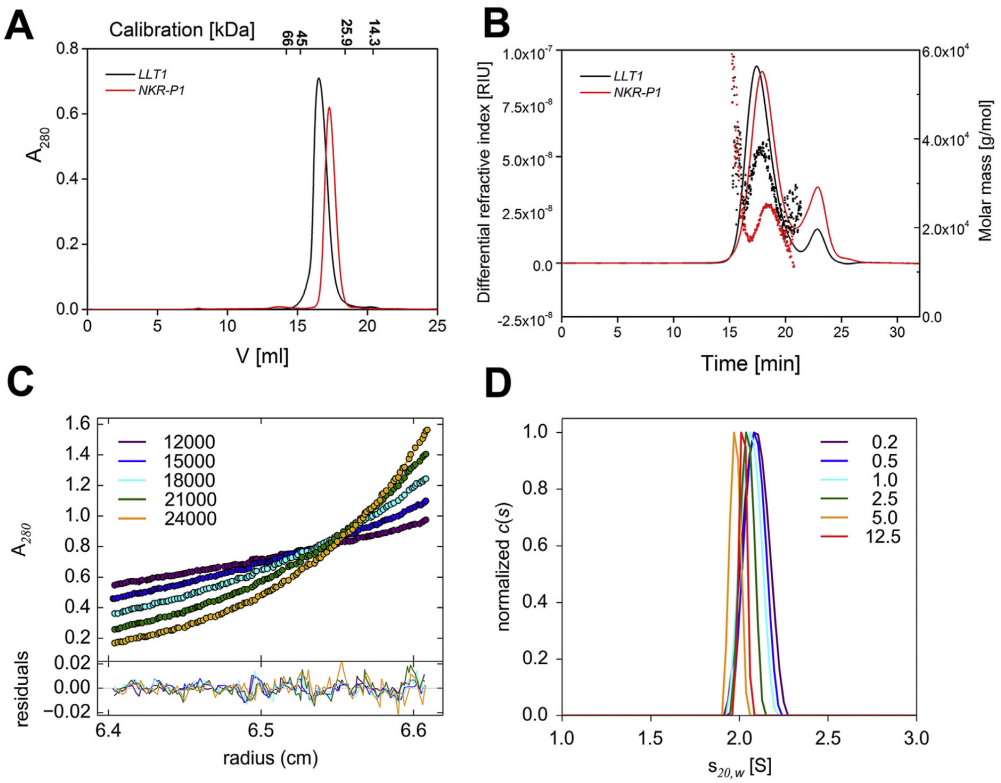

Fig. 4. Soluble NKR-P1 is monomeric in solution. (A) Comparison of size exclusion chromatography profiles of soluble LLT1 H176C mutant (black) and NKR-P1 (red). The LLT1 is forming non-covalent dimer [41] while NKR-P1 migrates rather as monomer. (B) Comparison of size exclusion chromatography with refractive index detection (line plot, left axis) and molar masses determined by multi angle light scattering (scatter plot, right axis) of soluble LLT1 H176C mutant (black) and NKR-P1 (red). (C) Sedimentation equilibrium analysis in analytical ultracentrifuge performed at 0.11 mg/ml concentration showed that NKR-P1 behaves as monomer; upper panel – absorbance data with fitted curves (single non-interacting discrete species model), lower panel – residual plot showing the goodness of fit. (D) Series of sedimentation velocity analyses in analytical ultracentrifuge at increasing protein concentration (given in mg/ml; normalized continuous size distributions of the sedimenting species) showed that NKR-P1 does not self-associate. (For interpretation of the references to colour in this figure legend, the reader is referred to the web version of this article.)

N-linked glycosylation sites occupied with the $GlcNAc_2Man_5$ oligosaccharide moieties (Fig. 3A). Furthermore, the prepared soluble human NKR-P1 with homogeneous $GlcNAc_2Man_5$ *N*-glycans (although still being in-homogeneous with respect to incomplete *N*-glycosylation site occupancy) was readily crystallized using the vapour diffusion method in sitting drop, forming bipyramidal crystals (Fig. 3B) up to 80 μm in size. These initial crystals already diffracted up to resolution of ca 2.0 Å and were later optimized leading to solution of NKR-P1 crystal structure (Bláha *et al.*, submitted).

Utilizing a mass spectrometry approach, we have identified cystic peptides in the soluble NKR-P1 ectodomain confirming canonical configuration of disulphides in CTL domain: C94-C105, C122-C210, and C189-C202 (Table S2, Fig. 1). Furthermore, we have been able to confirm presence of saccharide moieties at the three predicted *N*-linked glycosylation sites – N116, N157, and N169 (Table S2, Fig. 1). The incomplete occupancy of these sites accounts for the three different glycoforms observed on SDS-PAGE (Fig. 3A).

3.5. Stoichiometry of recombinant human NKR-P1 in solution

Comparison of SEC retention volumes for soluble LLT1(H176C) eluting as a non-covalent dimer [41] and for soluble NKR-P1 ectodomain suggests that soluble NKR-P1 elutes rather as a monomer (Fig. 4A). To confirm this, we repeated the analysis with multi-angle light scattering detection (Fig. 4B) providing a molecular weight of ca 22 kDa and 33 kDa for soluble NKR-P1 and LLT1(H176C) respectively, both with low polydispersity (Fig. 4B). Monomeric state of human NKR-P1 was further corroborated by sedimentation equilibrium analysis in analytical ultracentrifuge resulting in estimated molecular weight of 20.7 kDa (Fig. 4C). Sedimentation velocity experiment performed with samples of increasing protein concentration also showed no tendency to form homodimer or oligomeric species (Fig. 4D). Soluble human NKR-P1 behaves as particle with standard sedimentation coefficient $s_{20,w}$ 2.10 S and approximate dimensions of 4.5 × 3.5 nm corresponding well to expected values for monomeric protein.

Human NKR-P1 should form a covalently linked homodimer on the cell surface [19], but the produced soluble form of NKR-P1 lacks the odd cysteine residue in the stalk region implicated in such dimerization [13]. However, soluble ectodomains of the homologous subfamily of related *clec2* receptors – CD69 [61], LLT1 [40], and KACL [62] were previously reported to form stable non-covalent dimers in solution quite easily. On the other hand, recently published structure of NKp65 [62], a member of more closely related *klrf* subfamily, shows this receptor interacting with

its *clec2* ligand KACL while being in a monomeric state and its dimerization in the manner of *clec2* receptors would even hamper the interaction with its *clec2* ligand. Similarly, previously reported mouse NKR-P1A and NKR-P1C(B6) orthologues were observed in solution only as monomers [43,44]. Taken together with the presented low propensity of NKR-P1 to form a non-covalent dimer in solution, a different, less stable mode of dimerization should be expected than that of *clec2* receptors for the human NKR-P1 and its orthologues and close homologues – the *klrf* receptors; that requires covalent stabilization by a disulphide bridge(s) in the putative stalk region.

4. Conclusions

To conclude, we have recombinantly expressed soluble human NKR-P1 ectodomain in stable, deglycosylatable and crystallizable form. To our knowledge, this is the first attempt at structural characterization of human NKR-P1 immunoreceptor. The strategy of construct design described herein for NKR-P1 – i.e. the construction of stalk region deletion library – might be considered also for other C-type lectin-like receptors of NK cells, although in our case, it was rather the choice of proper expression system that was the most important factor. Selection of stably transfected HEK293 cell lines as expression host may be optimal both for protein production aimed at structural characterization and for production of soluble receptor domains that could be utilized in clinical therapy also for other NK cell CTL receptors and their ligands. Depending on the intended use, suitable HEK293 cell line with desired *N*-glycosylation profile could be chosen, i.e. HEK293S GnTI$^-$ or HEK293T cell lines with simple or complex *N*-glycans, respectively.

Acknowledgements

This study was supported by Czech Science Foundation (15-15181S), Ministry of Education, Youth and Sports of the Czech Republic (LG14009 and LM2015043 CIISB for CMS Biocev; LTC17065), Charles University (UNCE 204025/2012, SVV 260079/2014, GAUK 161216), Foundation "Nadání Josefa, Marie a Zdeňky Hlávkových", COST Action CA15126 (MOBIEU), and BioStruct-X (EC FP7 project 283570). The authors also acknowledge the support and the use of resources of Instruct, a Landmark ESFRI project through the R&D pilot scheme APPID 56 and 286.

Appendix A. Supplementary data

Supplementary data related to this article can be found at http://dx.doi.org/10.1016/j.pep.2017.07.016.

References

[1] E. Vivier, D.H. Raulet, A. Moretta, M.A. Caligiuri, L. Zitvogel, L.L. Lanier, W.M. Yokoyama, S. Ugolini, Innate or adaptive immunity? The example of natural killer cells, Science 331 (2011) 44–49.
[2] M.A. Caligiuri, Human natural killer cells, Blood 112 (2008) 461–469.
[3] E. Vivier, E. Tomasello, M. Baratin, T. Walzer, S. Ugolini, Functions of natural killer cells, Nat. Immunol. 9 (2008) 503–510.
[4] A. Cerwenka, L.L. Lanier, Natural killer cell memory in infection, inflammation and cancer, Nat. Rev. Immunol. 16 (2016) 112–123.
[5] E. Vivier, S. Ugolini, Natural killer cells: from basic research to treatments, Front. Immunol. 2 (2011) 18.
[6] M.A. Cooper, M. Colonna, W.M. Yokoyama, Hidden talents of natural killers: NK cells in innate and adaptive immunity, EMBO Rep. 10 (2009) 1103–1110.
[7] D.H. Raulet, N. Guerra, Oncogenic stress sensed by the immune system: role of natural killer cell receptors, Nat. Rev. Immunol. 9 (2009) 568–580.
[8] C.S. Brandt, M. Baratin, E.C. Yi, J. Kennedy, Z. Gao, B. Fox, B. Haldeman, C.D. Ostrander, T. Kaifu, C. Chabannon, A. Moretta, R. West, W. Xu, E. Vivier, S.D. Levin, The B7 family member B7-H6 is a tumor cell ligand for the activating natural killer cell receptor NKp30 in humans, J. Exp. Med. 206 (2009) 1495–1503.
[9] N. Anfossi, P. Andre, S. Guia, C.S. Falk, S. Roetynck, C.A. Stewart, V. Breso, C. Frassati, D. Reviron, D. Middleton, F. Romagne, S. Ugolini, E. Vivier, Human NK cell education by inhibitory receptors for MHC class I, Immunity 25 (2006) 331–342.
[10] C. Bottino, R. Castriconi, L. Moretta, A. Moretta, Cellular ligands of activating NK receptors, Trends Immunol. 26 (2005) 221–226.
[11] K. Karre, H.G. Ljunggren, G. Piontek, R. Kiessling, Selective rejection of H-2-deficient lymphoma variants suggests alternative immune defence strategy, Nature 319 (1986) 675–678.
[12] L.L. Lanier, B. Corliss, J.H. Phillips, Arousal and inhibition of human NK cells, Immunol. Rev. 155 (1997) 145–154.
[13] Y. Bartel, B. Bauer, A. Steinle, Modulation of NK cell function by genetically coupled C-type lectin-like receptor/ligand pairs encoded in the human natural killer gene complex, Front. Immunol. 4 (2013) 362.
[14] W.M. Yokoyama, B.F. Plougastel, Immune functions encoded by the natural killer gene complex, Nat. Rev. Immunol. 3 (2003) 304–316.
[15] D. Rozbesky, L. Ivanova, L. Hernychova, V. Grobarova, P. Novak, J. Cerny, Nkrp1 family, from lectins to protein interacting molecules, Molecules 20 (2015) 3463–3478.
[16] A.N. Zelensky, J.E. Gready, The C-type lectin-like domain superfamily, FEBS J. 272 (2005) 6179–6217.
[17] K.P. Kane, K.J. Lavender, B.J. Ma, Ly-49 receptors and their functions, Crit. Rev. Immunol. 24 (2004) 321–348.
[18] S. Bauer, V. Groh, J. Wu, A. Steinle, J.H. Phillips, L.L. Lanier, T. Spies, Activation of NK cells and T cells by NKG2D, a receptor for stress-inducible MICA, Science 285 (1999) 727–729.
[19] L.L. Lanier, C. Chang, J.H. Phillips, Human NKR-P1A. A disulfide-linked homodimer of the C-type lectin superfamily expressed by a subset of NK and T lymphocytes, J. Immunol. 153 (1994) 2417–2428.
[20] J. Spreu, S. Kuttruff, V. Stejfova, K.M. Dennehy, B. Schittek, A. Steinle, Interaction of C-type lectin-like receptors NKp65 and KACL facilitates dedicated immune recognition of human keratinocytes, Proc. Natl. Acad. Sci. U. S. A. 107 (2010) 5100–5105.
[21] S. Welte, S. Kuttruff, I. Waldhauer, A. Steinle, Mutual activation of natural killer cells and monocytes mediated by NKp80-AICL interaction, Nat. Immunol. 7 (2006) 1334–1342.
[22] I. Vogler, A. Steinle, Vis-a-vis in the NKC: genetically linked natural killer cell receptor/ligand pairs in the natural killer gene complex (NKC), J. Innate Immun. 3 (2011) 227–235.
[23] M. Exley, S. Porcelli, M. Furman, J. Garcia, S. Balk, CD161 (NKR-P1A) costimulation of CD1d-dependent activation of human T cells expressing invariant V alpha 24 J alpha Q T cell receptor alpha chains, J. Exp. Med. 188 (1998) 867–876.
[24] J.R. Fergusson, K.E. Smith, V.M. Fleming, N. Rajoriya, E.W. Newell, R. Simmons, E. Marchi, S. Bjorkander, Y.H. Kang, L. Swadling, A. Kurioka, N. Sahgal, H. Lockstone, D. Baban, G.J. Freeman, E. Sverremark-Ekstrom, M.M. Davis, M.P. Davenport, V. Venturi, J.E. Ussher, C.B. Willberg, P. Klenerman, CD161 defines a transcriptional and functional phenotype across distinct human T cell lineages, Cell Rep. 9 (2014) 1075–1088.
[25] B. Afzali, P.J. Mitchell, F.C. Edozie, G.A. Povoleri, S.E. Dowson, L. Demandt, G. Walter, J.B. Canavan, C. Scotta, B. Menon, P.S. Chana, W. Khamri, S.Y. Kordasti, S. Heck, B. Grimbacher, T. Tree, A.P. Cope, L.S. Taams, R.I. Lechler, S. John, G. Lombardi, CD161 expression characterizes a subpopulation of human regulatory T cells that produces IL-17 in a STAT3-dependent manner, Eur. J. Immunol. 43 (2013) 2043–2054.
[26] L. Cosmi, R. De Palma, V. Santarlasci, L. Maggi, M. Capone, F. Frosali, G. Rodolico, V. Querci, G. Abbate, R. Angeli, L. Berrino, M. Fambrini, M. Caproni, F. Tonelli, E. Lazzeri, P. Parronchi, F. Liotta, E. Maggi, S. Romagnani, F. Annunziato, Human interleukin 17-producing cells originate from a CD161+CD4+ T cell precursor, J. Exp. Med. 205 (2008) 1903–1916.
[27] E. Billerbeck, Y.H. Kang, L. Walker, H. Lockstone, S. Grafmueller, V. Fleming, J. Flint, C.B. Willberg, B. Bengsch, B. Seigel, N. Ramamurthy, N. Zitzmann, E.J. Barnes, J. Thevanayagam, A. Bhagwanani, A. Leslie, Y.H. Oo, S. Kollnberger, P. Bowness, O. Drognitz, D.H. Adams, H.E. Blum, R. Thimme, P. Klenerman, Analysis of CD161 expression on human CD8+ T cells defines a distinct functional subset with tissue-homing properties, Proc. Natl. Acad. Sci. U. S. A. 107 (2010) 3006–3011.
[28] V. Brucklacher-Waldert, K. Stuerner, M. Kolster, J. Wolthausen, E. Tolosa, Phenotypical and functional characterization of T helper 17 cells in multiple sclerosis, Brain J. Neurol. 132 (2009) 3329–3341.
[29] L. Estrada-Capetillo, B. Hernandez-Castro, A. Monsivais-Urenda, C. Alvarez-Quiroga, E. Layseca-Espinosa, C. Abud-Mendoza, L. Baranda, A. Urzainqui, F. Sanchez-Madrid, R. Gonzalez-Amaro, Induction of Th17 lymphocytes and Treg cells by monocyte-derived dendritic cells in patients with rheumatoid arthritis and systemic lupus erythematosus, Clin. Dev. Immunol. 2013 (2013) 584303.
[30] J.A. Smith, R.A. Colbert, Review: the interleukin-23/interleukin-17 axis in spondyloarthritis pathogenesis: Th17 and beyond, Arthritis & Rheumatol. 66 (2014) 231–241.
[31] A. Poggi, P. Costa, M.R. Zocchi, L. Moretta, Phenotypic and functional analysis of CD4+ NKRP1A+ human T lymphocytes. Direct evidence that the NKRP1A molecule is involved in transendothelial migration, Eur. J. Immunol. 27 (1997) 2345–2350.
[32] A. Poggi, P. Costa, M.R. Zocchi, L. Moretta, NKRP1A molecule is involved in

transendothelial migration of CD4+ human T lymphocytes, Immunol. Lett. 57 (1997) 121–123.
[33] V. Annibali, G. Ristori, D.F. Angelini, B. Serafini, R. Mechelli, S. Cannoni, S. Romano, A. Paolillo, H. Abderrahim, A. Diamantini, G. Borsellino, F. Aloisi, L. Battistini, M. Salvetti, CD161(high)CD8+T cells bear pathogenetic potential in multiple sclerosis, Brain J. Neurol. 134 (2011) 542–554.
[34] P. Chalan, J. Bijzet, M.G. Huitema, B.J. Kroesen, E. Brouwer, A.M. Boots, Expression of lectin-like transcript 1, the ligand for CD161, in rheumatoid arthritis, PLoS One 10 (2015) e0132436.
[35] H. Aldemir, V. Prod'homme, M.J. Dumaurier, C. Retiere, G. Poupon, J. Cazareth, F. Bihl, V.M. Braud, Cutting edge: lectin-like transcript 1 is a ligand for the CD161 receptor, J. Immunol. 175 (2005) 7791–7795.
[36] D.B. Rosen, J. Bettadapura, M. Alsharifi, P.A. Mathew, H.S. Warren, L.L. Lanier, Cutting edge: lectin-like transcript-1 is a ligand for the inhibitory human NKR-P1A receptor, J. Immunol. 175 (2005) 7796–7799.
[37] C. Germain, A. Meier, T. Jensen, P. Knapnougel, G. Poupon, A. Lazzari, A. Neisig, K. Hakansson, T. Dong, N. Wagtmann, E.D. Galsgaard, P. Spee, V.M. Braud, Induction of lectin-like transcript 1 (LLT1) protein cell surface expression by pathogens and interferon-gamma contributes to modulate immune responses, J. Biol. Chem. 286 (2011) 37964–37975.
[38] P. Roth, M. Mittelbronn, W. Wick, R. Meyermann, M. Tatagiba, M. Weller, Malignant glioma cells counteract antitumor immune responses through expression of lectin-like transcript-1, Cancer Res. 67 (2007) 3540–3544.
[39] C. Germain, T. Guillaudeux, E.D. Galsgaard, C. Hervouet, N. Tekaya, A.S. Gallouet, J. Fassy, F. Bihl, G. Poupon, A. Lazzari, P. Spee, F. Anjuere, C. Pangault, K. Tarte, P. Tas, L. Xerri, V.M. Braud, Lectin-like transcript 1 is a marker of germinal center-derived B-cell non-Hodgkin's lymphomas dampening natural killer cell functions, Oncoimmunology 4 (2015) e1026503.
[40] T. Skalova, J. Blaha, K. Harlos, J. Duskova, T. Koval, J. Stransky, J. Hasek, O. Vanek, J. Dohnalek, Four crystal structures of human LLT1, a ligand of human NKR-P1, in varied glycosylation and oligomerization states, Acta Crystallogr. D Biol. Crystallogr. 71 (2015) 578–591.
[41] J. Blaha, P. Pachl, P. Novak, O. Vanek, Expression and purification of soluble and stable ectodomain of natural killer cell receptor LLT1 through high-density transfection of suspension adapted HEK293S GnTI(-) cells, Protein Expr. Purif. 109 (2015) 7–13.
[42] J.V. Ravetch, L.L. Lanier, Immune inhibitory receptors, Science 290 (2000) 84–89.
[43] P. Kolenko, D. Rozbesky, O. Vanek, V. Kopecky Jr., K. Hofbauerova, P. Novak, P. Pompach, J. Hasek, T. Skalova, K. Bezouska, J. Dohnalek, Molecular architecture of mouse activating NKR-P1 receptors, J. Struct. Biol. 175 (2011) 434–441.
[44] D. Rozbesky, D. Kavan, J. Chmelik, P. Novak, O. Vanek, K. Bezouska, High-level expression of soluble form of mouse natural killer cell receptor NKR-P1C(B6) in Escherichia coli, Protein Expr. Purif. 77 (2011) 178–184.
[45] J. Kamishikiryo, H. Fukuhara, Y. Okabe, K. Kuroki, K. Maenaka, Molecular basis for LLT1 protein recognition by human CD161 protein (NKRP1A/KLRB1), J. Biol. Chem. 286 (2011) 23823–23830.
[46] P.J. Reeves, N. Callewaert, R. Contreras, H.G. Khorana, Structure and function in rhodopsin: high-level expression of rhodopsin with restricted and homogeneous N-glycosylation by a tetracycline-inducible N-acetylglucosaminyltransferase I-negative HEK293S stable mammalian cell line, Proc. Natl. Acad. Sci. U. S. A. 99 (2002) 13419–13424.
[47] N.S. Berrow, D. Alderton, S. Sainsbury, J. Nettleship, R. Assenberg, N. Rahman, D.I. Stuart, R.J. Owens, A versatile ligation-independent cloning method suitable for high-throughput expression screening applications, Nucleic Acids Res. 35 (2007) e45.
[48] L.E. Bird, High throughput construction and small scale expression screening of multi-tag vectors in Escherichia coli, Methods 55 (2011) 29–37.
[49] Y. Durocher, S. Perret, A. Kamen, High-level and high-throughput recombinant protein production by transient transfection of suspension-growing human 293-EBNA1 cells, Nucleic Acids Res. 30 (2002) E9.
[50] L.E. Bird, H. Rada, J. Flanagan, J.M. Diprose, R.J. Gilbert, R.J. Owens, Application of In-Fusion cloning for the parallel construction of E. coli expression vectors, Methods Mol. Biol. 1116 (2014) 209–234.
[51] J.E. Nettleship, P.J. Watson, N. Rahman-Huq, L. Fairall, M.G. Posner, A. Upadhyay, Y. Reddivari, J.M. Chamberlain, S.E. Kolstoe, S. Bagby, J.W. Schwabe, R.J. Owens, Transient expression in HEK 293 cells: an alternative to E. coli for the production of secreted and intracellular mammalian proteins, Methods Mol. Biol. 1258 (2015) 209–222.
[52] Y. Zhao, D.A. Chapman, I.M. Jones, Improving baculovirus recombination, Nucleic Acids Res. 31 (2003) E6. E6.
[53] P. Pompach, P. Man, D. Kavan, K. Hofbauerova, V. Kumar, K. Bezouska, V. Havlicek, P. Novak, Modified electrophoretic and digestion conditions allow a simplified mass spectrometric evaluation of disulfide bonds, J. Mass Spectrom. JMS 44 (2009) 1571–1578.
[54] M.M. Young, N. Tang, J.C. Hempel, C.M. Oshiro, E.W. Taylor, I.D. Kuntz, B.W. Gibson, G. Dollinger, High throughput protein fold identification by using experimental constraints derived from intramolecular cross-links and mass spectrometry, Proc. Natl. Acad. Sci. U. S. A. 97 (2000) 5802–5806.
[55] P. Schuck, Size-distribution analysis of macromolecules by sedimentation velocity ultracentrifugation and lamm equation modeling, Biophys. J. 78 (2000) 1606–1619.
[56] P. Schuck, On the analysis of protein self-association by sedimentation velocity analytical ultracentrifugation, Anal. Biochem. 320 (2003) 104–124.
[57] C.A. Brautigam, Calculations and publication-quality illustrations for analytical ultracentrifugation data, Methods Enzym. 562 (2015) 109–133.
[58] T. Skalova, K. Kotynkova, J. Duskova, J. Hasek, T. Koval, P. Kolenko, P. Novak, P. Man, P. Hanc, O. Vanek, K. Bezouska, J. Dohnalek, Mouse Clr-g, a ligand for NK cell activation receptor NKR-P1F: crystal structure and biophysical properties, J. Immunol. 189 (2012) 4881–4889.
[59] R. Linding, R.B. Russell, V. Neduva, T.J. Gibson, GlobPlot: exploring protein sequences for globularity and disorder, Nucleic Acids Res. 31 (2003) 3701–3708.
[60] A. Drozdetskiy, C. Cole, J. Procter, G.J. Barton, JPred4: a protein secondary structure prediction server, Nucleic Acids Res. 43 (2015) W389–W394.
[61] O. Vanek, M. Nalezkova, D. Kavan, I. Borovickova, P. Pompach, P. Novak, V. Kumar, L. Vannucci, J. Hudecek, K. Hofbauerova, V. Kopecky Jr., J. Brynda, P. Kolenko, J. Dohnalek, P. Kaderavek, J. Chmelik, L. Gorcik, L. Zidek, V. Sklenar, K. Bezouska, Soluble recombinant CD69 receptors optimized to have an exceptional physical and chemical stability display prolonged circulation and remain intact in the blood of mice, FEBS J. 275 (2008) 5589–5606.
[62] Y. Li, Q. Wang, S. Chen, P.H. Brown, R.A. Mariuzza, Structure of NKp65 bound to its keratinocyte ligand reveals basis for genetically linked recognition in natural killer gene complex, Proc. Natl. Acad. Sci. U. S. A. 110 (2013) 11505–11510.

Supplementary material

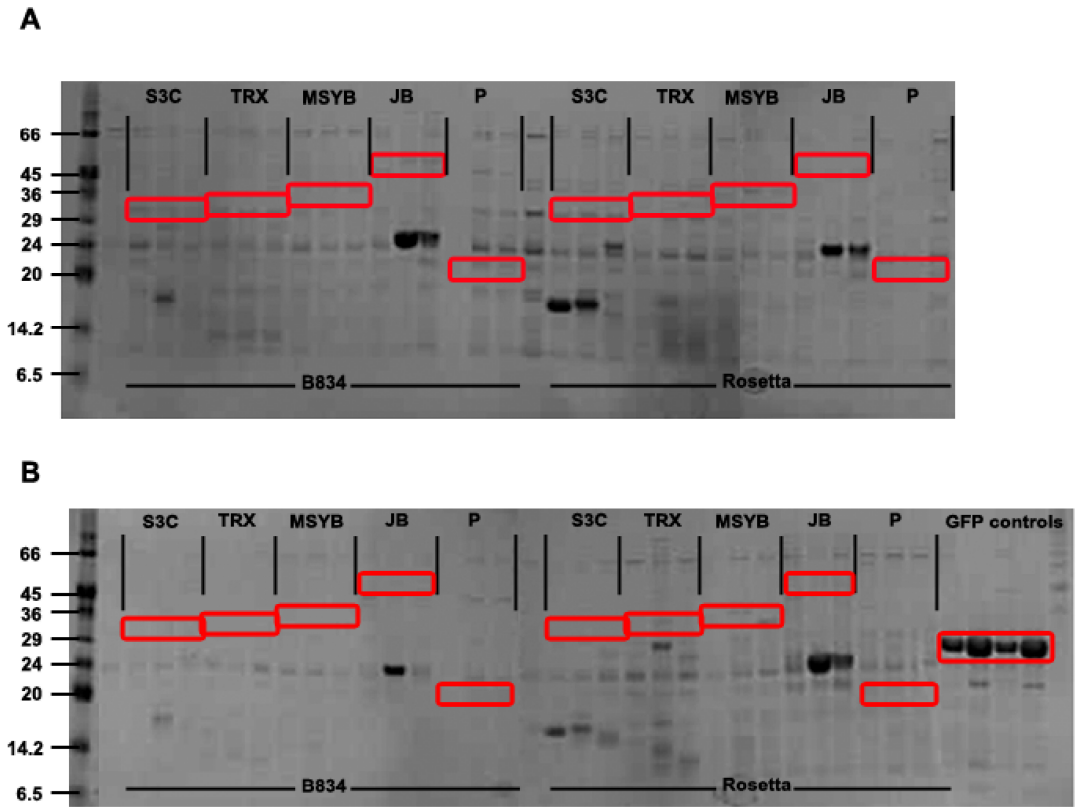

Fig. S1. Screening of the fusion tags for expression of NKR-P1 ectodomain in *E. coli*. Coomassie stained reducing 4-12% SDS-PAGE of His-tagged products enriched on Ni-NTA magnetic beads from soluble fraction of cell lysate of small-scale expression tests of three NKR-P1 constructs - I66/Q80/G90-S225 (displayed in that order); in pOPINS3C (S3C), pOPINTRX (TRX), pOPINMSYB (MSYB), pOPINJB (JB), and pOPINP (P) expression plasmids – annotated at the top. Expression tests were performed in *E. coli* B834(DE3) and Rosetta2(DE3) pLysS strains – annotated at the bottom, using two different production conditions – (A) an overnight production at 20°C after induction with 1 mM IPTG and (B) a production in Overnight Express Instant TB auto-induction media at 25°C for 20 h. Red rectangles highlight approximate area of expected products soluble fusion products. The positive GFP controls for the four experimental conditions are shown in the last four lanes in (B).

Table S1. Table of DNA primers used for PCR amplification. For In-Fusion cloning of the selected NKR-P1 construct into the set of pOPIN vectors, DNA primers contained a 5' overlap designed for the In-Fusion cloning into a linearized vector and a sequence specific for the selected NKR-P1 construct. The first part of the table shows the selected N-terminal/C-terminal NKR-P1 residue with the respective forward/reverse sequence specific for the given NKR-P1 construct. The second part of the table shows the pOPIN vectors used in this study with the respective set of restriction enzymes used for their linearization and specific 5' forward/reverse In-Fusion overlaps.

N-terminal AA	Construct specific forward sequence
I66	5'ATACAGAAATCATCAATAGAAAAATGCAGTGTGG3'
Q67	5'CAGAAATCATCAATAGAAAAATGCAGTGTGG3'
K68	5'AAATCATCAATAGAAAAATGCAGTGTGGAC3'
S69	5'TCATCAATAGAAAAATGCAGTGTGGACATTC3'
S70	5'TCAATAGAAAAATGCAGTGTGGACATTCAAC3'
I71	5'ATAGAAAAATGCAGTGTGGACATTCAACAG3'
E72	5'GAAAAATGCAGTGTGGACATTCAACAG3'
K73	5'AAATGCAGTGTGGACATTCAACAGAGC3'
C74	5'TGCAGTGTGGACATTCAACAGAGCAG3'
S75	5'AGTGTGGACATTCAACAGAGCAGGAATAAAAC3'
V76	5'GTGGACATTCAACAGAGCAGGAATAAAAC3'
D77	5'GACATTCAACAGAGCAGGAATAAAACAACAG3'
I78	5'ATTCAACAGAGCAGGAATAAAACAACAGAG3'
Q79	5'CAACAGAGCAGGAATAAAACAACAGAGAGACC3'
Q80	5'CAGAGCAGGAATAAAACAACAGAGAGACCG3'
S81	5'AGCAGGAATAAAACAACAGAGAGACCGGG3'
R82	5'AGGAATAAAACAACAGAGAGACCGGG3'
N83	5'AATAAAACAACAGAGAGACCGGGTCTCTTAAAC3'
K84	5'AAAACAACAGAGAGACCGGGTCTCTTAAACTG3'
T85	5'ACAACAGAGAGACCGGGTCTCTTAAACTGC3'
T86	5'ACAGAGAGACCGGGTCTCTTAAACTGCC3'
E87	5'GAGAGACCGGGTCTCTTAAACTGCCC3'
R88	5'AGACCGGGTCTCTTAAACTGCCC3'
P89	5'CCGGGTCTCTTAAACTGCCCAATATATTG3'
G90	5'GGTCTCTTAAACTGCCCAATATATTGGC3'
C-Terminal AA	**Construct specific reverse sequence**
S225	5'AGAGTCAGGATACACTTTATTTCTCACAGGTG3'

Vector	Restriction sites	Forward overlap	Reverse overlap
pOPINS3C pOPINTRX pOPINMSYB	KpnI HindIII	5'AAGTTCTGTTTCAGGGCC CG3'	5'ATGGTCTAGAAAGCTTTA3'
pOPINJB	KpnI SfoI	5'AAGTTCTGTTTCAGGGCC CG3'	5'AGATGTCGTTCAGGCC3'
pOPINP	KpnI PmeI	5'GCCCAGCCGGCGATGGC CATG3'	5'GTGATGGTGATGTTT3'
pOPING pOPINTTGneo	KpnI PmeI	5'GCGTAGCTGAAACCGGC3'	5'GTGATGGTGATGTTT3'

Table S2. Table of cystic peptides identified for NKR-P1. First column shows identified peptides/cystic dipeptides (numbered relative to the expressed NKR-P1 construct, i.e. ETG-G90-S225-KHHHHHH) based on which a disulphide bond or N-linked glycosylation was assigned in the second column (presence of N-bound HexNAc is also indicated, in this case this corresponds to the first GlcNAc unit left after the cleavage of protein by endoglycosidase Endo Hf). Theoretical and experimental masses of measured peptides, mass error and intensity are shown in the third, fourth, fifth and sixth column, respectively.

Identified peptide(s)	Cys-Cys cross-link	Theoretical mass	Experimental mass	Error (ppm)	Intensity
35-47/119-137	C122-C210	3834.0408	3834.037	0.9	2.30E+07
100-121	C189-C202	2497.0862	2497.083	1.4	2.40E+08
97-118	C189-C202	2413.0176	2413.012	2.3	4.11E+06
100-121	C189-C202	2497.0862	2497.081	2	1.14E+06
1-39/122-126	C94-C105, C122-C210, N116-HexNAc	5354.5532	5354.544	1.8	2.17E+07
1-34	C94-C105, N116-HexNAc	4146.022	4146.026	1.1	9.91E+08
61-80	N157-HexNAc	2612.3762	2612.372	1.5	1.72E+06
35-75	N157-HexNAc	4948.6133	4948.612	0.3	1.03E+08
48-80	N157-HexNAc	4188.2134	4188.208	1.3	9.24E+05
61-90	N157-HexNAc,N169-HexNAc	3947.9858	3947.98	1.4	4.39E+06
48-90	N157-HexNAc,N169-HexNAc	5523.8232	5523.812	2	9.39E+05
81-95	N169-HexNAc	1980.9666	1980.963	2	3.27E+08
81-99	N169-HexNAc	2352.147	2352.143	1.9	2.80E+07
78-95	N169-HexNAc	2409.1838	2409.179	1.8	5.11E+06
76-90	N169-HexNAc	2039.9827	2039.98	1.4	9.54E+07
81-95	N169-HexNAc	1980.9666	1980.964	1.4	7.60E+07
78-95	N169-HexNAc	2409.1838	2409.18	1.5	2.38E+06

PUBLICATION IV

Bláha, J., Skálová, T., Skořepa, O., Kalousková, B., Pažický, P., Poláchová, E., Stránský, J., Koval', J., Dušková, J., Zhao, Y., Harlos, K., Hašek, J., Dohnálek, J., Vaněk, O.

Structure of human natural killer cell receptor NKR-P1 bound to its cognate lymphocyte ligand LLT1

Submitted for publication

My contribution to the publication: *performing research (protein expression and purification, protein characterization and crystallization), data collection, data analysis and interpretation, manuscript writing*

Structure of human natural killer cell receptor NKR-P1 bound to its cognate lymphocyte ligand LLT1

Jan Bláha[1], Tereza Skálová[2], Ondřej Skořepa[1], Barbora Kalousková[1], Samuel Pažický[1], Edita Poláchová[1], Jan Stránský[2], Tomáš Koval'[2], Jarmila Dušková[2], Yuguang Zhao[3], Karl Harlos[3], Jindřich Hašek[2], Jan Dohnálek[2], Ondřej Vaněk[1,*]

[1]Department of Biochemistry, Faculty of Science, Charles University, Hlavova 2030/8, 12840 Prague, Czech Republic
[2]Institute of Biotechnology, The Czech Academy of Sciences, v.v.i., BIOCEV Centre, Průmyslová 595, 25250 Vestec, Czech Republic
[3]Division of Structural Biology, The Wellcome Trust Centre for Human Genetics, University of Oxford, Roosevelt Drive, OX37BN Oxford, United Kingdom

*Corresponding author: Department of Biochemistry, Faculty of Science, Charles University, Hlavova 2030, 12840 Prague, Czech Republic. Tel: +420221951272, Fax: +420221951283. E-mail address: ondrej.vanek@natur.cuni.cz.

Abstract

Human NKR-P1 (CD161, gene *klrb1*) and its physiological ligand LLT1 (gene *clec2d*) is a prototypical inhibitory C-type lectin-like receptor:ligand pair of NK cells. Being identified as a marker for Th17 cells, the role of NKR-P1 in homing lymphocytes into immune-privileged sites, where expression of LLT1 is increased, is of particular interest for multiple sclerosis, rheumatoid arthritis or Crohn's disease; while its inhibitory signalization is being exploited by overexpression of LLT1 on glioblastoma, non-Hodgkin's lymphoma and prostate cancer cells. We determined crystal structure of both NKR-P1 and NKR-P1:LLT1 complex. NKR-P1 is forming homodimer with unexpected symmetry that enables binding of LLT1 in two distinct binding modes bridging two LLT1 molecules, thus pointing to formation of potential interaction clusters suggestive of an inhibitory immune synapse. This structure explains previously observed interaction data and shows how avidity might improve affinity and signalization upon cellular contact.

Keywords

NKR-P1/ LLT1/CD161/NK cell/C-type lectin-like

Introduction

Natural killer (NK) cells are innate immune lymphocytes exceptional for their ability to detect and eliminate virally infected, malignantly transformed or stressed cells without prior antigen sensitization (Vivier et al, 2008). For these purposes, NK cells are equipped with a broad range of surface activating and inhibitory receptors that govern their activation through a fine balance of induced signals (Vivier et al, 2008). The inhibitory receptors engage the cellular health markers (MHC class I-like glycoproteins) that would be down-

regulated due to infection or cellular stress (Anfossi et al, 2006). In such an event, NK cell can recognize through such loss of its inhibitory signals the "missing-self" and promote cytotoxicity towards target cell (Karre et al, 1986). Similarly, the activation receptors recognize up-regulated surface disease markers in a recognition mode referred to as "induced-self" (Bottino et al, 2005). NK cells also contribute to the initiation and development of the adaptive immune response via production and secretion of several classes of cytokines, especially proinflammatory IFN-γ (Vivier et al, 2011). Moreover, recent findings showed that NK cells are capable of maintaining a form of immunological memory (Cerwenka & Lanier, 2016; Vivier et al, 2011). Thus, NK cells represent a bridge between innate and adaptive immunity (Caligiuri, 2008; Vivier et al, 2011).

The NK receptors comprise of two structurally divergent classes: the immunoglobulin-like receptors family and the C-type Lectin-like Receptors (CTLRs) family (Bartel et al, 2013; Yokoyama & Plougastel, 2003). CTLRs are encoded within the natural killer gene complex (NKC, human chromosome 12) and unlike C-type lectins CTLRs neither bind calcium ions nor engage carbohydrate ligands (Rozbesky et al, 2014; Zelensky & Gready, 2005). Instead, CTLRs are known to interact with protein ligands: while receptors such as Ly49, CD94/NKG2 or NKG2D recognize MHC class-I like molecules (Yokoyama & Plougastel, 2003), the NKR-P1 subfamily of receptors have been shown to recognize structurally highly related Clr/Ocil CTLRs from the *clec2* gene subfamily (Yokoyama & Plougastel, 2003; Zelensky & Gready, 2005) that is encoded in a tight genetic linkage with the *klr* genes of NKR-P1 receptors and represent a unique CTLR:CTLR interaction system serving both the non-MHC missing-self as well as the induced-self recognition (Bartel et al, 2013; Yokoyama & Plougastel, 2003; Zelensky & Gready, 2005). While several inhibitory and activating murine and rodent NKR-P1 receptors were described, the human receptor NKR-P1 (CD161, gene *klrb1*), identified in 1994 (Lanier et al, 1994), is still the only human orthologue described so far. However, based on the structural and functional homology with NKR-P1 it was proposed that the human activating C-type Lectin-like (CTL) receptor-ligand pairs NKp65:KACL (*klrf2*:*clec2a*) (Spreu et al, 2010) and NKp80:AICL (*klrf1*:*clec2b*) (Welte et al, 2006) represent the activating counterparts of human NKR-P1 (Bartel et al, 2013; Vogler & Steinle, 2011).

Human NKR-P1 was first identified as a marker of NK cells (Lanier et al, 1994), where it acts as an inhibitory receptor (Aldemir et al, 2005; Lanier et al, 1994; Rosen et al, 2005), that is up-regulated by IL-12 (Poggi et al, 1998). However, NKR-P1 is also expressed by natural killer T (NKT) cells (Exley et al, 1998), mucosal-associated invariant T (MAIT) cells (Ussher et al, 2014) and other subsets of T-lymphocytes (Fergusson et al, 2014), where it interestingly functions as a co-stimulatory receptor, increasing secretion of IFN-γ (Aldemir et al, 2005; Germain et al, 2011). NKR-P1 is already present on immature $CD16^-$ $CD56^-$ NK cells (Bennett et al, 1996) and also on precursors of Th17 and MAIT cells in the umbilical cord blood (Cosmi et al, 2008). Of particular interest is the presence of NKR-P1 on IL-17 producing regulatory T cells (Afzali et al, 2013), on subsets of Tc17 cells (Billerbeck et al, 2010) and on all Th17 cells, for which NKR-P1 is a marker (Cosmi et al, 2008). These IL-17 producing T lymphocytes are implicated in development of a number of autoimmune diseases – e.g. Crohn's disease (Smith & Colbert, 2014), multiple sclerosis (Brucklacher-Waldert et al, 2009), rheumatoid arthritis (RA) (Estrada-Capetillo et al, 2013), and psoriasis (Michalak-Stoma et al, 2013) – with NKR-P1 considered to aim or promote the transendothelial migration to immunologically privileged niches upon interaction with its endogenous ligand LLT1 (Cosmi et al, 2008; Chalan et al, 2015; Poggi et al, 1997).

LLT1 (gene *clec2d*) has been described to be primarily expressed on activated monocytes (APCs) and B-cells (Rosen et al, 2008) where it presumably contributes to defense against NK cell self-reaction (Rosen et al, 2008; Vogler & Steinle, 2011). However, its expression can be induced on NK cells and T cells by IL-2 (Boles et al, 1999). Furthermore, it was shown that LLT1 is up-regulated on glioblastoma (Roth et al, 2007), prostate cancer (Mathew et al, 2016), and B-cell non-Hodgkin's lymphoma (Germain et al, 2015) cells where LLT1 contributes to immune evasion by dampening the NK cell cytotoxicity. Interestingly, Th17 cells ($CD161^{+}$) have been reported to be present in the glioma tumor in increased number (Zambrano-Zaragoza et al, 2014). Six alternatively spliced isoforms of the *clec2* gene were identified, with isoform 1 (coding for full-length membrane bound LLT1) being the only one confirmed to interact with NKR-P1 (Germain et al, 2010). However, a soluble form of LLT1 was recently found elevated in sera of RA patients (Chalan et al, 2015).

Being a genetically coupled CTL receptor:ligand pair, human NKR-P1 and LLT1 share the general protein morphology (Bartel et al, 2013). They are type II transmembrane glycoproteins with an N-terminal cytoplasmic signalization tail, a transmembrane helix, a flexible stalk region and a C-terminal C-type Lectin-like domain(CTLD) (Germain et al, 2010; Lanier et al, 1994; Yokoyama & Plougastel, 2003). Both NKR-P1 and LLT1 were shown to form disulfidic homodimers (Germain et al, 2010; Lanier et al, 1994) linked most probably by cysteine residues in their stalk regions. Structure of the NKp65:KACL complex represents the only structural data currently available for complexes of the CTL receptor:ligand subfamily (Li et al, 2013). It was also shown that the interaction of NKp65:KACL is protein-based and independent of glycosylation (Bauer et al, 2015). Based on the available data an Surface plasmon resonance (SPR) analysis of NKR-P1 and LLT1 mutants was performed revealing fast kinetics of the interaction and key interaction residues and a model of this complex was proposed (Kamishikiryo et al, 2011; Kita et al, 2015).

Previously we reported the first structure of LLT1 (Skalova et al, 2015) forming a non-covalent dimer following the classical dimerization mode of CD69 independently on its glycosylation (Blaha et al, 2015). Here we show and discuss the first structure of the human NKR-P1 receptor, forming a non-covalent dimer that differs from the classical dimerization mode of CD69 and LLT1 (Kita et al, 2015; Natarajan et al, 2000; Skalova et al, 2015), as well as its complex with LLT1 that explains the previous solution interaction observations and yet totally differs from the previously proposed interaction model. For the first time, we can show how dimerization of NKR-P1, as a prototypic CTLR with weak affinity towards its ligand, helps overcome this by means of receptor oligomerization, leading to proposed clustering of the receptor:ligand complex within the immunological synapse.

Results

Structure of human NKR-P1 ectodomain

Two crystal structures of the human NKR-P1 ectodomain were solved: the structure of NKR-P1 with simple "$GlcNAc_2Man_5$" N-glycosylation (NKR-P1_glyco) and of NKR-P1 deglycosylated after the first GlcNAc residue (NKR-P1_deglyco); data statistics for all structures are given in Table 1. NKR-P1 in both crystal structures follows the fold characteristic for a CTLD – two α-helices (α1 and α2) and two antiparallel β-sheets with the conserved hydrophobic WIGL motif within the domain core (Fig. 1 and 2a). The two β-sheets are formed by β-strands β0, β1, β1', and β5 and by β-strands β2, β2′, β3, and β4, respectively (assignment according

to Zelensky and Gready (Zelensky & Gready, 2005) used also for description of other related CTL structures (Kita et al, 2015; Li et al, 2013)). The domain is stabilized by three intramolecular disulfide bonds Cys94-Cys105, Cys122-Cys210 and Cys189-Cys202.

Human NKR-P1 homodimer is similar to that of murine dectin-1

The asymmetric unit of NKR-P1_glyco contains two monomers, while the asymmetric unit of NKR-P1_deglyco contains eight monomers of NKR-P1. All these monomers are arranged into very similar homodimers, with pairwise RMSD on Cα atoms up to 0.5 Å (Fig. 2b). However, these homodimers are of an unexpected type: they do not resemble the classical dimerization mode of CD69 and other *clec2* ligands with helix α2 utilized in the dimerization interface. Instead, the dimerization interface of NKR-P1 is formed by helix α1, similarly as in the case of the murine C-type lectin-like pattern recognition receptor dectin-1 (Brown et al, 2007), with which human NKR-P1 shares only 32% sequence identity of the CTLD (Fig. 2c). RMSD of Cα atoms between NKR-P1 and the dimer of dectin-1 in structure 2CL8 is 3.7 Å. The overall position and orientation of the monomers of human NKR-P1 in the dimer resembles those of dectin-1 to some extent but still there are significant differences, e.g. the positions of helices α1 of the superimposed dimers differ up to 7 Å.

Dimerization interface of human NKR-P1 is stabilized by glycosylation

The dimerization interface of the NKR-P1 homodimer is formed by six protein-protein and several water-mediated hydrogen bonds (Tab. S1), a peptide bond interaction via delocalized electrons (Lys126-Glu127) and a small hydrophobic core comprising Leu119, Ala120 and Ile168 from both chains (Fig. 3a). The contact surface area is ca. 500 $Å^2$. In comparison with the classical α2-centred LLT1 dimer (7-12 hydrogen bonds, stronger hydrophobic core, contact surface area 500-800 $Å^2$) (Skalova et al, 2015), the α1-centred dimer of NKR-P1 is realized through smaller contact surface area with fewer contact residues.

Interestingly, the first localized GlcNAc units at Asn116 in NKR-P1_glyco and the overlapping GlcNAc units at Asn116 and Asn157 in NKR-P1_deglyco participate in dimerization contacts with residues of helix α1 and β2, L1, and β2' regions of the opposite subunit of the NKR-P1 homodimer (Fig. 3b). In NKR-P1_glyco five hydrogen bonds between Asn116:GlcNAc and the opposite subunit contribute to stabilization of the α1-centred homodimer (Tab. S1). The contact surface area between the opposite chain of NKR-P1 and the localized GlcNAc unit is about 125 $Å^2$.

Glycosylation of human NKR-P1

The NKR-P1 ectodomain contains three potential N-glycosylation sites at residues Asn116, Asn157, and Asn169 (Fig. 1a). Glycosylation on Asn169 is present in electron density in both glyco and deglyco structures - in NKR-P1_glyco the complete carbohydrate chain ($GlcNAc_2Man_5$) is localized in chain A, while a partial chain of $GlcNAc_2Man_3$ is localized in chain B (Fig. 3a); in NKR-P1_deglyco, the remaining first GlcNAc unit is well localized in all eight NKR-P1 chains. Interestingly, in NKR-P1_deglyco the remaining GlcNAc units on Asn116 and Asn157 of the opposite protein chains of the dimer occupy the same space and are found in alternative conformations together with Asn116 (for details see Methods, Tab. 1, and Fig. 3c). On the other

hand, in NKR-P1_glyco GlcNAc at Asn116 is well defined with full occupancy in both chains, while no electron density is present for glycosylation at Asn157.

Structure of human NKR-P1:LLT1 complex

The complex is composed of one NKR-P1 dimer and one LLT1 dimer

The crystal structure of the NKR-P1:LLT1 complex is formed by deglycosylated NKR-P1 and LLT1 ectodomains. The asymmetric unit of the crystal contains a complex of dimeric NKR-P1 with dimeric LLT1 and an extra dimer of NKR-P1 (Fig. 4a). The dimerization mode of these NKR-P1 dimers is of the same α1-centred type as in the structures of sole NKR-P1 described above (Fig. 2b). The LLT1 dimer follows the standard α2-centred dimerization mode (Fig. 2c), similar to CD69 and identical with that described in the LLT1 structures (Skalova et al, 2015). LLT1 has well localized GlcNAc units at residues Asn95 and Asn147. Glycosylation of NKR-P1 observed in electron density is the same as in the structure NKR-P1_deglyco.

The LLT1 homodimer engages its partner bivalently, i.e. one dimer interacts with two dimers of NKR-P1 related by crystallographic symmetry: each monomer of LLT1 binds to a different subunit of a distinct NKR-P1 homodimer (Fig. 4a). There is no apparent induced fit of the binding partners – the RMSD of Cα atoms between the non-interacting and interacting NKR-P1 dimers (NKR-P1_glyco and the complex) is 0.5 Å; for LLT1 (PDB ID 4QKH and the current complex) it is 0.7 Å. The localized N-linked glycosylation chains do not directly contribute to the interaction.

Two interaction modes of NKR-P1:LLT1 complex

There are two distinct types of engagement between NKR-P1 and LLT1 in the presented structure – the primary interaction mode (LLT1 chain B:NKR-P1 chain D) and the secondary interaction mode (LLT1 chain A:NKR-P1 symmetry-related chain C). The primary interaction mode corresponds well to the structure of the homologous NKp65:KACL complex (PDB ID 4IOP (Li et al, 2013)) – RMSD of Cα atoms of the two complexes is 1.3 Å (one chain of receptor and one chain of the ligand in each case, Fig. 4b, lower left). To the best of our knowledge no protein-protein interaction similar to the secondary interaction mode is known. The interaction interfaces of NKR-P1 involved in both interaction modes are fairly similar. They are formed mostly by the membrane-distal residues of the loops L0, L3, L5, and L6 and strands β3 and β4 (Fig. 4c,d) that form a flat surface for interaction with LLT1. Conversely, in the case of LLT1 the interaction interfaces of the primary and secondary mode are quite different, albeit sharing a small number of residues. The primary interaction patch of LLT1 is formed by residues of the loops L0', L0, L3, L5, L6 and strands β3 and β4 (Fig. 4c), whereas residues of the loops L2 and L5, strand β2'', and helix α2 (Fig. 4d) are employed in the secondary interaction interface. Both interaction modes place the membrane-proximal parts of the receptor and of the ligand on the opposite sides of the complex and suggest a plausible model of interaction realized between two cells.

The primary interaction is realized through nine hydrogen bonds, of which two are charge-supported, many water-mediated hydrogen bonds, and a π-π stacking interaction (Tyr201-Arg175) with a total contact surface area of ca. 800 Å^2 (Tab. S1). Hydrophobic interaction is not utilized in this contact. The four strongest bonds are between the NKR-P1 residues Arg181, Tyr201, Lys148, and Ser199 and LLT1 residues Glu179, Glu162, Ser129, and Tyr177, respectively (Fig. 4c). The secondary interaction mode is realized through five hydrogen bonds, of which two are charge-supported, and a hydrophobic interaction (LLT1:Pro156 – NKR-P1:Ala149,

Leu151) with a total contact surface area of ca. 550 Å^2 (Tab. S1). The three strongest bonds are between the NKR-P1 residues Asp147, Ser199, and Arg181 and LLT1 residues Arg153, Lys169, and Asn120, respectively (Fig. 4d).

Solution data for NKR-P1:LLT1 complex

To characterize the size and shape of the NKR-P1:LLT1 complex in solution we have performed small-angle X-ray scattering (SAXS) and analytical ultracentrifugation (AUC) measurements. The SAXS data are concentration-dependent due to an increasing ratio of the NKR-P1:LLT1 complex to the free constituents with increasing protein concentration. At total protein concentration 9.6 mg/ml, the molecular mass estimated from an extrapolated intensity at zero scattering angle I(0) is 63 kDa, which corresponds well with the expected mass of the dimer:dimer complex (66 kDa). Therefore, this concentration was selected for the complex solution state characterization. The scattering plot for these conditions, Kratky plot, P(r) plot and a DAM envelope with fitted crystal structure are shown in the supplemental Figure 1.

The SAXS envelope of the complex has a size and shape approximately corresponding to the size and shape of the dimer:dimer NKR-P1:LLT1 complex in both the primary or secondary mode. The CRYSOL fit between the experimental SAXS data and scattering curve simulated from coordinates of all possible monomeric or dimeric NKR-P1 and LLT1 domain combinations was checked. The best accordance was found for the dimer:dimer complex in primary and secondary interaction modes (χ^2 5.4 or 5.2, respectively). The CRYSOL fit for models composed of an LLT1 homodimer and two NKR-P1 monomers placed in either the primary/primary or primary/secondary combinations is much worse (χ^2 87.5 or 121.8, respectively) with shapes lacking good agreement with the SAXS envelope (not shown).

Similarly, AUC data are also concentration dependent. Whereas free human NKR-P1 ectodomain is monomeric with $s_{20,w}$ sedimentation coefficient 2.1 S (estimated molecular mass 18 kDa, expected 17.5 kDa) and LLT1 ectodomain is forming non-covalent dimer (2.9 S) dissociating to monomer at lower concentrations (previously characterized in Skalova *et al.*, 2015(Skalova et al, 2015)), upon increasing the total concentration of NKR-P1:LLT1 equimolar mixture a shift of apparent sedimentation coefficient corresponding to the complex formation is observable (Fig. S2a), reaching an $s_{20,w}$ value of 3.7 S at the highest analyzed protein concentration. While this value corresponds rather to an LLT1(dimer):NKR-P1(monomer) complex than to the particle of the expected dimer:dimer stoichiometry, when we take into account non-ideality resulting from the very high protein concentration used (18 mg/ml) and recalculate this $s_{20,w}$ value to zero protein concentration, the resultant estimated $^0s_{20,w}$ value for spherical particle is 4.4 S and for elongated particle 4.5–5 S with approximate dimensions 10–15 × 4–5 nm, which is within range expected for a dimer:dimer complex and correlates well with the observed SAXS envelope.

To analyze the sedimentation data further, binding isotherm was constructed by integrating individual c(s) curves and plotting the resulting weighted S values against the given protein concentrations used and fitted with two hetero-association binding models (Fig. S2b,c). The second bivalent binding model (A+B⇔AB+B⇔ABB) describes the data slightly better with estimated sAB and sABB values

3.3 and 4.0 S, and K_d values 36 and 144 μM, respectively, again pointing to the dimer:dimer overall stoichiometry.

Discussion

Comparison with homologous NKp65:KACL complex

Currently the only available structure of a homologous complex – NKp65:KACL (Li et al, 2013) describes two monomeric NKp65 units interacting separately and symmetrically with a dimeric KACL ligand with a topological similarity to the described primary interaction mode in the NKR-P1:LLT1 complex (Fig. 4b). However, the NKp65:KACL complex employs an entirely different set of interactions in the interface between the two proteins. Not a single amino acid interaction pair observed in the primary NKR-P1:LLT1 interface resembles those observed in the NKp65:KACL complex. The primary interaction mode in NKR-P1:LLT1 to a significant extent relies on main chain contacts permitting fast k_{on}/k_{off} kinetics, which agrees with the SPR experiments published previously as well as our AUC analysis. This implies that in both cases a topologically similar complex is formed while the responsible intermolecular recognition is realized semi-independently of the actual fold and amino acid composition.

Influence of α1-centred dimerization on complex affinity

Li *et al.* also reported that the orientation of NKp65 bound in the complex precludes the putative α2-centred dimerization of NKp65. An NKp65 α1-centred dimer model does not seem plausible for steric reasons and a lack of stabilizing interactions, too (based on our analysis, not shown). This contrasts with the α1-centred dimerization of NKR-P1 observed in both the unbound and complex crystal structures. Interestingly, a single-nucleotide polymorphism (SNP) c.503T>C of human *klrb1* gene causing mutation of the CTLD residue Ile168 to Thr168 was described recently (Rother et al, 2015). The authors reported a 37%-frequency of the Thr168 allele and showed that the Thr168 isoform of NKR-P1 has lower ability to bind LLT1 and subsequently smaller inhibitory effect on NK cells and further proposed that Ile168 forms a part of the interaction interface between NKR-P1 and LLT1 with a direct influence on the recognition of LLT1 by NKR-P1 (Rother et al, 2015). However, the structure of the NKR-P1 homodimer shows that Ile168 is present at the dimerization interface rather than at the membrane-distal interaction interface – actually, it participates in a small hydrophobic pocket within the dimerization interface (Fig. 3d). Therefore, we propose that the substitution of the nonpolar isoleucine residue by polar threonine caused by the c.503T>C SNP has an indirect effect on the binding affinity through destabilization of the α1-centred NKR-P1 homodimer and, furthermore, that the NKR-P1:LLT1 binding affinity is influenced by the oligomeric state of the receptor. The complex NKp65:KACL stands out for its high affinity (K_d ~ 0.67 nM)(Li et al, 2013) – ca. 3000× stronger than NKp80:AICL (K_d ~ 2.3 μM) (Welte et al, 2006) and 70000× than NKR-P1:LLT1 (K_d ~ 48 μM (Kamishikiryo et al, 2011); this study 36 μM). It is possible that due to this exceptionally high affinity in NKp65 the putative α1-centred dimerization interface evolved in a way that hinders such dimerization, while in the case of the low affinity NKR-P1, NKp80 receptors in a way supporting the α1-centred dimerization for an increased avidity effect.

Comparison with previously proposed NKR-P1:LLT1 binding model

The SPR analysis of single-residue mutants of both binding partners performed by Kamishikiryo *et al. (Kamishikiryo et al, 2011)* and updated by Kita *et al. (Kita et al, 2015)* (based on the published structure of LLT1) identified several key residues of NKR-P1 and LLT1 that are important for their interaction and proposed several pairs of interacting residues (Tab. S2). The proposed set of participating residues corresponds well with the observed primary interaction mode. The mutated residues with detrimental or moderate effect on binding in the SPR studies are mostly found in this interface (Fig. 1 and Tab. S2) – in LLT1: Tyr165, Asp167, Lys169, Arg175, Arg180, and Lys181, and in NKR-P1: Arg181, Asp183, Glu186, Tyr198, Tyr201, and Glu205. Also, their proposed interaction pairs agree with the mutual orientation of the interacting macromolecules. Namely, the proposed LLT1/NKR-P1 pairs Tyr177/Tyr198 and Arg175/Glu200 correspond well to our observed pairing of LLT1:Tyr177:OH/NKR-P1:Ser199:O and LLT1:Arg175:N/NKR-P1:Glu200:OE2, respectively. The proposed pairing of Glu179 from the LLT1 loop L6 with Ser193 or Thr195 from the NKR-P1 loop L5 resembles the crystal structure contacts of Glu179 with Arg181 (loop L3) and Tyr198 (strand β4), located just in the vicinity of the NKR-P1 loop L5. In contrast to the SPR studies we do not observe any contact between Tyr165 and Phe152, although LLT1:Tyr165 is employed in the primary interface and Phe152 is close to the interacting L0 region of NKR-P1. Lastly, we do not observe the suggested direct bond between LLT1:Lys169 and NKR-P1:Glu205. Although these residues are close to each other in the primary mode (the closest distance 4.3 Å), they clearly do not form a pivotal bond of the interaction interface and the Lys169 side chain is rather flexible as suggested by a low quality of its electron density map in the primary mode, contrary to all other side chains in the vicinity having well-defined positions.

As the secondary binding mode observed in the NKR-P1:LLT1 structure utilizes a significantly different region of LLT1 compared to the primary one, the orientation of LLT1 and NKR-P1 in this binding mode does not correspond to the interaction pairs proposed in the SPR studies. However, as the interaction interface of NKR-P1 in this mode is quite similar to the primary mode, some of the NKR-P1 residues with a previously identified effect on binding are also employed in the secondary mode (Arg181, Asp183, Tyr198, and Tyr201). Interestingly, the residue LLT1:Lys169 makes several contacts with NKR-P1 (Arg181, Ser199, and Glu200) in the secondary interaction mode. However, the proposed pair Lys169/Glu205 is not observed in this mode either and here they are located even further away – ca. 11 Å. The presence of Lys169 in both the primary and the secondary interface of LLT1 suggests that the role of this residue in the overall formation of the complex is significant. The reported mutation of Lys169 in LLT1 to Glu169 (Kamishikiryo et al, 2011) would lead to a co-localization of several negative side chains in the secondary interface (Glu200 and Asp183 of NKR-P1 and mutated Glu169). This explains that the observed disruption of the NKR-P1:LLT1 interaction in the previous SPR experiments was most likely caused by the weakening of the secondary interface rather than the primary one. The following restoration of binding due to the mutation of Glu205 in NKR-P1 to Lys205 could be, in the light of the current structure, explained as strengthening of the primary interface. Thus, the previously published SPR-based interaction data to a significant extent agree with the interaction modes between NKR-P1 and LLT1 observed in the presented crystal structure, although there are also previously suggested interaction pairs which cannot be observed in either interface.

Assembly of NKR-P1:LLT1 complex on cell surface

Previously, an avidity effect of multimerization upon interaction was suggested by several authors as a means of compensation for the low affinity of the NKR-P1:LLT1 complex (Kita et al, 2015; Li et al, 2013; Skalova et al, 2012). Interestingly, in the presented structure of this complex we do indeed observe formation of a chain of repeating NKR-P1 and LLT1 homodimers. This pseudo-linear multimer has a zig-zag shape with the membrane-proximal parts of the proteins on the opposite sides (Fig. 5). However, such multimer is based on the alternating α1/α2-centred homodimeric state of NKR-P1/LLT1 (the chain-forming effect) and by simultaneous involvement of both the primary and the secondary interaction modes (steric effect). An attempted multimeric model of NKR-P1:LLT1 engagement in the primary mode alone shows a chain of homodimers having non-linear, almost helical organization (Fig. S3a), with the NKR-P1 stalk regions clashing sterically and the LLT1 stalk regions exposed in many different directions out of the complex core. Such multimer is unlikely to be compatible with cell membrane anchoring and to form within an immunological synapse. The receptor:ligand engagement in the secondary mode alone would also lead to formation of a helical multimer with both the receptor and the ligand stalk regions pointing in many different directions out of the complex core (Fig. S3b). Therefore, we conclude that a combination of both interaction modes is necessary for a biologically plausible multimeric interaction.

Although such functional multimerization of NK CTLRs have not been much explored, formation of similar nanoclusters is well described for the immunoglobulin family of KIRs interacting with MHC class I glycoproteins (Davis et al, 1999). Moreover, in crystal structures of the co-stimulatory immunocomplexes B7-1:CTLA-4 and B7-2:CTLA-4 a periodic zipper-like network of interacting dimers was reported (Schwartz et al, 2001; Stamper et al, 2001). Interestingly, B7-1 exists on a cell surface in a dynamic equilibrium of monomers and non-covalent dimers, where upon interaction with co-stimulatory CD28 it forms an interaction network of B7-1:CD28 homodimers. The uncoupling of this interaction is facilitated by dissociation of the B7-1 to monomer, whereas an obligate dimer of B7-1 led to prolonged abnormal signalization between APC and T cells (Bhatia et al, 2010).

Although both LLT1 and NKR-P1 were shown to form covalent homodimers on the cell surface as full-length proteins (Germain et al, 2010; Lanier et al, 1994), the dimeric state of their CTL ectodomains was, to the best of our knowledge, not yet evaluated in native cells. The formation and stability of the α2-centred non-covalent homodimer of soluble LLT1 ectodomain was reported previously (Blaha et al, 2015; Kita et al, 2015; Skalova et al, 2015). The relevance of the α1-centred NKR-P1 non-covalent homodimer is discussed above; however, the human NKR-P1 α1-centred dimer utilizes fewer intermolecular contacts and has a smaller contact surface area than α2-centred dimeric CTLRs and is thus less stable as also shown in our AUC analysis where only monomeric NKR-P1 species were observed. Dimerization of human NKR-P1 CTLD would be expectedly promoted in the context of the full-length receptor cystic homodimer and yet the length of its stalk region (25 amino acids) may confer enough flexibility for a CTLD monomer/dimer equilibrium. It would be therefore interesting to assess the actual stoichiometry of NKR-P1 CTLD on cellular surface since similarly to B7-1/CD28 there could be an equilibrium of the monomeric/dimeric states (stabilized by cystic bond in the flexible stalk region) influencing the formation and dissociation of the above discussed interaction multimer and thus regulating the strength and signalization of the NKR-P1:LLT1 system, especially to distinguish between the membrane-bound dimeric and the soluble monomeric form of the ligand.

Methods

Protein expression and purification. The mutant (His176 to Cys176) form of soluble LLT1 ectodomain (Gln72-Val191) was produced transiently in HEK293S GnTI$^-$ cells as described before (Blaha et al, 2015). The lectin-like domain of human NKR-P1 was produced in a similar way in stably transfected pool of HEK293S GNTI$^-$ cells (Bláha *et al.*, submitted). Briefly, the expression construct corresponding to the CTL extracellular domain of NKR-P1 (Gly90-Ser225) was subcloned into the pOPINGGTneo plasmid (kindly provided by prof. Ray Owens, University of Oxford), flanked by N-terminal secretion leader and C-terminal His-tag (leaving ETG and KHHHHHH at secreted protein N- and C-termini, respectively). A suspension culture of HEK293S GnTI$^-$ cells (Reeves et al, 2002) was transfected with a 1:3 (w/w) mixture of the expression plasmid and 25 kDa linear polyethylenimine. The stably transfected cell pool was selected within 3 weeks on 200 ng/µl of geneticin G418 antibiotic. The secreted proteins were purified from the harvested media by two step chromatography – an IMAC was performed on a Talon column (GE Healthcare), followed by size-exclusion chromatography (SEC) on a Superdex 200 10/300 GL (GE Healthcare) in 10 mM HEPES pH 7.5 with 150 mM NaCl and 10 mM NaN_3. For deglycosylation, GST-fused Endo F1 (Grueninger-Leitch et al, 1996) was added to the protein (in SEC buffer with 50 mM citrate pH 5.5) in a 1:100 weight ratio and incubated for 2 hours at 37°C. The deglycosylated protein was then purified using batch affinity chromatography on Glutathione Sepharose 4B resin (GE Healthcare) with subsequent SEC as above.

Crystallization.

NKR-P1 glycosylated (structure NKR-P1_glyco) – Soluble human NKR-P1 ectodomain at 20 mg/ml in SEC buffer was crystallized using the sitting drop vapor-diffusion method. Drops (100 nl of reservoir solution and 100 nl of protein solution) were set up using a Cartesian Honeybee 961 robot (Genomic Solutions) at 294 K. The reservoir consisted of 20% w/v PEG 3350, 200 mM di-sodium tartrate pH 7.2 (PEG/Ion screen, condition 36; Hampton Research). A hexagonal crystal with dimensions of 150 × 150 × 20 µm was cryoprotected by soaking in the reservoir solution with addition of 25% (v/v) ethylene glycol.

NKR-P1 deglycosylated (structure NKR-P1_deglyco) – The ENDO F1-deglycosylated soluble human NKR-P1 ectodomain was concentrated to 12 mg/ml and crystallized as above. The reservoir consisted of 20% w/v PEG 3350, 200 mM ammonium fluoride, 200 mM lithium chloride pH 6.2 (PEG/Ion screen, condition 3, Additive screen, condition 17; Hampton Research). A rod-shaped crystal of dimensions 50 × 50 × 150 µm was cryoprotected as above using addition of 25% (v/v) glycerol.

NKR-P1:LLT1 complex (structure NKR-P1:LLT1) – The ENDO F1-deglycosylated soluble human NKR-P1 and LLT1 ectodomains were mixed in 1:1 molar ratio and concentrated to 8 mg/ml of total protein. The protein complex was crystallized as above; drops (200 nl of reservoir and 100 nl of protein solutions) were seeded with 50 nl of stock solution of crushed needle-shaped crystals of deglycosylated NKR-P1 grown in 20% w/v PEG 3350, 200 mM ammonium fluoride pH 6.2 (PEG/Ion screen, condition 3; Hampton Research). The reservoir consisted of 200 mM ammonium sulfate, 20% w/v PEG MME 5000, 100 mM Tris pH 7.5 (Proplex screen, condition 1-40; Molecular Dimensions). A tetragonal bipyramid crystal of dimensions 30 × 30 × 80 µm was cryoprotected as above using addition of 25% v/v glycerol.

Data collection. All diffraction data were collected at Diamond Light Source, beamline I03, with wavelength 0.97625 Å and using a PILATUS3 6M detector. The crystal-detector distance was set to 340 mm, exposure time per image was 0.02 s, oscillation width 0.1º, and temperature 100 K. 7200 images were collected for each of the data sets. In the case of the NKR-P1:LLT1 complex, only 5000 images were finally used for data processing.

Data processing and structure solution. All diffraction images were indexed and integrated using the XDS package (Kabsch, 2010) and scaled using AIMLESS (Evans & Murshudov, 2013). 5% randomly selected reflections were used as R_{free} set. The phase problem was solved by molecular replacement – NKR-P1_glyco: in program BALBES (Long et al, 2008) using the structure of the human NK cell receptor KLRG1 bound to E-cadherin (PDB ID 3FF7 (Li et al, 2009)); NKR-P1_deglyco: 6 chains found in PHASER(McCoy et al, 2007) using murine NKR-P1A (PDB ID 3T3A (Kolenko et al, 2011)) were completed by 2 chains found in MOLREP (Vagin & Teplyakov, 2010); NKR-P1:LLT1: 4 chains found in BALBES as NKR-P1 chains (using structure of murine dectin-1, PDB ID 2BPD (Brown et al, 2007)) were completed by two more chains in MOLREP and all 6 chains were manually reinterpreted as 4 NKR-P1 chains and 2 LLT1 chains. Refinement was performed using REFMAC5

(Murshudov et al, 2011) and manual editing in COOT (Emsley et al, 2010). The last cycle of refinement was done using all reflections. The final data processing and structure parameters are summarized in Tab. 1.

Structure quality assessment.
NKR-P1_glyco – The structure, comprising one dimer of the glycosylated CTLD of human NKR-P1, is overall well defined in electron density, corresponding to the high resolution of the structure (1.8 Å). Glycosylation at the dimerization interface does not show the overlapping features as observed in the structures of deglycosylated NKR-P1 (below). GlcNAc was modelled on Asn116 with full occupancy in both chains, while glycosylation at Asn157 was not observed on the level of electron density. All modelled glycosylation chains ($GlcNAc_2Man_5$ at A/Asn169, $GlcNAc_2Man_3$ at B/Asn169 and GlcNAc at residues Asn116 in both chains) are well localized in electron density.
NKR-P1_deglyco – The asymmetric unit comprises of four dimers of the CTLD of human NKR-P1 deglycosylated after the first GlcNAc unit. The length of the localized part of the protein chain varies from the shortest chains A, F and G with modelled residues Leu91–Leu214 to the longest chain H with residues Gly90–Arg218. GlcNAc at residue Asn169 is well localized, however, GlcNAc units bound to Asn157 and Asn116 at the dimerization interface are present in alternative and overlapping positions and residue Asn116 also shows alternative conformers. GlcNAc units bound to Asn157 and Asn116 were modeled with 0.5 occupancy and only the more distinct from each overlapping pair was modeled (Tab. 1).
NKR-P1:LLT1 – The asymmetric unit contains two dimers of the CTLD of human NKR-P1 and one dimer of the CTLD of LLT1. The structure has well defined electron density and all protein chains can be unambiguously assigned. The strongest difference peaks correspond to non-interpretable small ligands. LLT1 has well localized GlcNAc units at residues Asn95 and Asn147. Localized glycosylation chains of NKR-P1 are the same as in the structure NKR-P1_deglyco (previous paragraph).

PDB deposition. The crystal structures were deposited in the Protein Data Bank under the codes 5MGR (NKR-P1_glyco), 5MGS (NKR-P1_deglyco) and 5MGT (NKR-P1:LLT1).

Small-angle X-ray scattering. SAXS data for NKR-P1:LLT1 mixture/complex were collected on beamline P12 at DESY Petra III, Hamburg, Germany, using a Pilatus 2M detector, wavelength 1.24 Å and sample-to-detector distance 3 m. The human NKR-P1 and LLT1 ectodomains homogeneously glycosylated by $GlcNAc_2Man_5$ diluted in 10 mM HEPES, 150 mM NaCl, 10 mM NaN_3, pH 7.5 were mixed in 1:1 molar ratio. Data were collected at 293 K for buffer and protein samples at concentrations 0.6, 1.2, 2.4, 4.8, and 9.6 mg/ml and processed using the ATSAS package (Petoukhov et al, 2012). For data collected at concentration 9.6 mg/ml, 20 independent models were calculated with DAMMIN (Svergun, 1999). The models were superimposed and averaged using DAMAVER (Volkov & Svergun, 2003); no model was rejected. The DAMAVER model was filtered using the damfilt command and then refined with DAMMIN. The final model was visualized in CHIMERA (Pettersen et al, 2004) as an envelope 15 Å above the beads.

Analytical ultracentrifugation. NKR-P1:LLT1 complex formation was analyzed in an analytical ultracentrifuge ProteomeLab XL-I equipped with An-50 Ti rotor (Beckman Coulter, USA) using sedimentation velocity experiment. Samples of glycosylated NKR-P1, LLT1 and their equimolar mixtures with increasing concentration in SEC buffer were spun at 48000 rpm at 20 °C and 150 scans with 0.003 cm spatial resolution were recorded in 5 min steps using absorbance optics. Buffer density and proteins partial specific volumes were estimated in SEDNTERP (www.jphilo.mailway.com). Data were analyzed with SEDFIT (Schuck, 2000) using a c(s) continuous size distribution model. Binding isotherm (as well as figures illustrating AUC data) was prepared in GUSSI (Brautigam, 2015) and then fitted in SEDPHAT (Schuck, 2003) using hetero-association models A+B⇔AB or A+B⇔AB+B⇔ABB; only values for K_d, sAB, sABB were floated in the fit, other parameters were kept constant at known values.

Supplementary information

Figure S1 and S2 display the obtained SAXS and AUC data, respectively. Figure S3 shows a model of oligomeric assembly of NKR-P1:LLT1 complexes based on propagation of a single interaction mode. Table

S1 describes contacts of the NKR-P1 dimerization interface as well as the NKR-P1:LLT1 interaction interfaces. Table S2 compares the previously proposed NKR-P1:LLT1 binding model with the crystal structure.

Author contributions

JB, OS, BK, SP and EP contributed to protein expression and purification, JB and YZ performed the protein crystallization, YZ and KH performed the X-ray diffraction measurements, JB, TS, JS, TK, JD and JD contributed to the data processing and model refinement, TS performed the SAXS data analysis, OV performed the analytical ultracentrifugation measurements and analysis, JB, TS, JD and OV designed the experiments and wrote the manuscript, with critical input from JH.

Acknowledgements

This study was supported by BIOCEV (ERDF CZ.1.05/1.1.00/02.0109 and CZ.02.1.01/0.0/0.0/16_013/0001776), Czech Science Foundation (15-15181S), Ministry of Education, Youth and Sports of the Czech Republic (LG14009 and LM2015043 CIISB for CMS Biocev; LTC17065), Charles University (UNCE 204025/2012, SVV 260079/2014, GAUK 161216), Foundation "Nadání Josefa, Marie a Zdeňky Hlávkových", COST Action (CA15126 MOBIEU), and BioStruct-X (EC FP7 project 283570). The authors also acknowledge the support and the use of resources of Instruct, a Landmark ESFRI project through the R&D pilot scheme APPID 56 and 286. The Wellcome Trust Centre for Human Genetics is supported by the Wellcome Trust (grant 090532/Z/09/Z). We thank Diamond Light Source for beamtime (proposal MX10627) and the staff of beamline I03 for assistance with data collection.

Competing financial interests

The authors declare that they have no conflict of interest.

References

Afzali B, Mitchell PJ, Edozie FC, Povoleri GA, Dowson SE, Demandt L, Walter G, Canavan JB, Scotta C, Menon B, Chana PS, Khamri W, Kordasti SY, Heck S, Grimbacher B, Tree T, Cope AP, Taams LS, Lechler RI, John S, Lombardi G (2013) CD161 expression characterizes a subpopulation of human regulatory T cells that produces IL-17 in a STAT3-dependent manner. European journal of immunology **43:** 2043-2054

Aldemir H, Prod'homme V, Dumaurier MJ, Retiere C, Poupon G, Cazareth J, Bihl F, Braud VM (2005) Cutting edge: lectin-like transcript 1 is a ligand for the CD161 receptor. Journal of immunology **175:** 7791-7795

Anfossi N, Andre P, Guia S, Falk CS, Roetynck S, Stewart CA, Breso V, Frassati C, Reviron D, Middleton D, Romagne F, Ugolini S, Vivier E (2006) Human NK cell education by inhibitory receptors for MHC class I. Immunity **25:** 331-342

Bartel Y, Bauer B, Steinle A (2013) Modulation of NK cell function by genetically coupled C-type lectin-like receptor/ligand pairs encoded in the human natural killer gene complex. Frontiers in immunology **4:** 362

Bauer B, Spreu J, Rohe C, Vogler I, Steinle A (2015) Key residues at the membrane-distal surface of KACL, but not glycosylation, determine the functional interaction of the keratinocyte-specific C-type lectin-like receptor KACL with its high-affinity receptor NKp65. Immunology **145:** 114-123

Bennett IM, Zatsepina O, Zamai L, Azzoni L, Mikheeva T, Perussia B (1996) Definition of a natural killer NKR-P1A+/CD56-/CD16- functionally immature human NK cell subset that differentiates in vitro in the presence of interleukin 12. The Journal of experimental medicine **184:** 1845-1856

Bhatia S, Sun K, Almo SC, Nathenson SG, Hodes RJ (2010) Dynamic equilibrium of B7-1 dimers and monomers differentially affects immunological synapse formation and T cell activation in response to TCR/CD28 stimulation. Journal of immunology **184:** 1821-1828

Billerbeck E, Kang YH, Walker L, Lockstone H, Grafmueller S, Fleming V, Flint J, Willberg CB, Bengsch B, Seigel B, Ramamurthy N, Zitzmann N, Barnes EJ, Thevanayagam J, Bhagwanani A, Leslie A, Oo YH, Kollnberger S, Bowness P, Drognitz O, Adams DH, Blum HE, Thimme R, Klenerman P (2010) Analysis of CD161 expression on human CD8+ T cells defines a distinct functional subset with tissue-homing properties. Proceedings of the National Academy of Sciences of the United States of America **107:** 3006-3011

Blaha J, Pachl P, Novak P, Vanek O (2015) Expression and purification of soluble and stable ectodomain of natural killer cell receptor LLT1 through high-density transfection of suspension adapted HEK293S GnTI(-) cells. Protein expression and purification **109:** 7-13

Boles KS, Barten R, Kumaresan PR, Trowsdale J, Mathew PA (1999) Cloning of a new lectin-like receptor expressed on human NK cells. Immunogenetics **50:** 1-7

Bottino C, Castriconi R, Moretta L, Moretta A (2005) Cellular ligands of activating NK receptors. Trends in immunology **26:** 221-226

Brautigam CA (2015) Calculations and Publication-Quality Illustrations for Analytical Ultracentrifugation Data. Methods in enzymology **562:** 109-133

Brown J, O'Callaghan CA, Marshall AS, Gilbert RJ, Siebold C, Gordon S, Brown GD, Jones EY (2007) Structure of the fungal beta-glucan-binding immune receptor dectin-1: implications for function. Protein science : a publication of the Protein Society **16:** 1042-1052

Brucklacher-Waldert V, Stuerner K, Kolster M, Wolthausen J, Tolosa E (2009) Phenotypical and functional characterization of T helper 17 cells in multiple sclerosis. Brain : a journal of neurology **132:** 3329-3341

Caligiuri MA (2008) Human natural killer cells. Blood **112:** 461-469

Cerwenka A, Lanier LL (2016) Natural killer cell memory in infection, inflammation and cancer. Nature reviews Immunology **16:** 112-123

Cosmi L, De Palma R, Santarlasci V, Maggi L, Capone M, Frosali F, Rodolico G, Querci V, Abbate G, Angeli R, Berrino L, Fambrini M, Caproni M, Tonelli F, Lazzeri E, Parronchi P, Liotta F, Maggi E, Romagnani S, Annunziato F (2008) Human interleukin 17-producing cells originate from a CD161+CD4+ T cell precursor. The Journal of experimental medicine **205:** 1903-1916

Davis DM, Chiu I, Fassett M, Cohen GB, Mandelboim O, Strominger JL (1999) The human natural killer cell immune synapse. Proceedings of the National Academy of Sciences of the United States of America **96:** 15062-15067

Diederichs K, Karplus PA (1997) Improved R-factors for diffraction data analysis in macromolecular crystallography. Nature structural biology **4:** 269-275

Emsley P, Lohkamp B, Scott WG, Cowtan K (2010) Features and development of Coot. Acta crystallographica Section D, Biological crystallography **66:** 486-501

Estrada-Capetillo L, Hernandez-Castro B, Monsivais-Urenda A, Alvarez-Quiroga C, Layseca-Espinosa E, Abud-Mendoza C, Baranda L, Urzainqui A, Sanchez-Madrid F, Gonzalez-Amaro R (2013) Induction of Th17 lymphocytes and Treg cells by monocyte-derived dendritic cells in patients with rheumatoid arthritis and systemic lupus erythematosus. Clinical & developmental immunology **2013:** 584303

Evans PR, Murshudov GN (2013) How good are my data and what is the resolution? Acta crystallographica Section D, Biological crystallography **69:** 1204-1214

Exley M, Porcelli S, Furman M, Garcia J, Balk S (1998) CD161 (NKR-P1A) costimulation of CD1d-dependent activation of human T cells expressing invariant V alpha 24 J alpha Q T cell receptor alpha chains. The Journal of experimental medicine **188:** 867-876

Fergusson JR, Smith KE, Fleming VM, Rajoriya N, Newell EW, Simmons R, Marchi E, Bjorkander S, Kang YH, Swadling L, Kurioka A, Sahgal N, Lockstone H, Baban D, Freeman GJ, Sverremark-Ekstrom E, Davis MM, Davenport MP, Venturi V, Ussher JE, Willberg CB, Klenerman P (2014) CD161 defines a transcriptional and functional phenotype across distinct human T cell lineages. Cell reports **9:** 1075-1088

Germain C, Bihl F, Zahn S, Poupon G, Dumaurier MJ, Rampanarivo HH, Padkjaer SB, Spee P, Braud VM (2010) Characterization of alternatively spliced transcript variants of CLEC2D gene. The Journal of biological chemistry **285:** 36207-36215
Germain C, Guillaudeux T, Galsgaard ED, Hervouet C, Tekaya N, Gallouet AS, Fassy J, Bihl F, Poupon G, Lazzari A, Spee P, Anjuere F, Pangault C, Tarte K, Tas P, Xerri L, Braud VM (2015) Lectin-like transcript 1 is a marker of germinal center-derived B-cell non-Hodgkin's lymphomas dampening natural killer cell functions. Oncoimmunology **4:** e1026503
Germain C, Meier A, Jensen T, Knapnougel P, Poupon G, Lazzari A, Neisig A, Hakansson K, Dong T, Wagtmann N, Galsgaard ED, Spee P, Braud VM (2011) Induction of lectin-like transcript 1 (LLT1) protein cell surface expression by pathogens and interferon-gamma contributes to modulate immune responses. The Journal of biological chemistry **286:** 37964-37975
Grueninger-Leitch F, D'Arcy A, D'Arcy B, Chene C (1996) Deglycosylation of proteins for crystallization using recombinant fusion protein glycosidases. Protein science : a publication of the Protein Society **5:** 2617-2622
Chalan P, Bijzet J, Huitema MG, Kroesen BJ, Brouwer E, Boots AM (2015) Expression of Lectin-Like Transcript 1, the Ligand for CD161, in Rheumatoid Arthritis. PloS one **10:** e0132436
Kabsch W (2010) Xds. Acta crystallographica Section D, Biological crystallography **66:** 125-132
Kamishikiryo J, Fukuhara H, Okabe Y, Kuroki K, Maenaka K (2011) Molecular basis for LLT1 protein recognition by human CD161 protein (NKRP1A/KLRB1). The Journal of biological chemistry **286:** 23823-23830
Karre K, Ljunggren HG, Piontek G, Kiessling R (1986) Selective rejection of H-2-deficient lymphoma variants suggests alternative immune defence strategy. Nature **319:** 675-678
Kita S, Matsubara H, Kasai Y, Tamaoki T, Okabe Y, Fukuhara H, Kamishikiryo J, Krayukhina E, Uchiyama S, Ose T, Kuroki K, Maenaka K (2015) Crystal structure of extracellular domain of human lectin-like transcript 1 (LLT1), the ligand for natural killer receptor-P1A. European journal of immunology **45:** 1605-1613
Kolenko P, Rozbesky D, Vanek O, Kopecky V, Jr., Hofbauerova K, Novak P, Pompach P, Hasek J, Skalova T, Bezouska K, Dohnalek J (2011) Molecular architecture of mouse activating NKR-P1 receptors. Journal of structural biology **175:** 434-441
Lanier LL, Chang C, Phillips JH (1994) Human NKR-P1A. A disulfide-linked homodimer of the C-type lectin superfamily expressed by a subset of NK and T lymphocytes. Journal of immunology **153:** 2417-2428
Li Y, Hofmann M, Wang Q, Teng L, Chlewicki LK, Pircher H, Mariuzza RA (2009) Structure of natural killer cell receptor KLRG1 bound to E-cadherin reveals basis for MHC-independent missing self recognition. Immunity **31:** 35-46
Li Y, Wang Q, Chen S, Brown PH, Mariuzza RA (2013) Structure of NKp65 bound to its keratinocyte ligand reveals basis for genetically linked recognition in natural killer gene complex. Proceedings of the National Academy of Sciences of the United States of America **110:** 11505-11510
Long F, Vagin AA, Young P, Murshudov GN (2008) BALBES: a molecular-replacement pipeline. Acta crystallographica Section D, Biological crystallography **64:** 125-132
Lovell SC, Davis IW, Arendall WB, 3rd, de Bakker PI, Word JM, Prisant MG, Richardson JS, Richardson DC (2003) Structure validation by Calpha geometry: phi,psi and Cbeta deviation. Proteins **50:** 437-450
Mathew SO, Chaudhary P, Powers SB, Vishwanatha JK, Mathew PA (2016) Overexpression of LLT1 (OCIL, CLEC2D) on prostate cancer cells inhibits NK cell-mediated killing through LLT1-NKRP1A (CD161) interaction. Oncotarget **7:** 68650-68661
McCoy AJ, Grosse-Kunstleve RW, Adams PD, Winn MD, Storoni LC, Read RJ (2007) Phaser crystallographic software. Journal of applied crystallography **40:** 658-674
Michalak-Stoma A, Bartosinska J, Kowal M, Juszkiewicz-Borowiec M, Gerkowicz A, Chodorowska G (2013) Serum levels of selected Th17 and Th22 cytokines in psoriatic patients. Disease markers **35:** 625-631
Murshudov GN, Skubak P, Lebedev AA, Pannu NS, Steiner RA, Nicholls RA, Winn MD, Long F, Vagin AA (2011) REFMAC5 for the refinement of macromolecular crystal structures. Acta crystallographica Section D, Biological crystallography **67:** 355-367
Natarajan K, Sawicki MW, Margulies DH, Mariuzza RA (2000) Crystal structure of human CD69: a C-type lectin-like activation marker of hematopoietic cells. Biochemistry **39:** 14779-14786
Petoukhov MV, Franke D, Shkumatov AV, Tria G, Kikhney AG, Gajda M, Gorba C, Mertens HD, Konarev PV, Svergun DI (2012) New developments in the program package for small-angle scattering data analysis. Journal of applied crystallography **45:** 342-350
Pettersen EF, Goddard TD, Huang CC, Couch GS, Greenblatt DM, Meng EC, Ferrin TE (2004) UCSF Chimera--a visualization system for exploratory research and analysis. Journal of computational chemistry **25:** 1605-1612
Poggi A, Costa P, Tomasello E, Moretta L (1998) IL-12-induced up-regulation of NKRP1A expression in human NK cells and consequent NKRP1A-mediated down-regulation of NK cell activation. European journal of immunology **28:** 1611-1616
Poggi A, Costa P, Zocchi MR, Moretta L (1997) Phenotypic and functional analysis of CD4+ NKRP1A+ human T lymphocytes. Direct evidence that the NKRP1A molecule is involved in transendothelial migration. European journal of immunology **27:** 2345-2350
Reeves PJ, Callewaert N, Contreras R, Khorana HG (2002) Structure and function in rhodopsin: high-level expression of rhodopsin with restricted and homogeneous N-glycosylation by a tetracycline-inducible N-acetylglucosaminyltransferase I-negative HEK293S stable mammalian cell line. Proceedings of the National Academy of Sciences of the United States of America **99:** 13419-13424
Rosen DB, Bettadapura J, Alsharifi M, Mathew PA, Warren HS, Lanier LL (2005) Cutting edge: lectin-like transcript-1 is a ligand for the inhibitory human NKR-P1A receptor. Journal of immunology **175:** 7796-7799
Rosen DB, Cao W, Avery DT, Tangye SG, Liu YJ, Houchins JP, Lanier LL (2008) Functional consequences of interactions between human NKR-P1A and its ligand LLT1 expressed on activated dendritic cells and B cells. Journal of immunology **180:** 6508-6517
Roth P, Mittelbronn M, Wick W, Meyermann R, Tatagiba M, Weller M (2007) Malignant glioma cells counteract antitumor immune responses through expression of lectin-like transcript-1. Cancer research **67:** 3540-3544
Rother S, Hundrieser J, Pokoyski C, Kollrich S, Borns K, Blasczyk R, Poehnert D, Klempnauer J, Schwinzer R (2015) The c.503T>C Polymorphism in the Human KLRB1 Gene Alters Ligand Binding and Inhibitory Potential of CD161 Molecules. PloS one **10:** e0135682
Rozbesky D, Krejzova J, Krenek K, Prchal J, Hrabal R, Kozisek M, Weignerova L, Fiore M, Dumy P, Kren V, Renaudet O (2014) Re-evaluation of binding properties of recombinant lymphocyte receptors NKR-P1A and CD69 to chemically synthesized glycans and peptides. International journal of molecular sciences **15:** 1271-1283
Schuck P (2000) Size-distribution analysis of macromolecules by sedimentation velocity ultracentrifugation and lamm equation modeling. Biophysical journal **78:** 1606-1619
Schuck P (2003) On the analysis of protein self-association by sedimentation velocity analytical ultracentrifugation. Analytical biochemistry **320:** 104-124
Schwartz JC, Zhang X, Fedorov AA, Nathenson SG, Almo SC (2001) Structural basis for co-stimulation by the human CTLA-4/B7-2 complex. Nature **410:** 604-608
Skalova T, Blaha J, Harlos K, Duskova J, Koval T, Stransky J, Hasek J, Vanek O, Dohnalek J (2015) Four crystal structures of human LLT1, a ligand of human NKR-P1, in varied glycosylation and oligomerization states. Acta crystallographica Section D, Biological crystallography **71:** 578-591
Skalova T, Kotynkova K, Duskova J, Hasek J, Koval T, Kolenko P, Novak P, Man P, Hanc P, Vanek O, Bezouska K, Dohnalek J (2012) Mouse Clr-g, a ligand for NK cell activation receptor NKR-P1F: crystal structure and biophysical properties. Journal of immunology **189:** 4881-4889
Smith JA, Colbert RA (2014) Review: The interleukin-23/interleukin-17 axis in spondyloarthritis pathogenesis: Th17 and beyond. Arthritis & rheumatology **66:** 231-241
Spreu J, Kuttruff S, Stejfova V, Dennehy KM, Schittek B, Steinle A (2010) Interaction of C-type lectin-like receptors NKp65 and KACL facilitates dedicated immune recognition of human keratinocytes. Proceedings of the National Academy of Sciences of the United States of America **107:** 5100-5105
Stamper CC, Zhang Y, Tobin JF, Erbe DV, Ikemizu S, Davis SJ, Stahl ML, Seehra J, Somers WS, Mosyak L (2001) Crystal structure of the B7-1/CTLA-4 complex that inhibits human immune responses. Nature **410:** 608-611
Svergun DI (1999) Restoring low resolution structure of biological macromolecules from solution scattering using simulated annealing. Biophysical journal **76:** 2879-2886
Ussher JE, Bilton M, Attwod E, Shadwell J, Richardson R, de Lara C, Mettke E, Kurioka A, Hansen TH, Klenerman P, Willberg CB (2014) CD161++ CD8+ T cells, including the MAIT cell subset, are specifically activated by IL-12+IL-18 in a TCR-independent manner. European journal of immunology **44:** 195-203
Vagin A, Teplyakov A (2010) Molecular replacement with MOLREP. Acta crystallographica Section D, Biological crystallography **66:** 22-25
Vivier E, Raulet DH, Moretta A, Caligiuri MA, Zitvogel L, Lanier LL, Yokoyama WM, Ugolini S (2011) Innate or adaptive immunity? The example of natural killer cells. Science **331:** 44-49
Vivier E, Tomasello E, Baratin M, Walzer T, Ugolini S (2008) Functions of natural killer cells. Nature immunology **9:** 503-510
Vogler I, Steinle A (2011) Vis-a-vis in the NKC: genetically linked natural killer cell receptor/ligand pairs in the natural killer gene complex (NKC). Journal of innate immunity **3:** 227-235
Volkov VV, Svergun DI (2003) Uniqueness of ab initio shape determination in small-angle scattering. Journal of applied crystallography **36:** 860-864
Weiss MS (2001) Global indicators of X-ray data quality. Journal of applied crystallography **34:** 130-135
Welte S, Kuttruff S, Waldhauer I, Steinle A (2006) Mutual activation of natural killer cells and monocytes mediated by NKp80-AICL interaction. Nature immunology **7:** 1334-1342
Yokoyama WM, Plougastel BF (2003) Immune functions encoded by the natural killer gene complex. Nature reviews Immunology **3:** 304-316
Zambrano-Zaragoza JF, Romo-Martinez EJ, Duran-Avelar Mde J, Garcia-Magallanes N, Vibanco-Perez N (2014) Th17 cells in autoimmune and infectious diseases. International journal of inflammation **2014:** 651503
Zelensky AN, Gready JE (2005) The C-type lectin-like domain superfamily. The FEBS journal **272:** 6179-6217

Figures

Figure 1

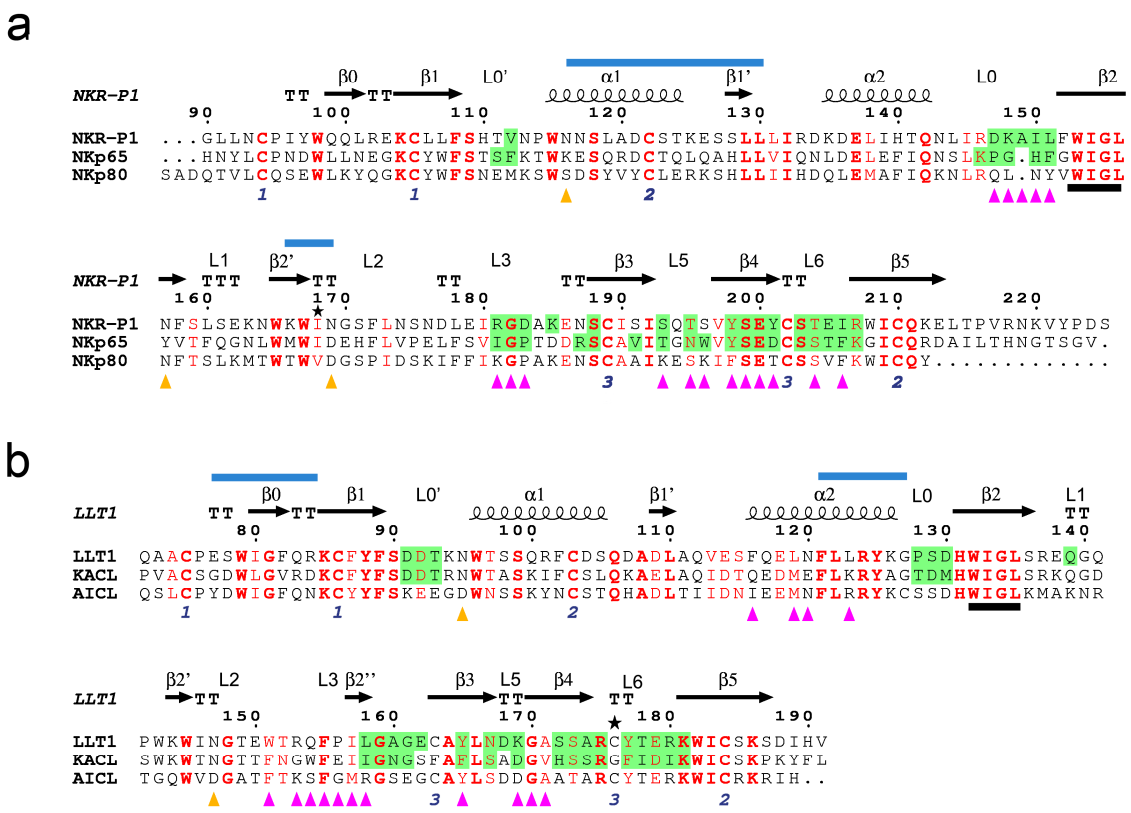

Figure 1. Sequence alignment of human NKC encoded receptor:ligand pairs. Secondary structure elements and loop regions (L) are denoted for NKR-P1 and LLT1 above the alignments. The paired numbers at the bottom indicate the cystic pairs in the NKR-P1 and LLT1 structures, mutation His176Cys in LLT1 and Ile168 in NKR-P1 are marked by asterisk. Predicted N-linked glycosylation sites of NKR-P1 and LLT1 are denoted with orange triangles. The conserved WIGL motifs are underlined with black line. The regions employed in formation of non-covalent dimer of NKR-P1 or LLT1 are denoted by blue lines above the sequence. Conserved residues are in red letters, bold denotes strictly conserved residues. (**a**) Sequence alignment of CTLDs of human NKR-P1, human NKp65 and human NKp80. NKR-P1 residues that contact LLT1 in the NKR-P1:LLT1 complex in primary binding mode and NKp65 residues that contact KACL in the NKp65:KACL complex are on green background. NKR-P1 residues that engage LLT1 in the NKR-P1:LLT1 complex in the secondary binding mode are marked with purple triangles. (**b**) Sequence alignment of CTLDs of human LLT1, human KACL and human AICL. LLT1 residues that contact NKR-P1 in the NKR-P1:LLT1 complex in the primary binding mode and KACL residues that contact NKp65 in the NKp65:KACL complex are on green background. LLT1 residues that engage NKR-P1 in the NKR-P1:LLT1 complex in the secondary binding mode are marked with purple triangles.

Figure 2

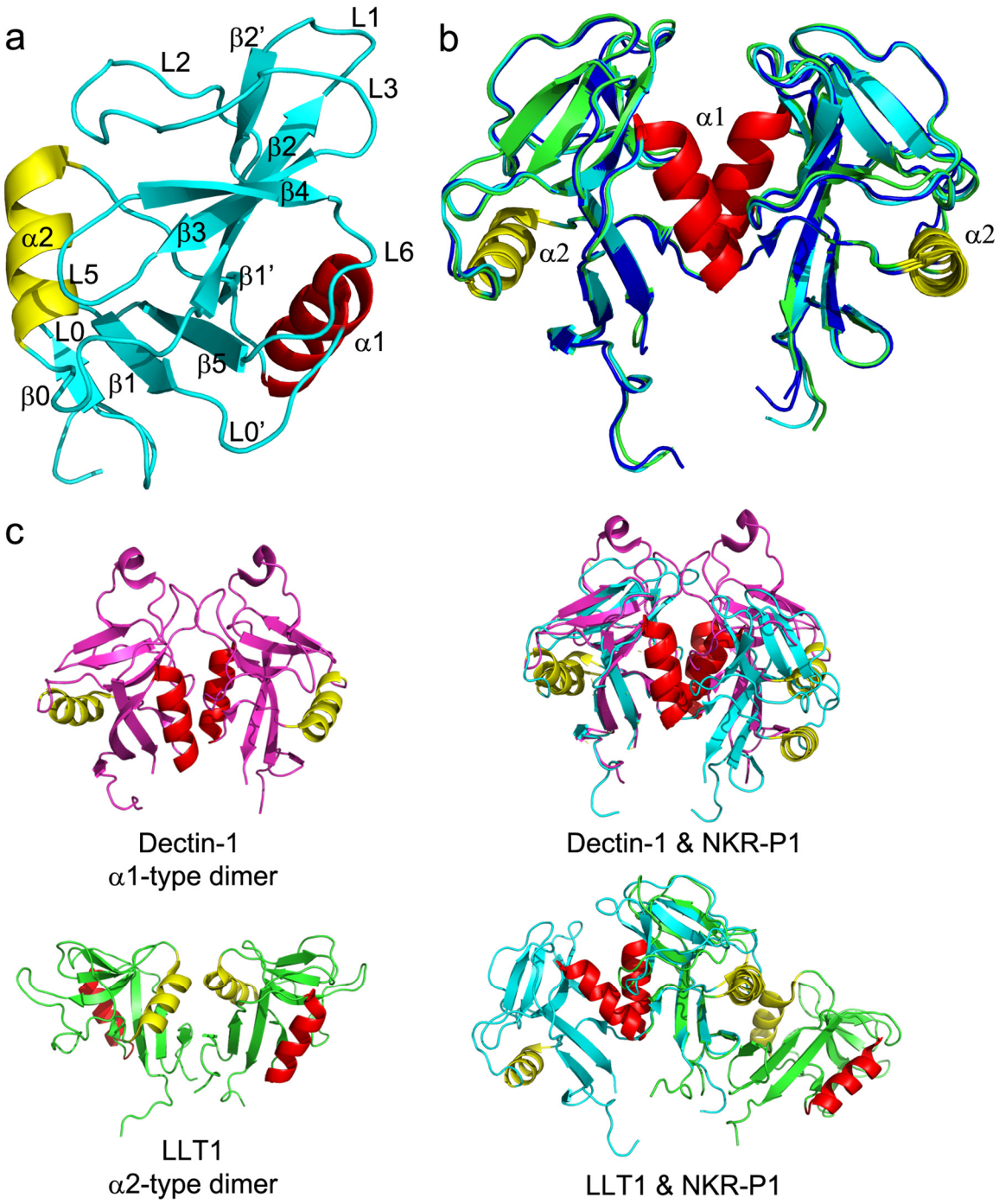

Figure 2. Structure of human NKR-P1 shows unique dimerization interface. (**a**) Ribbon diagram of the NKR-P1 CTLD. Secondary structure elements are labelled. Helix α1 is red and helix α2 is yellow; β-strands and loops are cyan. (**b**) Comparison of NKR-P1 dimer formation of glycosylated (cyan), deglycosylated free (green) and complex-bound (blue) form of NKR-P1. (**c**) Comparison of α1- and α2-centered dimerization of murine dectin-1 (PDB ID 2CL8, magenta) and LLT1 (PDB ID 4QKI, green), respectively, with helices α1 and α2 shown in red and yellow. On the right – structural alignments of dectin-1 and NKR-P1 monomers and LLT1 and NKR-P1 monomers are shown – while the CTLD fold is conserved in each pair of aligned proteins, the overall topology of α1- and α2- centered dimers is opposite.

Figure 3

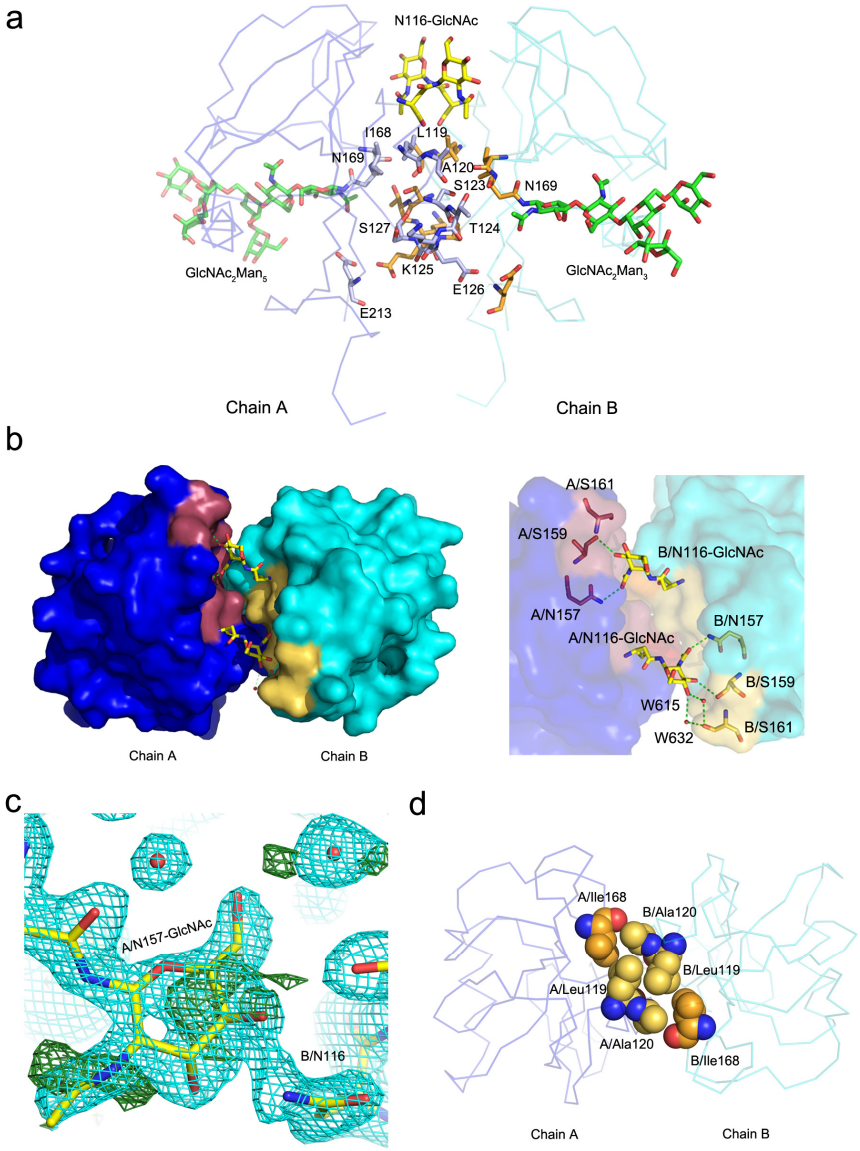

Figure 3. Glycosylation and dimerization interface of NKR-P1. (**a**) Dimerization interface of NKR-P1. Subunits of NKR-P1 are shown as Cα-trace (blue and cyan), the dimer contact residues are shown as sticks with carbon atoms colored in light blue (blue subunit) and orange (cyan subunit); for clarity only residues from the blue subunit are labelled. The first GlcNAc unit N-linked to Asn116 and the carbohydrate chain N-linked to Asn169 observable in the NKR-P1_glyco structure are shown with carbon atoms colored in yellow and green, respectively. (**b**) Top view into the dimerization interface. The NKR-P1 subunits surfaces are colored in blue and cyan. The GlcNAc units bound to Asn116 are shown as sticks with carbon atoms in yellow. The contact residues between GlcNAc bound to chain A and the chain B are in yellow, the contact residues between GlcNAc bound to chain B and the chain A are in purple. Hydrogen bonds are depicted by green dashed lines with a detailed view in top right. (**c**) Mixture of glycosylation states at the dimer interface in NKR-P1_deglyco structure. A GlcNAc unit is N-linked to Asn157, chain A, and it is modelled with 0.5 occupancy. The second GlcNAc unit present alternatively at Asn116 of chain B is not modelled. Contours of $2mF_o$-DF_c (2.8 σ, cyan) and mF_o-DF_c (1 σ, green) electron density maps are shown. (**d**) Small hydrophobic core in the central part of the NKR-P1 dimerization interface (subunits colored as in a). The principle residues are shown as spheres with carbon atoms in yellow. The Ille168 residues (whose mutation decreases the ability of NKR-P1 to bind LLT1) are shown with carbon atoms in orange.

Figure 4

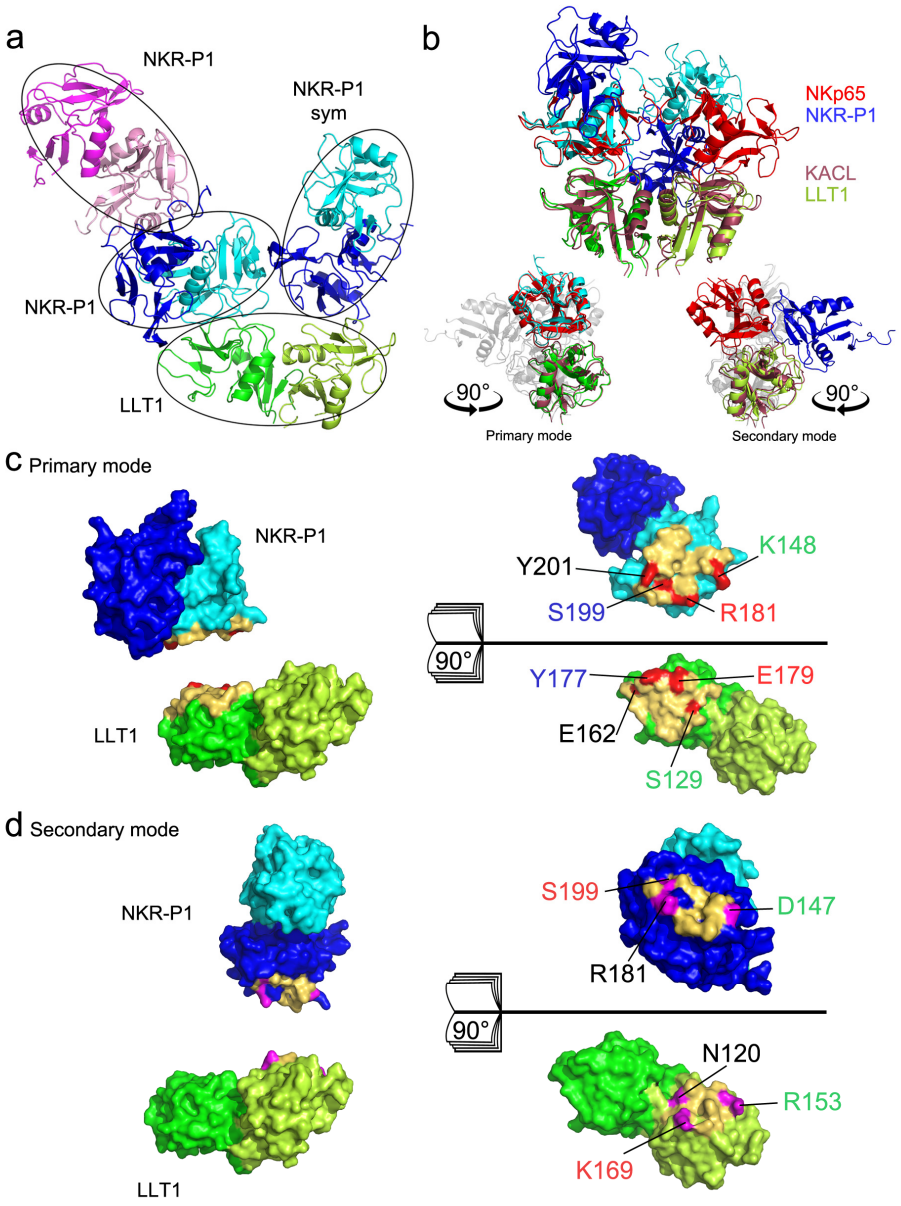

Figure 4. Organization of NKR-P1:LLT1 complex. (**a**) Overall organization of the complex crystal structure. The LLT1 dimer (green/lemon) has contact with the NKR-P1 dimer, formed by the blue monomer and the cyan monomer. The second blue-cyan NKR-P1 dimer is related to the first one by crystal symmetry. The cyan NKR-P1 monomer forms the primary mode contact with LLT1, while the blue NKR-P1 monomer forms the secondary mode contact with LLT1. Additionally, the asymmetric unit of the crystal contains another NKR-P1 dimer (pink/magenta), not engaging in any contacts with LLT1. (**b**) Overall comparison of the structure of dimeric KACL in the complex with two NKp65 monomers (PDB ID 4IOP, dark purple and red, respectively) and the structure of the LLT1 dimer (green/lemon) with two NKR-P1 dimers in the primary (cyan, left side) and secondary (blue, right side) binding mode. In the lower part – the comparisons with only the primary or secondary (both in side view using 90° y-axis rotation) interaction modes of NKR-P1:LLT1 are highlighted; the second molecules in NKR-P1 dimers were omitted for clarity. (**c**) The NKR-P1:LLT1 primary interaction mode. Contact residues within 5 Å distance are colored in yellow. Amino acids forming the four strongest contacts are highlighted in red. (**d**) NKR-P1:LLT1 secondary interaction mode. Contact residues within 5 Å distance are colored in yellow. Amino acids forming the three strongest contacts are highlighted in magenta.

Figure 5

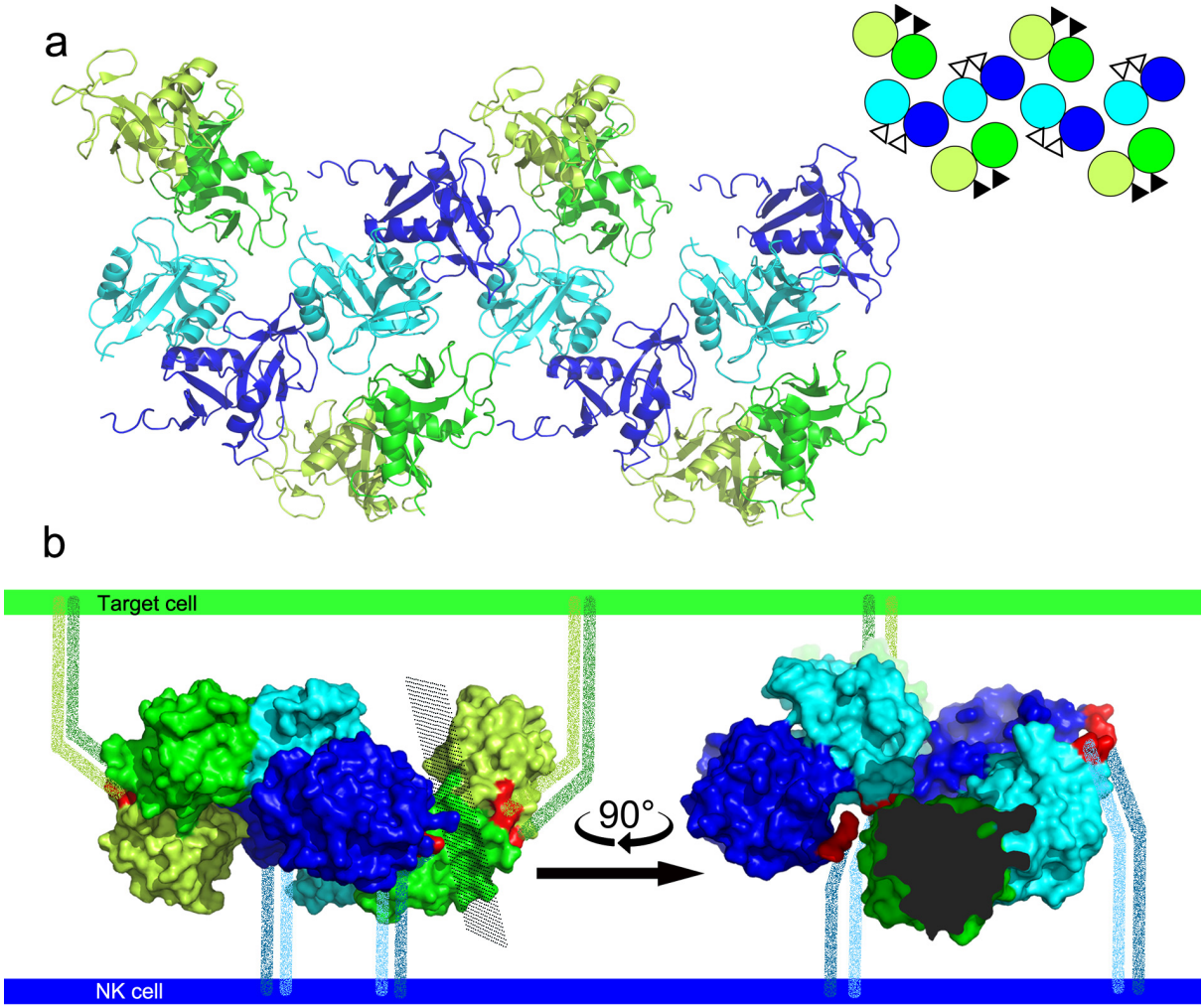

Figure 5. Organization of the chain-forming NKR-P1:LLT1 complexes. (**a**) **Representation** of four neighboring asymmetric units within the NKR-P1:LLT1 complex crystal, excluding the additional receptor dimer. The NKR-P1 (blue and cyan) and LLT1 (green and lemon) dimers alternate participating in the primary (cyan and green) and secondary (blue and lemon) interactions, forming a chain-like structure. The schematic depiction of this arrangement is shown in the inset with the same color code. The black and white triangles represent the positions of the N-termini, pointing behind and in front of the display plane, respectively. (**b**) Depiction of the hypothetical arrangement of the chain-like structure upon the contact of an NK (bottom, blue) and a target cell (top, green). Crystal structure of two NKR-P1 dimers (cyan and blue) interacting with two LLT1 dimers (green and lemon) in the primary (cyan and green) and secondary (blue and lemon) modes are shown. The first three N-terminal residues in the structures are highlighted in red. The symbolic representation of the flexible stalk regions connecting the N-termini and cellular membranes is drawn in speckled lines in the corresponding color coding. The view on the right is clipped for better clarity at the plane indicated in the view on the left.

Tables

Table 1. Data processing statistics and structure refinement parameters. Values in parentheses refer to the highest resolution shell.

	NKR-P1 glyco	NKR-P1 deglyco	NKR-P1:LLT1
PDB code	5MGR	5MGS	5MGT
Data processing statistics			
Space group	$P3_12_1$	P1	$P2_12_12_1$
Unit-cell parameters *a*, *b*, *c* (Å); α, β, γ (°)	68.24, 68.24, 127.19; 90, 90, 120	44.81, 68.40, 101.56; 101.88, 100.72, 100.64	44.58, 80.15, 272.95; 90, 90, 90
Resolution range (Å)	43.3 – 1.8 (1.84 – 1.80)	48.68 – 1.90 (1.93 – 1.90)	76.90 – 1.90 (1.94 – 1.90)
No. of observations	1287150 (76917)	610421 (26224)	1452154 (80494)
No. of unique reflections	32555 (1900)	87081 (4353)	78617 (4472)
Data completeness (%)	100 (100)	97.9 (95.1)	100 (99.9)
Average redundancy	39.5 (40.5)	7.0 (6.0)	18.5 (18.0)
Mosaicity (°)	0.08	0.09	0.05
Average $I/\sigma(I)$	41.0 (7.4)	12.9 (1.7)	14.0 (3.0)
Solvent content (%)	47	42	57
Matthews coefficient (Å^3/Da)	2.32	2.13	2.32
R_{merge}[a]	0.061 (0.637)	0.085 (0.894)	0.153 (0.976)
R_{pim}[b]	0.010 (0.102)	0.053 (0.618)	0.052 (0.337)
CC1/2	1.000 (0.975)	0.999 (0.671)	0.998 (0.890)
Structure refinement parameters			
R_{work}[c]	0.167	0.157	0.166
R_{free}	0.202	0.207	0.201
R_{all}	0.168	0.157	0.166
Average *B*-factor (Å^2)	33	32	26
RMSD bond lengths from ideal (Å)	0.016	0.018	0.019
RMSD bond angles from ideal (°)	1.7	1.8	1.8
Number of non-hydrogen atoms	2481	8344	7030
Number of dimers per asymmetric unit (chains)	1 NKR-P1 (AB)	4 NKR-P1 (AB, CD, EF, GH)	1 LLT1 (AB), 2 NKR-P1 (CD, EF)
Number of water molecules	225	682	691
Positions of modeled GlcNAc residues	AB 116, AB 169	C 116, ABCEFGH 157, ABCDEFGH 169	AB 95, AB 147, F 116, CDF 157, CDEF 169
Ramachandran statistics: residues in favored regions (%); number of outliers(Lovell et al, 2003)	98; 0	98; 0	98; 0

a $$R_{merge} = \sum_{hkl}\sum_{i} | I_i(hkl) - \overline{I(hkl)} / \sum_{hkl}\sum_{i} | I_i(hkl) |$$ (Diederichs & Karplus, 1997), where $I_i(hkl)$ and $\overline{I(hkl)}$ are the observed individual and mean intensities of a reflection with indices *hkl*, respectively, $\sum_{i}$ is the sum over the individual measurements of a reflection with indices *hkl* and $\sum_{hkl}$ is the sum over all reflections.

b $$R_{pim} = \sum_{hkl} \sqrt{\frac{1}{n-1}} \sum_{i=1}^{n} | I_i(hkl) - \overline{I(hkl)} / \sum_{hkl}\sum_{i=1}^{n} | I_i(hkl) |$$ (Weiss, 2001), where *n* is the redundancy of the reflection with indices *hkl*.

c $$R_{work} = \sum_{hkl} (| F_o(hkl) | - | F_c(hkl) |) / \sum_{hkl} | F_o(hkl) |$$, where $F_o(hkl)$ and $F_c(hkl)$ are the observed and calculated structure-factor amplitudes for reflection with indices *hkl*, for working set of reflections. R_{free} is the same as R_{work} but it is calculated for 5% of the data omitted from refinement. R_{all} sums over all reflections. Friedel pairs were treated as independent observations.

Supplementary information

Figure S1

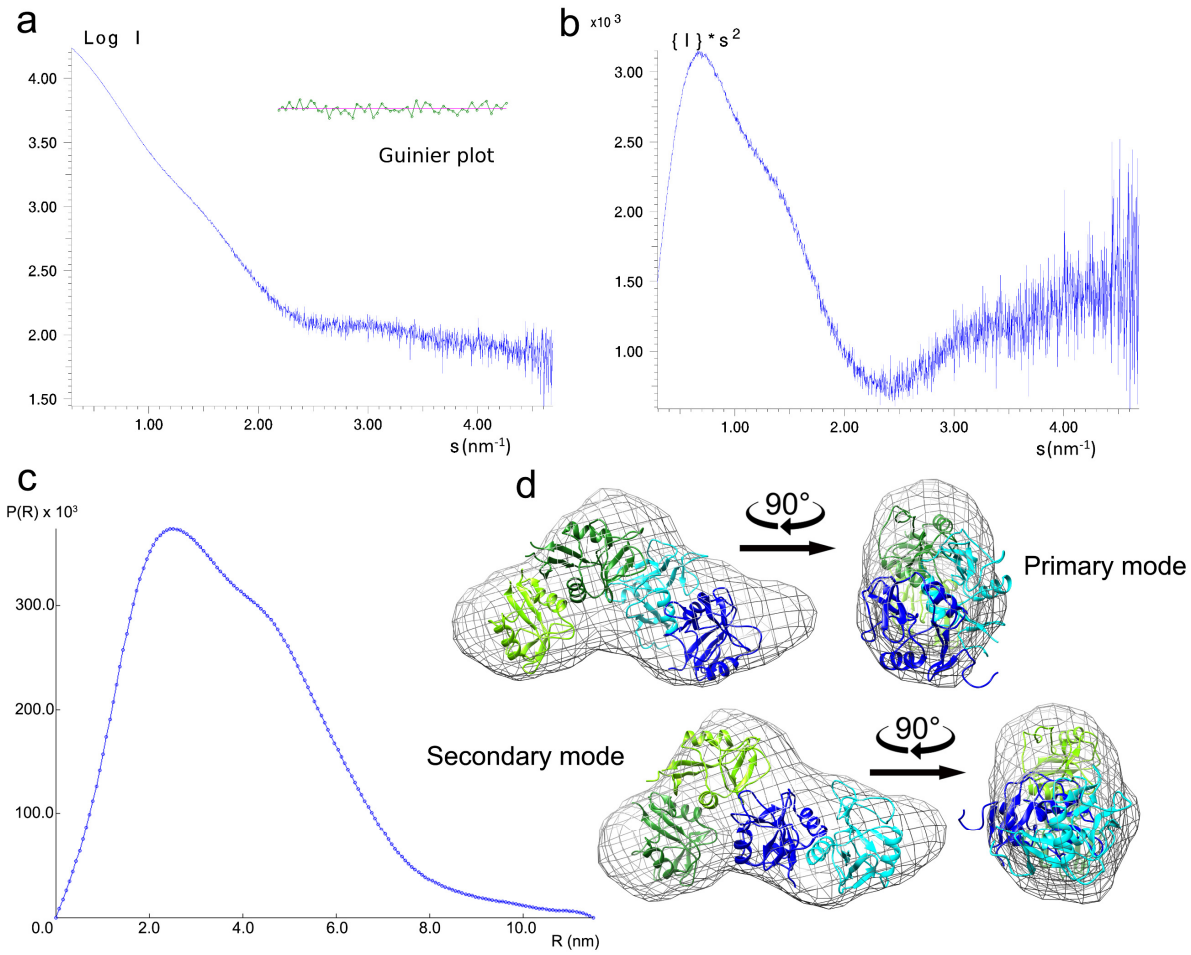

Figure S1. SAXS data for NKR-P1:LLT1 complex at 9.6 mg/ml. (**a**) Scattering plot in logarithmic scale with inserted behavior of Guinier region; (**b**) Kratky plot; (**c**) P(r) plot with D_{max} 11.5 nm; (**d**) The final DAM envelope fitted with X-ray structure of NKR-P1:LLT1 dimer:dimer complex in primary mode (top figure) and secondary mode (bottom figure). Color coding is the same as in figures 3 and 4.

Figure S2

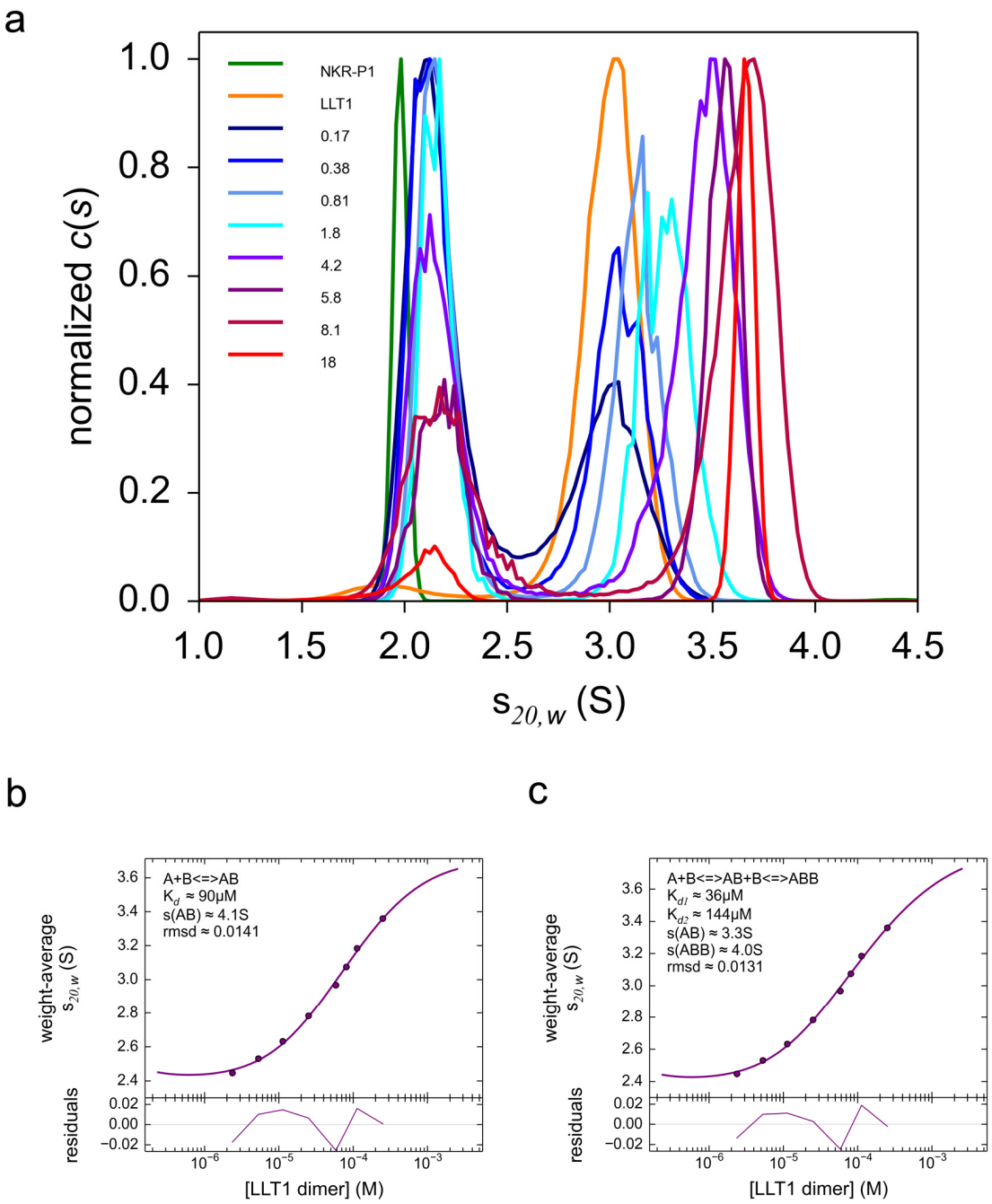

Figure S2. AUC data for NKR-P1:LLT1 complex. (**a**) Normalized sedimentation coefficient distributions transformed to standard conditions ($s_{20,w}$) for free NKR-P1 (green, 5 mg/ml), free LLT1 (orange, 3.5 mg/ml), and their equimolar mixtures at increasing concentration (blue to red, total concentration in mg/ml). Shifting of the distribution to higher S values corresponds to NKR-P1:LLT1 complex formation with fast kinetics. (**b**) and (**c**) Binding isotherms were constructed using the distributions for the proteins mixtures shown in (a) integrated per whole range and fitted using A+B⇔AB model in (b) or with A+B⇔AB+B⇔ABB model in (c) where A is LLT1 dimer and B is NKR-P1 monomer.

Figure S3

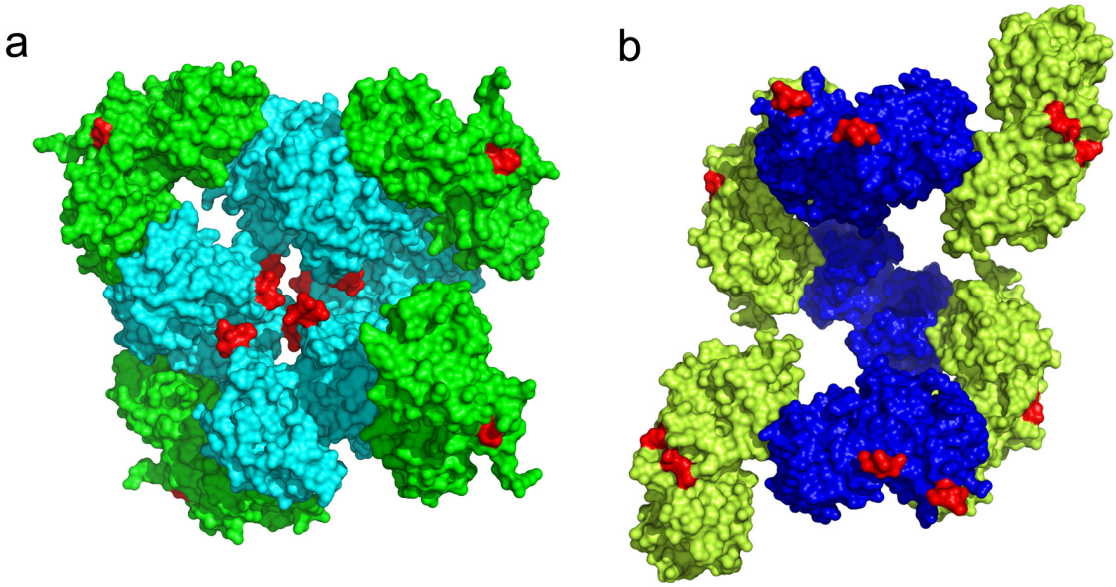

Figure S3. Oligomeric assemblies of the NKR-P1:LLT1 complexes based on propagation of a single interaction mode. (**a**) Primary interaction mode. LLT1 is in green, NKR-P1 in cyan. (**b**) Secondary interaction mode. LLT1 is in lemon, NKR-P1 in blue. The first three N-terminal residues of the proteins are highlighted in red.

Table S1

Table S1. Hydrogen bonds in the dimerization interface of NKR-P1 and in the primary and secondary binding modes of the NKR-P1:LLT1 complex. Water-mediated protein-protein hydrogen bonds are not shown.

NKR-P1 – chain A	NKR-P1 – chain B	Hydrogen bonds	Distance [Å]
α1-centered dimerization (NKR-P1_glyco: chain A, NKR-P1_glyco: chain B)			
Ser127	Ser123	A/Ser127 O:B/Ser123 Oγ	2.8
Ile168	Thr124	A/Ile168 O:B/Thr124 Oγ1	3.1
Glu213	Glu126	A/Glu213 N:B/Glu126 Oε2	2.8
Ser123	Ser127	A/Ser123 Oγ:B/Ser127 O	2.7
Thr124	Ile168	A/Thr124 Oγ1:B/Ile168 O	3.1
Glu126	Glu213	A/Glu126 Oε2:B/Glu213 N	2.8
Asn157	NAG501	A/Asn157 Nδ2:B/NAG501 O7	3.0
Ser159	NAG501	A/Ser159 Oγ:B/NAG501 O3	3.3
NAG501	Asn157	A/NAG501 O7:B/Asn157 Nδ2	2.9
NAG501	Ser159	A/NAG501 O4:B/Ser159 Oγ	3.3
NAG501	Ser161	A/NAG501 O4:W615/W632:B/Ser161 Oγ	4.8
LLT1	**NKR-P1**	**Hydrogen bonds**	**Distance [Å]**
Primary mode (LLT1: chain B, NKR-P1: chain D)			
Ser129	Lys148	Ser129 Oγ:Lys148 O	2.6
Asp130	Ala149	Asp130 N:Ala149 O	3.0
Glu162	Tyr201	Glu162 Oε1:Tyr201 OH	2.5
Arg175	Asp183	Arg175 Nη1:Asp183 Oδ2	2.9
Arg175	Asp183	Arg175 Nη2:Asp183 Oδ2	3.2
Arg175	Glu200	Arg175 N:Glu200 Oε2	3.0
Tyr177	Asp183	Tyr177 OH:Asp183 N	3.2
Tyr177	Ser199	Tyr177 OH:Ser199 O	2.6
Glu179	Arg181	Glu179 Oε1:Arg181 Nη1	3.1
Glu179	Arg181	Glu179 Oε1:Arg181 Nη2	3.0
Glu179	Tyr198	Glu179 N:Tyr198 OH	3.2
Secondary mode (LLT1: chain A, NKR-P1: chain C)			
Asn120	Arg181	Asn120 Oδ1:Arg181 Nη1	3.0
Asn120	Arg181	Asn120 Oδ1:Arg181 Nη2	3.0
Arg153	Asp147	Arg153 Nε:Asp147 Oδ1	3.2
Arg153	Asp147	Arg153 Nη2:Asp147 Oδ2	2.8
Lys169	Arg181	Lys169 O:Arg181 Nη1	3.1
Lys169	Arg181	Lys169 O:Arg181 Nε	3.2
Lys169	Ser199	Lys169 Nζ:Ser199 O	2.6
Lys169	Glu200	Lys169 Nζ:Glu200 Oε1	3.1

Table S2

Table S2. Comparison of the previously proposed NKR-P1:LLT1 binding model with the crystal structure. The table lists point mutations of LLT1 and NKR-P1 residues that had either a detrimental or moderate negative effect on binding of its partner as determined by SPR analyses in the previous binding model proposed by Kamishikiryo *et al.* and Kita *et al.* (Kamishikiryo et al, 2011; Kita et al, 2015); the previously proposed interaction pairs are listed at the bottom. The presence or absence of such residue or interaction pair within the primary or secondary binding mode interface in the observed NKR-P1:LLT1 complex crystal structure is indicated with upper indices (P – primary, S – secondary, - – absence).

LLT1	NKR-P1
Detrimental effect on binding	
Lys169Glu $^{P/S}$	Glu162Arg $^{-/-}$
Arg175Glu $^{P/-}$	Asp183Arg $^{P/S}$
Arg180Glu $^{P/-}$	Tyr198Ala $^{P/S}$
Lys181Glu $^{P/-}$	Tyr201Ala $^{P/S}$
	Glu205Arg $^{P/-}$
Moderate effect on binding	
Tyr165Ala $^{P/S}$	Arg181Glu $^{P/S}$
Asn167Ala $^{P/-}$	Glu186Arg $^{-/-}$
Proposed LLT1:NKR-P1 interaction pairs	
Lys169:Glu205 $^{-/-}$	
Arg175:Glu200 $^{P/-}$	
Glu179:Ser193/Thr195 $^{P/-}$	
Tyr177:Tyr198 $^{P/-}$	
Tyr165:Phe152 $^{-/-}$	

LIST OF PUBLICATIONS

Blaha, J., Pachl, P., Novak, P. and Vanek, O. (2015). "Expression and purification of soluble and stable ectodomain of natural killer cell receptor LLT1 through high-density transfection of suspension adapted HEK293S GnTI$^-$ cells." Protein Expr Purif **109**: 7-13.
DOI 10.1016/j.pep.2015.01.006

Skalova, T., Blaha, J., Harlos, K., Duskova, J., Koval, T., Stransky, J., Hasek, J., Vanek, O. and Dohnalek, J. (2015). "Four crystal structures of human LLT1, a ligand of human NKR-P1, in varied glycosylation and oligomerization states." Acta Crystallogr D Biol Crystallogr **71**(Pt 3): 578-591.
DOI 10.1107/S1399004714027928

Blaha, J., Kalouskova B., Skorepa O., Pazicky S., Novak P. and Vanek O. (2017). "High-level expression and purification of soluble form of human natural killer cell receptor NKR-P1 in HEK293S GnTI- cells." Protein Expr Purif **140**: 36-43.
DOI 10.1016/j.pep.2017.07.016

Blaha, J., Skalova, T., Skorepa, O., Kalouskova, B., Pazicky, S., Polachova, E., Stransky, J., Koval', T., Duskova, J., Zhao, Y., Harlos, K., Hasek, J., Dohnalek, J. and Vanek, O. (2017). "Structure of human natural killer cell receptor NKR-P1 bound to its cognate lymphocyte ligand LLT1." **Submitted**

Skerlova, J., Blaha, J., Pachl, P., Hofbauerova, K., Kukacka, Z., Man, P., Pompach, P., Novak, P., Otwinowski, Z., Brynda, J., Vanek, O. and Rezacova, P. (2017). "Crystal structure of native β-N-acetylhexosaminidase isolated from Aspergillus oryzae sheds light onto its substrate specificity, high stability, and regulation by propeptide." **Submitted**

Stranava, M., Man, P., Skalova, T., Kolenko, P., Blaha, J., Fojtikova, V., Martinek, V., Dohnalek, J., Lengalova, A., Rosulek, M., Shimizu, T. and Martinkova, M. (2017). "Structural basis of the catalytic regulation caused by the heme redox state and ligand-binding of heme-based oxygen sensor histidine kinase, AfGcHK." **Submitted**